THE ROLE OF MATURE MYCOLIC ACIDS IN MYCOBACTERIAL PELLICLE BIOFILM FORMATION AND INTERACTIONS WITH THE HUMAN COMPLEMENT SYSTEM

by

RACHEL KEIRA HALKERSTON

A thesis submitted to the University of Birmingham for the degree of

DOCTOR OF PHILOSOPHY

The Institute of Microbiology and Infection
School of Biosciences
College of Life and Environmental Sciences
University of Birmingham
August 2021

UNIVERSITY OF
BIRMINGHAM

University of Birmingham Research Archive

e-theses repository

This unpublished thesis/dissertation is copyright of the author and/or third parties. The intellectual property rights of the author or third parties in respect of this work are as defined by The Copyright Designs and Patents Act 1988 or as modified by any successor legislation.

Any use made of information contained in this thesis/dissertation must be in accordance with that legislation and must be properly acknowledged. Further distribution or reproduction in any format is prohibited without the permission of the copyright holder.

Abstract

M. tuberculosis cell wall components are essential for host-pathogen interactions and modulating the immune response. *M. tuberculosis* may persist as pellicle-like biofilms within the peripheries of human cavities, and expectorated bacteria from these biofilms may establish infection in a new host. The complement system is an early cascade of the innate immune response, which plays an important role in *M. tuberculosis* access to alveolar macrophages. The impact of mycobacterial biofilms on complement activation has not been studied in-depth. This thesis aims to evaluate the role of mycolic acid maturation in pellicle biofilm formation and interactions of the mycobacterial cell envelope with the human complement system.

Mycolic acids are a major cell wall component, and their accumulation is a hallmark of pellicle biofilm formation. *M. smegmatis,* a surrogate organism for *M. tuberculosis,* was mutated in gene *MSMEG4722* (ortholog of *M. tuberculosis Rv2509*) (*ΔMSMEG4722*), causing the loss of mature mycolic acids for mycolic acid intermediates (Bhatt *et al.*, 2008). As a result, *ΔMSMEG4722* pellicle biofilms could form on the air-liquid interface but could not mature and produced significantly less extracellular material.

Biochemical changes in the cell envelope of *ΔMSMEG4722* were examined using thin layer chromatography. Changes included alteration to the distribution of glycolipids (TDM, TMM and GMM) within the apolar lipid fractions, occurring in bacteria cultured in Middlebrook 7H9 and as planktonic cells and pellicle biofilms. Within pellicle biofilms, mature free mycolic acids and free mycolic acid intermediates/ pre-mycolates decarboxylated to unsaturated ketones accumulated in the apolar lipid fractions for *M. smegmatis* mc^2 155 and *ΔMSMEG4722*, respectively.

Flow cytometry and ELISA demonstrated increased complement system activation, both on whole bacterial cells and the apolar lipid fractions of *ΔMSMEG4722* compared to *M. smegmatis* mc^2 155. Increased complement activator binding was also observed. When examining *M. smegmatis* mc^2 155 pellicle biofilms, comparable complement activation was observed on planktonic cells and pellicle biofilm-derived cells. However, overall activator binding was lower, and there was decreased complement activation by the apolar lipid fractions. *ΔMSMEG4722*, in contrast, showed higher complement activation by both phenotypes compared to *M. smegmatis* mc^2 155, but activator binding was only increased on biofilm-derived cells and both phenotypes demonstrated decreased complement activation by the outer apolar lipid fraction.

The implications of these findings in understanding mycobacterial pellicle biofilm formation and deciphering mycobacterial cell wall component activation of the complement system are discussed.

Acknowledgements

First and foremost, I would like to thank my supervisors Joanna Bacon (Public Health England (PHE)-Porton), Stephen Taylor (PHE-Porton) and Luke Alderwick (University of Birmingham) for their guidance, knowledge, feedback and help throughout the past four and a half years. With your support, I have developed a wide range of skills and enjoyed the diverse aspects of this project that evolved over time. Thanks go to PHE for my doctoral funding.

Thanks also go to all the members, past and present, of the Tuberculosis Drug Discovery Group and Pathogen Immunology Group at PHE-Porton, including; Charlotte, Chris, Rose, Eden, Vanessa, Charlotte, Alex, Frances, Steve, Breeze, Holly, Andy, Charlotte, Stephanie, Lauren, Emily, Liz and Collette. The training, help, guidance, feedback, difficult to acquire consumables and cake that has been provided throughout has been immeasurable. Finally, a special thanks go to Adam and Jordan, who have been my 'ride or dies' over the years. You have supported me at every stage of this journey, picked me up at my lowest points, celebrated my wins and always provided friendship, board games and laughter. Thanks to Katherine Davies and Howard Tolley (Electron Microscopy Department PHE-Porton) for the SEM imaging.

Thanks to all the members of the IMI lab at the University of Birmingham, who welcomed me for the various short stints over the project and provided me with ample guidance, support, training and biochemistry tips and tricks. Special thanks go to Sarah, Natacha, Bala, Helen and Stephen. Thanks go to Apoorva Bhatt (University of Birmingham) for providing the mutant used throughout this project.

Finally, I would like to thank my parents. Mum and dad, as you pointed out when I accepted my PhD position, 452 miles was about as far away from home as I could get whilst staying in the UK. At times it has been challenging but thank you for always being there. Throughout my whole life, you have supported and encouraged my every endeavour. I hope that I have made you very proud.

This thesis is dedicated to my family

Contents

Abstract i

Acknowledgements iii

Contents v

List of Figures xvii

List of Tables xxiv

List of Abbreviations xxvi

1 Introduction 1

1.1 Overview 1

1.2 What is Tuberculosis? 1

1.2.1 *M. tuberculosis* and TB incidence 1

1.2.2 The current state of antibiotics and vaccines against TB 2

1.3 Overview of the mycobacterial cell envelope and its interactions with the immune system 4

1.3.1 Surrogate organisms 4

1.3.2 The mycobacterial cell envelope 4

1.3.3 The plasma membrane 6

1.3.4 Peptidoglycan 7

1.3.5 Arabinogalactan 8

1.3.6 Mycolic acids 8

1.3.7 The mycomembrane outer leaflet and ‘free’ lipids 11

1.3.8 Capsule 12

1.4 Pathophysiology of TB including the role of the complement system 13

1.4.1 Aerosol transmission of *M. tuberculosis* 13

1.4.2 Phagocytosis by macrophages 14

1.4.3 Granulomas 17

1.4.4 The model of biofilm formation for mycobacterial survival and re-activation 19

1.5 Mycobacterial biofilms 22

1.5.1 What are biofilms? 22

1.5.2 The role of biofilms in chronic infections 22

1.5.3 NTM biofilms 23

1.5.4 Pellicle biofilms 24

1.5.5 Mycobacterial biofilm extracellular material 25

1.5.6 Using mutants to understand biofilm formation 26

1.5.7 Mycolic acid mutants and pellicle biofilm formation 27

1.6 The human complement system and interactions with mycobacteria 29

1.6.1 The role of the complement system in the immune system 29

1.6.2 The three complement pathways 30

1.6.3 Mycobacteria and the complement cascade 33

1.6.4 The role of anaphylatoxins in mycobacterial infection 35

1.7 Thesis aims 36

2 The role of IgM in complement activation by planktonic and pellicle biofilm *M. smegmatis* mc^2 155 39

2.1 Introduction 39

2.1.1 Mycobacterial biofilms 39

2.1.2 The role of IgM in complement activation of the classical pathway 41

2.1.3 Aims 42

2.1.4 Hypotheses 43

2.2 Results 44

2.2.1 A reduction in glycerol concentration increases *M. smegmatis* mc^2 155 pellicle reticulation 44

2.2.2 SYTO 40 can separate *M. smegmatis* mc^2 155 bacterial events from flow cytometry background 'noise' 45

2.2.3 Planktonic and pellicle biofilm *M. smegmatis* mc^2 155 bacterial concentration can be standardised using Flow-Count Fluorospheres™ ... 48

2.2.4 Summary of Flow Cytometry optimisation 49

2.2.5 IgM from the IgG-depleted complement source can bind both *M. smegmatis* mc^2 155 and *M. tuberculosis* H37Rv 50

2.2.6 IgM significantly enhances complement activation by both planktonic and pellicle biofilm *M. smegmatis* mc^2 155 53

2.2.7 Summary of IgM binding and complement activation for planktonic and pellicle biofilm *M. smegmatis* mc^2 155 57

2.3 Discussion 58

2.3.1 IgM can facilitate complement activation against both planktonic and pellicle biofilm *M. smegmatis* mc^2 155 58

2.3.2 IgM is a potent activator of complement against *M. smegmatis* mc^2 155 and *M. tuberculosis* H37Rv 59

2.4 Technical discussion 62

2.4.1 Culture condition variations for pellicle biofilms 62

2.4.2 Optimisation of flow cytometry....63

2.4.3 Potential implications of using 4% (v/v) formaldehyde-treated bacteria....65

3 Pellicle biofilm formation by the *M. smegmatis* mutant *ΔMSMEG4722*....66

3.1 Introduction....66

3.1.1 The mycolic acid biosynthesis reductase....66

3.1.2 Aims and Hypothesis....69

3.2 Results....70

3.2.1 Two PCR primer sets were used to confirm the deletion of the *MSMEG4722* gene in *ΔMSMEG4722* and its re-introduction in the complemented strain....70

3.2.2 Defining the growth rate and assessing the effects of selective antibiotics…....76

3.2.2.1 *ΔMSMEG4722* displayed a significantly lower optical density and a log lower total viable counts compared to *M. smegmatis* mc^2 155 by stationary phase, but has a comparable doubling time....76

3.2.2.2 Selective antibiotics had a negative effect on optical density and total viable count of *ΔMSMEG4722*-C....80

3.2.2.3 Selective antibiotics had a negative effect on the culture of *ΔMSMEG4722*-C compared to zero-antibiotic conditions....83

3.2.3 Selective antibiotics inhibit *ΔMSMEG4722* and *ΔMSMEG4722*-C pellicle biofilm formation....83

3.2.3.1 *ΔMSMEG4722* was unable to produce reticulated pellicle biofilms and selective antibiotics inhibited *ΔMSMEG4722*-C pellicle biofilm formation....84

3.2.3.2 Kanamycin has a stronger inhibitory effect than hygromycin on *ΔMSMEG4722*-C pellicle biofilm formation....86

3.2.4 *ΔMSMEG4722* and *ΔMSMEG4722*-C planktonic and pellicle biofilm cultures are stable without the addition of selective antibiotics....88

3.2.5 *ΔMSMEG4722* pellicle biofilms produce significantly less biomass than *M. smegmatis* mc^2 155....93

3.2.6 *ΔMSMEG4722* pellicle biofilm formation visually diverges from day one of culture....96

3.2.7 *ΔMSMEG4722* pellicle biofilms do not mature and reticulate after prolonged incubation....97

3.2.8 Scanning Electron Microscopy to determine the topographical characteristics of *M. smegmatis* mc^2 155, *ΔMSMEG4722* and *ΔMSMEG4722*-C shaking planktonic cultures and pellicle biofilms....98

3.2.8.1 Planktonic *ΔMSMEG4722* are more dispersed than *M. smegmatis* mc^2 155....99

3.2.8.2 *ΔMSMEG4722* pellicle biofilms are significantly flatter with less extracellular material....102

3.3 Discussion....105

3.3.1 Pellicle biofilm development is inhibited in *ΔMSMEG4722*....105

3.3.1.1 The inability to progress past surface aggregation could be an inability to accumulate unreduced free mycolate....105

3.3.1.2 Failure to reticulate could be related to the mycolate change in other mycolate-containing cell wall components....108

3.3.1.3 Failure to reticulate could be influenced by structural changes to mycolates....109

3.3.2 *ΔMSMEG4722* pellicle biofilms produce less extracellular material....110

3.3.3 The growth rate of *ΔMSMEG4722* and *ΔMSMEG4722*-C was comparable to *M. smegmatis* mc^2 155....111

3.4 Technical Discussion....113

3.4.1 Culturing planktonic cells and pellicle biofilms with selective antibiotics....113

3.4.2 Limitations of Middlebrook 7H9 growth analysis for comparing planktonic and pellicle biofilm culture....114

4 Analysis of the outermost lipids of planktonic and pellicle biofilm *ΔMSMEG4722*....115

4.1 Introduction....115

4.1.1 Summary of progress in earlier chapters 115

4.1.2 The lipid profile of *ΔMSMEG4722* in liquid culture 115

4.1.3 Analyses of the lipid profiles of mycobacterial pellicle biofilms 116

4.1.4 TLC solvent systems to characterise lipids 117

4.1.5 Aims 118

4.1.6 Hypotheses 119

4.2 Results 120

4.2.1 Analysis of apolar, polar and FAMEs and MAMEs lipids comparing *M. smegmatis* mc^2 155 and *ΔMSMEG4722* 120

4.2.1.1 *ΔMSMEG4722* has unreduced free mycolic acid intermediates that replace mature free mycolic acids 121

4.2.1.2 TDM and GMM are present in *ΔMSMEG4722* in both the outer and inner apolar lipid fractions, but only the outer apolar lipid fraction of *M. smegmatis* mc^2 155 123

4.2.1.3 No differences were observed in the polar lipid fractions 126

4.2.1.4 Mycolic acid intermediates were esterified to arabinogalactan in *ΔMSMEG4722,* replacing α, α' and epoxy mycolates 126

4.2.2 Analysis of apolar, polar and FAMEs and MAMEs lipids comparing planktonic and pellicle biofilm cultures of *M. smegmatis* mc^2 155 and *ΔMSMEG4722* 130

4.2.2.1 *ΔMSMEG4722* pellicle biofilms accumulate unreduced free mycolate in the apolar lipid fractions 131

4.2.2.2 FMA accumulates in *M. smegmatis* mc^2 155 pellicle biofilms compared to planktonic cells 133

4.2.2.3 TDM is distributed differently between the apolar lipid fractions of planktonic and pellicle biofilm *ΔMSMEG4722* 135

4.2.2.4 Polar lipids displayed a plethora of unidentified lipid spots in both phenotypes of *M. smegmatis* mc^2 155, lost in *ΔMSMEG4722*. 138

4.2.2.5 Unreduced MAMEs are esterified to arabinogalactan for both phenotypes 139

4.2.2.6 Summary tables of lipid changes observed between strains and phenotypes....141

4.3 Discussion....145

4.3.1 Mature mycolates are required for pellicle biofilm maturation....145

4.3.2 TDM, TMM (and GMM) were found in the inner apolar lipids of *ΔMSMEG4722* regardless of phenotype....147

4.3.3 Changes to TDM distribution may affect *ΔMSMEG4722* pellicle biofilm development....149

4.4 Technical Discussion....152

4.4.1 Radiolabelling lipids....152

4.4.2 Deciphering polar lipid spots....152

5 Complement activation by *ΔMSMEG4722*....153

5.1 Introduction....153

5.1.1 Summary of progress in earlier chapters....153

5.1.2 Complement pathway activation by mycobacteria....153

5.1.3 Identified mycobacterial cell wall ligands of complement activators....156

5.1.4 Biofilms and complement activation....157

5.1.5 Aims....158

5.1.6 Hypotheses....159

5.2 Results Aim 1: Functional activation of the complement cascade by *ΔMSMEG4722* and *M. smegmatis* mc^2 155....161

5.2.1 Complement protein deposition and C5a generation onto *M. smegmatis* mc^2 155 and *ΔMSMEG4722*....161

5.2.1.1 Increased C3b/iC3b deposition was observed on *ΔMSMEG4722* compared to *M. smegmatis* mc^2 155....161

5.2.1.2 C5a generation was comparable between *M. smegmatis* mc^2 155 and *ΔMSMEG4722* 162

5.2.2 Activator binding to *M. smegmatis* mc^2 155 and *ΔMSMEG4722* 165

5.2.2.1 Activator binding screen to identify positive controls 165

5.2.2.2 Ficolin-1 was the only activator to show increased binding to *ΔMSMEG4722* compared to *M. smegmatis* mc^2 155 165

5.2.3 C3b/iC3b deposition onto lipid fractions extracted from *M. smegmatis* mc^2 155 and *ΔMSMEG4722* 167

5.2.3.1 Development of a lipid-based C3b/iC3b ELISA 167

5.2.3.2 Only the outer apolar lipids displayed increased C3b/iC3b binding to *ΔMSMEG4722* compared to *M. smegmatis* mc^2 155 168

5.2.4 C3b/iC3b deposition onto *M. smegmatis* mc^2 155 and *ΔMSMEG4722* carbohydrate fractions 170

5.2.4.1 Development of a carbohydrate-based ELISA 170

5.2.4.2 Comparable C3b/iC3b deposition levels were observed between *M. smegmatis* mc^2 155 and *ΔMSMEG4722* extracted lipoglycans 170

5.2.5 Summary of Aim 1 results 172

5.3 Results Aim 2: Functional activation of the complement cascade by planktonic and pellicle biofilm *M. smegmatis* mc^2 155 and *ΔMSMEG4722* 173

5.3.1 Complement protein deposition and C5a generation onto planktonic and pellicle biofilm mycobacteria 173

5.3.1.1 Increased C3b/iC3b deposition was observed on both phenotypes of *ΔMSMEG7422* compared to *M. smegmatis* mc^2 155 173

5.3.1.2 C5a generation was increased in the supernatant of planktonic and pellicle biofilm *ΔMSMEG4722* compared to *M. smegmatis* mc^2 155 176

5.3.2 Activator binding to planktonic and pellicle biofilm mycobacteria 177

5.3.2.1 C1q binding decreases on pellicle biofilm-derived *M. smegmatis* mc^2 155 compared to planktonic *M. smegmatis* mc^2 155 178

5.3.2.2 *ΔMSMEG4722* pellicle biofilm-derived bacteria bind more ficolin-1 and ficolin-2 than planktonic *ΔMSMEG4722* 178

5.3.2.3 C1q binding is lower on planktonic *ΔMSMEG4722* compared to planktonic *M. smegmatis* mc^2 155 178

5.3.3 C3b/iC3b deposition measured onto lipid fractions from extracted planktonic and pellicle biofilm mycobacteria 181

5.3.3.1 *M. smegmatis* mc^2 155 pellicle biofilm-derived apolar lipid fractions have lower C3b/iC3b deposition compared to planktonic cells 181

5.3.3.2 For all lipid fractions of *ΔMSMEG4722*, C3b/iC3b deposition was comparable between planktonic and pellicle biofilm lipids 182

5.3.3.3 Decreased C3b/iC3b deposition was observed on the outer apolar lipids of both phenotypes of *ΔMSMEG4722* compared to *M. smegmatis* mc^2 155 182

5.3.4 Minimal C3b/iC3b deposition was observed onto both planktonic and pellicle biofilm lipoglycans of *M. smegmatis* mc^2 155 and *ΔMSMEG4722*..... 186

5.3.5 Summary of Aim 2 results 188

5.4 Results Aim 3: Purified *Mycobacterium* spp. cell envelope components show a range of C3b/iC3b deposition 191

5.4.1 C3b/iC3b deposition on solvent-soluble cell envelope components 191

5.4.2 C3b/iC3b deposition onto water-soluble cell envelope components 194

5.5 Discussion Aim 1 196

5.5.1 Increased activation of the complement cascade was observed on *ΔMSMEG4722* 196

5.5.2 Mycolic acids (mature and unreduced) are unlikely to facilitate complement activation 197

5.5.3 Redistributed glycolipids in *ΔMSMEG4722* may facilitate increased activation of the complement cascade 199

5.5.4 Changes in distribution to cell wall components other than lipids may facilitate increased activation on *ΔMSMEG4722* 201

5.6 Discussion Aim 2 203

5.6.1 Comparable complement activation was observed on planktonic and pellicle biofilm *M. smegmatis* mc^2 155 203

5.6.2 Activator binding decreases on pellicle biofilm-derived *M. smegmatis* mc^2 155 compared to planktonic cells 204

5.6.3 *ΔMSMEG4722* phenotypes highlight that the picture of complement activation by mycobacteria is complicated and incomplete 206

5.7 Discussion Aim 3 209

5.7.1 Arabinogalactan does not activate the complement system 209

5.7.2 *M. leprae* PGL-1 is a more potent activator of the complement system than *M. canetti* PGL-tb 209

5.7.3 The biosynthetically related $PIM_{1,2}$, PIM_6, LM and ManLAM in *M. tuberculosis* H37Rv showed different activation of complement 211

5.7.4 Species-specific differences in C3b/iC3b deposition onto LAM was observed 214

5.7.5 Sulpholipid-1 and PDIM were potent activators of the complement system 215

6 General Discussion 218

6.1 Do biofilms aid the dissemination of *M. tuberculosis* to a new host? 222

6.2 Do biofilms protect *M. tuberculosis* from antibody-mediated complement activation and killing by immune cells? 224

6.3 Could complement aid anti-Tuberculosis drug evaluation through synergy? 226

6.4 What role do anaphylatoxins play in TB disease, and could changes to the cell wall alter the innate and adaptive immune response to *M. tuberculosis*? 229

6.5 Further assessment of the role of mycolic acids and other cell envelope components in pellicle biofilm development 233

6.6 Further assessment of the cell envelope components that activate the complement system 235

6.7 Concluding Statement 237

7 Materials and Methods 239

7.1 *M. smegmatis* Middlebrook 7H9 and Sauton's 40 planktonic and pellicle biofilm culture 239

7.2 Alternative culture of *M. smegmatis* mc^2 155, *M. tuberculosis* H37Rv and non-mycobacterial bacteria for use in various assays 240

7.3 Preparation of heat-inactivated biomass 241

7.4 Preparation of single-cell *M. smegmatis* stocks 241

7.5 Crystal Violet staining and imaging of pellicle biofilms 242

7.6 Visualisation of *M. smegmatis* mc^2 155 with nucleic acid stains 242

7.7 Gating strategy and compensation matrix for flow cytometry 244

7.8 Calculating bacterial stock concentrations 246

7.9 IgM deposition flow cytometry assays 246

7.10 Complement deposition flow cytometry assays determining C3b/iC3b and C5b-9 deposition 247

7.11 C1q, MBL, ficolin-1 and ficolin-2 flow cytometry binding assay 249

7.12 DNA extraction 250

7.13 Polymerase Chain Reaction 251

7.14 Testing the stability of the *ΔMSMEG4722* and *ΔMSMEG4722*-C *MSMEG4722* gene deletion and complementation 253

7.15 *M. smegmatis* mc^2 155, *ΔMSMEG4722* and *ΔMSMEG4722*-C optical density and total viable count growth curves 253

7.16 Full lipid extraction of *M. smegmatis* mc^2 155, *ΔMSMEG4722* and *ΔMSMEG4722*-C 254

7.16.1 Extraction of free lipids (outer apolar lipid fraction) 255

7.16.2 Extraction of non-polar lipids (inner apolar lipid fraction) 256

7.16.3 Extraction of polar lipids (polar lipid fraction) 256

7.16.4 Extraction of FAMEs and MAMEs (FAMEs and MAMEs lipid fraction) .. 257

7.17 Thin-layer chromatography analysis of lipid extractions 257

7.18 Densitometry analysis of TLC lipid spots 258

7.19 Lipoglycan extraction of *M. smegmatis* mc^2 155, *ΔMSMEG4722* and *ΔMSMEG4722*-C 259

7.20 C3 Standard Curve 259

7.21 C3b/iC3b lipid ELISA 260

7.22 C3b/iC3b carbohydrate ELISA 262

7.23 SEM of *M. smegmatis* planktonic cultures and pellicle biofilms 264

7.24 C5a ELISA 266

8 List of References 268

Appendix 1 284

Appendix 2 288

Appendix 3 313

List of Figures

Figure 1.1: Schematic of the mycobacterial cell envelope.....6

Figure 1.2: Species-specific mycolic acids with a conserved mycolic motif.....10

Figure 1.3 Schematic overview of the complement cascade.....33

Figure 1.4: Thesis aim.....37

Figure 2.1: *M. smegmatis* mc^2 155 pellicle biofilm growth in 24-well plates. 44

Figure 2.2: Evaluating nucleic acid dye staining of *M. smegmatis* mc^2 155 for flow cytometry assays.....47

Figure 2.3: Standardising the starting bacterial concentrations in flow cytometry assays. 49

Figure 2.4: IgM binding onto NTHi, GBS, *M. smegmatis* mc^2 155 and *M. tuberculosis* H37Rv from an IgG-depleted complement source. 51

Figure 2.5: IgM binding over a serial dilution of IgG-depleted complement onto *M. tuberculosis* H37Rv, *M. smegmatis* mc^2 155 and NTHi. 53

Figure 2.6: C3b/iC3b deposition, C5b-9 deposition and IgM binding on planktonic and pellicle biofilm *M. smegmatis* mc^2 155 using IgG-depleted and IgG- and IgM-depleted complement sources. 56

Figure 3.1: *MSMEG4722* encoded reduction of the mycolic motif.....68

Figure 3.2: Schematic representation of the *MSMEG4722* gene region and predicted PCR amplification products using primer set 1.....71

Figure 3.3: PCR confirmation of *M. smegmatis* mc^2 155, *ΔMSMEG4722* and *ΔMSMEG4722*-C using primer set 1. 73

Figure 3.4: Schematic representation of the *MSMEG4722* gene region and predicted PCR amplification products using primer set 2.....74

Figure 3.5: PCR confirmation of *M. smegmatis* mc^2 155, *ΔMSMEG4722* and *ΔMSMEG4722*-C using primer set 2. 75

Figure 3.6: Culture of *M. smegmatis* mc^2 155, *ΔMSMEG4722* and *ΔMSMEG4722*-C without selective antibiotics. 79

Figure 3.7: Culture of *M. smegmatis* mc^2 155, *ΔMSMEG4722* and *ΔMSMEG4722*-C with selective antibiotics. 82

Figure 3.8: The effect of selective antibiotics on pellicle biofilm formation. 85

Figure 3.9: The effect of selective antibiotics on *ΔMSMEG4722*-C pellicle biofilm formation. 87

Figure 3.10: Stability of *ΔMSMEG4722* and *ΔMSMEG4722*-C after Middlebrook 7H9 culture with selective antibiotics. 90

Figure 3.11: Stability of *ΔMSMEG4722* and *ΔMSMEG4722*-C after planktonic culture without selective antibiotics. 91

Figure 3.12: Stability of *ΔMSMEG4722* and *ΔMSMEG4722*-C after pellicle biofilm culture without selective antibiotics. 93

Figure 3.13: *M. smegmatis* mc^2 155, *ΔMSMEG4722* and *ΔMSMEG4722*-C pellicle biofilm formation. 95

Figure 3.14: Imaging pellicle biofilm development over time. 97

Figure 3.15: Prolonged pellicle biofilm development of *M. smegmatis* mc^2 155, *ΔMSMEG4722* and *ΔMSMEG4722*-C. 98

Figure 3.16: Schematic of an *M. smegmatis* pellicle biofilm on the air-liquid interface in a well. 99

Figure 3.17: Scanning electron micrographs of shaking planktonic culture *M. smegmatis* mc^2 155, *ΔMSMEG4722* and *ΔMSMEG4722*-C. 100

Figure 3.18: Scanning electron micrographs of shaking planktonic culture *M. smegmatis* mc^2 155, *ΔMSMEG4722* and *ΔMSMEG4722*-C. 101

Figure 3.19: Scanning electron micrographs of air- and liquid-interface pellicle biofilms of *M. smegmatis* mc^2 155, *ΔMSMEG4722* and *ΔMSMEG4722*-C. 103

Figure 3.20: Scanning electron micrographs of air- and liquid-interface pellicle biofilms of *M. smegmatis* mc^2 155, *ΔMSMEG4722* and *ΔMSMEG4722*-C. 104

Figure 4.1: Outer and inner apolar lipid analysis of *M. smegmatis* mc^2 155, *ΔMSMEG4722* and *ΔMSMEG4722*-C (solvent system A). 122

Figure 4.2: Outer and inner apolar lipid analysis of *M. smegmatis* mc^2 155, *ΔMSMEG4722* and *ΔMSMEG4722*-C (solvent system C). 123

Figure 4.3: Outer and inner apolar lipid fraction analysis of *M. smegmatis* mc^2 155, *ΔMSMEG4722* and *ΔMSMEG4722*-C (solvent system D). 125

Figure 4.4: Polar lipid analysis of *M. smegmatis* mc^2 155, *ΔMSMEG4722* and *ΔMSMEG4722*-C (solvent system D) 126

Figure 4.5: FAMEs and MAMEs analysis of *M. smegmatis* mc^2 155, *ΔMSMEG4722* and *ΔMSMEG4722*-C.....127

Figure 4.6: Outer and Inner apolar lipid analysis of planktonic and pellicle biofilm *M. smegmatis* mc^2 155, *ΔMSMEG4722* and *ΔMSMEG4722*-C (solvent system A) 132

Figure 4.7: Outer and Inner apolar lipid analysis of planktonic and pellicle biofilm *M. smegmatis* mc^2 155, *ΔMSMEG4722* and *ΔMSMEG4722*-C (solvent system C) 134

Figure 4.8: Outer and inner apolar lipid analysis of planktonic and pellicle biofilm *M. smegmatis* mc^2 155, *ΔMSMEG4722* and *ΔMSMEG4722*-C (solvent system D). 136

Figure 4.9: Outer and inner apolar lipid analysis of planktonic and pellicle biofilm *M. smegmatis* mc^2 155, *ΔMSMEG4722* and *ΔMSMEG4722*-C (solvent system D). 137

Figure 4.10: Polar lipid analysis of planktonic and pellicle biofilm culture *M. smegmatis* mc^2 155, *ΔMSMEG4722* and *ΔMSMEG4722*-C (solvent system D) 138

Figure 4.11: FAMEs and MAMEs analysis of planktonic and pellicle biofilm *M. smegmatis* mc^2 155, *ΔMSMEG4722* and *ΔMSMEG4722*-C.....140

Figure 5.1: Overview of the complement cascade with components measured in this chapter highlighted. 154

Figure 5.2: C3b/iC3b and C5b-9 deposition on *M. smegmatis* mc^2 155, *ΔMSMEG4722* and *ΔMSMEG4722*-C. 162

Figure 5.3: C5a anaphylatoxin generation in the supernatant of *M. smegmatis* mc^2 155, *ΔMSMEG4722* and *ΔMSMEG4722*-C incubated with complement. 164

Figure 5.4: Complement activator binding to *M. smegmatis* mc^2 155, *ΔMSMEG4722* and *ΔMSMEG4722*-C.....166

Figure 5.5: C3b/iC3b deposition on *M. smegmatis* mc^2 155, *ΔMSMEG4722* and *ΔMSMEG4722*-C lipid fractions.....169

Figure 5.6: C3b/iC3b deposition on *M. smegmatis* mc^2 155, *ΔMSMEG4722* and *ΔMSMEG4722*-C carbohydrate/ lipoglycan extractions.....171

Figure 5.7: C3b/iC3b and C5b-9 deposition on planktonic and pellicle biofilm *M. smegmatis* mc^2 155, *ΔMSMEG4722* and *ΔMSMEG4722*-C.....175

Figure 5.8: C5a anaphylatoxin generation in the supernatant of planktonic and pellicle biofilm *M. smegmatis* mc^2 155, *ΔMSMEG4722* or *ΔMSMEG4722*-C incubated with complement. 177

Figure 5.9: Complement activator binding to planktonic and pellicle biofilm *M. smegmatis* mc^2 155, *ΔMSMEG4722* and *ΔMSMEG4722*-C.....180

Figure 5.10: C3b/iC3b deposition on lipid extracts from planktonic and pellicle biofilm *M. smegmatis* mc^2 155, *ΔMSMEG4722* and *ΔMSMEG4722*-C.....185

Figure 5.11: C3b/iC3b deposition on planktonic and pellicle biofilm *M. smegmatis* mc^2 155, *ΔMSMEG4722* and *ΔMSMEG4722*-C carbohydrate/lipoglycan extractions.....188

Figure 5.12: C3b/iC3b deposition on purified mycobacterial spp. cell wall components using the lipid-based ELISA. 193

Figure 5.13: C3b/iC3b deposition on purified mycobacterial spp. cell wall components using the carbohydrate-based ELISA.....195

Figure 7.1: Channel and gating strategy for separating *M. smegmatis* mc^2 155 events from unstained background events by flow cytometry.....243

Figure 7.2: Gating strategy for flow cytometry assays.....245

Figure 7.3: Flowchart of full lipid extraction. 255

Figure A.1.1: Culture of *M. smegmatis* mc^2 155 with and without selective antibiotics. 284

Figure A.1.2: Culture of *ΔMSMEG4722* with and without the addition of hygromycin. 285

Figure A.1.3: Culture of *ΔMSMEG4722* with the addition of kanamycin.....286

Figure A.1.4: Culture of *ΔMSMEG4722*-C with and without selective antibiotics. ...287

Figure A.2.1: Outer apolar lipid analysis of *M. smegmatis* mc^2 155, *ΔMSMEG4722* and *ΔMSMEG4722*-C (solvent system A). 288

Figure A.2.2: Inner apolar lipid analysis of *M. smegmatis* mc^2 155, *ΔMSMEG4722* and *ΔMSMEG4722*-C (solvent system A). 289

Figure A.2.3: Outer apolar lipid analysis of *M. smegmatis* mc^2 155, *ΔMSMEG4722* and *ΔMSMEG4722*-C (solvent system B). 290

Figure A.2.4: Inner apolar lipid analysis of *M. smegmatis* mc^2 155, *ΔMSMEG4722* and *ΔMSMEG4722*-C (solvent system B). 291

Figure A.2.5: Outer apolar lipid analysis of *M. smegmatis* mc^2 155, *ΔMSMEG4722* and *ΔMSMEG4722*-C (solvent system C). 292

Figure A.2.6: Inner apolar lipid analysis of *M. smegmatis* mc^2 155, *ΔMSMEG4722* and *ΔMSMEG4722*-C (solvent system C). 293

Figure A.2.7: Outer apolar lipid fraction analysis of *M. smegmatis* mc^2 155, *ΔMSMEG4722* and *ΔMSMEG4722*-C (solvent system D). 294

Figure A.2.8: Inner apolar lipid fraction analysis of *M. smegmatis* mc^2 155, *ΔMSMEG4722* and *ΔMSMEG4722*-C (solvent system D). 295

Figure A.2.9: Outer apolar lipid fraction analysis of *M. smegmatis* mc^2 155, *ΔMSMEG4722* and *ΔMSMEG4722*-C (solvent system D). 296

Figure A.2.10: Inner apolar lipid fraction analysis of *M. smegmatis* mc^2 155, *ΔMSMEG4722* and *ΔMSMEG4722*-C (solvent system D). 297

Figure A.2.11: Polar lipid analysis *M. smegmatis* mc^2 155, *ΔMSMEG4722* and *ΔMSMEG4722*-C (solvent system D).....298

Figure A.2.12: Polar lipid analysis of *M. smegmatis* mc^2 155, *ΔMSMEG4722* and *ΔMSMEG4722*-C (solvent system D).....299

Figure A.2.13: Outer apolar lipid analysis of planktonic and biofilm *M. smegmatis* mc^2 155, *ΔMSMEG4722* and *ΔMSMEG4722*-C (solvent system A).....300

Figure A.2.14: Inner apolar lipid analysis of planktonic and biofilm *M. smegmatis* mc^2 155, *ΔMSMEG4722* and *ΔMSMEG4722*-C (solvent system A).....301

Figure A.2.15: Outer apolar lipid analysis of planktonic and biofilm *M. smegmatis* mc^2 155, *ΔMSMEG4722* and *ΔMSMEG4722*-C (solvent system B).....302

Figure A.2.16: Inner apolar lipid analysis of planktonic and biofilm *M. smegmatis* mc^2 155, *ΔMSMEG4722* and *ΔMSMEG4722*-C (solvent system B).....303

Figure A.2.17: Outer apolar lipid analysis of planktonic and biofilm *M. smegmatis* mc^2 155, *ΔMSMEG4722* and *ΔMSMEG4722*-C (solvent system C).....304

Figure A.2.18: Inner apolar lipid analysis of planktonic and biofilm *M. smegmatis* mc^2 155, *ΔMSMEG4722* and *ΔMSMEG4722*-C (solvent system C).....305

Figure A.2.19: Outer apolar lipid analysis of planktonic and biofilm *M. smegmatis* mc^2 155, *ΔMSMEG4722* and *ΔMSMEG4722*-C (solvent system D).....306

Figure A.2.20: Inner apolar lipid analysis of planktonic and biofilm *M. smegmatis* mc^2 155, *ΔMSMEG4722* and *ΔMSMEG4722*-C (solvent system D).....307

Figure A.2.21: Outer apolar lipid analysis of planktonic and biofilm *M. smegmatis* mc^2 155, *ΔMSMEG4722* and *ΔMSMEG4722*-C (solvent system D).....308

Figure A.2.22: Inner apolar lipid analysis of planktonic and biofilm *M. smegmatis* mc^2 155, *ΔMSMEG4722* and *ΔMSMEG4722*-C (solvent system D).....309

Figure A.2.23: Polar lipid analysis of planktonic and biofilm culture *M. smegmatis* mc^2 155, *ΔMSMEG4722* and *ΔMSMEG4722*-C (solvent system D).....310

Figure A.2.24: Polar lipid analysis of planktonic and biofilm culture *M. smegmatis* mc^2 155, *ΔMSMEG4722* and *ΔMSMEG4722*-C (solvent system D).....311

Figure A.2.25: FAMEs and MAMEs analysis of planktonic and biofilm *M. smegmatis* mc^2 155, *ΔMSMEG4722* and *ΔMSMEG4722*-C.....312

Figure A.3.1: Complement activator binding screen for positive controls.....313

Figure A.3.2: Initial blocking buffer screen for the lipid-based C3b/iC3b ELISA. 314

Figure A.3.3: Second blocking buffer screen for the lipid-based C3b/iC3b ELISA. .315

Figure A.3.4: Third blocking buffer screen for the lipid-based C3b/iC3b ELISA. 316

Figure A.3.5: Optimal lipid coating concentration for the C3b/iC3b lipid-based ELISA. 317

Figure A.3.6: Evaluating the effect of barbitone on complement activation in the lipid-based C3b/iC3b ELISA. 318

Figure A.3.7: C3 standard curve.....319

Figure A.3.8: Evaluating the effect of barbitone on complement activation in the carbohydrate-based C3b/iC3b ELISA. 320

Figure A.3.9: Blocking buffer screen for the C3b/iC3b carbohydrate-based ELISA.321

Figure A.3.10: Determining the optimal coating concentration for the C3b/iC3b carbohydrate-based ELISA. 322

Figure A.3.11: Activator binding to planktonic and biofilm-derived bacteria for each strain. 323

List of Tables

Table 1.1: Species of the *Mycobacterium tuberculosis* complex. 2

Table 2.1: Z-factor analysis of the mean fluorescence intensity of unstained vs stained bacteria.....48

Table 4.1: Mycobacterial lipid profile using the solvent system combinations 118

Table 4.2: Changes to lipids in *ΔMSMEG4722* when *M. smegmatis* mc^2 155 is used as the control lipid profile.....128

Table 4.3: Lipid changes in pellicle biofilms compared to planktonic for both *M. smegmatis* mc^2 155 and *ΔMSMEG4722* (planktonic used as the control). 141

Table 4.4: Lipid changes between *ΔMSMEG4722* and *M. smegmatis* mc^2 155 (*M. smegmatis* mc^2 155 phenotypes used as the control). 143

Table 5.1: C3b/iC3b deposition onto extracted lipid fractions comparing pellicle biofilms and planktonic cells for both *M. smegmatis* mc^2 155 and *ΔMSMEG4722* (planktonic used as the control).....186

Table 5.2: C3b/iC3b deposition onto extracted lipid fractions comparing *ΔMSMEG4722* and *M. smegmatis* mc^2 155 (*M. smegmatis* mc^2 155 phenotype used as the control). 186

Table 5.3: Purified mycobacterial cell wall components. 191

Table 7.1: Sauton's 40 media defined composition 239

Table 7.2: Z-factor ranges. 244

Table 7.3: Primer pairs. 252

Table 7.4: Thermocycler conditions.....252

Table 7.5: Antibiotic conditions for $OD540_{nm}$ and total viable count growth curves. 254

Table 7.6: Solvent systems for TLC lipid analysis. 258

Table 7.7: 12-point 2:3 C3 standard curve dilution series. 260

Table 7.8: Purified solvent-soluble cell wall components obtained through BEI Resources, NAID, NIH. 261

Table 7.9: Purified water-soluble cell wall components obtained through BEI Resources, NAID, NIH. 263

List of Abbreviations

Bacille Calmette-Guérin	BCG
Basic Local Alignment Search Tool	BLAST
Bone-marrow-derived macrophages	BMDM
Bronchoalveolar lavage fluid	BALF
Calcium ions	Ca^{2+}
CAMR Mycobacterium Medium MOD2	CMM MOD2
Chronic obstructive pulmonary disease	COPD
Collectin	CL
Complement receptors	CR
Collagen like region	CLR
Curli-like pili	MTP
Dendritic Cell-Specific Intercellular adhesion molecule-3-Grabbing Non-integrin	DC-SIGN
Diacylglyceride	DAG
Extensively drug-resistant Tuberculosis	XDR-TB
Extracellular material	ECM
Extracellular nucleic acids	eDNA
Extracellular polymeric substances	EPS
Fatty acid methyl esters	FAMEs
Fatty acid synthases	FAS
Free fatty acids	FFA
Free mycolic acids	FMA
Glucose monomycolate	GMM
Glycopeptidolipids	GPLs
Proton nuclear magnetic resonance	^{1}H-NMR
Interferon gamma	IFN-γ
Interleukin	IL
Lipoarabinomannan	LAM
Lipomannan	LM
Mannose receptor	MR
Mannose binding lectin	MBL
Mannosylated lipoarabinomannan	ManLAM
Mass spectrometry	MS
Membrane attack complex	MAC
Micrograms per millilitre	µg mL^{-1}
Mycobacterial membrane protein large 11 transporter	MmpL11
Molybdophosphoric acid	MPA
Monocyte-derived macrophages	MDM
Monomeromycolyl diacylglycerols	MMMDAGs
Monomycoloyl glycerols	MMG
Multi-drug resistant Tuberculosis	MDR-TB
Mycobacterium tuberculosis complex	MTBC
Mycolic acid methyl esters	MAMEs
Mycolyl-arabinogalactan-peptidoglycan complex	mAGP

Mycolyl-diacylglycerols	MDAGs
N-Acetylglucosamine	GlcNAc
N-Acetylmuramic acid	MurNAc
Necrosis-associated extracellular clusters	NECs
Nitric oxide	NO
Non-capped lipoarabinomannan	AraLAM
Nontuberculous mycobacteria	NTM
Non-typeable *Haemophilus influenzae*	NTHi
Nucleotide-binding oligomerization domain 2	NOD-2
Optical density	OD
Pathogen Immunology Group	PIG
Pathogen-associated molecular patterns	PAMPs
Phenolic glycolipid	PGL-tb
Phenolic glycolipid-1	PGL-1
Phenolic glycolipids	PGL
Phosphate buffered saline	PBS
Phosphatidylinositol mannoside 1,2 ($PIM_{1,2)}$	$PIM_{1,2}$
Phosphatidylinositol mannoside 6 (PIM_6)	PIM_6
Phosphatidyl-myo-inositol-mannosides	PIMs
Phosphoinositol lipoarabinomannan	PILAM
Phthiocerol dimycocerosates	PDIM
Polymerase chain reaction	PCR
Public Health England	PHE
Rifampicin-resistant Tuberculosis	RR-TB
Scanning Electron Microscopy	SEM
Streptococcus agalactiae	GBS
Sucrose counter-selectable and hygromycin antibiotic marker	*SacB-Hyg*^{R} cassette
Sulfolipid-1	SL-1
Sulpholipids	SL
Thin Layer Chromatography	TLC
Toll-like receptor	TLR
Total viable counts	TVC
Trehalose dimycolate	TDM
Trehalose monomycolate	TMM
Triacylglycerols	TAG
Tuberculosis disease	TB
Tumor necrosis factor	TNF
United Kingdom	UK
World Health Organisation	WHO

1 Introduction

1.1 Overview

This thesis investigates the innate interactions and activation of the human complement system with *Mycobacterium smegmatis,* a surrogate organism for *Mycobacterium tuberculosis*. Complement system activation by mycobacteria is documented (Ferguson *et al.*, 2004; Carroll *et al.*, 2009; Bartlomiejczyk *et al.*, 2014), but little is known about the role mycolic acids and individual cell envelope components play in these interactions. Even less is known about the role of biofilms, which are emerging as an important phenotype in Tuberculosis disease (TB) (Hunter, 2011). The role of mature mycolic acids in complement interactions and pellicle biofilm formation will be explored with a mycolic acid mutant, *ΔMSMEG4722.*

1.2 What is Tuberculosis?

1.2.1 *M. tuberculosis* and TB incidence

The genus Mycobacterium contains over 170 species, ranging from harmless environmental dwellers to obligate pathogens (Fedrizzi *et al.*, 2017). Most species are Nontuberculous mycobacteria (NTM), including pathogenic *Mycobacterium abscessus* and the *Mycobacterium avium* complex. However, research has focused on *M. tuberculosis*, the predominant species of the *Mycobacterium tuberculosis* complex (MTBC) that causes TB (Table 1.1) (Riojas *et al.*, 2018). The rod-shaped bacterium was first identified in 1882 by Robert Koch (Koch, 1882). TB is the leading worldwide cause of death from an infectious disease. It typically affects the lungs (pulmonary TB) and is spread through aerosol transmission of *M. tuberculosis*. In 2019, there were 7.1

million new reported cases, 10 million people fell ill, with an estimated 1.4 million deaths. An estimated 2 billion people are latently infected, defined as; “the presence of immune responses to *M. tuberculosis* antigens without clinical evidence of active TB”. A challenge of TB diagnosis and treatment is that those latently infected individuals are asymptomatic, with only 5-15% progressing to active TB (re-activation) over their lifetime (WHO, 2020a).

Table 1.1: Species of the *Mycobacterium tuberculosis* complex.

MTBC Member	Typically isolated from
Mycobacterium tuberculosis	humans
Mycobacterium africanum	humans
Mycobacterium caprae	goats
Mycobacterium microti	rodents
Mycobacterium bovis	bovids and humans
Mycobacterium pinnipedii	marine mammals

1.2.2 The current state of antibiotics and vaccines against TB

Issues facing the healthcare response to TB are drug resistance and lack of an effective vaccine. Drug-susceptible TB is treated with a 6-month multi-drug regime (2-months HRZE/4-months HR where H = isoniazid, R = rifampicin, Z = pyrazinamide and E = ethambutol) (WHO, 2017), but mono- and multi-drug resistance, treatment of children, HIV-positive status, extrapulmonary disease and pregnancy/lactation can make TB treatment regimens complicated and long (up to 20 months) (WHO, 2020b). In the latest World Health Organisation (WHO) annual report on TB, in 2019, approximately 500,000 cases of developed TB were rifampicin-resistant (RR-TB). Of these, 78% were multi-drug resistant (MDR-TB), defined as “resistance to rifampicin and isoniazid”. Of previously treated cases, 17.7% were MDR/RR-TB. Extensively drug-resistant TB (XDR-TB), defined as “MDR-TB plus resistance to at least one

fluoroquinolone and second-line injectable agent (amikacin, capreomycin or kanamycin)", had been reported from 123 WHO member states by the end of 2019 and made up 0.17% of all new and relapse TB notifications. There are currently twenty-two drugs in phase I, II or III clinical trials; thirteen new compounds, two drugs with accelerated regulatory approval, one drug approved for limited use in the USA and six repurposed drugs (WHO, 2020a).

The only licenced vaccine, Bacille Calmette-Guérin (BCG), was first administered 100 years ago (1921) and prevents severe TB in children but is less effective in adults (WHO, 2020a). Several countries have discontinued their blanket BCG programmes, including the UK in 2005 (Zwerling and Pai, 2011). An effective T cell response, primarily $CD4^+$, is important for controlling and eliminating *M. tuberculosis,* driving vaccine research to focus on eliciting cell-mediated immunity (Flynn and Chan, 2001). In pre-clinical studies, MVA85A, given as a booster to BCG vaccination, elicited an *ex vivo* Ag85A-specific $CD4^+$ T cell response that secreted Tumour Necrosis Factor (TNF-α), Interferon Gamma (IFN-γ) and IL-12 (McShane *et al.*, 2004; Beveridge *et al.*, 2007). However, in phase 2b clinical trials carried out in South Africa where TB is endemic, MVA85A induced low cell-mediated immunity and lacked efficacy in protection against TB and *M. tuberculosis* in BCG-vaccinated infants when administered as a booster vaccine (Tameris *et al.*, 2013). This has prompted the WHO to declare a re-evaluation of TB vaccine development, with candidates aiming to either prevent the establishment of infection or prevent TB disease progression. Fourteen vaccine candidates are in phase I, II or III clinical trials; three in phase I, nine in phase II and two in phase III. Five of the fourteen candidates contain an Ag85 complex subunit component (WHO, 2020a).

There are no known correlates of protection for TB (Tameris *et al.*, 2013) and drug-treatment regimens are long due to 'persistent' bacteria and drug resistance (Ginsberg and Spigelman, 2007). Therefore, a greater understanding of host-pathogen interactions with the cell wall and modulations of the immune system is essential in developing new vaccines and antibiotics.

1.3 Overview of the mycobacterial cell envelope and its interactions with the immune system

1.3.1 Surrogate organisms

Work evaluating the mycobacterial cell envelope has primarily been conducted in *M. tuberculosis* and its surrogate model organisms *Mycobacterium bovis* BCG, *Mycobacterium marinum* and *M. smegmatis. M. smegmatis* does not need to be handled at containment level three conditions, has a fast doubling time in liquid culture (four hours compared to twenty-two for *M. tuberculosis*), and there is extensive knowledge and expertise in its' genetic manipulation (Shiloh and Champion, 2010).

1.3.2 The mycobacterial cell envelope

The cell envelope is an important interface between mycobacteria and the host immune system, consisting of multiple immunomodulatory constituents and providing intrinsic protection against antibiotics and the host immune response. Mycobacteria present as weakly gram-positive bacteria but have an outer permeability barrier that acts as a pseudo-outer membrane with a periplasmic space akin to gram-negative bacteria (Jarlier and Nikaido, 1994; Jackson, 2014; Rodriguez-Rivera *et al.*, 2017). Genome phylogenetic analysis found that *M. tuberculosis* clusters more closely to gram-negative than gram-positive bacteria (Wolf *et al.*, 2001; Fu and Fu-Liu, 2002).

Schematically, the mycobacterial cell envelope consists of an inner plasma membrane, peptidoglycan layer, arabinogalactan layer, mycomembrane (inner and outer leaflet) and a capsule (Figure 1.1). The peptidoglycan, arabinogalactan and mycolic acid-rich inner leaflet of the mycomembrane make up the mycolyl-arabinogalactan-peptidoglycan complex (mAGP) (Rodriguez-Rivera *et al.*, 2017). The three-dimensional topology of the mAGP complex is still to be elucidated, but the model proposed by Minnikin in 1982 stands up to experimental scrutiny to this day (Minnikin, 1982; Alderwick *et al.*, 2015). The location of many cell wall components within the cell envelope remains ambiguous.

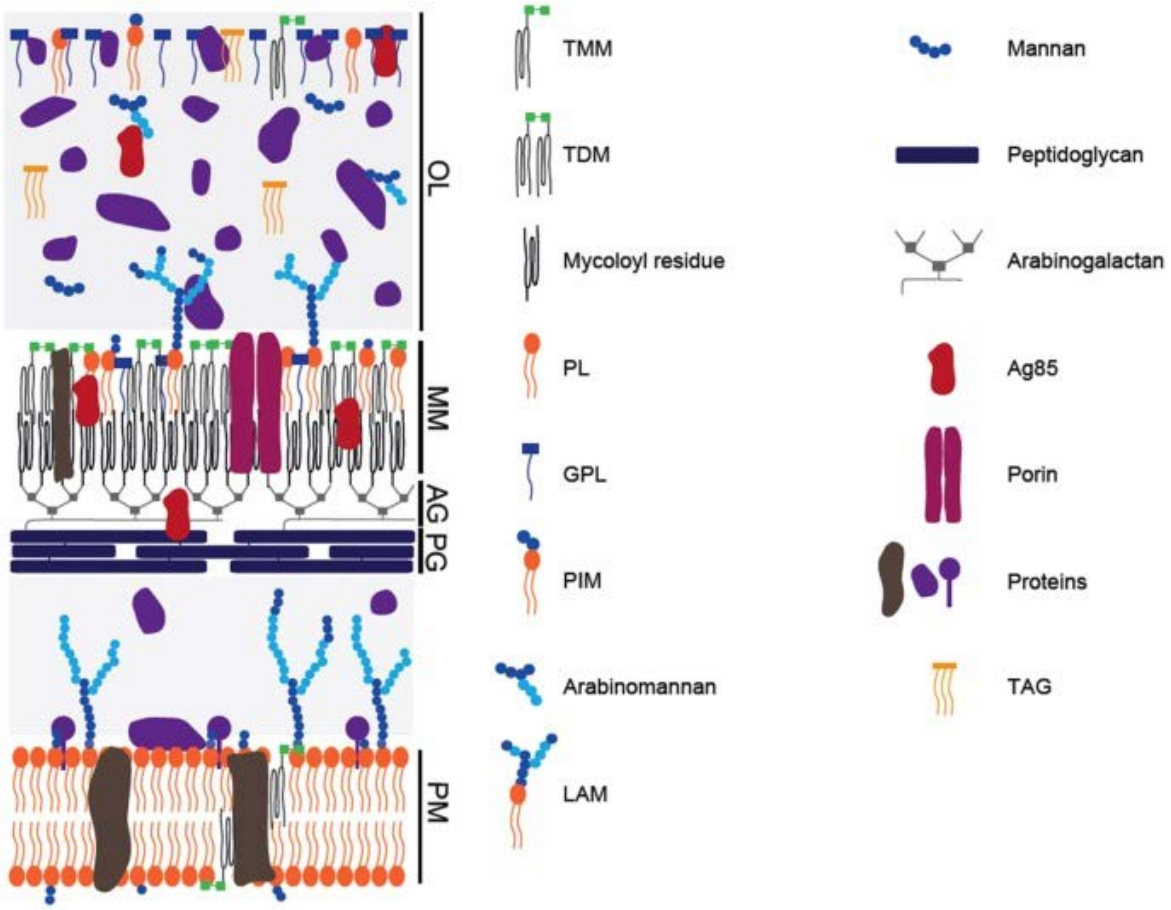


Figure 1.1: Schematic of the mycobacterial cell envelope.

Outermost layer (OL), mycomembrane (MM), arabinogalactan (AG), peptidoglycan (PG), plasma membrane (PM), Trehalose monomycolate (TMM), trehalose dimycolate (TDM), phospholipids (PL), glycopeptidolipids (GPL), phosphatidyl-myo-inositol-mannosides (PIM), lipoarabinomannans (LAM), antigen 85 complex proteins (Ag85), triacylglycerols (TAG). Image reproduced from Chiaradia *et al.*, (2017) (permission to reuse via a Creative Commons Attribution Licence).

1.3.3 The plasma membrane

The inner plasma membrane has an inner and outer leaflet primarily composed of phospholipids and proteins. The main phospholipids in mycobacteria are the phosphatidyl-myo-inositol-mannosides (PIMs); $AcPIM_2$, $AcPIM_6$, Ac_2PIM_2 and Ac_2PIM_6. PIM_2 and PIM_6 are thought to be unevenly distributed across the plasma membrane leaflets. PIM_2 primarily resides in the inner leaflet, which could contribute

to the structural integrity of the cell wall. PIM_6 is proposed to anchor to the outer leaflet and project into the periplasmic space. Projecting into the periplasmic space is also a proposed (transient) location for lipomannan (LM) and lipoarabinomannan (LAM) as they share a common lipid anchor (PI) with the PIMs (Minnikin *et al.*, 2015; Daffé and Marrakchi, 2019). PIMs, LM, and LAM have been implicated with multiple immunomodulatory properties. Mannosylated LAM (ManLAM) induces phagosome maturation arrest through inhibiting calcium ion (Ca^{2+}) increase. PIMs stimulate fusion with early endosomes to provide a source of nutrients to phagosome-residing mycobacteria. ManLAM and PIM_6 are ligands of the mannose receptor (MR) (Mishra *et al.*, 2011) and complement receptors (CR) (Thorson *et al.*, 2001; Villeneuve *et al.*, 2005) that aid phagocytosis. PIM_6 and ManLAM are also ligands of the C-type lectin receptor DC-SIGN on dendritic cells. Binding DC-SIGN can enhance the transcription of the anti-inflammatory cytokine gene for interleukin (IL)-10 upon toll-like receptor (TLR) signalling, but the physiological roles of ManLAM and PIM_6 and their effect on IL-10 production are ambiguous (Driessen *et al.*, 2009; Mishra *et al.*, 2011).

1.3.4 Peptidoglycan

The first ‘layer’ surrounding the inner plasma membrane is peptidoglycan, composed of cross-linked repeating disaccharide units *N*-Acetylglucosamine (GlcNAc) and *N*-Acetylmuramic acid (MurNAc). Cross-linking in *Mycobacterium* spp. is significantly higher at 70%–80% compared to 50% in *Escherichia coli.* This mesh-like arrangement confers rigidity allowing the bacteria to withstand osmotic pressure and degradation by lysozymes (Alderwick *et al.*, 2015). Some muramic acids are oxidised to *N*-glycolylmuramic acids, which may be important in overall strength and resilience

against the host immune response by tightening the peptidoglycan structure through additional hydrogen bonding (Brennan and Nikaido, 1995). Peptidoglycan containing *N*-glycolyl groups has greater NOD2-like receptor stimulating activity. This results in activation of NFκb-pathways, producing the proinflammatory cytokines TNF-α and IL-6 and activation of macrophages and T cells (Coulombe *et al.*, 2009).

1.3.5 Arabinogalactan

Covalently tethered via a phosphodiester bond to 10%–12% of peptidoglycans muramic acid residues is the next 'layer' of the cell envelope, arabinogalactan, which is the second most common macromolecule found in the cell wall after mycolic acids (Birch *et al.*, 2008; Alderwick *et al.*, 2015). Its structure comprises three units; the linker unit, galactan and arabinan, and constitutes around 35% of the cell envelope total mass (Alderwick *et al.*, 2015; Jankute *et al.*, 2015).

Modifications to arabinogalactan may promote efficient infection by mycobacteria, including succinyl or unusual non-*N*-acetylated galactosamine additions to arabinan, which has been observed in the pathogenic gram-negative coccobacillus *Francisella tularensis* (Kieser and Rubin, 2014).

1.3.6 Mycolic acids

The arabinan domain of arabinogalactan is a highly branched polysaccharide that provides the attachment sites for the covalently anchored 70-90 carbon-long mycolic acids (2-alkyl, 3-hydroxy long-chain fatty acids), which consist of a shorter alpha-branch and longer meromycolate chain. Esterified mycolic acids make up the inner leaflet of the mycomembrane (Marrakchi, Lanéelle and Daffé, 2014). Mycolic acids

account for up to 60% of the whole cell dry weight (Lambert, 2002; Nataraj *et al.*, 2015) and give mycobacteria their characteristic waxy, thick coat (Rodriguez-Rivera *et al.*, 2017).

Mycobacterial species produce different mycolic acids; *M. tuberculosis* produces alpha- (α), methoxy- and keto-mycolic acids, whereas *M. smegmatis* produces α-, α prime- (α') and epoxy-mycolic acids. Structural and chemical adaptations to the longer meromycolate chain to produce the various species include double bonds, oxygenation and *cis*- or *trans*-cyclopropane rings with an adjacent methyl branch (Figure 1.2). The most abundant form in *M. tuberculosis* are α-mycolic acids (50-70%) and are primarily found in a 'U' conformation, where the alpha-branch and meromycolate chains are fully extended. This could provide interaction sites with 'free' outer leaflet lipids. In contrast, keto-mycolates are primarily observed as a tightly packed 'W' conformation with the alpha-branch, and longer meromycolate chain folded into three are in parallel, potentially important for the low permeability of the cell wall. Methoxy-mycolates adopt a meromycolate semi-folded 'Z' form (Marrakchi, Lanéelle and Daffé, 2014; Minnikin *et al.*, 2015). The conserved mycolic motif anchors all mycolic acids, and mycolic acids reach maturation after the reduction of a β-oxo group to a hydroxyl group on the motif. The reductase is encoded by the *Rv2509* gene in *M. tuberculosis* (Lea-Smith *et al.*, 2007) and the *MSMEG4722* gene in *M. smegmatis* mc^2 155 (Bhatt *et al.*, 2008).

Mycolic acids give mycobacteria their highly hydrophobic surface, rendering them impermeable to many hydrophilic molecules such as isoniazid and ethambutol. Mycolic acids may trigger the differentiation of macrophages into foamy macrophages, which mycobacteria use as a protective barrier within the lungs (Marrakchi, Lanéelle and

Daffé, 2014). As will be discussed in section 1.5, they are heavily implicated in pellicle biofilm formation *in vitro*.

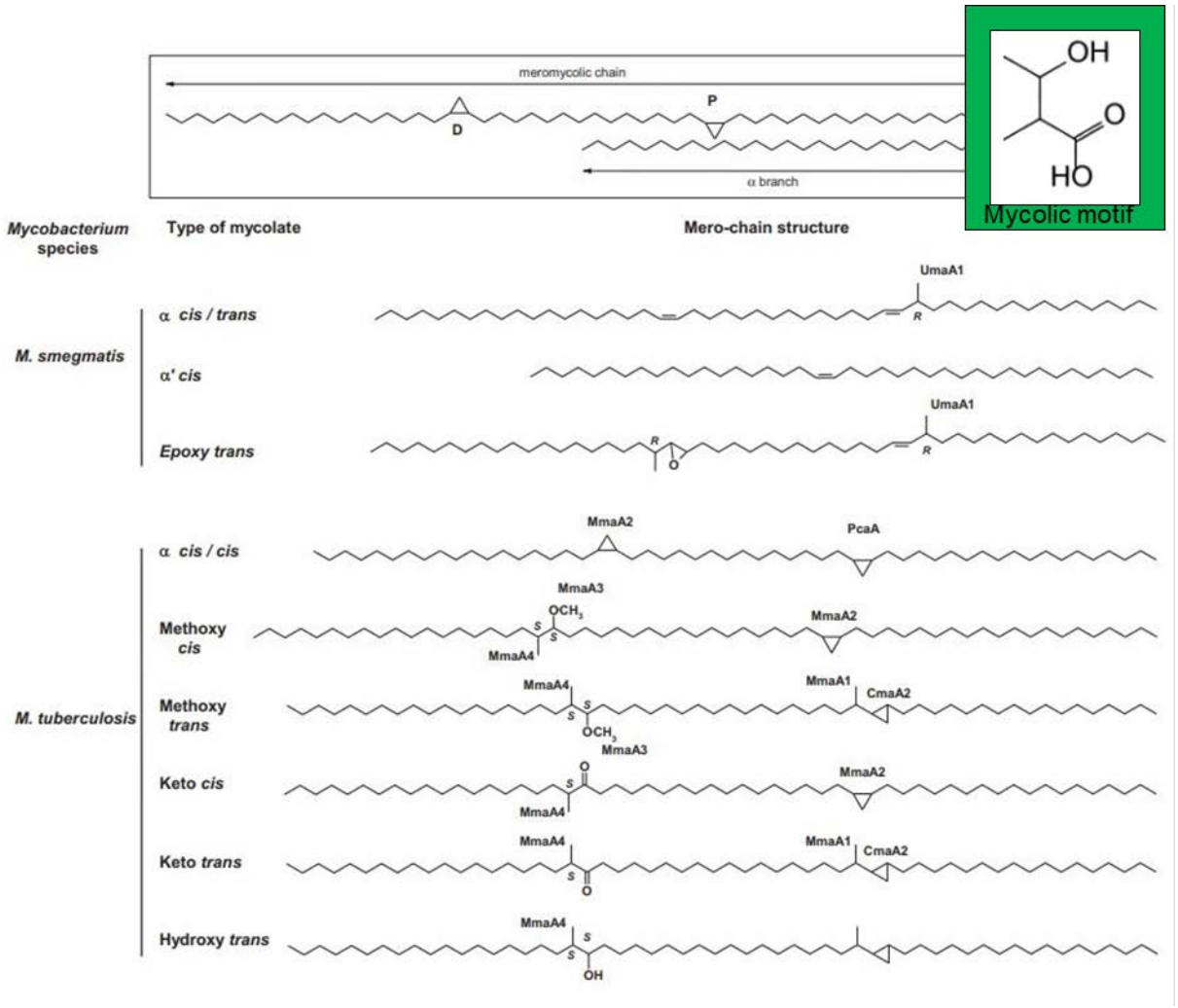


Figure 1.2: Species-specific mycolic acids with a conserved mycolic motif.

Species-specific mycolic acids of *M. smegmatis* and *M. tuberculosis.* Alterations to the longer meromycolate chains within species are characterised by various chemical functions, including double bonds, oxygenation and *cis*- or *trans*-cyclopropane rings with an adjacent methyl branch. The conserved mycolic motif found present on all mycolates is highlighted in a green box. Image adapted from Marrakchi, Lanéelle and Daffé, (2014) (permission to reuse via an Elsevier Copyright Clearance Center Licence).

1.3.7 The mycomembrane outer leaflet and ‘free’ lipids

Mycolic acid esters primarily exist as non-covalently attached ‘free’ lipids in the outer leaflet. These include trehalose monomycolate (TMM), trehalose dimycolate (TDM), glucose monomycolate (GMM), monomycoloyl glycerols (MMG) and di- and triacylglycerols (DAG and TAG). TDM and TMM are the most abundant ‘free’ lipid in the cell envelope, making up 1.5-3% of the dry cell weight of *M. smegmatis* (Woodruff *et al.*, 2004; Yang *et al.*, 2013). TDM is a well-established virulence factor implicated in granuloma formation (Borders *et al.*, 2005; Welsh *et al.*, 2008) and induction of cytokine and nitric oxide (NO) production in macrophages via Mincle binding (C-type lectin receptor). TDM also potentially contributes to phagosome maturation delay through inhibiting phagosome-lysosome fusion (Madacki *et al.,* 2019). Oxygenated functions of the mycolic acids can suppress proinflammatory IL-12 production (Dao *et al.*, 2008). The role of TMM is primarily proposed as a mycolate chain donor to produce TDM. Mycolic acid also exists freely in the cell envelope (Ojha *et al.,* 2010).

Other lipids in the mycomembrane include; phenolic glycolipids (PGL), sulpholipids (SL), phthiocerol dimycocerosates (PDIM), LM, LAM, TMM, TDM and the glycopeptidolipids (GPL) in NTMs, many of which have been implicated in host-pathogen interactions. So far, PDIMs, SL and PGL have only been identified in pathogenic mycobacteria (Jackson, 2014; Jankute *et al.*, 2015; Rodriguez-Rivera *et al.*, 2017). The immunomodulatory properties conveyed by these 'free' lipids, glycolipids and other macromolecules arise from interacting with the large plethora of pattern-recognition receptors present in the immune system, activating various signalling pathways. For example, LM is primarily associated with TLR signalling and

ManLAM by C-type lectin receptor signalling. These interactions are important for the inflammatory response by inducing cytokine production, including IL-8, matrix metallopeptidase 9 from macrophages (associated with tissue damage) and the release of the proinflammatory factors TNF-α and NO (Mishra *et al.*, 2011). They may also be important for interactions with complement and CRs, for access to macrophages, which will be discussed in detail in section 1.4.2.

1.3.8 Capsule

The final 'layer' of the mycobacterial envelope, the capsule, has been visualised using light microscopy techniques as an unstable 'halo' around the bacterial cell wall (Hanks, 1961). Early biochemical works determined the capsule to be composed of a mixture of polysaccharides, proteins and lipids. Lipids account for 2-5% of total material when extracted, indicating most lipids are present in the inner layers, but the lipoglycans LM and ManLAM are present in the capsule. Whether polysaccharides or proteins dominate as the capsular constituent depends on the mycobacterial species. *M. tuberculosis, Mycobacterium kansasii* and *Mycobacterium gastri* are polysaccharide dominant, whilst *Mycobacterium phlei* and *M. smegmatis* are mainly protein. The main polysaccharides composing the capsule are α-glucan (dominant in *M. tuberculosis*), arabinomannan, and mannan (Daffé *et al.*, 1999). There are a wide variety of proteins present. However, due to the current extraction methods (detergents and agitation with glass beads), it is difficult to determine which part of the cell envelope they originate from (Daffé *et al.*, 1999; Daffé and Lanée, 2001; Jackson, 2014).

1.4 Pathophysiology of TB including the role of the complement system

TB is primarily a pulmonary disease. Caseous granulomas located in lung lesions are characteristic of human pathology. When infected with *M. tuberculosis*, individuals progress rapidly to active disease (primary or primary-progressive TB) or contain the initial infection and become latently infected, with the potential for re-activation. How specific disease outcomes arise is not well understood but is likely determined by both the host-immune response and modulation by the bacterium (O'Garra *et al.*, 2013; WHO, 2020a). The pathophysiology of TB is complex and not fully elicited, so described below is an overview of the model pathophysiology of TB, with a focus on CR-mediated entry into macrophages, followed by a new model that implicates biofilms as an important phenotype in TB disease.

1.4.1 Aerosol transmission of *M. tuberculosis*

Viable *M. tuberculosis* is spread through aerosol transmission from (re)active TB patients, with an estimated particle size of 0.65 to 4.7μm aerodynamic diameter (Fennelly *et al.,* 2012). *M. tuberculosis* rods are on average 2-4μM in length and 0.2-0.5μM in width (Todar, 2006), indicating that the aerosols are primarily single bacteria or small aggregates. Shed aerosolised bacteria traverse the respiratory tract. In most cases, the bacilli are trapped within mucus and degraded by antimicrobial proteins, then removed via beating cilia, sterilising the infection. Bacilli that are not sterilised penetrate deep into the distal pulmonary alveoli. They infect resident alveolar macrophages, neutrophils and type II pneumocytes, establishing infection in the

airways and lung parenchyma (Knechel, 2009; Silva Miranda *et al.,* 2012; O'Garra *et al.,* 2013).

1.4.2 Phagocytosis by macrophages

The primary mode of access to the intracellular niche (macrophages) is through opsonophagocytosis. The collectins (mannose-binding lectin (MBL) and surfactant proteins A and D), and activators of the complement system (MBL, C1q, ficolin-1, ficolin-2 and ficolin-3) all facilitate *M. tuberculosis* opsonisation (Gaynor *et al.*, 1995; Ferguson *et al.*, 2004; Carroll *et al.*, 2009; Bartlomiejczyk *et al.*, 2014; Świerzko *et al.*, 2016). The collectins primarily recognise complex carbohydrates (Hickling *et al.*, 2004).

Complement-opsonised *M. tuberculosis* is marked for destruction with C3 fragments including C3b/iC3b that serve as bridging molecules with CR; CR1, CR3 and CR4 (Schlesinger *et al.*, 1990; Schlesinger, 1993; Hirsch *et al.*, 1994). CR1 expression occurs on monocytes, macrophages and neutrophils and CR3 and CR4 on macrophages, monocytes, dendritic cells, neutrophils and natural killer cells. CR1 recognises C1q, C3b, C4b and CR3 and CR4 recognise iC3b (Merle *et al.*, 2015). For human alveolar macrophages, CR4 is the primary receptor for opsonophagocytosis (Hirsch *et al.*, 1994). For human monocytes, CR3 facilitates approximately 80% of complement-opsonised phagocytosis of *M. tuberculosis.* CR1 can also facilitate opsonophagocytosis (Schlesinger *et al.*, 1990; Schlesinger, 1993).

There is a limited concentration of some complement components in the alveolar space, but cells can synthesise complement proteins. This may provide a localised complement micro-environment in the lung at the onset of infection (Watford *et al.*,

2000). In human bronchoalveolar lavage fluid (BALF), compared to serum, C3a, C3b, C4a, and C4b were present at comparable concentrations when normalised to total protein concentrations, but there was significantly less C1q and Factor B. Reduced, but functional classical pathway activity was observed in BALF compared to serum (Watford *et al.*, 2000; Ferguson *et al.*, 2004). Cleavage products of Factor B (alternative pathway protein) were found in the BALF by Western blot, despite no functional alternative pathway activity detected (Watford *et al.*, 2000). Activators of the lectin pathway, ficolin-2, ficolin-3 and MBL, are detectable but at significantly lower levels in BALF than serum (Vogt *et al.*, 2020). *In vitro,* pulmonary alveolar type II epithelial cells synthesise and secrete C2, Factor B, C3, C4 and C5, and human bronchoalveolar macrophages synthesise and secrete C2 and Factor B (Cole *et al.*, 1983; Strunk, Eidlen and Mason, 1988). Macrophages and monocytes can synthesis Factor D, but whether this is to a physiologically relevant concentration is unknown (Morgan and Gasque, 1997).

Non-opsonic phagocytosis may also play a role in early *M. tuberculosis* infection (Watford *et al.*, 2000). CR3 is the primary receptor for non-opsonic *M. tuberculosis* phagocytosis (Schlesinger *et al.*, 1990; Schlesinger, 1993; Hirsch *et al.*, 1994; Cywes *et al.*, 1997), but CR4-mediated phagocytosis has also been observed (Zaffran, Zhang and Ellner, 1998). In addition, MBL can mediate direct opsonophagocytosis via the MR or trigger the lectin pathway of the complement cascade (Schlesinger, 1993; Astarie-Dequeker *et al.*, 1999; Hickling *et al.*, 2004; Kang *et al.*, 2005).

The role that opsonised CR-mediated entry plays in immune subversion by *M. tuberculosis* within macrophages is unclear. *In vitro,* opsonised engagement of CR

facilitates increased association of *M. tuberculosis* with macrophages and faster phagocytosis kinetics than non-opsonised engagement, but neither condition significantly impacts *M. tuberculosis* survival (Hirsch *et al.*, 1994; Zimmerli, Edwards and Ernst, 1996). Reduced bacterial association and opsonophagocytosis kinetics of macrophages *in vitro*, but no overall disadvantage to bacterial burdens and survival *in vivo* have been observed for *M. tuberculosis* and *M. avium* infection using $CR3^{-/-}$ mouse models (Hu *et al.*, 2000; Melo *et al.*, 2000; Bohlson *et al.*, 2001; Rooyakkers and Stokes, 2005).

In contrast, Malik, Denning and Kusner, (2000) evaluated cytosolic Ca^{2+} levels in macrophages (necessary for cellular defence signalling) after the opsonophagocytosis of zymosan and live *M. tuberculosis.* Only zymosan induced an increase in cytosolic Ca^{2+} levels. Mycobacterial phagocytosis via FcyR induced by coating with Anti-LAM antibodies increased cytosolic Ca^{2+} levels. Recoverable CFU was higher after CR-mediated entry than FcyR-mediated entry. Opsonophagocytosed bacteria resided in phagosomes that exhibited low amounts of the lysosomal protein markers, indicating a lack of phagosome-lysosome fusion (Malik, Denning and Kusner, 2000).

Mycobacteria engage a plethora of cell wall components and secreted molecules to induce immune subversion mechanisms, including; inhibiting acidification of the phagosome, inhibiting maturation of the lysosome and preventing phagosome-lysosome fusion. They can also inhibit the production and function of reactive oxygen and nitrogen intermediates, inhibit apoptosis and autophagy of infected/damaged macrophages and suppress the activation and recruitment of T cells through modulating dendritic cell antigen-presenting functions (Pieters, 2008; Zhai *et al.*, 2019).

It is thought that *M. tuberculosis* subversion of cell functions within macrophages exists almost exclusively in nonactivated macrophages (Pieters, 2008). *In vitro* activation of human and mouse macrophages by IFN-γ reduces opsonophagocytosis of *M. tuberculosis* (Douvas *et al.*, 1985; Rooyakkers and Stokes, 2005), *Mycobacterium leprae* (L S Schlesinger and Horwitz, 1991b) and *M. avium* (Toba, Crawford and Ellner, 1989). CR may facilitate entry, but receptors are known to work cooperatively in response to pathogens. Several other receptors have been implicated in mycobacterial recognition and intracellular signalling, including TLR2, TLR4, TLR9, Mincle, Dectin-1, DC-SIGN, FcyR and NOD2 (Silva Miranda *et al.*, 2012).

1.4.3 Granulomas

Despite immune subversion by *M. tuberculosis*, an immune response can be mounted, cumulating in the formation of granulomas (reservoirs for latent infections). Alveolar macrophages produce and secrete antimicrobial peptides, inflammatory cytokines (IL-1α/β, TNF-α, IL-12p40 and IL-6) and chemokines (MCP-1, IL-8, MIP-1a, MIP-1b, RANTES) which attract a variety of immune cells to the site, including blood-derived macrophages, dendritic cells and lymphocytes. Macrophages undergo apoptosis, aiding bacterial control, but primarily necrosis, with the latter resulting in uptake and potentially further replication in macrophages. Activated epithelial cells and neutrophils also release cytokines and chemokines, contributing to cell recruitment prior to necrosis. Through the phagocytosis of apoptotic macrophages and neutrophils, dendritic cells present mycobacterial peptides on their surface and migrate from early forming granulomas to the lymph nodes under the influence of IL-12 and the chemokines CCL19 and CCL21, to drive naive T0 cell differentiation toward a Th1

phenotype (T helper cells). Bacteria can also drain to the lymph nodes. T helper cells return to the lungs and release the cytokine IFN-γ, kick-starting macrophage activation, cytokine production, the induction of microbicidal factors, inflammation and bacterial control. This initiates a proinflammatory response and the progression of granuloma formation. Regulators, including IL-10 and TGF-β, produced by T-regs primary role is to limit host-induced immune pathology but may accidentally aid mycobacterial persistence by dampening the proinflammatory response. The adaptive immune response can take two to three weeks post *M. tuberculosis* exposure to become effective (Silva Miranda *et al.*, 2012; O'Garra *et al.*, 2013).

Most people with a healthy immune system control the initial infection but cannot eliminate bacilli resulting in granuloma formation. Classical granulomas are composed of a central mass of infected macrophages, multinucleated giant cells, epithelioid cells and foamy macrophages loaded with lipid droplets. This central mass is surrounded by layers of B cells, $CD4^+$ and $CD8^+$ T cells and fibroblasts, forming a peripheral fibrotic capsule that acts as a layer of containment. Breakdown of infected cells at the centre of the granuloma results in solid necrotic tissue. As solid necrotic tissue progresses to a caseous material, the granulomas' microenvironment changes, becoming hypoxic, low pH and nutrient-limited, inducing metabolically altered 'dormant' bacilli; those that have entered a metabolically quiescent non-replicative state. Successful granuloma formation results in the primary lesions calcifying and healing, establishing a latent infection with a residual population of viable mycobacteria that can remain 'dormant' within macrophages for decades. In immunocompromised individuals, this process is unsuccessful, and primary-TB develops. The necrotic tissue within the granulomas becomes liquefied, and the fibrous wall loses integrity, allowing caseous material to

drain into a bronchus or nearby blood vessels. This can result in bacilli dispersal and the formation of new granulomas, bacilli expulsion in aerosol droplet nuclei and in some cases, bacilli spread to new tissue resulting in extrapulmonary-TB. Re-activation is thought to occur when a patient has negative changes to their immune status, resulting in the breakdown of focal lesions, extensive lung damage and re-activation of the 'dormant' bacilli leading to active disease (Stewart, Robertson and Young, 2003; Knechel, 2009; Silva Miranda *et al.*, 2012; O'Garra *et al.*, 2013). A hallmark of re-activation is cavitation; the estimated rate of cavitation at the time of diagnosis ranges from 29% to 87%. Cavitation is a consequence of the inflammatory erosion from a granulomatous lung abscess into an airway. It is associated with an increased risk of person-to-person transmission (Urbanowski *et al.*, 2020).

1.4.4 The model of biofilm formation for mycobacterial survival and re-activation

There is increasing evidence that biofilm formation may be a critical step in the survival and persistence of *M. tuberculosis* in latent TB. *M. tuberculosis* bacilli have been observed as extracellular colonies or biofilm-like structures in immunologically naive cotton rats (Basaraba, 2008), guinea pigs (Lenaerts *et al.*, 2007; Ryan *et al.*, 2010; Hoff *et al.*, 2011; Guirado and Schlesinger, 2013), mice and macaques (Chakraborty *et al.*, 2021). In humans, although not explicitly described as 'biofilms', live *M. tuberculosis* has been found post-mortem in lung lesions containing granulomas (Shaler *et al.*, 2013; Chakraborty *et al.*, 2021), and further microbiological examinations have revealed that live bacilli also occur in surrounding lung tissue (Shaler *et al.*, 2013). There is also histological evidence for *M. tuberculosis* biofilm-like structures within

human cavities (Nyka, 1963, 1967, 1977; Nyka and O'Neill, 1970; Hunter *et al.*, 2006; Hunter, 2011).

Within these necrotic cavities, Orme (2014) proposes a challenge to the conventional pathogenesis of TB disease, suggesting that for the majority of its human 'life-cycle' within the lung, *M. tuberculosis* exists as an extracellular pathogen. The initial infection of parenchyma and alveolar macrophages creates local inflammation that assists the influx of tissue fluid, containing primarily macrophages but also neutrophils and dendritic cells. Bacteria drive replication and macrophage necrosis, infecting and replicating within newly arrived macrophages, amplifying the process. The inflammation and necrotic damage caused to host lung tissue during primary granulomatous lesion formation through the release of oxygen radicals and degranulation of neutrophils damage the local capillary bed, inducing the region to become more hypoxic and form necrotic foci. This, coupled with the necrosis of neutrophils and macrophages releasing large numbers of bacilli, result in adapted bacilli that can persist extracellularly within necrosis of a classical granuloma as biofilm-like clusters or communities; termed 'Necrosis-associated extracellular clusters' (NECs). Orme suggests the NECs confer high phenotypic resistance to antibiotics during latent infection and argues that the bacteria will not be nutrient-starved due to the extensive necrosis of neutrophils providing a lipid source.

Re-activation originates from the vicinity of residual primary lesions and can occur from minimal residual necrosis. The theory is that as they heal and calcify, the necrosis becomes highly compressed. The NECs are gradually pushed towards the edge of the lesion into airspace (akin to a pellicle biofilm). The bacteria on the 'air-interface' sense

the increase in partial pressure of oxygen and start to replicate with the potential to disperse. The NECs cause local inflammation, attracting macrophages that will destroy the bacteria, but some become infected, resulting in re-activation. Within cavitation, it is proposed that small aggregates are expelled from NECs and help successful transmission as a larger 'starting dose'. A productive site of infection can establish, implicating biofilm-derived bacteria as the starting inoculum of new infections (Orme, 2014).

Mahamed *et al.*, (2017) examined the uptake of heterogeneous clumps of *M. tuberculosis* by monocyte-derived macrophages (MDMs) using time-lapse microscopy when the bacilli were mCherry fluorescent. When clumps of ≥30 bacilli were ingested, macrophages had a significant probability of death, and ingested clumps of ≥50 bacilli were the threshold for death. Death was faster and more frequent when larger clumps were ingested than multiple small clumps by the same macrophage. *M. tuberculosis* replicated within the cell detritus as a clump faster than in live cells or extracellularly. Activation by IFN-γ before infection did not improve macrophage survival, and alveolar macrophages showed the same death and replication pattern as MDMs. *M. tuberculosis* typically induced macrophage necrosis. Under these conditions, they also observed 'chains' of macrophage infection and necrosis; a macrophage ingested a clump of bacilli, underwent necrosis then the necrotic macrophage-bacilli clump was taken up by another macrophage, with the onset time to macrophage necrosis decreasing down the 'chain'.

1.5 Mycobacterial biofilms

1.5.1 What are biofilms?

Microbial species can persist against environmental stresses and hostile environments by forming heterogeneous mono- or multispecies biofilms; surface-associated, structured, multicellular communities enclosed in a self-produced extracellular polymeric substances matrix (EPS) composed of exopolysaccharides, proteins and extracellular nucleic acids (eDNA), interspersed with nutrient and water channels. Biofilm formation is a developmental process in which bacteria undergo a regulated lifestyle switch from a planktonic 'free-living' state to a sedentary multicellular state influenced by physical, chemical and biological processes. Biofilms develop highly heterogeneous populations in local microenvironments, influenced by the availability of space, oxygen and nutrient gradients, temperature and pH. Key steps include adhesion to a surface, microcolony formation through bacterium division or aggregation and differentiation and maturation of these microcolonies to produce EPS. The EPS makes up to 90% of the biofilm mass (Costerton *et al.*, 1999; Flemming and Wingender, 2010) and is important for structural stability (Chakraborty and Kumar, 2019). Numerous bacteria that cause chronic infections have been isolated as biofilms from live and dead host tissue and medical devices, including *Pseudomonas aeruginosa* and uropathogenic *E. coli* (Costerton *et al.*, 1999; Islam, Richards and Ojha, 2012).

1.5.2 The role of biofilms in chronic infections

Work on isolated bacteria from *in vivo* biofilms and *in vitro* biofilm models have developed multiple proposed roles of biofilms in chronic infections. These include 1)

increasing phenotypic resistance to antibiotics compared to their planktonic state, 2) making bacteria less conspicuous to the immune system, 3) protection against free radicals from phagocytic cells, 4) modulating the cellular immune response, including inducing immune complex damage to surrounding tissue, 5) hiding or repressing key ligands and 6) being fundamental in re-seeding of biofilms through the release of planktonic bacteria or clumps of bacteria (Costerton *et al.*, 1999; Parsek and Singh, 2003; Hall-Stoodley, Costerton and Stoodley, 2004; Islam, Richards and Ojha, 2012; Pang *et al.*, 2012; Chakraborty *et al.*, 2021).

1.5.3 NTM biofilms

NTMs, including members of the *M. avium* complex, *Mycobacterium chelonae*, *Mycobacterium fortuitum,* and *Mycobacterium gordonae,* which are ubiquitous in the environment, have all shown natural attached biofilm formation in aquatic conditions such as drinking water supply systems, showerheads and hospital equipment (Schulze-Röbbecke, Janning and Fischeder, 1992; Wallace *et al.*, 2013; Falkinham, 2010; Kohler *et al.*, 2015; Sax *et al.*, 2015). *M. avium* can form aggregates on the surface of cell monolayers, and within vacuoles of cells (Yamazaki *et al.*, 2006), *Mycobacterium ulcerans* produce a multicellular structure containing bacteria encapsulated by an extracellular matrix within the aquatic insect *Naucoris cimicoides* (Marsollier *et al.*, 2005). *M. abscessus* has been reported to have formed a biofilm within a Chronic Obstructive Pulmonary Disease (COPD) patient (Fennelly *et al.,* 2016).

1.5.4 Pellicle biofilms

Traditionally, biofilms are associated with a solid interface, but biofilms formed on an air-liquid interface under static conditions are described as pellicle biofilms (Armitano, Méjean and Jourlin-Castelli, 2014). Pellicle biofilms have access to high oxygen concentrations from the air, and nutrients from the liquid, through opposing gradients. Pathogenic bacteria that can form pellicle biofilms *in vitro* include *Acinetobacter baumannii, P. aeruginosa,* uropathogenic *E. coli, Salmonella enterica and Vibrio cholerae.* Pellicles are hypothesised to form from initial attachment to a surface adjacent to the air-liquid interface before spreading or through bacterial aggregation on the air-liquid interface. Using the model organism *Bacillus subtilis,* phenotypically pellicle development occurs over three steps; formation of the pellicle, thickening with the appearance of wrinkles then thickening of those wrinkles (Armitano, Méjean and Jourlin-Castelli, 2014). As described in section 1.4.4, there is increasing evidence that *M. tuberculosis* biofilms may be an important phenotype in TB disease.

The ability of *M. avium* and *M. tuberculosis* to form organised pellicle-like structures at the air-liquid interface has been inferred from work as far back as Löwenstein (1920), Calmette (1936), and Koch (1882) (Esteban and García-Coca, 2018). Darzins and Fahr (1956) described *in vitro* mycobacterial growth on the air-liquid interface explicitly as “pellicles”. Under controlled environmental conditions including limited oxygen concentration, high carbon dioxide concentration, and sufficient iron and zinc in the medium, *M. tuberculosis, M. bovis* BCG and *M. smegmatis* have a predisposition to produce macroscopic, phenotypically thick, organised, multicellular structures with net-like patterns at the air-liquid interface (Ojha *et al.*, 2008). Mycobacterial pellicles

develop as a thin film before producing ridging that expands over prolonged incubation (Ojha *et al.*, 2005).

1.5.5 Mycobacterial biofilm extracellular material

A key feature of biofilm formation is the development of EPS. For most biofilm-forming bacteria, EPS composition is mainly exopolysaccharides, including cellulose, D-mannose, D-glucose and L-rhamnose (Flemming and Wingender, 2010). Mycobacterial extracellular material (ECM) is lipid-rich and shows high interspecies variation that is not fully characterised. An ECM component identified in *M. tuberculosis* biofilms formed within *in vitro* granulomas and *in vivo* mouse, macaque and human lung tissue is the glucose polymer cellulose (Chakraborty *et al.*, 2021).

For attached biofilms, GPLs ('smooth' morphotype) have been heavily implicated for *M. avium* (Martínez, Torello and Kolter, 1999; Carter *et al.*, 2003), *M. smegmatis* (Recht *et al.*, 2000) *and M. abscessus* (Howard *et al.*, 2006). Conversely, *M. avium, M. abscessus* and *M. smegmatis* strains lacking GPLs ('rough' morphotype) have been associated with an inability to form attached biofilms (Martínez, Torello and Kolter, 1999; Torrelles *et al.*, 2002; Howard *et al.*, 2006).

M. tuberculosis lacks GPLs and has been described as having "a highly conserved rough morphotype" (Brambilla *et al.*, 2016). However, biofilm formation is still achieved *in vitro* as pellicles (Ojha *et al.*, 2008). *M. smegmatis* and *M. tuberculosis* pellicle biofilm ECM is primarily composed of free mycolic acids. Heterogeneous bacterial persisters from pellicle biofilms exhibit higher drug tolerance than their planktonic counterparts (Ojha *et al.*, 2005, 2008). Multiple cell wall components and cellular processes are

involved in mycobacterial biofilm formation, and ECM could be biofilm-type specific, e.g. attached vs pellicle.

1.5.6 Using mutants to understand biofilm formation

Work understanding the different phenotypic and genotypic properties of mycobacterial biofilms has primarily been undertaken *in vitro*. Multiple clinical *M. tuberculosis* isolates from various lineages can form biofilms, suggesting it is a general characteristic (Pang *et al.*, 2012). For genotypic research, using gene knockout strains of mycobacteria, researchers have deciphered some of the critical genes and pathways involved in biofilm formation, including cell-cell adhesion, cell wall formation and mycolic acid synthesis.

Biofilm formation in human infection by *Staphylococcus epidermidis* is associated with cell adhesion molecules (Hall-Stoodley, Costerton and Stoodley, 2004). *M. tuberculosis* expresses multiple cell adhesion molecules on its cell wall surface, including heparin-binding hemagglutinin adhesin, which adheres to epithelial cells, induces bacterial auto-aggregation and aids the formation of microcolonies (Menozzi *et al.,* 1996). Curli-like pili (MTP) play a vital role in the biofilm formation of *E. coli* and *Salmonella* spp. and were recently identified in *Mycobacterium* spp. through the identification of the *Rv3312A* (mtp) gene product. The *M. tuberculosis* wild-type bacteria showed auto-aggregation, whereas MTP mutants showed defective biofilm growth with no formation at the air-liquid interface (Ramsugit *et al.,* 2013).

Cell wall components implicated in biofilm formation include GPL associated genes; *mps* (GPL biosynthesis), *tmtpC* (GPL transport across the plasma membrane) (Recht

et al., 2000) and *atf1* (transfer of acetyl groups to the glycolipid core of GPLs) (Recht and Kolter, 2001). A *Δupk* mutant, which has a putative role in peptidoglycan synthesis, could only form an attachment of aggregates (Röse, Kaufmann and Daugelat, 2004).

Screening a transposon mutant library of *M. tuberculosis,* a mutant in the *Rv2946c* (*pks1*) gene, essential for PGL production, showed an inability to produce a pellicle biofilm past the initial spreading over the well. The screen also identified genes involved in nitrogen metabolism (*Rv0021c* and *nirB*), cell surface protease activity (*mycP1*), and a gene of unknown function (*Rv0199*) to have attenuated pellicle biofilm-forming function (Pang *et al.*, 2012). An *M. marinum* mutant deficient in producing the 'free' surface-exposed antigenic glycolipid, lipooligosaccharide II, was unable to produce attached biofilms (Ren *et al.*, 2007).

1.5.7 Mycolic acid mutants and pellicle biofilm formation

Mycolic acids, a defining feature of the mycobacterial cell wall, have been highly implicated in pellicle biofilm formation. Fatty acids are the precursors to mycolic acids and are produced through the fatty acid synthases (FASs): FAS I and FAS II. FAS I catalyse the *de novo* synthesis of two long-chain Acyl-CoA fatty acids, C_{16}–C_{18} and C_{24}–C_{26}, from Acetyl-CoA. The C_{24}–C_{26} fatty acid is the substrate for the final α-branch of mycolic acids after carboxylation. FAS II elongates C_{12}-C_{16} fatty acids from FAS I to C_{18}–C_{30} acyl-acyl carrier proteins that undergo iterative elongation cycles as enzyme-bound intermediates. Each elongation cycle includes four steps involving different proteins; MabA, HadAB/HadBC, InhA and KasA/KasB. Within each step, proteins may differ between initial extensions and later extensions of the fatty acid chain. After elongation, the long-chain fatty acids undergo modifications, including the addition of

double bonds, cyclopropyl and methyl groups and oxygenated functions. The Claisen condensation by Pks13 of the long-chain fatty acids from FAS II to the carboxylated α-branch produced by FAS I results in the formation of the unreduced mycolic motif (Marrakchi, Lanéelle and Daffé, 2014).

In several studies, proteins directly involved in elongation of fatty acid chains; InhA, KasB (Ojha *et al.*, 2005), HadC (Jamet *et al.*, 2015) and HadD (Lefebvre *et al.*, 2018), FAS I and II-associated proteins; GroEL (Ojha *et al.*, 2005) and aceE (Chen *et al.*, 2006), and proteins involved in long-chain fatty acid modifications; mmaA4 and pcaA (Sambandan *et al.*, 2013), have shown either delayed, partial, or complete inhibition of pellicle biofilm formation.

Free mycolic acid generation is upregulated in pellicle biofilm formation and hydrolysed from newly synthesised TDM (Ojha *et al.*, 2010). Cell wall components containing mycolate chains can also impact pellicle biofilm formation. The novel apolar mycolyl-diacylglycerols (MDAGs) lipids are α- or α'-mycolates esterified to a glycerol moiety. In an *M. smegmatis* mutant of the cytoplasmic protein Lsr2, inhibited pellicle biofilm formation was observed (Chen *et al.*, 2006). Lsr2 is a histone-like DNA binding protein and is important for conjugative DNA transfer within pellicles (Nguyen *et al.*, 2010). A mutant in the mycobacterial membrane protein large 11 transporter (MmpL11) failed to translocate MDAGs and mycolate ester wax to the bacterial surface, instead accumulating a mycolic acid precursor. This mutant produced a flatter, less reticulated pellicle than *M. smegmatis* mc^2 155 (Pacheco *et al.*, 2013). *rpoZ*, which encodes the ω-subunit of the bacterial polymerase and is involved in β' subunit folding and

recruitment, has shown defective sliding motility and pellicle biofilm formation, associated with the loss of short-chain mycolic acids (Mathew *et al.*, 2006).

1.6 The human complement system and interactions with mycobacteria

1.6.1 The role of the complement system in the immune system

The human complement system plays an intrinsic role in first-line defence against invading pathogens. It is facilitated by a tightly regulated network of >30 proteins primarily synthesised in the liver, circulating in tissues as inactive precursors. They activate upon recognition and interaction with microorganisms' molecular components, including cell wall constituents, so they could play a role in host-pathogen interactions with mycobacteria.

The complement system is a component of innate immunity, providing complement opsonins for phagocytosis, forming the membrane attack complex (MAC) and releasing anaphylatoxins that trigger inflammation and immune and non-immune cell activation. There is now mounting evidence for its role in the adaptive immune response. This includes the early selection and expansion of the B cell pool, maintenance of long-term memory B cells and priming both $CD4^+$ and $CD8^+$ T cells via the marking of foreign antigens (Merle *et al.*, 2015). Additionally, both antigen-presenting cells and T cells express CR3a, which could link the innate and adaptive immune response (Carroll, 2004).

1.6.2 The three complement pathways

The system is composed of three pathways; the classical, lectin and alternative pathways. They are activated by a plethora of pathogen-associated molecular patterns (PAMPs) interacting with pathway-specific activators that all form C3-convertases, which cleaves the central component of complement, C3.

C1q is the recognition molecule of the classical pathway that makes up the circulating inactive C1-complex through associations with C1r and C1s. C1q is not synthesised in the liver, instead primarily by immature dendritic cells, monocytes, and macrophages. C1q comprises an N-terminal region, a collagen-like region (CLR) and a hexameric C-terminal globular head domain (Kishore *et al.,* 2004). Antibodies have a high affinity for C1q, with IgG and IgM being part of the complexes that can activate complement, potentially through ionic interactions with an exposed Ca^{2+} ion in the globular head region of C1q. Classical activating antibody-C1q complexes are made up of multiple IgG or a single IgM antibody. IgM is primarily pentameric and the most potent complement-activating immunoglobulin. The binding of the inactive C1q-complex to antibodies induces conformational changes that activate C1r then C1s. C1s cleaves C4 and C2 to form the C3-convertase C4bC2a (Schroeder and Cavacini, 2010; Merle *et al.*, 2015; Quidel, 2018). Serum C1q levels have been reported to range between 56 and 276 µg mL^{-1} (Dillon *et al.*, 2009).

The lectin pathway has multiple activators; the collectins (CL) (MBL, CL-10, CL-11) and ficolins (ficolin-1, ficolin-2, ficolin-3), which recognise and bind carbohydrates on the pathogen surface. MBL is structurally similar to C1q but has a C-terminal carbohydrate recognition domain. It primarily consists in the oligomeric form of trimers

and tetramers of subunits but can also form pentamers, hexamers and monomers. MBL is found at 1µg mL^{-1} in human serum and recognises a range of ligands, including mannose, GlcNAc and nucleic acids. Each MBL molecule is associated with a serine protease, either MASP-1 or MASP-2. MBL with differing MASPs come together on the ligand surface to allow MASP-1 to activate MASP-2. Both MASPs cleave C2 and MASP-2 can also cleave C4, producing C4b and C2a that form the C3-convertase C4bC2a (Merle *et al.*, 2015; Garred *et al.*, 2016).

The ficolins are structurally similar to MBL with a C-terminal fibrinogen-like recognition domain. Ficolin-1 and ficolin-2 have the highest amino acid similarity at 79%. Ficolin-3 has 48% homology to ficolin-1 and ficolin-2. Ficolin-3 is the most abundant in serum (25µg mL^{-1}), then ficolin-2 (5µg mL^{-1}) and ficolin-1 (0.3µg mL^{-1}). Ficolin-1 is primarily tethered to the cell that secretes it. All three ficolins recognise acetylated compounds, including GlcNAc and sialic acid, but overall, ficolin-2 recognises the broadest range of ligands. Ficolin-2 contains four recognition domains compared to one in both ficolin-1 and ficolin-3. Ficolins also trigger the lectin pathway through interactions with MASPs. The collectins CL-10 and CL-11 are structurally like MBL and ficolins and primarily exist as a complex, but currently, very few ligands have been determined (Garred *et al.*, 2016).

Finally, for the alternative pathway, complement cascade activation is facilitated by spontaneous hydrolysis of C3 into bioactive C3(H_2O), which exposes a Factor B binding site. Unless Factor B binds, C3(H_2O) is rapidly degraded. C3(H_2O)FB is then cleaved by Factor D to form the fluid phase C3-convertase C3(H_2O)Bb that continuously cleaves low levels of C3 into C3a and C3b. This spontaneous hydrolysis

is known as ‘tick-over’ and results in the alternative pathway being permanently active at a low level providing immune surveillance.

After formation through one of the three pathways, C3-convertases cleave C3 into C3a and C3b. The opsonin C3b is a nucleophile binding to primary amine or hydroxyl groups. C3b is the central component of C5-convertases (C4bC2aC3b for the classical and lectin pathway and $(C3b)_2Bb$ for the alternative pathway), triggering the production of C5b, which drives the terminal complement pathway resulting in the formation of the lytic MAC; also known as the C5b-9 complex (Figure 1.3). The formation of $(C3b)_2Bb$ is also amplified by the positive feedback loop of the alternative pathway. The C5b-9 complex penetrates the cell membrane at C5b-8 before recruiting 12-18 C9 proteins, which polymerise to form a pore, facilitating death through Ca^{2+} influx and lysis. As the complement cascade progresses from C3 cleavage, different products released initiate various aspects of the immune response. The anaphylatoxins C3a and C5a can bind to CRs and have various functions, including triggering mast cell degranulation, increased neutrophil and monocyte adherence, act as chemoattractants and activate T-cells and macrophages. C3b is degraded quickly into products including iC3b and C3dg. These, like the anaphylatoxins, can mediate adaptive immune stimulation, opsonophagocytosis and immune adhesion through interaction with CRs (Merle *et al.*, 2015; Ricklin, Reis and Lambris, 2016; Quidel, 2018).

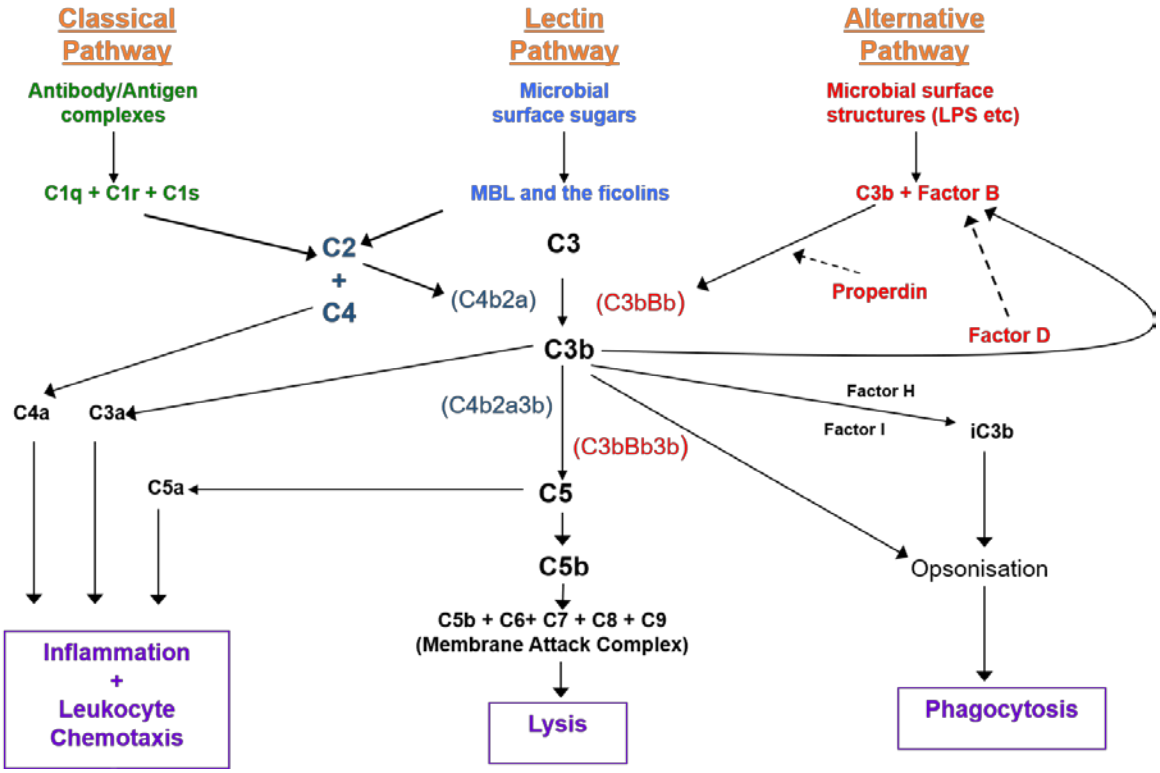


Figure 1.3 Schematic overview of the complement cascade.

The three pathways, classical, lectin and alternative, all lead to the formation of C5b-9 via cleavage of the central component of complement, C3. Image created by and reproduced with permission from Stephen Taylor, PHE.

1.6.3 Mycobacteria and the complement cascade

Mycobacteria are thought to exploit opsonins of the complement cascade and their receptors on host phagocytes to gain entry to their intracellular niche and evade the host immune response, as was described in section 1.4.2.

The cell wall components involved in direct interactions with CRs are still being elicited but may include GlcNAc (Thornton *et al.*, 1996), LAM, LM (Thorson *et al.*, 2001), PIM_2, PIM_6 (Thorson *et al.*, 2001; Villeneuve *et al.*, 2005), PGL-1 of *M. leprae* (Larry S Schlesinger and Horwitz, 1991), polar glycopeptidolipid III (Villeneuve *et al.*, 2005) and

Ag85 complex proteins of *M. tuberculosis* and *M. bovis* BCG (Hetland and Wiker, 1994).

For mycobacteria, *in vitro* activation of the cascade for C3b/iC3b deposition and the cascade's continuation to C5b-9 formation can be facilitated by the activators of all three pathways. Opsonisation by anti-cell wall antibodies via the C1q complex triggers the classical pathway (Ferguson *et al.*, 2004). Antibodies against mycobacterial cell wall components that can trigger the classical pathway include ManLAM for *M. bovis* BCG and *M. tuberculosis* (Hetland *et al.*, 1998) and PGL-1 for *M. leprae* (Larry S Schlesinger and Horwitz, 1991). Carroll *et al.,* (2009) demonstrated antibody-independent binding of C1q onto whole-cell *M. bovis* BCG, but the potential ligands are yet to be elicited.

Lectin pathway activators interact with multiple mycobacterial species; MBL can bind *M. tuberculosis*, *M. bovis* BCG, *M. kansasii, M. gordonae* and *M. smegmatis.* Ficolin-1 and ficolin-2 can bind *M. tuberculosis*, and *M. bovis* BCG and ficolin-3 can bind *M. tuberculosis*, *M. bovis* BCG and *M. kansasii* (Carroll *et al.*, 2009; Bartlomiejczyk *et al.*, 2014). However, Carroll *et al.,* (2009) did not observe any ficolin-3 binding to *M. bovis* BCG. For *M. tuberculosis,* identified lectin pathway activating ligands are ManLAM and Ag85 complex proteins (Bartlomiejczyk *et al.*, 2014; Świerzko *et al.*, 2016). Ficolin-2 was found to block the infection of human lung epithelial cells, and opsonophagocytosis was promoted (Luo *et al.*, 2013).

The alternative pathway has been proposed as the only way for complement to activate against mycobacteria (Ramanathan, Curtis and Turk, 1980; Swartz *et al.*, 1988), but

the classical and lectin pathway activity demonstrated above means it likely acts as the main amplifier of the system. Another unique way that pathogenic mycobacteria may exploit CR interactions is to recruit complement fragment C2a to form a C3-convertase that generates C3b in the absence of the complement activators (Schorey, Carroll and Brown, 1997).

1.6.4 The role of anaphylatoxins in mycobacterial infection

With opsonophagocytosis being the primary focus of mycobacteria and complement research, the lytic C5b-9 complex role regarding mycobacterial infection is relatively unexplored. Gram-positive bacteria such as *Streptococcus pyogenes* and *B. subtilis* have been observed to have C5b-9 on their surface in specialised regions (Berends *et al.,* 2013). Mycobacteria demonstrate C5b-9 deposition but are widely believed to be impermissible to lysis. The C5b-9 deposition was primarily from cell wall-specific antibody-mediated classical activation, with serum from TB patients eliciting significantly more C5b-9 deposition on *M. bovis* BCG bacilli than serum from healthy individuals (Hetland *et al.,* 1998). Whether the formation of the C5b-9 complexes is beneficial for human pathology or mycobacterial survival is complicated. Welsh *et al.,* (2012) observed in C7-deficient mice reduced lung pathology when infected with *M. tuberculosis*, compared to wild-type mice with changes observed in multiple aspects of the immune response. These included lung cytokine expressions, macrophage cytokine expression, reduced bacterial burden in the liver and immune cell composition in the lungs (large clusters of lymphocytes near granulomas with fewer macrophages). They suggest that C7 in the host response contributes to *M. tuberculosis*'s persistence

and dissemination. C7 insertion into the cell membrane is the essential step in the formation of the lysing C5b-9 complex.

In comparison, Actor *et al.,* (2001) used mice naturally deficient in C5 and found accelerated TB infection in these C5-deficient mice compared to wild-type. Changes include increased bacterial load in the lung, negative changes to lung architecture, the inability to contain bacteria within granulomas and defective chemokine secretion from macrophages. They suggest the negative changes seen in the C5-deficient mice were due to their inability to mount an early immune response, early activation of macrophages and subsequent T-cell responses, mainly due to a lack of the anaphylatoxin C5a and its downstream effects.

1.7 Thesis aims

All three pathways of the complement system have been implicated in activating in response to mycobacteria. Cell wall composition and existing in a biofilm-like state within the host are likely to modulate interactions with the complement system.

Mycolic acids are a crucial component of the mycobacterial cell wall and a hallmark of pellicle biofilm formation. This thesis aims to evaluate the role of mycolic acid maturation in pellicle biofilm formation and interactions of the mycobacterial cell envelope with the complement system (Figure 1.4). In this thesis, comparisons are made between the mycolic acid biosynthesis reductase mutant *ΔMSMEG4722,* the complemented strain *ΔMSMEG4722*-C and wild-type *M. smegmatis* mc^2 155.

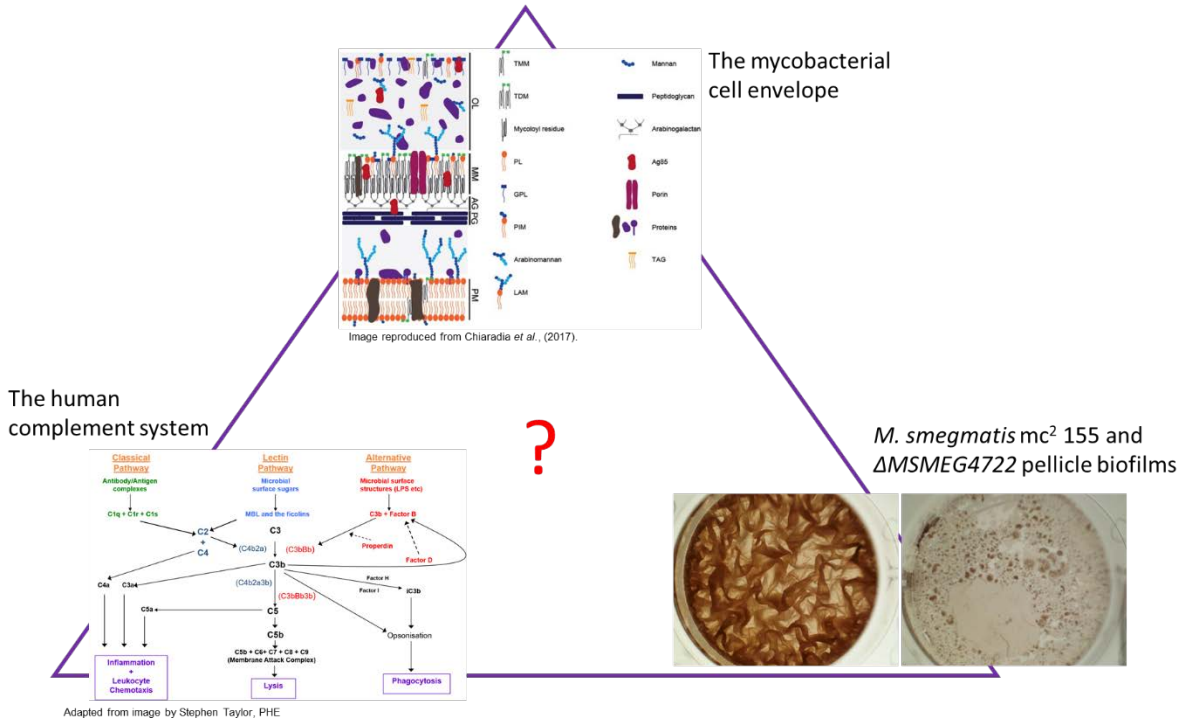


Figure 1.4: Thesis aim.

To understand the role of mature mycolic acids in pellicle biofilm formation and how they affect innate cell envelope complement interactions when cultured as a pellicle biofilm. Complement cascade image created by and reproduced with permission from Stephen Taylor, PHE. Cell envelope image reproduced from Chiaradia *et al.*, (2017) (permission to reuse via a Creative Commons Attribution Licence). Pellicle biofilm images from this thesis (chapter 3).

The overarching aims of this thesis are to:

1) Determine the role of IgM in complement activation on planktonic and pellicle biofilm *M. smegmatis* mc^2 155 (chapter 2).

2) Determine whether the loss of mature mycolic acids for mycolic acid intermediates using *ΔMSMEG4722* affects pellicle biofilm formation (chapter 3).

3) Identify changes to cell envelope lipids between *M. smegmatis* mc^2 155 and *ΔMSMEG4722.* Extracted characterised lipid fractions will then be assessed for complement activation (chapter 4/5).

4) Identify changes to cell envelope lipids between planktonic and pellicle biofilm *M. smegmatis* mc^2 155 and *ΔMSMEG4722.* Extracted characterised lipid fractions will then be assessed for complement activation (chapter 4/5).

5) Determine whether the loss of mature mycolic acids affects activation (C3b/iC3b, C5a and C5b-9) and interactions of the complement system (C1q, MBL, ficolin-1 and ficolin-2) with *M. smegmatis* mc^2 155 and *ΔMSMEG4722* (chapter 5).

6) Determine alterations in complement activation and activator binding between whole-cell planktonic and pellicle biofilm-derived *M. smegmatis* mc^2 155 and *ΔMSMEG4722* (chapter 5).

7) Evaluate purified *Mycobacterium* spp. cell envelope components (sourced from BEI Resources, NAID, NIH) ability to activate the complement system (chapter 5).

2 The role of IgM in complement activation by planktonic and pellicle biofilm *M. smegmatis* mc^2 155

2.1 Introduction

2.1.1 Mycobacterial biofilms

Biofilms are defined as “a structured community of bacterial cells enclosed in a self-produced polymeric matrix and adherent to an inert or living surface” and are established in chronic infections caused by bacteria including *P. aeruginosa* and *S. epidermidis* (Costerton *et al.*, 1999). Biofilms contrast to planktonic bacteria that exist as 'freely suspended’ cells (Donlan, 2002).

There is extensive evidence that Nontuberculous mycobacteria naturally form biofilms within water systems (Schulze-Röbbecke, Janning and Fischeder, 1992; Wallace *et al.*, 2013) and on medical devices causing disease (Falkinham, 2010; Kohler *et al.*, 2015; Sax *et al.*, 2015).

In contrast, the role of biofilms in TB disease is less well established. However, histological evidence from human lungs indicates pellicle biofilms could be a physiologically relevant phenotype during *M. tuberculosis* infection (Nyka, 1963, 1967, 1977; Nyka and O’Neill, 1970; Hunter *et al.*, 2006; Hunter, 2011; Chakraborty *et al.*, 2021). Cavitation is a hallmark of pulmonary TB and the proposed site for the role of biofilms in TB disease (Orme, 2014). Cavities occur after the inflammatory erosion from a granulomatous lung abscess into an airway. The cavity walls contain loose necrotic debris along the interior surface, which provides an immune sheltered zone with a high oxygen concentration that facilitates the proliferation of *M. tuberculosis* to a high

extracellular bacterial burden. Cavitation is associated with an increased risk of person-to-person transmission due to a higher bacterial load in the sputum and the proximity of cavities to airways (Urbanowski *et al.*, 2020).

Robert Koch potentially gave the first description of *M. tuberculosis* biofilms *in vivo* when identifying the 'Tubercule virus' in 1882 after staining infected human histological material. He observed that "they ordinarily form small groups of cells which are pressed together and arranged in bundles, and frequently are lying within tissue cells...many times the bacteria occur in large numbers outside of cells as well. Especially at the edge of large, cheesy masses, the bacilli occur almost exclusively in large numbers free of the tissue cells...even when they are present in large numbers, they are generally mixed with finely granular detritus in such a way that they are completely hidden" (Koch, 1882).

In multiple studies, Nyka *et al.,* showed that when stained with Ziehl-Neelsen followed by oxidation within the caseous material of cavities, large numbers of *M. tuberculosis* that began acid-fast negative were then observable. When present in large numbers, "they were spread out into sheets of agglomerated and single cells or assembled into firm, dense masses. Filamentous bacilli grew in cords, either single or entwined and forming loose, lacy structures". They proposed these structures as a way for *M. tuberculosis* to maintain latent infections and be a potential reservoir of bacterial release during relapse, as the lung material stained were from patients who had undergone intensive chemotherapy with a range of drugs that targeted metabolically active bacteria. The structures were comparable to *M. tuberculosis* slide cultures that formed a meshwork of weakly acid-fast filamentous forms (Nyka, 1963, 1967, 1977;

Nyka and O'Neill, 1970). In addition, Hunter *et al.*, (2006) observed extracellular *M. tuberculosis* growth at "the interface of air with the fluid that continuously seeps into the cavity", akin to the *in vitro* air-liquid interface pellicle biofilm model (Hunter *et al.*, 2006; Hunter, 2011).

Studies of mycobacterial biofilms are primarily performed *in vitro*, and *M. tuberculosis*, *M. bovis* BCG and *M. smegmatis* can form pellicle biofilms at the air-liquid interface (Ojha *et al.,* 2008, 2010). However, pellicle biofilm development is not standardised. For the surrogate organism *M. smegmatis* mc^2 155, variations throughout the literature for pellicle biofilm culture include temperature, culture vessel, culture media, media pH, carbon source and carbon concentration (Ojha *et al.*, 2005; Mathew *et al.*, 2006; Ojha and Hatfull, 2007; Naresh *et al.*, 2011; Pacheco *et al.*, 2013; Syal *et al.*, 2016, 2017).

2.1.2 The role of IgM in complement activation of the classical pathway

The complement system classical pathway activator is C1q, a protein of the C1-complex that activates upon interactions with a ligand. The primary ligands of C1q are IgG and IgM that exist as part of immune complexes (Kojouharova, Reid and Gadjeva, 2010). IgG and IgM need to undergo conformational changes induced by binding to an antigen to interact with C1q. It is estimated that one C1q activates after binding one antigen-bound IgM, compared to requiring two antigen-bound IgG that must be spatially close together (30-40nm) (Schroeder and Cavacini, 2010; Murphy, 2012). Aggregates of IgG have an increased ability to bind C1q than IgG monomers (Hughes-Jones, 1977). However, due to its polyreactive nature, high avidity and pentameric form, natural IgM is a more efficient activator of the complement system (Murphy,

2012). IgM is primarily pentameric, but hexameric IgM is present at low levels in human serum and can activate human complement 4-13 fold greater than the pentameric form (Collins, Tsui and Shulman, 2002). To study the effects of vaccine-induced IgG antibodies from sera on complement activation, the Pathogen Immunology Group (PIG) at PHE-Porton, has developed a 'large-scale' IgG-depleted complement source (Brookes *et al.*, 2013). This was also applied to study the innate activation of complement by *M. tuberculosis* (Keating *et al.*, 2021).

IgG and IgM present in non-immune sera has been observed to bind and induce complement activation against *M. tuberculosis* and *M. bovis* BCG (Hetland *et al.*, 1998; Ferguson *et al.*, 2004), but IgM alone has only been studied for *M. leprae* (Schlesinger and Horwitz, 1994). The 'enhancing' effect of natural IgM to trigger the classical pathway in a non-vaccine antibody-induced manner has been observed for Non-typeable *Haemophilus influenzae* (NTHi) and *Streptococcus agalactiae* (GBS) (personal communication, Steve Thomas, PIG, PHE-Porton), so a complement source further depleted of both IgG and IgM has been developed. Innate complement-cell wall interactions with mycobacteria could be obscured by the presence of IgM in the complement source.

2.1.3 Aims

To determine if IgM can activate the complement system against *M. smegmatis* mc^2 155 grown either planktonically or as pellicle biofilms, an IgG-depleted complement source was assessed for IgM binding to *M. smegmatis* mc^2 155. Following this, IgG-depleted complement and IgG- and IgM-depleted complement sources were compared for complement activation via C3b/iC3b and C5b-9 deposition onto pellicle

biofilm-derived or planktonic *M. smegmatis* mc^2 155. The assessment was facilitated after optimising the flow cytometry method by distinguishing bacteria from background events using a nucleic acid stain and standardising bacterial concentrations using a known concentration of fluorescent beads.

2.1.4 Hypotheses

1) IgM will facilitate complement activation and deposition of C3b/iC3b and C5b-9 onto *M. smegmatis* mc^2 155.

2) *M. smegmatis* mc^2 155 pellicle biofilm-derived bacilli will have reduced activation of the human complement system compared to a planktonic *M. smegmatis* mc^2 155.

2.2 Results

2.2.1 A reduction in glycerol concentration increases *M. smegmatis* mc^2 155 pellicle reticulation

M. smegmatis mc^2 155 pellicle biofilm culture is described in methods section 7.1. In summary, *M. smegmatis* mc^2 155 was cultured in 24 well-plates, statically at 37^{o}C in Sauton's medium (a defined minimal media) with a reduction in the glycerol concentration from 6% to 4% (Sauton's 40 medium), for six days in an airtight container, which was lined with a damp tissue to maintain humidity.

Multiple variables were assessed to determine the optimal culture conditions for *M. smegmatis* mc^2 155 pellicle biofilm formation, including; plate type, pH, and glycerol concentration. There was ambiguity to the glycerol concentration in the Sauton's media recipe (Media Department at PHE-Porton), so both 4% and 6% glycerol were tested for *M. smegmatis* mc^2 155 pellicle biofilm formation. A reduction in final glycerol concentration from 6% to 4% results in increased visible pellicle biofilm reticulation (Figure 2.1).



1: Standard Sauton's medium (media department)

2: Standard Sauton's medium (in-lab)

3: Sauton's 40 medium (media department)

4: Sauton's 40 medium (in-lab)

Figure 2.1: *M. smegmatis* mc^2 155 pellicle biofilm growth in 24-well plates.

Representative *M. smegmatis* mc^2 155 pellicle biofilms. Sauton's media containing 6% glycerol (rows 1 and 2) or 4% glycerol (rows 3 and 4), produced from the PHE-Porton Media Department (rows 1 and 3) or in-lab (rows 2 and 4).

2.2.2 SYTO 40 can separate *M. smegmatis* mc^2 155 bacterial events from flow cytometry background 'noise'

Flow cytometry is a semi-quantitative technique that can be utilised to determine complement activation via complement component deposition onto planktonic and pellicle biofilm *M. smegmatis* once efficiently dispersed using glass beads (Ortalo-Magne *et al.*, 1995; Sani *et al.*, 2010). A limitation in quantifying complement activation by flow cytometry is the inability to distinguish bacteria from background 'noise' due to their similar size and granularity. Background 'noise' will typically include salt crystals, sheath particulate, electronic noise and air bubbles that generate a signal picked up by the flow cytometer detectors. PB450 fluorescing nucleic acid dyes allow us to distinguish bacteria from 'noise', which is the first step in standardising bacterial concentrations across flow cytometry. Briefly, three biological replicates of 4% (v/v) formaldehyde-treated *M. smegmatis* mc^2 155 cultured in Middlebrook 7H9 were standardised to an optical density ($OD540_{nm}$) of 0.05, pelleted, and re-suspended in either phosphate-buffered saline (PBS) (containing no dye) or PBS-DAPI, SYTOX BLUE, or SYTO 40 at three different concentrations. Three technical repeats of three biological replicates for the three dyes were averaged (methods section 7.6).

When a nucleic acid dye was present, unstained background 'noise' events accounted for 13.76% ± 0.87% SD of all events. Bacteria accounted for 86.24% ± 0.82% of all events (Figure 2.2A). SYTO 40 showed the strongest binding to bacterial cell DNA (mean PB450 fluorescence intensity). This was reflected with an 'excellent' Z-factor across all three concentrations tested compared to an unstained control (5µM 0.754, 10µM 0.681 and 20µM 0.795). DAPI showed lower binding and gave a 'marginal' Z-factor until the highest dye concentration was tested (5µM 0.374, 10µM 0.440 and

20µM 0.753). SYTOX BLUE gave a ‘marginal’ Z-factor at all three concentrations tested and showed variability between biological replicates (5µM 0.240, 10µM 0.193 and 20µM 0.248) (Figure 2.2B and Table 2.1). On dot plot overlays, background ‘noise’ events are indistinguishable from the unstained bacterial control, but the presence of 20µM SYTO 40 and SYTOX BLUE allows the gating of bacterial events. For DAPI, even at 20µM, the stained population sits partially on top of the unstained control, which is mixed with background ‘noise’ (Figure 2.2C).

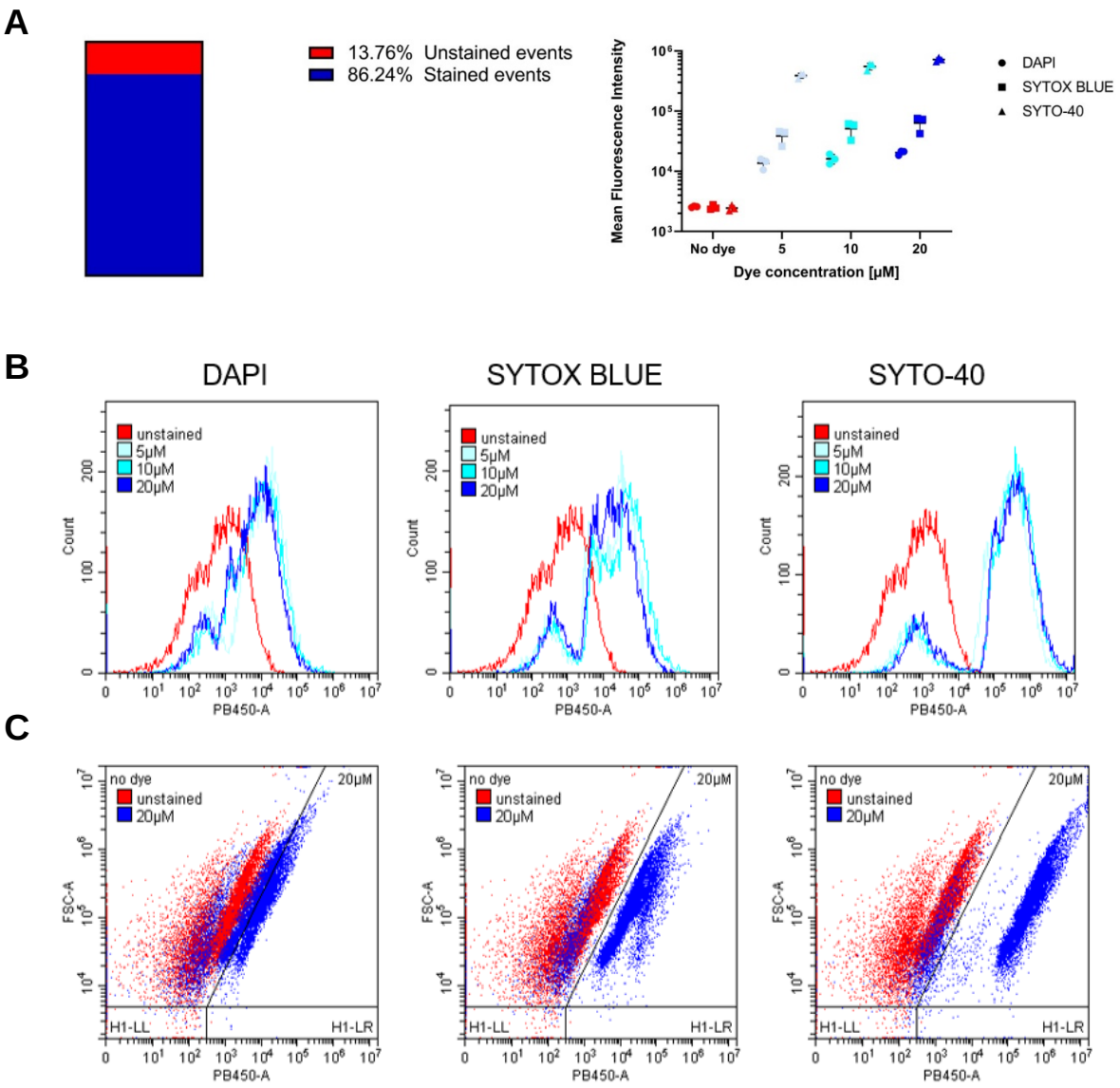


Figure 2.2: Evaluating nucleic acid dye staining of *M. smegmatis* mc² 155 for flow cytometry assays.

(A) (Left) % stained (blue) vs % unstained (red) events. (Right) mean fluorescence intensity of stained *M. smegmatis* mc² 155 cultured in Middlebrook 7H9 and treated with 4% (v/v) formaldehyde. Bacteria were stained with increasing concentrations of DAPI (circles), SYTOX BLUE (squares) or SYTO 40 (triangles). Unstained (red), 5µM (light blue), 10µM (turquoise) and 20µM (blue). Error bars = standard deviation of three biological replicates. (B) Representative overlay histograms of bacteria; unstained (red) 5µM (light blue),10µM (turquoise), or 20µM (blue) DAPI, SYTOX BLUE and SYTO 40 staining. (C) Representative overlay dot plots of bacteria; unstained bacteria (red) were used to set the PB450 negative gate vs 20µM staining (blue) for DAPI, SYTOX BLUE and SYTO 40.

Table 2.1: Z-factor analysis of the mean fluorescence intensity of unstained vs stained bacteria.

Z-factor analysis of the mean fluorescence intensity of unstained vs stained bacteria with 5µM, 10µM and 20µM DAPI, SYTOX BLUE and SYTO 40. Bacterial populations mean fluorescence intensity calculated from three technical replicates of three biological replicates for each dye. Z-factor: excellent (green), marginal (yellow).

Z-Factor			
Dye concentration	**DAPI**	**SYTOX BLUE**	**SYTO 40**
5µM	0.374	0.240	0.754
10µM	0.441	0.193	0.682
20µM	0.753	0.248	0.795

2.2.3 Planktonic and pellicle biofilm *M. smegmatis* mc^2 155 bacterial concentration can be standardised using Flow-Count Fluorospheres™

After defining bacterial events, to optimise flow cytometry assays, a standardised starting bacterial concentration was needed. Three biological replicates of single-cell planktonic and pellicle biofilm *M. smegmatis* mc^2 155 (methods section 7.4) at an $OD540_{nm}$ of either 0.05, 0.5 or 1.0 were counted with bacterial Flow-Count Fluorospheres™, which have a known concentration of fluorescent beads μl^{-1}. This allowed the determination of the robustness of $OD540_{nm}$ to standardise bacterial concentration (methods section 7.8). There was no statistical difference between phenotypes at any $OD540_{nm}$ dilution. However, pellicle biofilms possessed higher variability between biological replicates, which were most prominent at an $OD540_{nm}$ of 1 (planktonic $6.7x10^7 \pm 1.3x10^6$ bacteria mL^{-1} compared to pellicle biofilm $5.1x10^7 \pm 1.8x10^7$ bacteria mL^{-1}) (Figure 2.3).

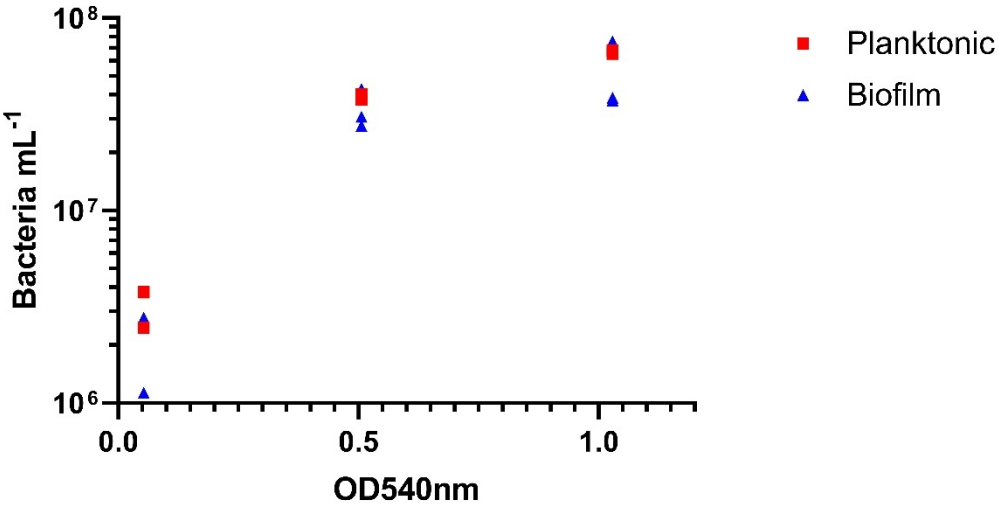


Figure 2.3: Standardising the starting bacterial concentrations in flow cytometry assays.

$OD540_{nm}$ and bacteria mL^{-1} were compared using single-cell planktonic (red squares) and pellicle biofilm (blue triangles) *M. smegmatis* mc^2 155. $OD540_{nm}$ values tested were 0.05, 0.5 and 1 counted with Flow-Count™ Fluorospheres with a known concentration of fluorescent beads μl^{-1} to give bacteria mL^{-1}. For statistical analysis, the data were log10 transformed, and a two-way ANOVA was performed with Šidák correction for multiple comparisons. No statistical differences were observed between phenotypes at any concentration. Three biological replicates are plotted at each dilution for both phenotypes.

2.2.4 Summary of Flow Cytometry optimisation

Based on its 'excellent' Z-factor of 0.682 and visible distinction of bacteria from background events using PB450 fluorescence gating, 10µM SYTO 40 was chosen as the stain and concentration used throughout the rest of this thesis. To allow phenotypic comparisons, Flow-Count Fluorospheres™ were used to standardise cultured bacterial stocks during flow cytometry assays. However, this was not optimised until after the initial evaluations of IgM-binding to *M. smegmatis* mc^2 155 reported in section 2.2.5.

2.2.5 IgM from the IgG-depleted complement source can bind both *M. smegmatis* mc^2 155 and *M. tuberculosis* H37Rv

The initial aim was to determine whether IgM present in IgG-depleted exogeneous human complement could bind to bacteria including NTHi, GBS, Middlebrook 7H9 cultured *M. smegmatis* mc^2 155 and CAMR Mycobacterium Medium MOD2 (CMM MOD2) chemostat cultured *M. tuberculosis* H37Rv (James, Williams and Marsh, 2000). Three biological replicates of 4% (v/v) formaldehyde-treated bacteria at an $OD540_{nm}$ of 0.1 were incubated with 10% or 2% IgG-depleted complement. The bacteria were then labelled with a fluorescent antibody to measure IgM-binding (methods section 7.9).

IgM-binding was observed on NTHi, GBS, *M. smegmatis* mc^2 155 and *M. tuberculosis* H37Rv at both complement concentrations. Incubating with 10% complement, IgM-binding was significantly higher on NTHi than *M. smegmatis* mc^2 155 and *M. tuberculosis* H37Rv ($P = 0.0089$ and $P = 0.0032$, respectively). There was no difference between *M. smegmatis* and *M. tuberculosis* (Figure 2.4)

At 2% complement, NTHi had significantly higher IgM binding than the other three bacterial strains tested ($P = 0.0499$ for GBS, $P = 0.0019$ for *M. smegmatis* mc^2 155 and $P < 0.0001$ for *M. tuberculosis* H37Rv). IgM-binding was significantly higher on GBS than *M. tuberculosis* H37Rv only ($P = 0.0001$). When comparing *M. smegmatis* mc^2 155 and *M. tuberculosis* H37Rv, at 2% complement, there was significantly more IgM-binding to *M. smegmatis* mc^2 155 ($P = 0.0032$).

Comparable IgM binding was observed on *M. smegmatis* mc^2 155 between 10% and 2% complement. There was significantly less IgM binding to *M. tuberculosis* H37Rv at 2% than 10% complement (P= 0.0002) (Figure 2.4).

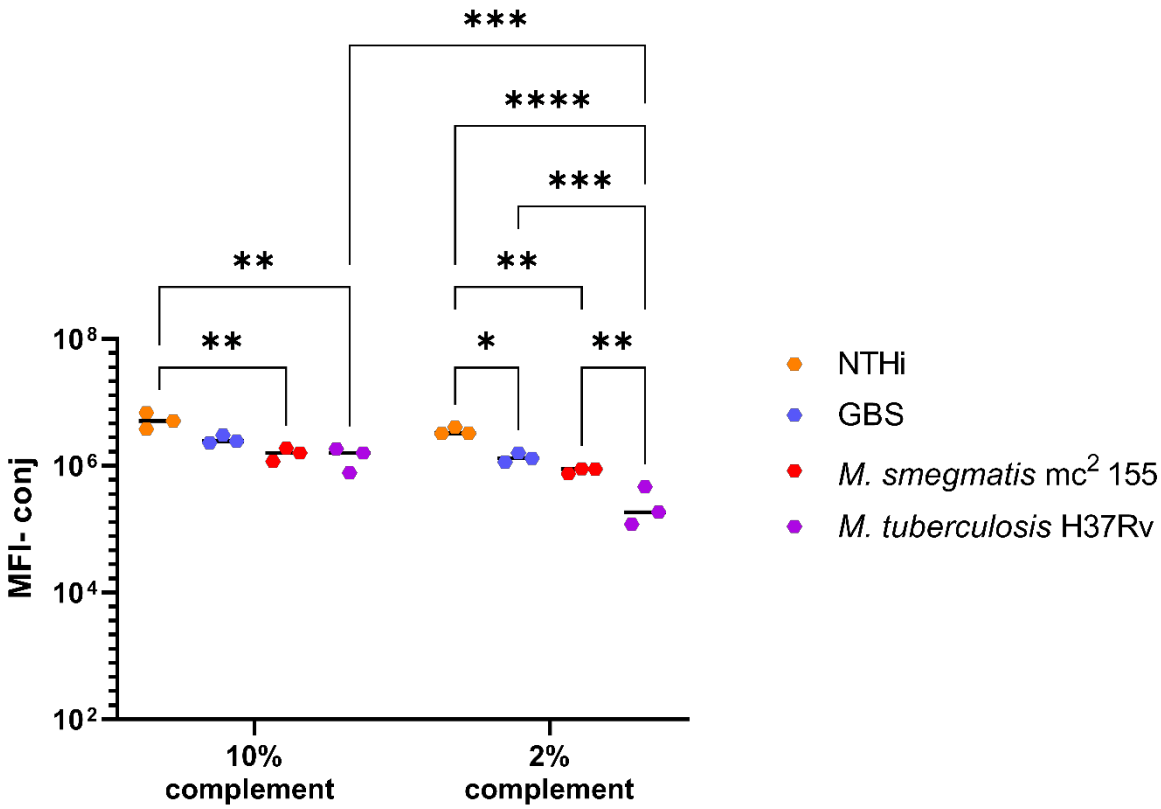


Figure 2.4: IgM binding onto NTHi, GBS, *M. smegmatis* mc^2 155 and *M. tuberculosis* H37Rv from an IgG-depleted complement source.

Median fluorescence intensity – conjugate only fluorescence (MFI-conj) corresponds to IgM-binding. *M. smegmatis* mc^2 155 cultured in Middlebrook 7H9 (red), *M. tuberculosis* H37Rv sourced from a CMM MOD2 chemostat culture (purple), NTHi (orange) and GBS (lilac) were assessed for IgM-binding. All bacteria were 4% (v/v) formaldehyde-treated before incubation with 10% or 2% IgG-depleted complement. Error bars = standard deviation of three biological replicates. For statistical analysis, data were log10 transformed followed by performing a two-way ANOVA with Tukey's multiple comparison correction. 10%; ** P = 0.0089 (NTHi vs *M. smegmatis* mc^2 155), ** P = 0.0032 (NTHi vs *M. tuberculosis* H37Rv). 2%; * P = 0.0499, ** P = 0.0019 (NTHi vs *M. smegmatis* mc^2 155), ** P = 0.0032 (*M. smegmatis* mc^2 155 vs *M. tuberculosis* H37Rv), *** P = 0.0001, **** P < 0.0001. 10% vs 2%; *** P = 0.0002.

As IgM binding levels appeared similar at 10% complement and 2% complement for *M. smegmatis* mc^2 155, a serial dilution was performed to determine at what concentration of complement IgM binding reached baseline levels (conjugate only fluorescence). Two biological replicates of 4% (v/v) formaldehyde-treated NTHi, CMM MOD2 chemostat-cultured *M. tuberculosis* H37Rv and CMM MOD2-cultured *M. smegmatis* mc^2 155 at an $OD540_{nm}$ of 0.1, were incubated with a 1:2 serial dilution of IgG-depleted complement from 10% to 0.3125%. CMM MOD2 was used to culture *M. smegmatis* mc^2 155 to allow a fairer comparison of IgM binding between *M. smegmatis* mc^2 155 and *M. tuberculosis* H37Rv. Bacteria were then labelled with the appropriate fluorescent antibodies to measure IgM binding (methods section 7.9).

A decrease in IgM binding was observed between 10% complement and 0.3125% complement for all three bacteria, but fluorescence was still higher than the conjugate only baseline (~10^5 compared to ~10^2). NTHi showed statistically lower IgM binding at 2.5% complement compared to 10% complement ($P = 0.0227$). For *M. tuberculosis* H37Rv, a statistical drop in IgM binding was observed by 5% complement compared to 10% complement ($P = 0.0127$). No statistical drop was observed for *M. smegmatis* mc^2 155 until 1.25% complement was used ($P = 0.0099$). There was significantly more IgM binding onto *M. tuberculosis* H37Rv than *M. smegmatis* mc^2 155 at 10% complement ($P = 0.0002$). There was also statistically more IgM binding to *M. tuberculosis* H37Rv than NTHi at 10% complement only ($P = 0.0021$) (Figure 2.5).

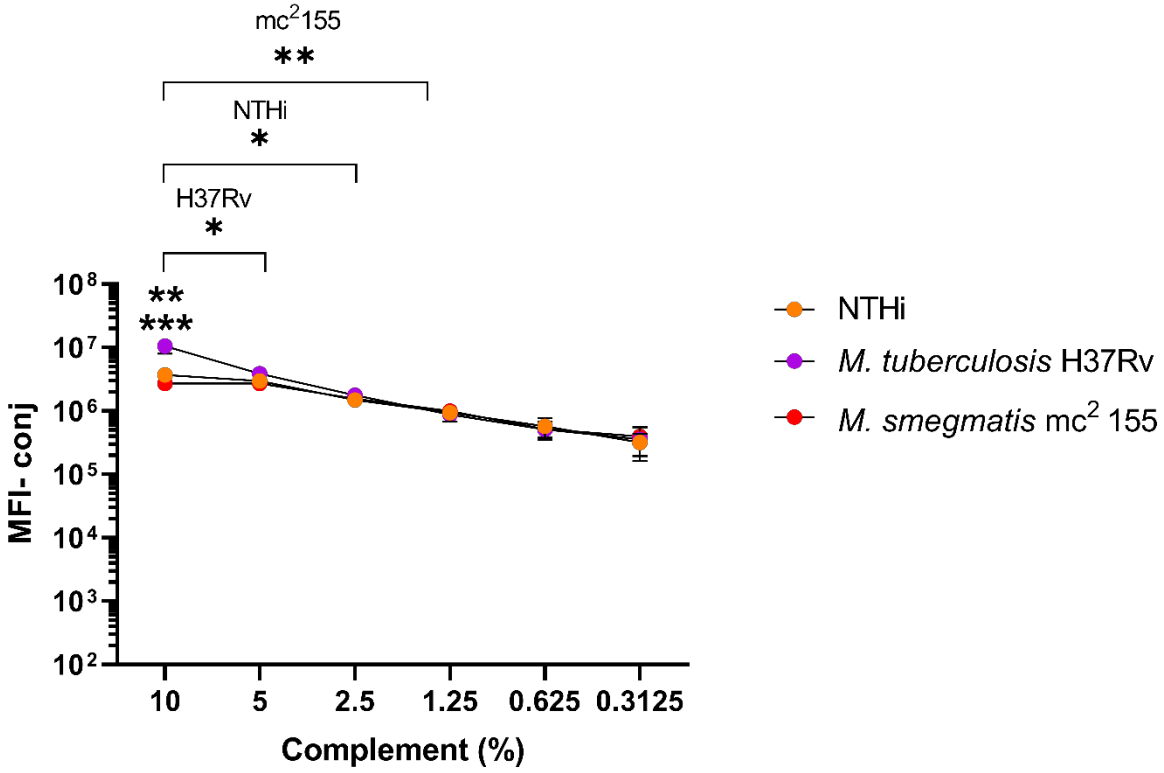


Figure 2.5: IgM binding over a serial dilution of IgG-depleted complement onto *M. tuberculosis* H37Rv, *M. smegmatis* mc² 155 and NTHi.

Median fluorescence intensity – conjugate only fluorescence (MFI-conj) corresponds to IgM binding. *M. smegmatis* mc² 155 cultured in Middlebrook 7H9 (red), *M. tuberculosis* H37Rv sourced from a CMM MOD2 chemostat culture (purple) and NTHi (orange) were assessed for IgM binding. Bacteria were treated with 4% (v/v) formaldehyde prior to incubation with a 1:2 serial dilution of IgG-depleted complement from 10% to 0.3125%. Data was log10 transformed then statistical analysis performed using a two-way ANOVA with Tukey's multiple comparison correction. ** P = 0.0021 (*M. tuberculosis* H37Rv vs NTHi at 10%), *** P = 0.0002 (*M. tuberculosis* H37Rv vs *M. smegmatis* mc² 155 at 10%), * = P 0.0127 (*M. tuberculosis* H37Rv 10% vs 5%), * P =0.0227 (NTHi 10% vs 2.5%), ** P = 0.0099 (*M. smegmatis* mc² 155 10% vs 1.25%). Error bars = standard deviation of two biological replicates.

2.2.6 IgM significantly enhances complement activation by both planktonic and pellicle biofilm *M. smegmatis* mc² 155

The effect of planktonic or pellicle biofilm growth of *M. smegmatis* mc² 155 on complement activation by IgM was investigated using flow cytometry. Three biological replicates of 4% (v/v) formaldehyde-treated planktonic or pellicle biofilm-derived *M.*

smegmatis mc^2 155 were normalised to 1x10^7 bacteria mL^{-1}. Bacteria and the positive control zymosan were incubated with either 10% or 2% IgG depleted or IgG- and IgM-depleted exogenous human complement. Bacteria were labelled with the appropriate fluorescent antibodies to measure IgM binding (IgG-depleted complement only) or complement activation via deposition of C3b/iC3b and C5b-9 by flow cytometry (methods section 7.10)

When examining complement activation, 10% is used to determine activation when all three complement pathways are active. At 2% complement, only the classical and lectin pathways are active. Alternative pathway inhibition at 2% complement is due to the lack of available Factor D (Nilsson and Nilsson, 1984). Overall, as there is a 1:5 dilution of all complement components, there is less overall complement activation at 2% than 10% complement.

No deposition of either C3b/iC3b or C5b-9 was observed on either phenotype when the alternative pathway was inhibited. When all three pathways were active, there was significantly more deposition of C3b/iC3b onto both phenotypes of *M. smegmatis* mc^2 155 when incubated with IgG-depleted complement compared to IgG- and IgM-depleted complement (both $P < 0.0001$). There was no statistical difference in C3b/iC3b deposition between phenotypes using either complement source (Figure 2.6A).

For C5b-9 deposition, again, there was significantly more deposition onto both phenotypes of *M. smegmatis* mc^2 155 when incubated with IgG-depleted complement compared to IgG- and IgM-depleted complement ($P = 0.0399$ for planktonic and $P =$

0.0025 for pellicle biofilm) and no statistical difference in C5b-9 deposition between phenotypes using either complement source (Figure 2.6B).

Despite not observing complement activation via complement component deposition when the alternative pathway was inhibited, IgM binding onto planktonic and pellicle biofilm *M. smegmatis* mc^2 155 from the IgG-depleted complement source was seen when all three pathways were active and when the alternative pathway was inhibited. At both complement concentrations, the IgM binding was comparable between phenotypes. There was significantly less binding of IgM when only the classical and lectin pathways were active compared to all three pathways active for both phenotypes (P = 0.0004 for both) (Figure 2.6C).

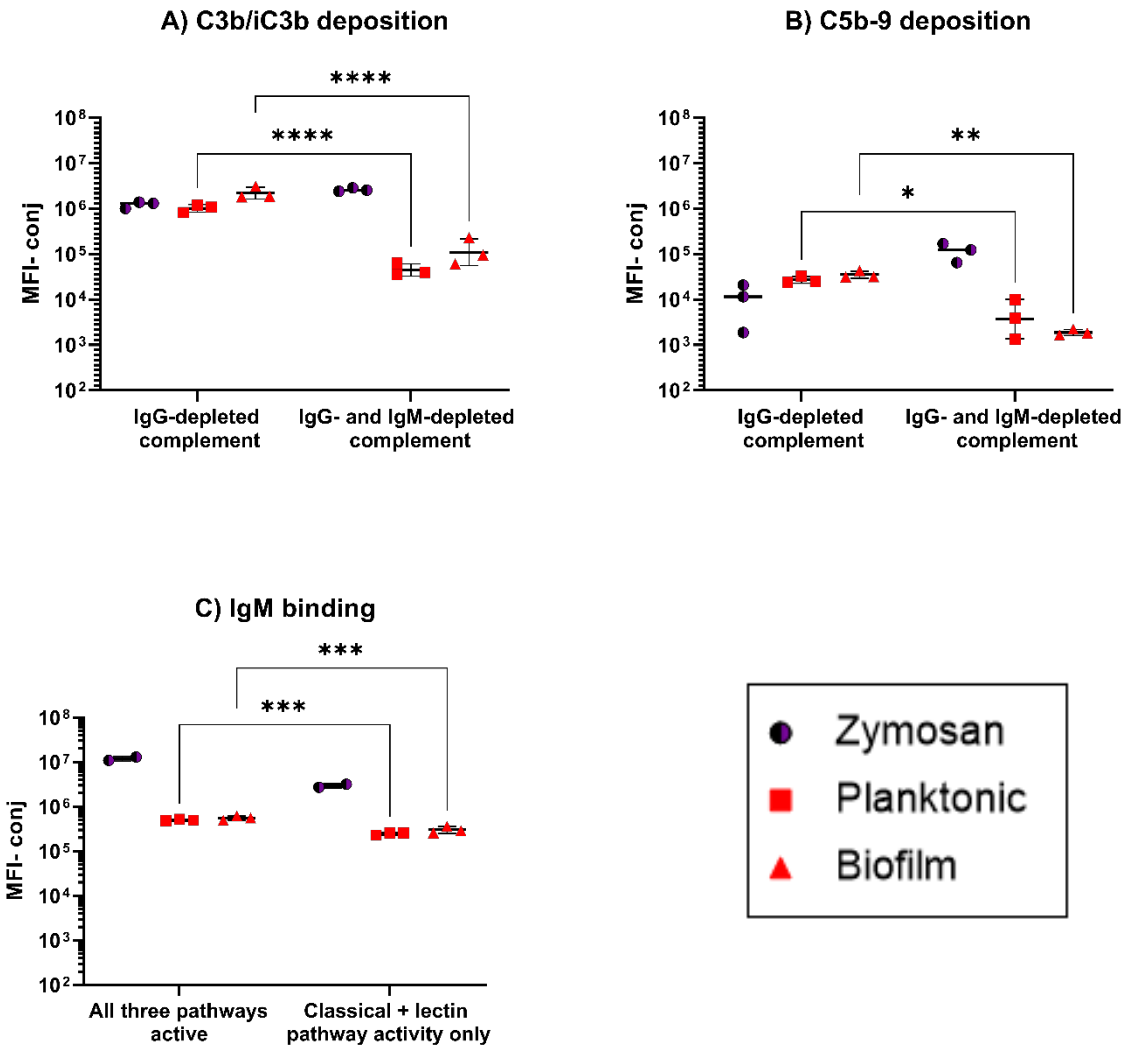


Figure 2.6: C3b/iC3b deposition, C5b-9 deposition and IgM binding on planktonic and pellicle biofilm *M. smegmatis* mc^2 155 using IgG-depleted and IgG- and IgM-depleted complement sources.

Median fluorescence intensity – conjugate only fluorescence (MFI-conj) corresponding to (A) C3b/iC3b deposition or (B) C5b-9 deposition on planktonic (squares) and pellicle biofilm (triangles) *M. smegmatis* mc^2 155 at 10% IgG-depleted or IgG- and IgM-depleted complement. (C) MFI-conj corresponds to IgM binding on planktonic and pellicle biofilm *M. smegmatis* mc^2 155 from an IgG-depleted complement source at 10% complement and 2% complement. For statistical analysis data was log10 transformed before performing a two-way ANOVA with Tukey's multiple comparison correction. (A) **** $P < 0.0001$ (B) ** $P = 0.0025$, * $P = 0.0399$ (C) *** $P = 0.0004$. Error bars = standard deviation of three biological replicates. Zymosan (black/purple circles) was used as a positive control.

2.2.7 Summary of IgM binding and complement activation for planktonic and pellicle biofilm *M. smegmatis* mc^2 155

IgM present in the IgG-depleted complement source could bind *M. smegmatis* mc^2 155 and *M. tuberculosis* H37Rv. IgM enhanced the activation of complement on both phenotypes of *M. smegmatis* mc^2 155. There were no differences in IgM binding, C3b/iC3b or C5b-9 deposition between planktonic and pellicle biofilm-derived *M. smegmatis* mc^2 155 using either complement source (IgG-depleted complement for IgM binding only). Complement deposition was only observed when all three complement system pathways were active for both complement sources. IgM will have to be removed from the complement source to study innate interactions of complement with the *M. smegmatis* cell envelope.

2.3 Discussion

2.3.1 IgM can facilitate complement activation against both planktonic and pellicle biofilm *M. smegmatis* mc^2 155

On *M. smegmatis* mc^2 155, comparable complement activation was observed via C3b/iC3b and C5b-9 deposition between planktonic and pellicle biofilm-derived bacteria in the IgG-depleted and IgG- and IgM-depleted complement sources. When IgM was removed, complement activation was significantly reduced when all three pathways were active. The IgG and IgM antibody-driven classical pathway play a role in complement deposition on mycobacteria (Hetland *et al.*, 1998; Ferguson *et al.*, 2004). The research around the effect of IgM alone on complement activation is limited, and there is currently no literary evidence of mycobacterial biofilms and IgG or IgM antibody interactions. Schlesinger and Horwitz (1994) separated C3 fixation activated by IgG and IgM on *M. leprae.* C3 fixation only required a small amount of antibody from non-immune serum, estimating around 100 to 1000 IgG molecules or 100 IgM molecules. The fewer IgM needed to activate complement deposition on mycobacteria could be due to its pentameric or hexameric form. Only one IgM antibody needs to associate with C1q to activate the classical cascade, compared to multiple IgG molecules (Schroeder and Cavacini, 2010; Murphy, 2012). As flow is only semi-quantitative, it cannot quantify the number of IgM binding to planktonic and pellicle biofilm-derived *M. smegmatis* mc^2 155.

Despite the removal of IgM, complement activation was still observed when all three pathways were active. Classical pathway C1q antibody-independent binding to *M. bovis* BCG has been reported previously (Carroll *et al.*, 2009) as well as lectin pathway activation (Bartlomiejczyk *et al.*, 2014; Świerzko *et al.*, 2016), indicating innate

complement-cell wall interactions were being obscured by the presence of IgM in the complement source.

When the alternative pathway was inhibited, no activation of the complement system was observed despite high levels of IgM binding. Classical and lectin pathway activity could be at too low a concentration to be observed under the current flow cytometry parameters. This highlights the likely importance of the alternative pathway positive feedback amplification loop in response to mycobacteria that utilises classical and lectin pathway generated C3b (Merle *et al.*, 2015).

2.3.2 IgM is a potent activator of complement against *M. smegmatis* mc^2 155 and *M. tuberculosis* H37Rv

IgG-depleted exogeneous human complement characterisation showed approximately 3-fold less IgM than IgG in the native plasma pool (Brookes *et al.*, 2013). IgM from the IgG-depleted complement source has been observed to bind the commensal bacteria NTHi and GBS (personal communication, Steve Thomas, PIG, PHE-Porton). This work has shown that for non-commensal *M. tuberculosis* H37Rv and *M. smegmatis* mc^2 155, IgM from pooled exogeneous complement can also bind.

Although the highest titres of anti-mycobacterial antibodies are consistently seen in individuals who either have active or latent TB, these studies also acknowledged that anti-mycobacterial antibodies were present in their healthy control cohorts. A proportion of these were IgM. Carroll *et al.*, (2009) saw individuals with no BCG vaccination with IgG and IgM antibodies that could bind *M. bovis* BCG. In another study by Perley *et al.*, (2014), BCG-unvaccinated individuals were found to have plasma that reacted to the surface of live *M. tuberculosis* H37Rv and whole cell lysate (cell wall

proteins, lipids and carbohydrates) and purified LAM. The anti-IgG titres for every condition tested were around 10^2. Evaluating the ratio of IgG: IgM in these individuals gave roughly equal amounts of each isotype against each fraction. A limitation is that no uninfected individuals were BCG vaccinated, so its potential effects on IgG and IgM titres were not evaluated. The presence of cross-species reactive mycobacterial antibodies, focused on IgG, in healthy individuals has been attributed to the exposure and sensitisation by environmental mycobacteria (Andersen *et al.*, 1986; Andersen and Doherty, 2005; Perley *et al.*, 2014). Andersen *et al.*, (1986) took five purified monoclonal IgG antibodies (HYT 6, HYT 27, HYT 28, HAT 1 and HAT 3) generated against *M. tuberculosis* H37Rv. They looked for cross-reactivity with a range of environmental mycobacteria, including *Mycobacterium Intracellulare, M. avium* and *M. marinum*. They found only HYT 28 was specific for *M. bovis* BCG and *M. tuberculosis* H37Rv, with the other four mAbs binding to most, if not all, the environmental mycobacteria tested. Perley *et al.*, (2014) observed that uninfected, non-BCG vaccinated individuals had modest antibody titres against *M. tuberculosis* lysates and *M. intracellulare, M. avium and M. fortuitum*. Cross-reactivity could also arise from exposure to NTM biofilms as they have been frequently sampled from environmental water sources (Schulze-Röbbecke, Janning and Fischeder, 1992; Wallace *et al.*, 2013).

The previous findings of anti-mycobacterial IgM in plasma from healthy individuals support this study's observation that anti-mycobacterial IgM is present in the IgG-depleted complement source. IgM-binding did not deplete out to conjugate only baseline fluorescence levels even at a very low concentration of complement (0.3125%), so it could be a potent activator of the complement system at the 10% and

2% complement conditions used throughout this thesis. It was unknown whether the donors were previously given the BCG vaccine because immunisation of 10-14 year-olds was stopped in the UK in 2005 (Zwerling and Pai, 2011). There is evidence that intradermal BCG vaccination can induce IgG and IgM antibodies (Tanner *et al.*, 2019). Therefore, those who received the vaccine would likely produce antibodies that could cross-react with *M. tuberculosis* H37Rv and *M. smegmatis* mc^2 155. Differences in the phenotypic binding of IgM may have been expected (despite the overall low affinity of IgM molecules) as *M. bovis* BCG production for vaccines is grown as a pellicle biofilm (Venkataswamy *et al.*, 2012; Sefidi *et al.*, 2017), which are physiologically similar to *M. tuberculosis* pellicle biofilms (Ojha *et al.*, 2008). A hallmark of both *M. smegmatis* and *M. tuberculosis* pellicle biofilm formation is the accumulation of free mycolic acids (Ojha *et al.*, 2005, 2008). In the serial dilution of complement, *M. tuberculosis* H37Rv appeared to have more IgM binding, which was not observed in the original experiment with 10% complement or 2% complement. This could be due to when the bacteria from the chemostat was harvested. Late-stage chemostat cultures form cell wall growth on the culture vessel (personal communication, Jordan Pascoe, TB Drug Discovery Group, PHE-Porton), which may alter interactions with natural IgM.

2.4 Technical discussion

2.4.1 Culture condition variations for pellicle biofilms

Biofilms are potentially a physiologically relevant phenotype of *M. tuberculosis* disease (Nyka, 1963, 1967, 1977; Nyka and O'Neill, 1970; Hunter *et al.*, 2006; Hunter, 2011; Orme, 2014; Chakraborty *et al.*, 2021).

For mycobacterial pellicle biofilm culture, the literature is split between the use of M63; a minimal media used to propagate *E. coli* at a slower growth rate (Recht and Kolter, 2001; Ojha *et al.*, 2005; Gopalaswamy *et al.*, 2007; Ojha and Hatfull, 2007) and variations of Sauton's media (Mathew *et al.*, 2006; Ojha *et al.*, 2008; Naresh *et al.*, 2011; Kulka, Hatfull and Ojha, 2012; Pacheco *et al.*, 2013; Syal *et al.*, 2017). Variations in Sauton's media for the culture of mycobacteria since its original formulation in 1912 is summarised by Guallar-Garrido *et al.*, (2020). The main variant is glycerol concentration, which has ranged from 0.2% to 6%, although most formulations are between 3-6%. There was ambiguity to the glycerol concentration in the Sauton's media recipe made by the Media Department at PHE-Porton, so both 4% and 6% glycerol were tested for *M. smegmatis* mc^2 155 pellicle biofilm formation. The addition of 4% glycerol appeared to increase the reticulation of the pellicles compared to 6%. This contrasts with Guallar-Garrido *et al.*, (2020) for *M. bovis* BCG and *Mycobacterium brumae*. They observed more pronounced reticulation and pellicle thickness cultured in Sauton's with 6% glycerol compared to 3% glycerol. For *M. brumae,* the effect of glycerol concentration on pellicle thickness was only observed under an L-asparagine amino acid source, not L-glutamate. The amino acid source in the PHE Sauton's media recipe is L-asparagine (methods section 7.1, Table 7.1). They suggest that optimal

pellicle culture conditions are mycobacterial strain specific. The same amino acid source produced significantly different biomass in *M. bovis* BCG compared to *M. brumae,* with an L-asparagine amino acid source favouring *M. bovis* BCG biomass development compared to L-glutamate favouring *M. brumae* biomass development.

The change to the architecture of the pellicle biofilm could be linked to carbon availability. For *P. aeruginosa,* using flow cell chambers and citrate as the carbon source, under carbon-replete conditions biomass and biofilm thickness increased as biofilms developed, but roughness and surface-to-area volume remained steady. When switched to carbon-limited conditions, the biomass plateaued, but biofilm roughness and surface-to-area volume increased over time, indicating an increase in biofilm surface area (Bester *et al.*, 2011). An increase in *M. smegmatis* mc^2 155 pellicle reticulation would likely increase the biofilm surface area, although this was not measured. To determine if the biofilm cultures go into a carbon-limited environment, this would have to be measured over time.

2.4.2 Optimisation of flow cytometry

To allow comparable measurements between planktonic and pellicle biofilm-derived *M. smegmatis* in flow cytometry analysis, the ability to standardise bacterial concentration is necessary. Two factors were optimised; identification of the bacteria by nucleic acid staining and standardising the starting bacterial concentration using Flow-Count Fluorospheres™.

Staining was necessary as due to flow cytometer sensitivity; unstained bacteria appear at the same size and granularity as non-specific background ‘noise’ events. Staining

allows us to distinguish the bacteria from the background ‘noise’. The impermeable nature of the mycobacterial cell wall makes it difficult to stain. Stains used during clinical diagnosis are Ziehl-Neelsen and Auramine-rhodamine fluorochrome but are unsuitable for flow cytometry due to their multi-step process (Remel, 2004, 2013). Of the three dyes tested, SYTO 40 allowed the best distinction from the background ‘noise’. An advantage of using an SYTO dye is that it will not interfere with or be inhibited by potential complement deposition onto the mycobacterial surface, unlike an Auramine-rhodamine fluorochrome that complexes with mycolic acids (Remel, 2004).

Optical density measurements indirectly determine bacterial concentrations based on the scattering of light. An unknown variable with dispersed planktonic and pellicle biofilm cells is whether having a comparable optical density corresponds to having a comparable bacterial concentration, which could be affected by factors including the presence and composition of free ECM with biofilm-cultured bacteria (Ojha *et al.*, 2008; Trivedi *et al.*, 2016), overall shorter bacterial cell length in stationary phase and biofilm-derived bacteria, different bacterial shape distributions between phenotypes (Thanky, Young and Robertson, 2007; Sochorová *et al.*, 2014) and differences to the cell wall composition between phenotypes (Ojha *et al.*, 2005). Although no statistical differences were seen between planktonic and pellicle biofilm bacteria mL^{-1} measured from a known optical density, more variability within the pellicle biofilm replicates highlights the importance of standardisation. This method was continued throughout this thesis for flow cytometry analysis.

2.4.3 Potential implications of using 4% (v/v) formaldehyde-treated bacteria

This initial flow cytometry complement work used bacteria treated with 4% (v/v) formaldehyde pre-incubation with the complement source. Formaldehyde preserves cellular morphology by inducing cross-linking of protein functional groups. For histological material, formaldehyde treatment alters the physicochemical state of the tissue, including surface charges and membrane potentials, altering the reactivity of cellular components (Thavarajah *et al.*, 2012). Previously, for *M. tuberculosis* H37Rv, it was demonstrated that paraformaldehyde-inactivation of bacteria resulted in weaker MBL binding than heat-inactivation, hypothesised to be influenced by exposure of different glycosylation patterns (Bartlomiejczyk *et al.*, 2014). For the most biologically relevant assessment of complement interactions with *M. smegmatis* going forward, the bacteria will be incubated live with the complement source then treated with 4% (v/v) formaldehyde to allow flow cytometer assessment.

3 Pellicle biofilm formation by the *M. smegmatis* mutant *ΔMSMEG4722*

3.1 Introduction

3.1.1 The mycolic acid biosynthesis reductase

Mycolic acids are an important component of mycobacterial pellicle biofilms. Their accumulation as free mycolate is a hallmark of *M. smegmatis* and *M. tuberculosis* pellicle biofilm development (Ojha *et al.*, 2008, 2010). Mature mycolates are esterified to arabinogalactan to form the mAGP complex. They also exist as free lipids within the cell envelope and are components of cell wall glycolipids, including TDM, TMM and GMM (Marrakchi, Lanéelle and Daffé, 2014).

The final step in the production of mycolic acids is proposed to be the reduction of the β-oxo group on the mycolic motif to a hydroxyl group. The reductase catalysing this reaction was identified by Lea-Smith *et al.*, (2007) in *M. tuberculosis* as encoded by gene *Rv2509*. Using Basic Local Alignment Search Tool (BLAST) on a transposon mutagenesis library of *M. tuberculosis* H37Rv and *M. bovis* BCG Pasteur, genes of unknown function identified as either essential or inducing a slow-growth phenotype were selected. Amino acid similarities and conserved residues found in the short-chain type reductase family were identified in *Rv2509*. In *Corynebacterium glutamicum,* the ortholog gene to *Rv2509* was identified as *NCgl2385*, with 70% amino acid similarity. Belonging to the same suborder Corynebacterineae, mycolates of the genus *Corynebacterium* are shorter than those found in *Mycobacterium* (C_{22}-C_{36} vs C_{60}-C_{90}), but the mycolic motif is conserved within the suborder. An *NCgl2385* knockout mutant grew as smaller colonies on a solid medium and had a slower growth rate when

cultured in a liquid medium compared to the wild-type strain. Using MALDI-TOF/Mass Spectrometry (MS), Thin Layer Chromatography (TLC) and sodium borodeuteride reduction, a β-keto motif instead of the hydroxyl motif in the mycolates of trehalose monocorynomycolate and trehalose dicorynomycolate was observed (Lea-Smith *et al.*, 2007).

Bhatt *et al.*, (2008) identified the orthologue gene of *M. tuberculosis Rv2509* in *M. smegmatis* mc^2 155 as *MSMEG4722* (Figure 3.1). Knocking out the *MSMEG4722* gene (*ΔMSMEG4722)* resulted in altered colony morphology on solid medium and a slightly slower growth rate when measured by optical density (OD) in a liquid medium compared to *M. smegmatis* mc^2 155. Observed by TLC, the mutant lost the lipid spots for mature mycolates, replaced by a rapidly migrating lipid spot in extracts from both the mAGP complex and as a free lipid in the outer cell envelope. These rapidly migrating lipid spots were identified as decarboxylated α-alkyl, β-oxo mycolate intermediates/ pre-mycolates through MALDI-TOF/MS. *ΔMSMEG4722* cells pre-treated with sodium borohydride, which reduces the β-oxo group on the mycolic motif, had restored mature mycolic acids. TDM and TMM lipid spot mobilities also migrated more rapidly in *ΔMSMEG4722*, confirming that the reductase function of *MSMEG4722* affected all mycolates throughout the cell envelope. Potential changes to cell wall permeability through increased susceptibility to the lipophilic antibiotic rifampicin was also observed (Bhatt *et al.*, 2008). The cell wall was also proposed to be more hydrophobic, observed through n-hexadecane partitioning. *ΔMSMEG4722* had a lower absorbance in the aqueous phase than *M. smegmatis* mc^2 155 (Asma Javid, Thesis, University of Birmingham, 2017).

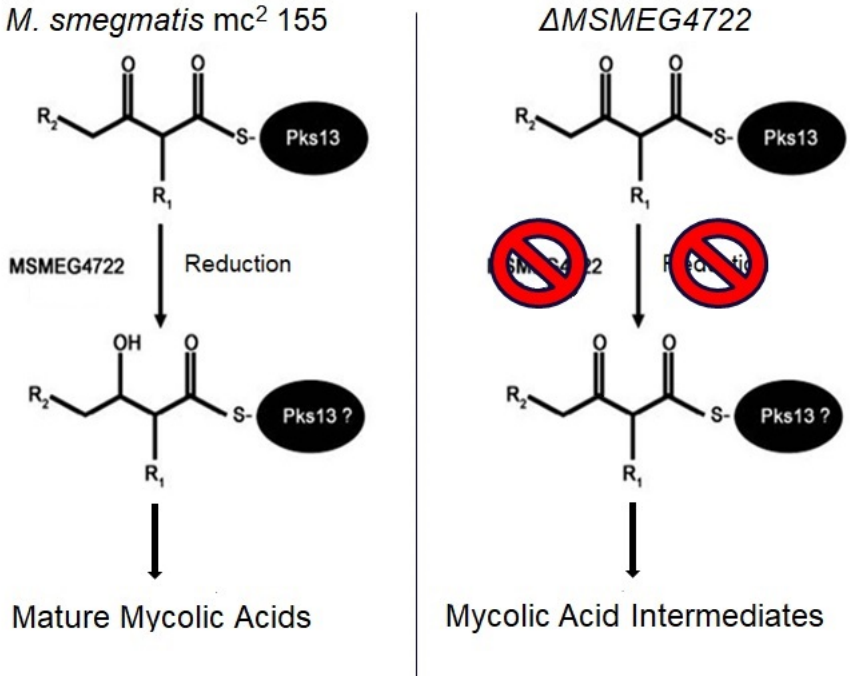


Figure 3.1: *MSMEG4722* encoded reduction of the mycolic motif.

The gene product of *MSMEG4722* reduces the β-oxo group on the mycolic motif to a hydroxyl group. This is proposed to be the final step in the production of mature mycolic acids. Image adapted from Bhatt *et al.*, (2008) (permission to reuse via a Creative Commons Attribution Licence).

Complementation of the *ΔMSMEG4722* mutant with the genes *MSMEG4722* (*ΔMSMEG4722*-C) and *Rv2509*, reintroduced on an episomal plasmid (pMV261, which contains a kanamycin resistance marker), indicated that *MSMEG4722* is a functional homologue of *Rv2509* (Bhatt *et al.*, 2008). In *M. tuberculosis* and *M. bovis* BCG, knocking out *Rv2509* and the BCG homologue *BCG2529* respectively, are lethal mutations, showing the gene is essential in these species (Javid *et al.*, 2020); however, *MSMEG4722* does not appear to be essential in *M. smegmatis* mc^2 155. Thereby, providing a useful strain to study the function of this biosynthetic enzyme.

3.1.2 Aims and Hypothesis

Using the *ΔMSMEG4722* mutant and the complemented strain *ΔMSMEG4722*-C (constructed and provided by Apoorva Bhatt, School of Biosciences, University of Birmingham), this chapter aimed to:

1) Characterise *ΔMSMEG4722* in Middlebrook 7H9 culture conditions.

2) Understand the effect of losing mature mycolic acids for mycolic acid intermediates on pellicle biofilm formation when cultured in the minimal media Sauton's 40 without detergent.

Hypothesis: The loss of mature mycolates for mycolic acid intermediates will alter the ability of *M. smegmatis* to produce pellicle biofilms.

3.2 Results

3.2.1 Two PCR primer sets were used to confirm the deletion of the *MSMEG4722* gene in *ΔMSMEG4722* and its re-introduction in the complemented strain

The genetics of *ΔMSMEG4722* and *ΔMSMEG4722*-C were investigated to confirm that the gene had been deleted and complemented, as expected. Visualising the construction of *ΔMSMEG4722* by Bhatt *et al.*, (2008) in DNAStar SeqBuilder™ showed the deletion of the *MSMEG4722* gene and replacement with a sucrose counter-selectable and hygromycin antibiotic marker (*SacB-Hyg*^{R} cassette) did not result in the complete removal of the gene. Instead, small residual regions of genomic DNA from *MSMEG4722* flank the *SacB-Hyg*^{R} cassette; 86bp from the beginning of the gene and 174bp from the end. The amino acid sequences for these residual flanking regions were identified, and polymerase chain reaction (PCR) primers designed for this thesis were used to re-confirm the mutation and are hereafter referred to as primer set 1 (methods section 7.13, Table 7.3) (Figure 3.2).

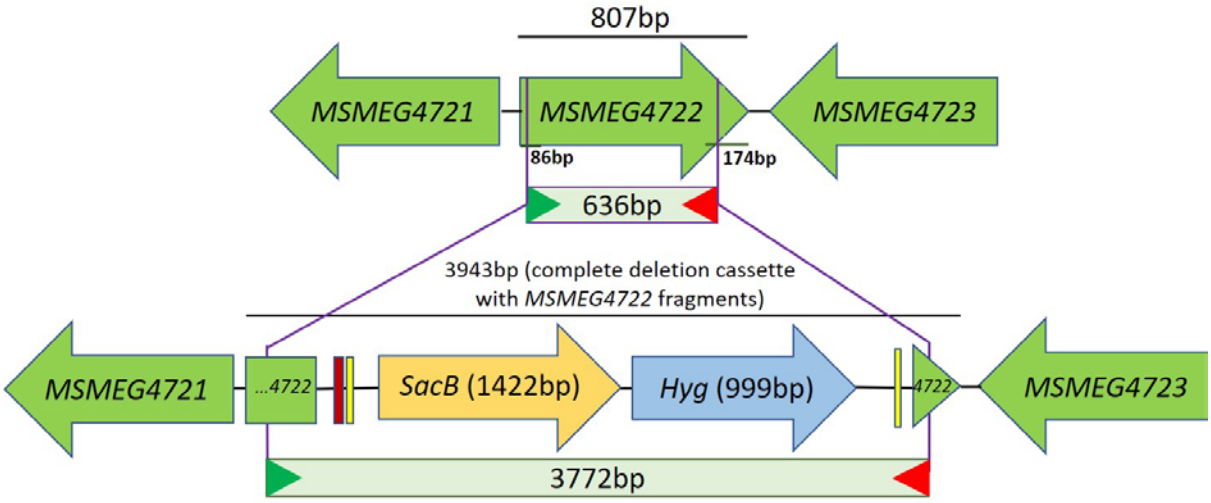


Figure 3.2: Schematic representation of the *MSMEG4722* gene region and predicted PCR amplification products using primer set 1.

In *ΔMSMEG4722* and *ΔMSMEG4722*-C, the *MSMEG4722* gene has been replaced by a *SacB-Hyg*^{R} cassette. In *ΔMSMEG4722*-C, the *MSMEG4722* gene has been re-introduced via a pMV261 plasmid. Primer set 1: forward primer (green) that sits within the residual 86bp from the beginning of the *MSMEG4722* gene, and reverse primer (red) that sits within the 174bp from the end of the *MSMEG4722* gene after its deletion. In *M. smegmatis* mc^2 155 and *ΔMSMEG4722*-C, the predicted PCR product for the wild-type gene is 636bp. In *ΔMSMEG4722* and *ΔMSMEG4722*-C (second PCR product), the predicted PCR product for replacement with the *SacB-Hyg*^{R} cassette is 3772bp. The schematic is based on Bhatt *et al.,* (2008).

Amplification via PCR using primer set 1 was expected to produce a band size of 636bp in *M. smegmatis* mc^2 155 corresponding to the wild-type gene, a band size of 3772bp in *ΔMSMEG4722* corresponding to the replacement of *MSMEG4722* with the *SacB-Hyg*^{R} cassette, or both fragments in *ΔMSMEG4722*-C due to the complementation of the gene via the pMV261 plasmid.

Two independent cultures of either *M. smegmatis* mc^2 155, *ΔMSMEG4722* or *ΔMSMEG4722*-C were cultured in Middlebrook 7H9 with selective antibiotics hygromycin (*ΔMSMEG4722 and ΔMSMEG4722*-C) and kanamycin (*ΔMSMEG4722*-C only) (methods section 7.1). DNA was extracted and amplified using PCR (method

sections 7.12 and 7.13) before the DNA products were analysed by agarose gel electrophoresis.

For *M. smegmatis* mc^2 155, the 636bp band was present which corresponds to the wild-type gene. For *ΔMSMEG4722*, the 3772bp band was present which corresponds to the *SacB-Hyg*^{R} cassette replacement of *MSMEG4722*. For *ΔMSMEG4722*-C, the 636bp band was present, but the PCR conditions could not amplify the 3772bp band, confirming the wild-type gene complementation but not the initial knockout and replacement with the *SacB-Hyg*^{R} cassette (Figure 3.3).

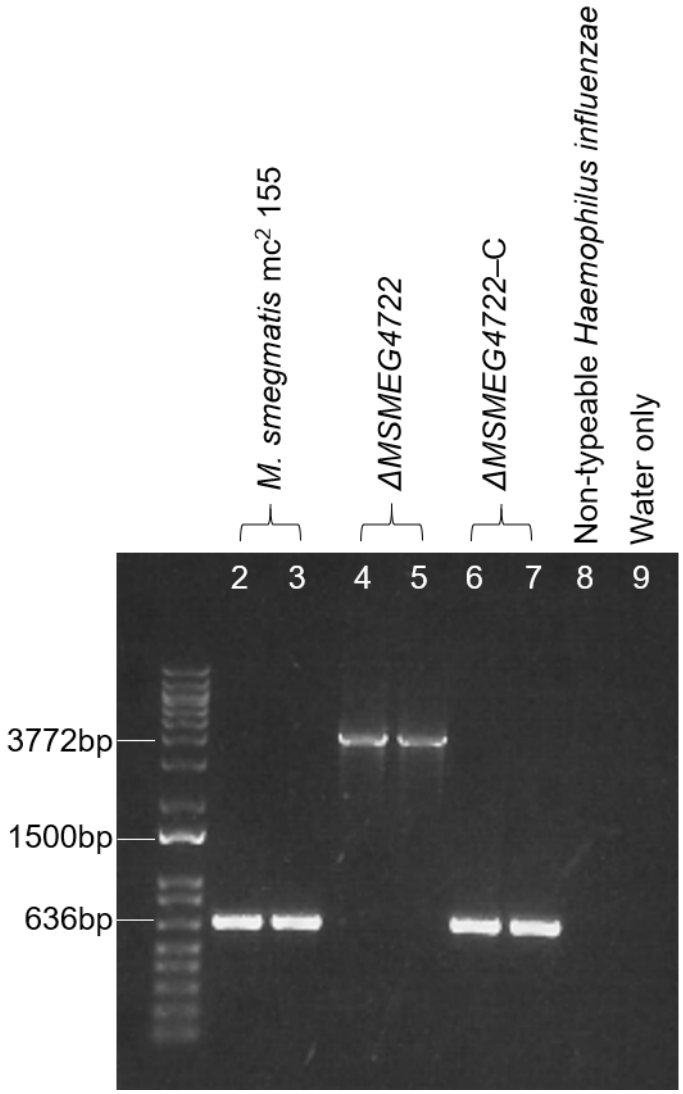


Figure 3.3: PCR confirmation of *M. smegmatis* mc² 155, *ΔMSMEG4722* and *ΔMSMEG4722*-C using primer set 1.

Confirmation of *M. smegmatis* mc² 155, *ΔMSMEG4722* and *ΔMSMEG4722*-C using PCR amplifications of the *MSMEG4722* gene and *SacB-Hyg*^{R} cassette with electrophoresis on a 1% TAE agarose gel. Gel electrophoresis of PCR amplifications for primer set 1: molecular weight marker, lanes 2-3 *M. smegmatis* mc² 155 (636bp), lanes 4-5 *ΔMSMEG4722* (3772bp), lanes 6-7 *ΔMSMEG4722*-C (636bp), lane 8 genomic DNA from Non-typeable *Haemophilus influenzae* (negative control), lane 9 water only (negative control).

Due to the inability to amplify both the 636bp and the 3772bp bands in *ΔMSMEG4722*-C, a second primer set was designed with the same forward primer from primer set 1, and a complementary reverse primer to the *SacB* gene of the *SacB-Hyg*^{R} cassette.

These will hereafter be referred to as primer set 2 (methods section 7.13, Table 7.3) (Figure 3.4). These primers should not produce a band in *M. smegmatis* mc^2 155 and produce a 1238bp band in both *ΔMSMEG4722* and *ΔMSMEG4722*-C.

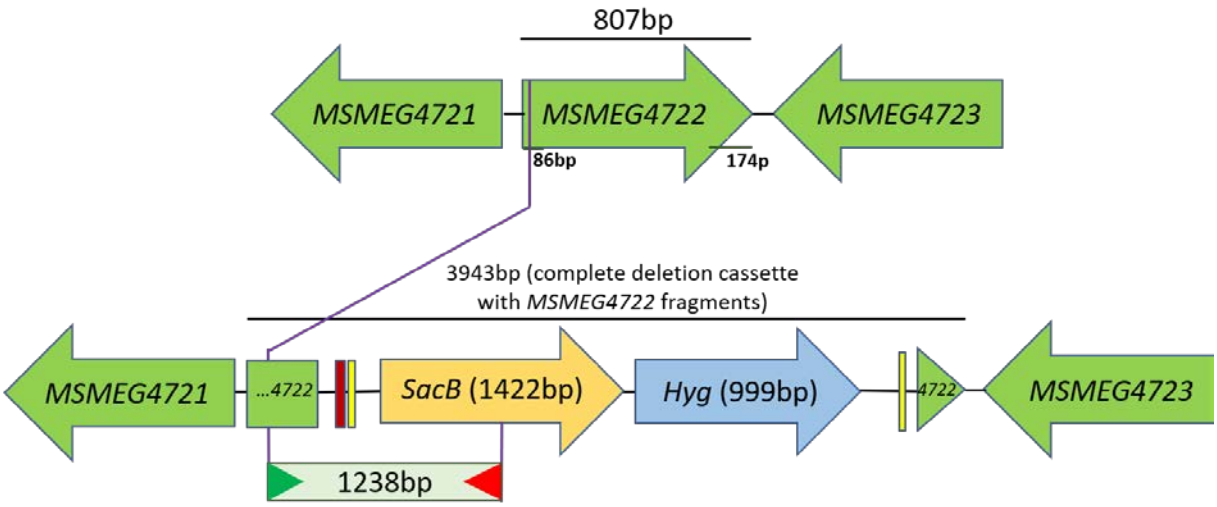


Figure 3.4: Schematic representation of the *MSMEG4722* gene region and predicted PCR amplification products using primer set 2.

Predicted PCR amplification products within *M. smegmatis* mc^2 155, *ΔMSMEG4722* and *ΔMSMEG4722*-C with PCR primer set 2. Primer set 2: forward primer (green) that sits within the residual 86bp from the beginning of the *MSMEG4722* gene and reverse primer (red) that sits within the *SacB* gene of the *SacB-Hyg*^{R} cassette. In *M. smegmatis* mc^2 155, there is no predicted PCR product. In *ΔMSMEG4722* and *ΔMSMEG4722*-C, the predicted PCR product is 1238bp. The schematic is based on Bhatt *et al.,* (2008).

PCR using primer set 2 resulted in no bands in *M. smegmatis* mc^2 155. The presence of the 1238bp band in both *ΔMSMEG4722* and *ΔMSMEG4722*-C confirmed the deletion of the *MSMEG4722* gene in both strains (Figure 3.5).

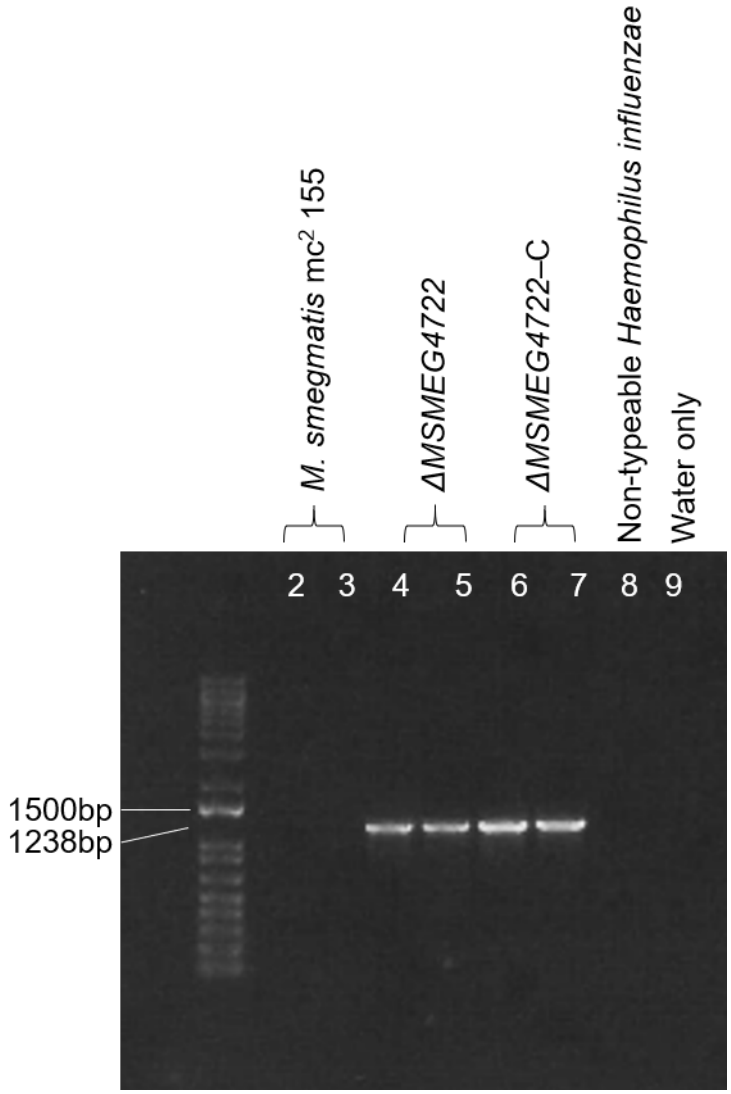


Figure 3.5: PCR confirmation of *M. smegmatis* mc² 155, *ΔMSMEG4722* and *ΔMSMEG4722*-C using primer set 2.

Confirmation of *M. smegmatis* mc² 155, *ΔMSMEG4722* and *ΔMSMEG4722*-C using PCR amplification of the *MSMEG4722* gene and *SacB-Hyg*^{R} cassette with electrophoresis on a 1% TAE agarose gel. Gel electrophoresis of PCR amplification for primer set 2: molecular weight marker, lanes 2-3 *M. smegmatis* mc² 155 (no band), lanes 4-5 *ΔMSMEG4722* (1238bp), lanes 6-7 *ΔMSMEG4722*-C (1238bp), lane 8 genomic DNA from Non-typeable *Haemophilus influenzae* (negative control) and lane 9 water only (negative control).

3.2.2 Defining the growth rate and assessing the effects of selective antibiotics

A change in the culture characteristics ($OD600_{nm}$) of *ΔMSMEG4722* compared to *M. smegmatis* mc^2 155 cultured in TSB had been observed by Bhatt *et al.*, (2008). Here, culture characteristics were evaluated by both $OD540_{nm}$ and total viable counts (TVC), defining the bacterial growth rate and exponential phase of growth of *ΔMSMEG4722* and *ΔMSMEG4722*-C compared to *M. smegmatis* mc^2 155. The effect of selective antibiotics on growth was also evaluated.

Three independent cultures of *M. smegmatis* mc^2 155, *ΔMSMEG4722* and *ΔMSMEG4722*-C were grown in Middlebrook 7H9 supplemented with 10% OADC + 0.05% Tween-80 with or without the selective antibiotics hygromycin and kanamycin (methods section 7.15). To confirm no cross-contamination of strains during culture, additional flasks of *M. smegmatis* were cultured with hygromycin and kanamycin and *ΔMSMEG4722* with kanamycin (appendix A Figure A.1.1 and Figure A.1.3).

3.2.2.1 *ΔMSMEG4722* displayed a significantly lower optical density and a log lower total viable counts compared to *M. smegmatis* mc^2 155 by stationary phase, but has a comparable doubling time

When evaluating $OD540_{nm}$ measurements, *M. smegmatis* mc^2 155 saw $OD540_{nm}$ increase from 0.05 ± 0.01 [$OD540_{nm}$ ± SD] at the start of the time course (T0) to $OD540_{nm}$ 1.69 ± 1.68 by 15-hours indicating a lag phase. Between 15-28 hours, the $OD540_{nm}$ increased to 6.86 ± 1.50, consistent with exponential growth. The cultures plateaued into stationary phase after 32-36 hours at $OD540_{nm}$ 8.02 ± 1.34 and remained at this $OD540_{nm}$ to the end of the time course. *ΔMSMEG4722* cultured without hygromycin saw $OD540_{nm}$ increase from 0.02 ± 0.01 at T0 to 0.20 ± 0.16 over

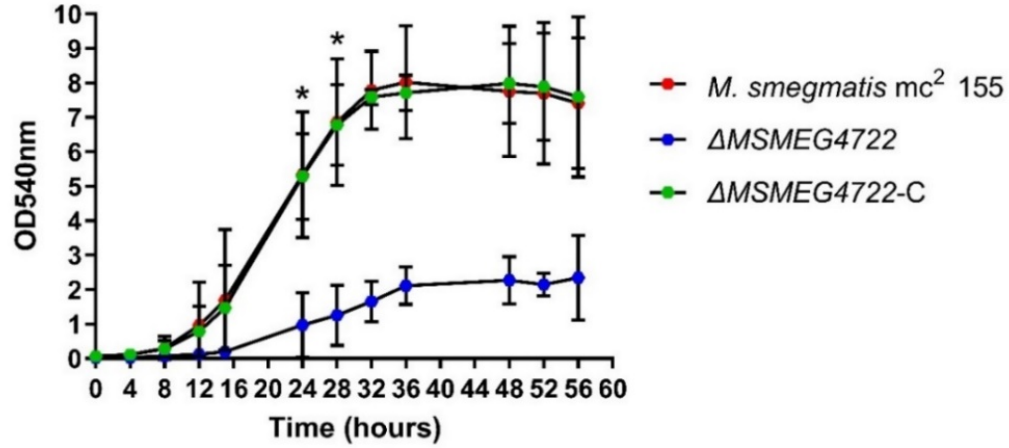
15-hours indicating a lag phase. The $OD540_{nm}$ increased to 1.65 ± 0.49 by 32-hours indicating an exponential phase before it plateaued after 36-hours at an $OD540_{nm}$ of 2.11 ± 0.44 for the remainder of the time course. For *ΔMSMEG4722*-C cultured without selective antibiotics, the $OD540_{nm}$ started at 0.06 ± 0.03 and rose to 1.47 ± 1.0 after 15-hours indicating a lag phase. Between 15-24 hours, the $OD540_{nm}$ rose to 5.29 ± 1.00, akin to the exponential phase. The $OD540_{nm}$ plateaued at 28-hours at $OD540_{nm}$ 6.78 ± 0.95, where it remained until the end of the time course (stationary phase) (Figure 3.6A).

For TVC (TVC; CFU mL^{-1}), the *M. smegmatis* mc^2 155 CFU mL^{-1} was $8.06x10^6$ ± $2.16x10^6$ [CFU mL^{-1} ± SD] at T0 and rose to $1.38x10^8$ ± $1.62x10^8$ after 15-hours, indicating a lag phase. Between 15-28 hours, the CFU mL^{-1} rose to $1.03x10^9$ ± $3.75x10^8$ indicating an exponential phase where it then plateaued at this CFU mL^{-1} until the end of the time course (stationary phase). For *ΔMSMEG4722* cultured without hygromycin, the CFU mL^{-1} was $1.11x10^5$ ± $6.43x10^4$ at T0, which rose to $2.01x10^7$ ± $1.89x10^7$ after 15-hours of culture, indicating a lag phase. Between 15-28 hours, the CFU mL^{-1} rose to $1.88x10^8$ ± $7.83x10^7$, indicating an exponential phase. The CFU mL^{-1} plateaued into the stationary phase after 32-hours at $2.67x10^8$ ± $6.66x10^7$, where it remained at this CFU mL^{-1} for the remained of the time course. *ΔMSMEG4722*-C cultured without selective antibiotics were inoculated at T0 to a CFU mL^{-1} of $9.61x10^6$ ± $5.17x10^6$. By 15-hours it had increased to $3.78x10^7$ ± $6.98x10^6$ (lag phase), between 15-24 hours the CFU mL^{-1} increased to $3.72x10^8$ ± $6.98x10^7$ (exponential phase). After 32-hours, the culture plateaued at $4.58x10^8$ ± $4.17x10^7$ CFU mL^{-1} until the end of the time course (stationary phase) (Figure 3.6B).

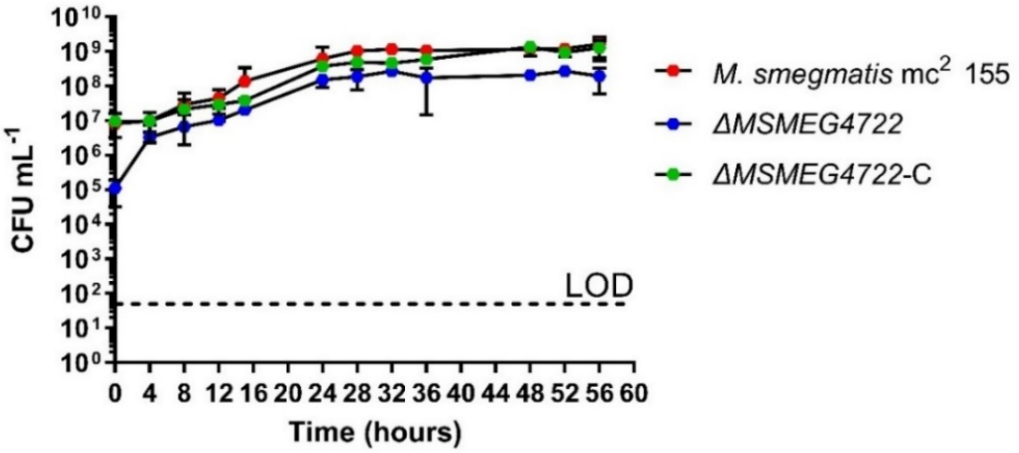
The bacterial growth rate was calculated as the doubling time, based on both $OD540_{nm}$ and TVC. For *M. smegmatis,* the doubling time was 4:12 ± 1:22 [mean hours: minutes ± SD] based on $OD540_{nm}$ and 4:07 ± 0:47 hours based on TVC. For *ΔMSMEG4722* cultured without hygromycin, the doubling time was 4:26 ± 0:16 hours based on $OD540_{nm}$ and 3:23 ± 0:58 hours based on TVC. *ΔMSMEG4722*-C cultured without selective antibiotics had a doubling time of 4:14 ± 1:00 hours for $OD540_{nm}$ and 3:45 ± 0:43 hours for TVC (Figure 3.6C).

When comparing *M. smegmatis* mc^2 155 and *ΔMSMEG4722* cultures without selective antibiotics, the $OD540_{nm}$ measurements were statistically significantly lower from the 28-hour timepoint to the end of the time course for ($P = 0.0383$). For *ΔMSMEG4722* compared to *ΔMSMEG4722*-C, the $OD540_{nm}$ was statistically significantly lower from the 24-hour time point to the end of the time course ($P = 0.0223$). For TVC, there was no statistical difference between the three strains at any time point, although the viable count of *ΔMSMEG4722* was 1 $\log_{10}$CFU mL^{-1} lower than *M. smegmatis* mc^2 155 and *ΔMSMEG4722*-C from 36-hours of culture to the conclusion of the time course at 56-hours. There were no statistical differences in the doubling times calculated from the optical density ($OD540_{nm}$) or TVC between strains or comparing the same strain under the two measurements. All three strains were in the exponential growth phase from 15-24 hours of culture.

A



B



C

Strain	Doubling time based on $OD540_{nm}$	Doubling time based on CFU mL^{-1}
M. smegmatis mc^2 155	4:12 [±1:22]	4:07 [±0:47]
ΔMSMEG4722	4:26 [± 0.16]	3:23 [±0:58]
ΔMSMEG4722-C	4:14 [±1:00]	3:45 [±0:43]

Figure 3.6: Culture of *M. smegmatis* mc^2 155, *ΔMSMEG4722* and *ΔMSMEG4722*-C without selective antibiotics.

$OD540_{nm}$ and CFU mL^{-1} of *M. smegmatis* mc^2 155 (red), *ΔMSMEG4722* (blue) and *ΔMSMEG4722*-C (green) cultured in Middlebrook 7H9 supplemented with 10% OADC + 0.05% Tween-80. (A) $OD540_{nm}$ over 56-hours at intervals of approximately every 4-hours. (B) CFU mL^{-1} over 56-hours at intervals of approximately every 4-hours. (C) Calculated bacterial doubling time based on $OD540_{nm}$ or CFU mL^{-1}. Three independent biological replicates. Error bars = standard deviation. LOD = limit of detection (50 CFU mL^{-1}). Statistical analysis was performed by a matched two-way ANOVA ($OD540_{nm}$) or matched mixed effect analysis (CFU mL^{-1}) using the Geisser-Greenhouse correction.

3.2.2.2 Selective antibiotics had a negative effect on optical density and total viable count of *ΔMSMEG4722*-C

For *ΔMSMEG4722* cultured with hygromycin, the $OD540_{nm}$ increase from 0.01 ± 0.004 at T0 to 0.18 ± 0.18 after 15-hours (lag phase). The $OD540_{nm}$ increased to 1.84 ± 0.57 by 32-hours (exponential phase) before it plateaued after 36-hours at an $OD540_{nm}$ of 2.28 ± 0.32 for the remained of the time course (stationary phase). For *ΔMSMEG4722*-C cultures with hygromycin and kanamycin, the $OD540_{nm}$ started at 0.07 ± 0.02, which increased to 0.61 ± 0.23 after 15-hours. Between 15-24 hours, the $OD540_{nm}$ increased to 3.77 ± 0.84. The culture plateaued at an $OD540_{nm}$ of 7.24 ± 0.10 after 36-hours, and it remained at this $OD540_{nm}$ until the end of the time course (Figure 3.7A).

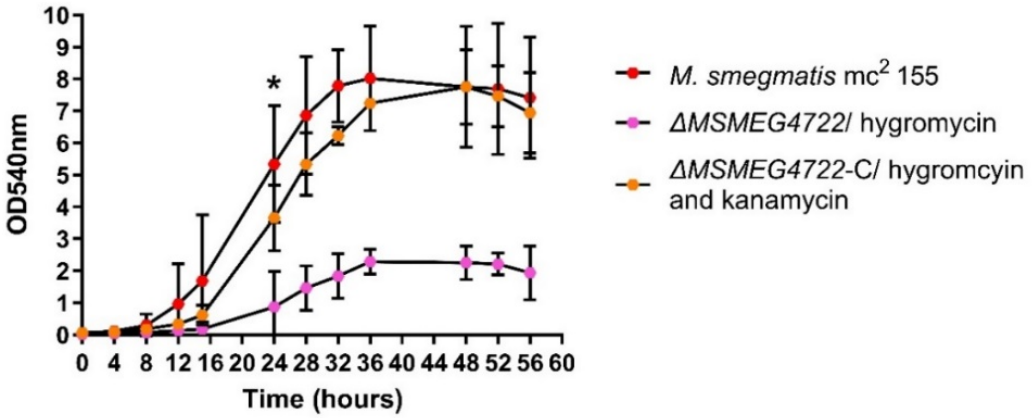
For TVC analyses, *ΔMSMEG4722* cultured with hygromycin had a starting CFU mL^{-1} of $1.50x10^5 \pm 6.23x10^4$ CFU mL^{-1} at T0, which rose to $2.36x10^7 \pm 1.89x10^7$ CFU mL^{-1} after 15-hours of culture (lag phase). Between 15-24 hours the viable count rose to $1.49x10^8 \pm 4.15x10^7$ CFU mL^{-1} (exponential phase). The viable count plateaued into stationary phase after 28-hours at $2.91x10^8 \pm 4.17x10^7$ CFU mL^{-1} and remained at this level for the rest of the time course. For *ΔMSMEG4722*-C cultured with hygromycin and kanamycin, the viable count started at $6.94x10^6 \pm 4.52x10^6$ and rose to $3.00x10^7 \pm 1.52x10^7$ CFU mL^{-1} after 15-hours (lag phase). Between 15-24 hours the CFU mL^{-1} increased to $1.53x10^8 \pm 4.98x10^7$ (exponential phase). The culture entered stationary phase around 36-hours with a CFU mL^{-1} of $3.22x10^8 \pm 4.37x10^7$. The culture remained at this CFU mL^{-1} (Figure 3.7B).

For *ΔMSMEG4722* cultured with hygromycin, the bacterial doubling time was 4:37 ± 0:34 hours based on $OD540_{nm}$ and 3:23 ± 0:54 hours based on CFU mL^{-1}. For

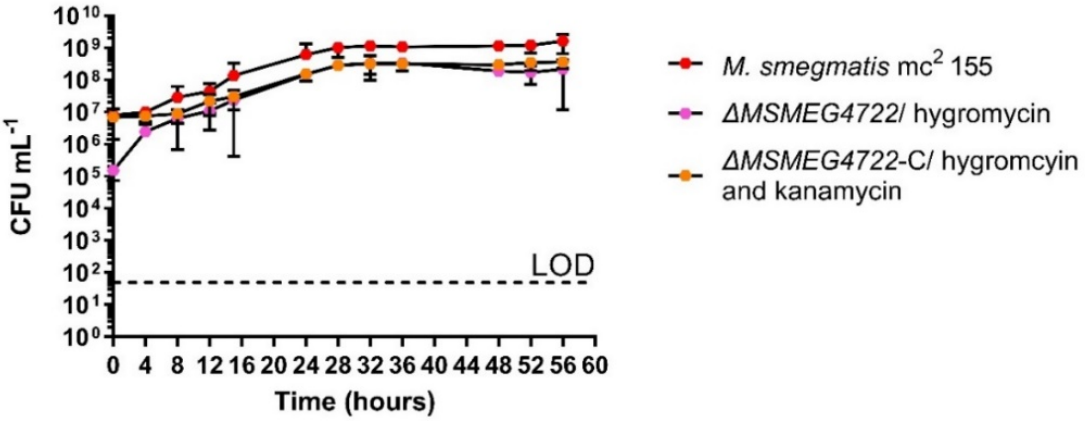
ΔMSMEG4722-C cultured with hygromycin and kanamycin, the $OD540_{nm}$ doubling time was 3:52 ± 0:12 hours and for CFU mL^{-1} 4:04 ± 0:1 hours. There was no statistical difference between any bacterial culture conditions doubling times for either $OD540_{nm}$ or CFU mL^{-1} over the 56-hour time course (Figure 3.7C).

When comparing *M. smegmatis* mc^2 155 to *ΔMSMEG4722* and *ΔMSMEG4722*-C cultured with their respective selective antibiotics; from 28-hours of culture, the $OD540_{nm}$ of *ΔMSMEG4722* was significantly lower than both *M. smegmatis* mc^2 155 and *ΔMSMEG4722*-C (P = 0.0479 and 0.0145 respectively). For TVC, there was no statistical difference between the strains, although *ΔMSMEG4722* and *ΔMSMEG4722*-C TVC was 1 log_{10}CFU mL^{-1} lower than *M. smegmatis* mc^2 155 from the 36-hour time point until the end of the time course. There were no statistical differences in the doubling times calculated from $OD540_{nm}$ or TVC between strains or comparing the same strain under the two measurements.

A



B



C

Strain	Doubling time based on $OD540_{nm}$	Doubling time based on CFU mL^{-1}
M. smegmatis mc^2 155	4:12 [±1:22]	4:07 [±0:47]
ΔMSMEG4722/ hygromycin	4:26 [±0:16]	3:23 [±0:58]
ΔMSMEG4722-C/ hygromycin and kanamycin	4:14 [±1:00]	3:45 [±0:43]

Figure 3.7: Culture of *M. smegmatis* mc^2 155, *ΔMSMEG4722* and *ΔMSMEG4722*-C with selective antibiotics.

$OD540_{nm}$ and CFU mL^{-1} of *M. smegmatis* mc^2 155 *(*red), *ΔMSMEG4722* (pink) and *ΔMSMEG4722*-C (orange) cultured in Middlebrook 7H9 supplemented with 10% OADC + 0.05% Tween-80 and their respective selective antibiotics hygromycin and kanamycin. (A) $OD540_{nm}$ over 56-hours at intervals of approximately every 4-hours. (B) CFU mL^{-1} over 56-hours at intervals of approximately every 4-hours. (C) Calculated bacterial doubling time based on $OD540_{nm}$ or CFU mL^{-1}. Three independent biological replicates. Error bars = standard deviation. LOD = limit of detection (50 CFU mL^{-1}). Statistical analysis by a matched two-way ANOVA ($OD540_{nm}$) or matched mixed effect analysis (CFU mL^{-1}) using the Geisser-Greenhouse correction.

3.2.2.3 Selective antibiotics had a negative effect on the culture of *ΔMSMEG4722*-C compared to zero-antibiotic conditions

When comparing drugged and zero drug conditions, there were no statistical differences in $OD540_{nm}$ readings or TVC for *ΔMSMEG4722* cultures with or without the addition of hygromycin at any time point over the time course. There was no statistical difference between the doubling times of *ΔMSMEG4722* cultured with or without hygromycin (appendix 1 Figure A.1.2).

ΔMSMEG4722-C was also cultured with hygromycin or kanamycin alone to evaluate the effects of each selective antibiotic. There was no statistical difference between any of the culture conditions of *ΔMSMEG4722*-C for $OD540_{nm}$ or TVC at any time point. However, the presence of kanamycin appears to delay or inhibit the growth of *ΔMSMEG4722*-C ($OD540_{nm}$ and TVC) compared to culture without selective antibiotics. *ΔMSMEG4722*-C cultured with hygromycin only had an $OD540_{nm}$ and TVC that mirrored no drug conditions. For cultures with hygromycin or kanamycin, the $OD540_{nm}$ doubling times were 4:22 ± 1:14 hours and 4:34 ± 1:10 hours, respectively. For the TVC, the doubling times were 4:46 ± 1:34 hours and 4:49 ± 0:49 hours, respectively (appendix 1 Figure A.1.4).

3.2.3 Selective antibiotics inhibit *ΔMSMEG4722* and *ΔMSMEG4722*-C pellicle biofilm formation

Any potential inhibitory effects caused by selective antibiotics in pellicle biofilm cultures (in Sauton's 40 medium) were identified. Two independent cultures of *M. smegmatis* mc^2 155, *ΔMSMEG4722* and *ΔMSMEG4722*-C were cultured as pellicle biofilms (methods section 7.1) with or without the selective antibiotics hygromycin and

kanamycin alongside zero-antibiotic controls. Pellicle biofilm formation was assessed visually and by quantifying biomass with crystal violet (methods section 7.5).

3.2.3.1 *ΔMSMEG4722* was unable to produce reticulated pellicle biofilms and selective antibiotics inhibited *ΔMSMEG4722*-C pellicle biofilm formation

Without the addition of selective antibiotics, the complemented strain *ΔMSMEG4722*-C produced creamy reticulated pellicle biofilms with ridges and troughs comparable to *M. smegmatis* mc^2 155 pellicle biofilms (Figure 3.8A). The biomass concentration was also comparable after staining with crystal violet ($Ab595_{nm}$ 4-6 for both strains) (Figure 3.8B). The mutant *ΔMSMEG4722,* in comparison, developed a thin, opaque pellicle biofilm with little ridging (Figure 3.8A) and produced significantly less biomass than both *M. smegmatis* mc^2 155 and *ΔMSMEG4722*-C pellicle biofilms ($Ab595_{nm}$ of 3-4 for *ΔMSMEG4722*) ($P < 0.0001$) (Figure 3.8B).

When evaluating the effect of selective antibiotics on pellicle biofilm formation, for *ΔMSMEG4722,* the addition of hygromycin to the culture inhibited pellicle biofilm formation. There was significantly less biomass produced compared to the *ΔMSMEG4722* pellicle biofilms grown in antibiotic-free culture ($Ab595_{nm}$ 2-3 compared to $Ab595_{nm}$ 3-4) ($P = 0.0139$). For *ΔMSMEG4722*-C, the addition of hygromycin and kanamycin resulted in the formation of a thin, translucent pellicle biofilm with no ridging and the pellicle biofilms produced significantly less biomass than the *ΔMSMEG4722*-C pellicle biofilms cultured in antibiotic-free culture ($Ab595_{nm}$ of 2 compared to $Ab595_{nm}$ of 4-6) ($P < 0.0001$) (Figure 3.8A and Figure 3.8B).

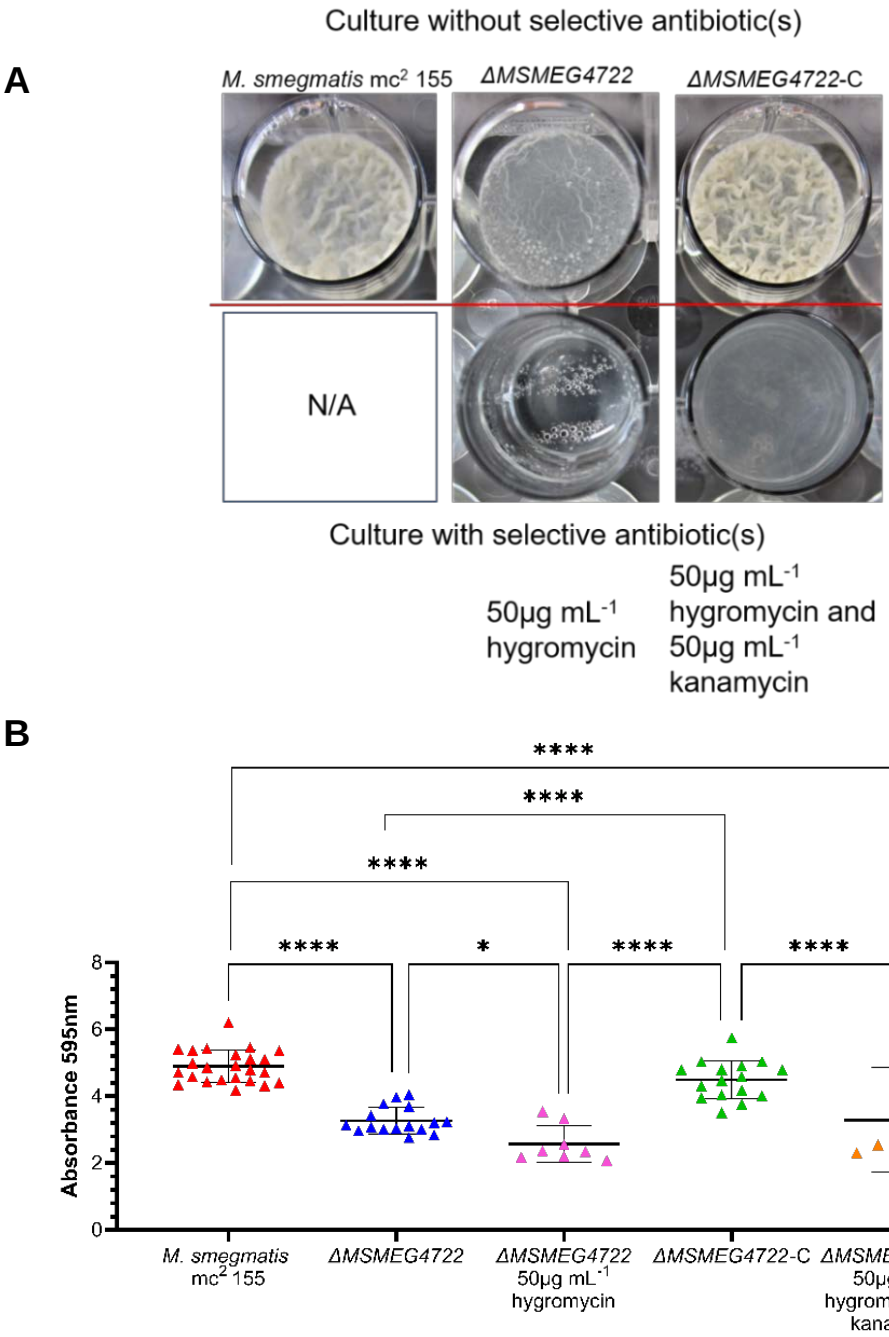


Figure 3.8: The effect of selective antibiotics on pellicle biofilm formation.

(A) Representative photographs of *ΔMSMEG4722* and *ΔMSMEG4722*-C pellicle biofilms cultured with or without selective antibiotics. *M. smegmatis* mc^2 155 was used as a pellicle biofilm forming control. (B) Crystal violet biomass quantification of *ΔMSMEG4722* (blue), *ΔMSMEG4722* with hygromycin (pink), *ΔMSMEG4722*-C (green) and *ΔMSMEG4722*-C with hygromycin and kanamycin (orange). *M. smegmatis* mc^2 155 was used as a pellicle biofilm forming control (red). Absorbance was read at a wavelength of 595$_{nm}$. Two independent biological replicates consisting of 4-12 technical replicates (independent pellicle biofilms formed in a well of a 24-well plate). Error bars = standard deviation. Statistical analysis was performed by log10 transforming the data and performing a one-way ANOVA, **** $P < 0.0001$, * $P = 0.0139$.

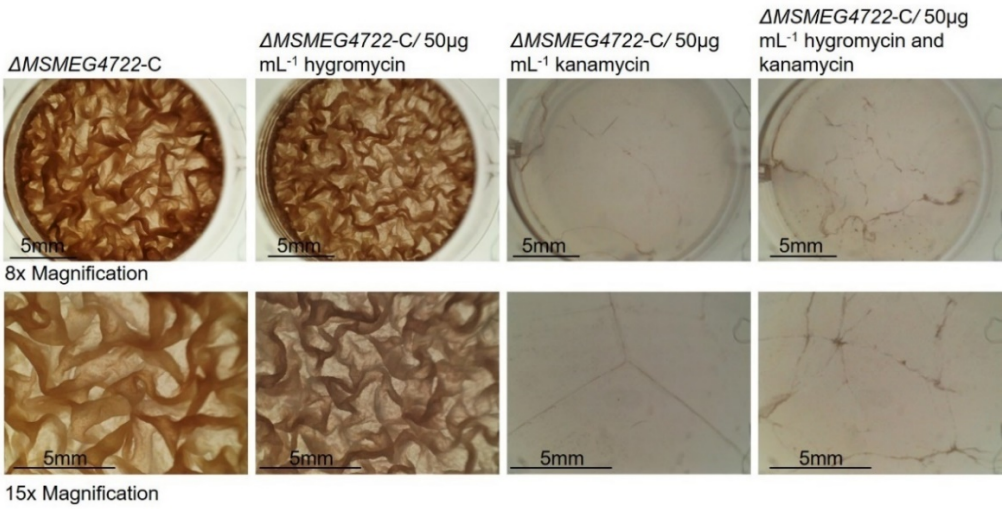
3.2.3.2 Kanamycin has a stronger inhibitory effect than hygromycin on *ΔMSMEG4722*-C pellicle biofilm formation

To assess the inhibitory effect of hygromycin and kanamycin independently on *ΔMSMEG4722*-C pellicle biofilm formation, three independent biological replicates of *ΔMSMEG4722*-C were cultured in Sauton's 40 under pellicle biofilm conditions (methods section 7.1); with or without selective antibiotics. Each condition consisted of 8-16 technical replicates. Pellicle biofilm formation was assessed using microscopy and quantifying biomass with crystal violet (methods section 7.5).

As observed in Figure 3.8A, *ΔMSMEG4722*-C cultured without selective antibiotics formed creamy, reticulated, ridged pellicle biofilms, and this was also observed for *ΔMSMEG4722*-C cultured with hygromycin. The pellicle biofilms formed when cultured with kanamycin, or hygromycin and kanamycin were thin and translucent (Figure 3.9A). Although phenotypically indistinguishable, when quantified for biomass, the pellicle biofilms of *ΔMSMEG4722*-C cultured with hygromycin produced significantly less biomass than *ΔMSMEG4722*-C pellicles cultured with zero antibiotics ($Ab595_{nm}$ of 3-4 compared to $Ab595_{nm}$ of 4-6) ($P < 0.0001$). *ΔMSMEG4722*-C pellicle biofilms cultured with kanamycin produced significantly less biomass than pellicle biofilms cultured under the other three conditions; zero antibiotics, hygromycin only, or hygromycin and kanamycin ($Ab595_{nm}$ of 2 compared to 4-6, 3-4 and 3-5 respectively) (all $P < 0.0001$). *ΔMSMEG4722*-C pellicle biofilms cultured with both hygromycin and kanamycin produced statistically less biomass than *ΔMSMEG4722*-C pellicle biofilms cultured with zero antibiotics ($Ab595_{nm}$ ranged from 3-5 compared to 4-6) ($P < 0.0001$). There was no statistical difference between *ΔMSMEG4722*-C pellicle biofilms cultured with

hygromycin and *ΔMSMEG4722*-C pellicle biofilms cultured with hygromycin and kanamycin (Figure 3.9B).

A



B

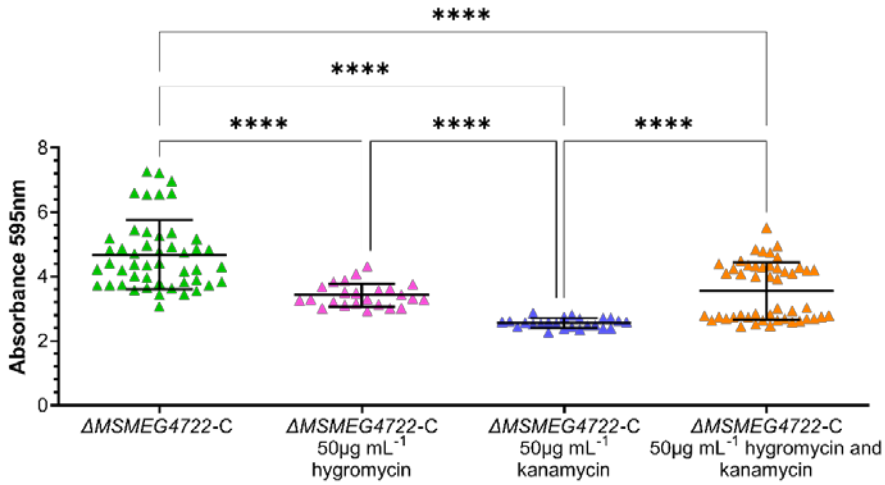


Figure 3.9: The effect of selective antibiotics on *ΔMSMEG4722*-C pellicle biofilm formation.

(A) Representative microscopic photographs of *ΔMSMEG4722*-C cultured either without antibiotics, with 50µg mL^{-1} hygromycin, with 50µg mL^{-1} kanamycin or with 50µg mL^{-1} hygromycin and kanamycin at 8x and 15x magnification. (B) Crystal violet biomass quantification (measured at an absorbance of 595$_{nm}$) of *ΔMSMEG4722*-C cultured without antibiotics (green), with 50µg mL^{-1} hygromycin (pink), with 50µg mL^{-1} kanamycin (lilac) or with 50µg mL^{-1} hygromycin and kanamycin (orange). Three independent biological replicates containing 8-16 technical replicates (independent pellicle biofilms formed in each well of a 24-well plate). Error bars = standard deviation. Statistical analysis was performed by log10 transforming the data and performing a one-way ANOVA Tukey's multiple comparison correction, ** P = 0.0019, **** P < 0.0001.

3.2.4 *ΔMSMEG4722* and *ΔMSMEG4722*-C planktonic and pellicle biofilm cultures are stable without the addition of selective antibiotics

Selective antibiotics present during pellicle biofilm culture inhibited the ability of *ΔMSMEG4722*-C to produce creamy, reticulated pellicle biofilms and reduced the biomass produced by both *ΔMSMEG4722* and *ΔMSMEG4722*-C pellicle biofilms. The selective antibiotics were removed from both pellicle biofilm and shaking planktonic cultures to allow future comparison work between phenotypes. The genetic stability of the *MSMEG4722* gene deletion and its complementation were confirmed.

Three independent biological replicates of either *M. smegmatis* mc^2 155, *ΔMSMEG4722* and *ΔMSMEG4722*-C were cultured as planktonic cells without selective antibiotics. DNA was extracted at three time points; 1) from the initial bacterial culture in Middlebrook 7H9 with selective antibiotics that were used to inoculate planktonic cultures, 2) after twenty-four hours of planktonic culture (standard planktonic culture time), and 3) after six days of planktonic culture (to mimic the culture length of pellicle biofilms). DNA was also extracted from one biological replicate of pooled and evaporated six-day pellicle biofilm biomass that had been cultured without selective antibiotics. Genomic DNA was extracted and amplified using PCR before the DNA products were analysed by agarose gel electrophoresis (methods section 7.14).

For all three time points of the planktonic *M. smegmatis* mc^2 155 cultures, using primer set 1, the 636bp band was present corresponding to the wild-type gene. Using primer set 2, no bands were seen that correspond to the deletion of the *MSMEG4722* gene with the replacement *SacB-Hyg*^{R} selection cassette (Figure 3.10 and Figure 3.11).

For *ΔMSMEG4722*, using primer set 1, the 3772bp band corresponding to the deletion of the *MSMEG4722* gene and presence of the *SacB-Hyg*^{R} cassette was only observed in one of the three cultures and only at the timepoint 'twenty-four hours of planktonic culture' (Figure 3.11A). Using primer set 2, the presence of the 1238bp band in all three biological replicates at all three timepoints confirmed the stable deletion of the *MSMEG4722* gene (Figure 3.10 and Figure 3.11A and B).

For *ΔMSMEG4722*-C, using primer set 1, the 636bp band was present corresponding to the wild-type gene at all time points (Figure 3.10 and Figure 3.11A and B). Using primer set 2, the presence of the 1238bp band in all three biological replicates of the 'Middlebrook 7H9 culture' and 'twenty-four hours of planktonic culture' timepoints confirmed the deletion of the *MSMEG4722* gene (Figure 3.10 and Figure 3.11A). At the 'six-days of planktonic culture' timepoint, one of the cultures had lost the 1238bp band (Figure 3.11B).

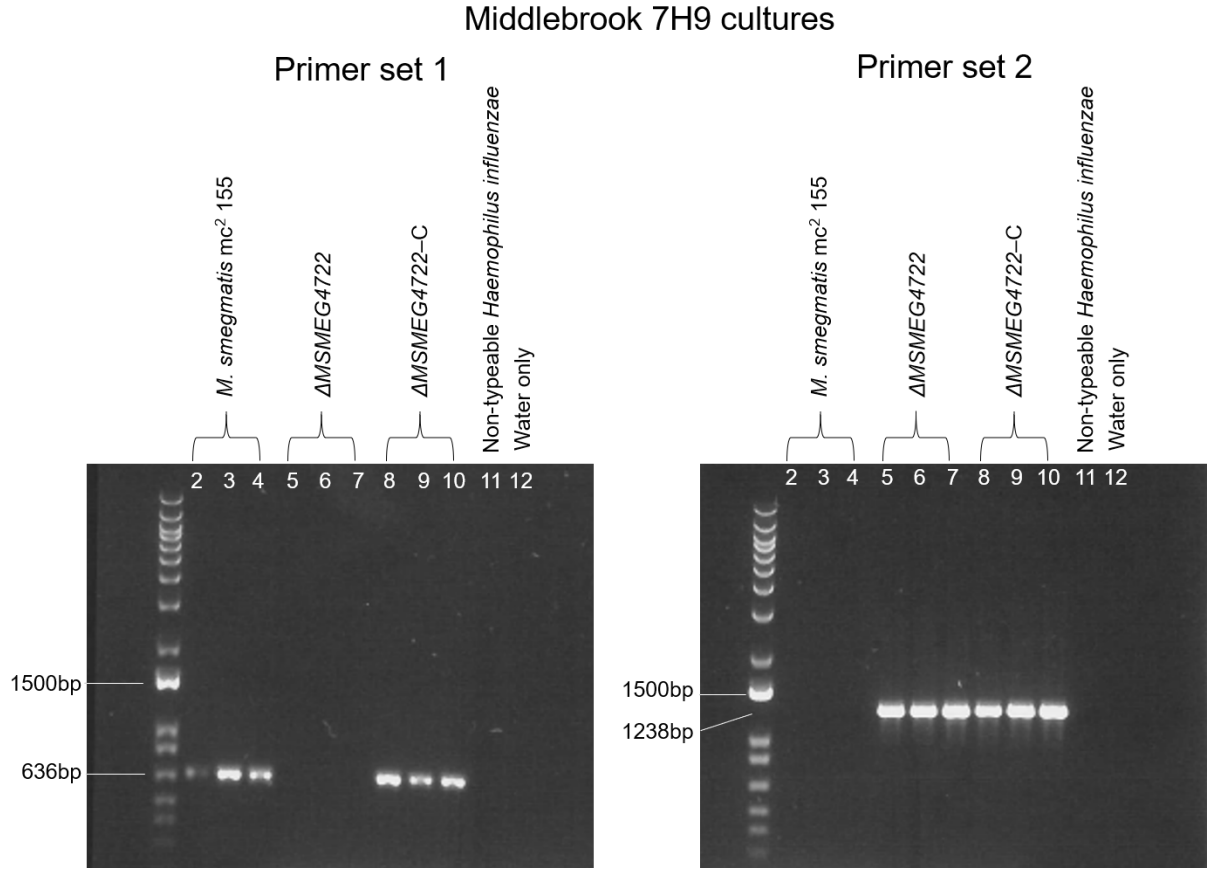


Figure 3.10: Stability of *ΔMSMEG4722* and *ΔMSMEG4722*-C after Middlebrook 7H9 culture with selective antibiotics.

Confirmation of *M. smegmatis* mc^2 155, *ΔMSMEG4722* and *ΔMSMEG4722*-C stability after Middlebrook 7H9 culture with selective antibiotics using PCR and gel electrophoresis on a 1% TAE agarose gel. (Left) PCR products from primer set 1: molecular weight marker, lanes 2-4 *M. smegmatis* mc^2 155 (636bp), lanes 5-7 *ΔMSMEG4722* (3772bp), lanes 8-10 *ΔMSMEG4722*-C (636bp), lane 11 Non-typeable *Haemophilus influenzae* (negative control), lane 12 water only (negative control). (Right) PCR products from primer set 2: molecular weight marker, lanes 2-4 *M. smegmatis* mc^2 155 (negative control), lanes 5-7 *ΔMSMEG4722* (1238bp), lanes 8-10 *ΔMSMEG4722*-C (1238bp), lane 11 Non-typeable *Haemophilus influenzae* (negative control) and lane 12 water only (negative control).

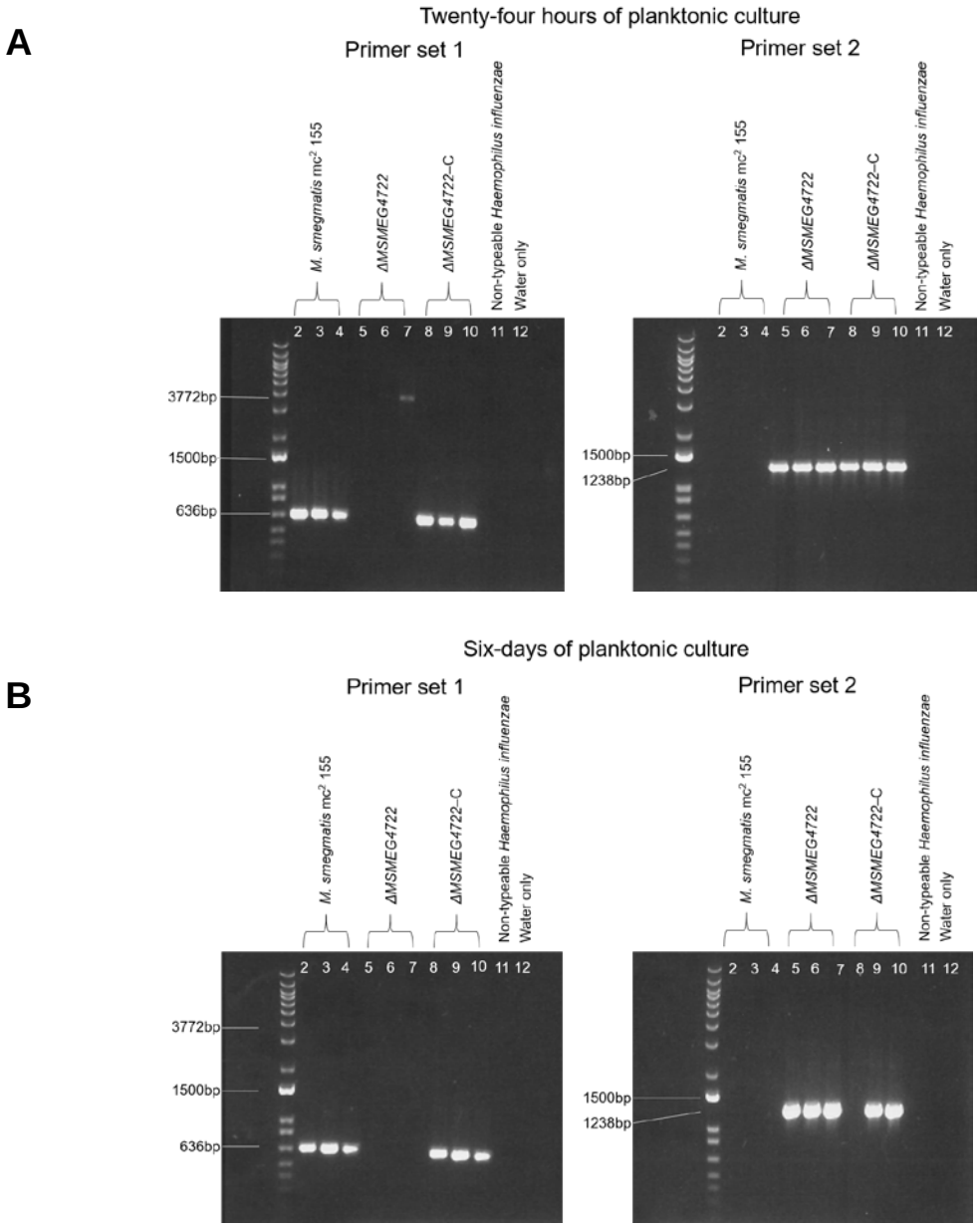


Figure 3.11: Stability of *ΔMSMEG4722* and *ΔMSMEG4722*-C after planktonic culture without selective antibiotics.

Confirmation of *M. smegmatis* mc^2 155, *ΔMSMEG4722* and *ΔMSMEG4722*-C stability without selective antibiotics after (A) Twenty-four hours of planktonic culture and (B) Six-days of planktonic culture using PCR and gel electrophoresis on a 1% TAE agarose gel. (Left) PCR products from primer set 1: molecular weight marker, lanes 2-4 *M. smegmatis* mc^2 155 (636bp), lanes 5-7 *ΔMSMEG4722* (3772bp), lanes 8-10 *ΔMSMEG4722*-C (636bp), lane 11 Non-typeable *Haemophilus influenzae* (negative control), lane 12 water only (negative control). (Right) PCR products from primer set 2: molecular weight marker, lanes 2-4 *M. smegmatis* mc^2 155 (negative control), lanes 5-7 *ΔMSMEG4722* (1238bp), lanes 8-10 *ΔMSMEG4722*-C (1238bp), lane 11 Non-typeable *Haemophilus influenzae* (negative control) and lane 12 water only (negative control).

In DNA extracted from pellicle biofilm biomass, using primer set 1, *M. smegmatis* mc^2 155 and *ΔMSMEG4722*-C showed the 636bp band corresponding to the wild-type gene. *ΔMSMEG4722* showed the 3772bp band corresponding to the deletion of *MSMEG4722* and the presence of the *SacB-Hyg*^{R} cassette. The 3772bp band was not present in *ΔMSMEG4722*-C (Figure 3.12A). Using primer set 2, no band was present in *M. smegmatis* mc^2 155. Both *ΔMSMEG4722* and *ΔMSMEG4722*-C showed the 1238bp band complementary to the residual 86bp from the start of the *MSMEG4722* gene and the *SacB* gene of the *SacB-Hyg*^{R} cassette, confirming the knockout of *MSMEG4722* (Figure 3.12B).

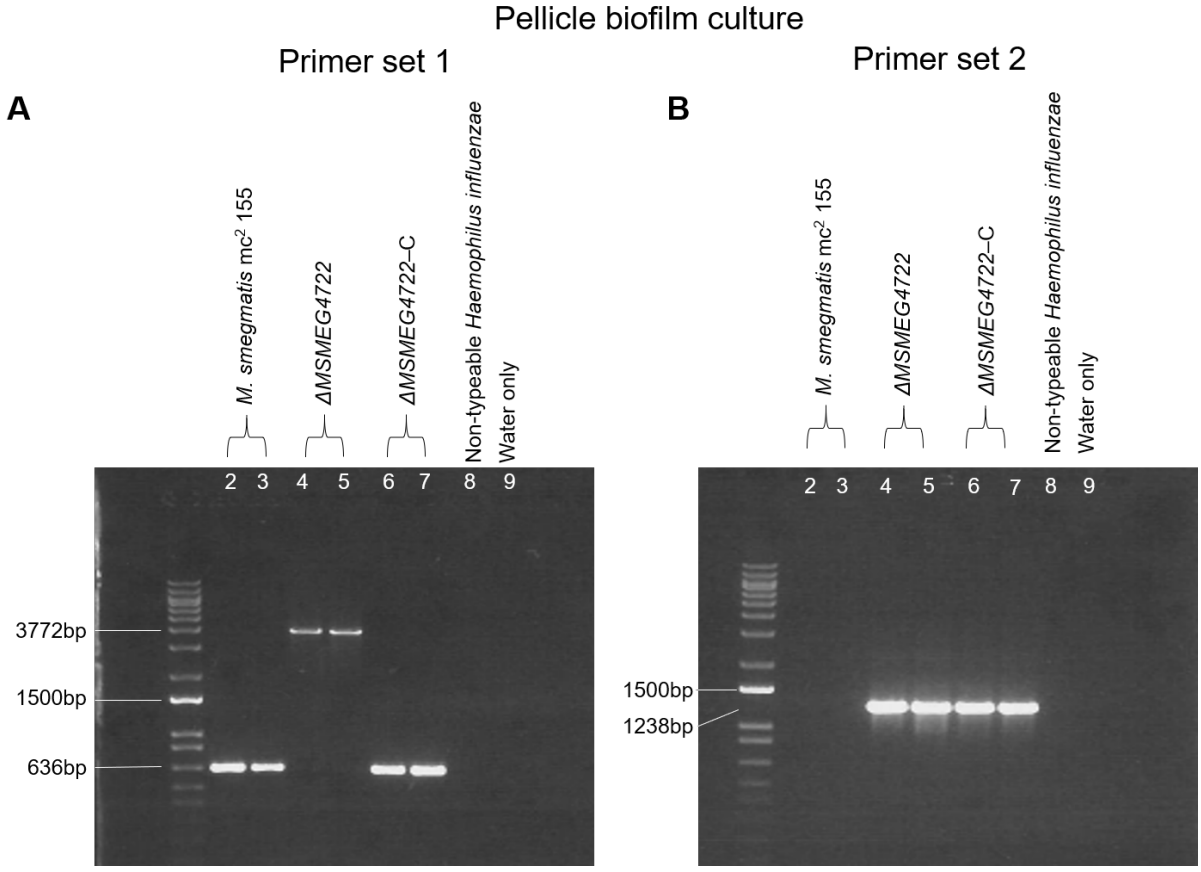


Figure 3.12: Stability of *ΔMSMEG4722* and *ΔMSMEG4722*-C after pellicle biofilm culture without selective antibiotics.

Confirmation of *M. smegmatis* mc^2 155, *ΔMSMEG4722* and *ΔMSMEG4722*-C after pellicle biofilm culture in Sauton's 40 without the presence of selective antibiotics using PCR and gel electrophoresis on a 1% TAE agarose gel. (A) PCR products from primer set 1: molecular weight marker, lanes 2-3 *M. smegmatis* mc^2 155 (636bp), lanes 4-5 *ΔMSMEG4722* (3772bp), lanes 6-7 *ΔMSMEG4722*-C (636bp), lane 8 Non-typeable *Haemophilus influenzae* (negative control) and lane 9 water only (negative control). (B) PCR products from primer set 2: Molecular weight marker, lanes 2-3 *M. smegmatis* mc^2 155 (negative control), lanes 4-5 *ΔMSMEG4722* (1238bp), lanes 6-7 *ΔMSMEG4722*-C (1238bp), lane 8 Non-typeable *Haemophilus influenzae* (negative control) and lane 9 water only (negative control).

3.2.5 *ΔMSMEG4722* pellicle biofilms produce significantly less biomass than *M. smegmatis* mc^2 155

After confirming the stability of *ΔMSMEG4722* and *ΔMSMEG4722*-C during planktonic and pellicle biofilm culture, *M. smegmatis* mc^2 155, *ΔMSMEG4722,* and *ΔMSMEG4722*-C pellicle biofilms were cultured without selective antibiotics to

determine the effect of losing mature mycolic acids for mycolic acid intermediates on pellicle biofilm formation.

Three independent pellicle biofilm cultures of either *M. smegmatis* mc^2 155, *ΔMSMEG4722 a*nd *ΔMSMEG4722*-C were set up (methods section 7.1). Each condition consisted of 8-16 technical replicates (independent pellicle biofilm formed in a well of a 24-well plate). Pellicle biofilm formation was assessed using microscopy and quantifying biomass with crystal violet (methods section 7.5).

ΔMSMEG4722 could not form a mature pellicle biofilm as observed for *M. smegmatis* mc^2 155 and *ΔMSMEG4722*-C, instead forming a thin film interspersed with bacterial aggregates (Figure 3.13A). *ΔMSMEG4722* pellicle biofilms produced significantly less biomass compared to *M. smegmatis* mc^2 155 and *ΔMSMEG4722*-C ($Ab595_{nm}$ 2-3 for *ΔMSMEG4722* compared to 4-6 for *M. smegmatis* mc^2 155 and *ΔMSMEG4722*-C) (both $P < 0.0001$) (Figure 3.13B).

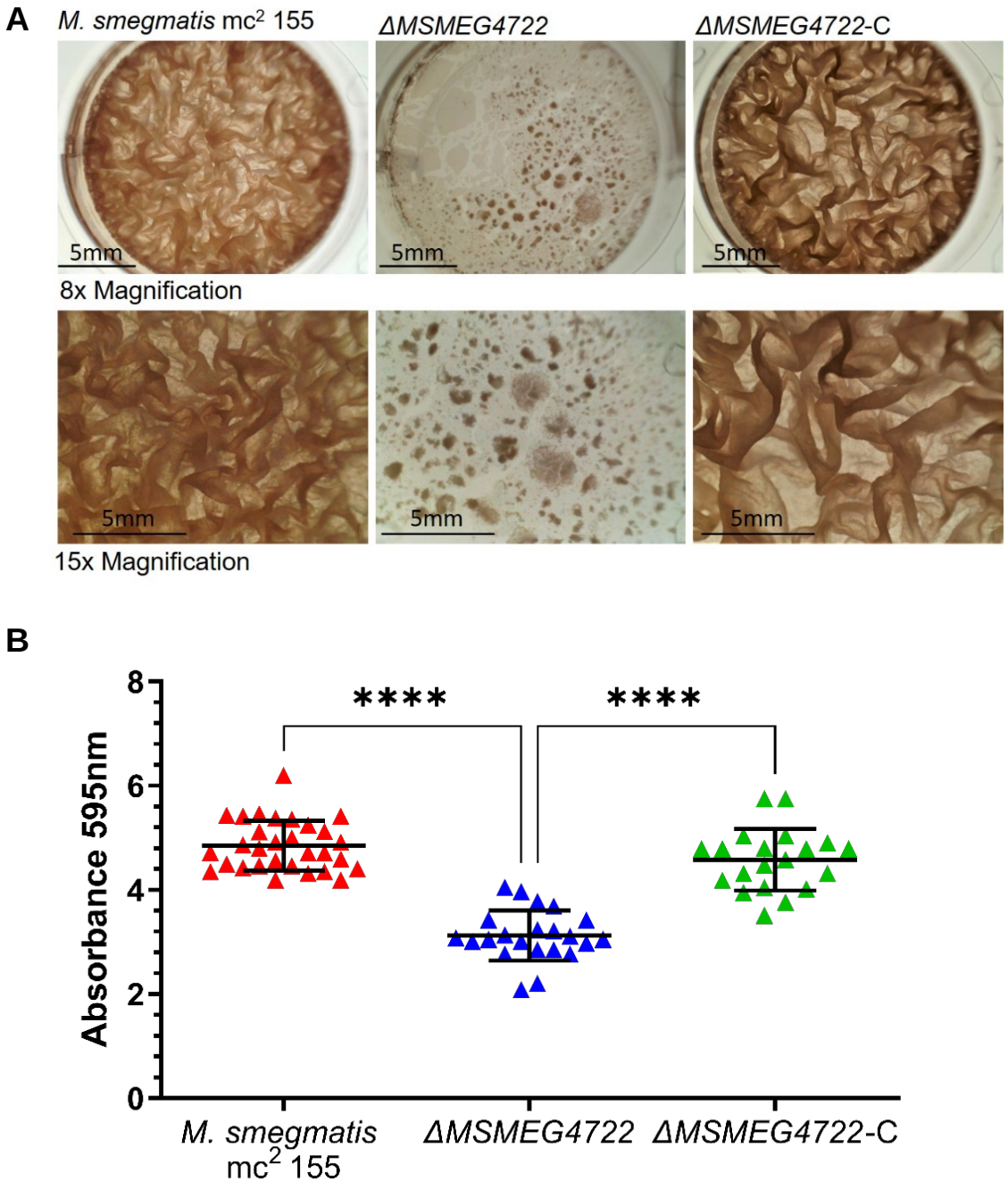


Figure 3.13: *M. smegmatis* mc² 155, *ΔMSMEG4722* and *ΔMSMEG4722*-C pellicle biofilm formation.

(A) Representative microscopic photographs of pellicle biofilms at 8x and 15x magnification. (B) Crystal violet biomass quantification (measured at an absorbance of 595_{nm}) for *M. smegmatis* mc² 155 (red), *ΔMSMEG4722* (blue) and *ΔMSMEG4722*-C (green). Three independent biological replicates containing 8-16 technical replicates (independent pellicle biofilms formed in a well of a 24-well plate). Error bars = standard deviation. Statistical analysis was performed by log10 transforming the data and performing a one-way ANOVA, **** $P < 0.0001$.

3.2.6 *ΔMSMEG4722* pellicle biofilm formation visually diverges from day one of culture

To determine at which stage phenotypically *ΔMSMEG4722* pellicle biofilm development diverges from *M. smegmatis* mc^2 155 and *ΔMSMEG4722*-C, seven 24-well plates were inoculated (methods section 7.1) and sacrificially imaged over a six-day time course of pellicle biofilm development. Sacrificial imaging prevented altering the aeration of the plates over the time course.

By visual inspection, *ΔMSMEG4722* diverges from *M. smegmatis* mc^2 155 and *ΔMSMEG4722*-C during the early stage of pellicle biofilm development. By day one of culture, a thin film develops with bacterial aggregates for all three strains, but for *ΔMSMEG4722,* only the bacterial aggregates cluster near the centre of the well. By day two of culture, *M. smegmatis* mc^2 155 and *ΔMSMEG4722*-C, as well as having bacterial aggregates, start to form ridges compared to *ΔMSMEG4722,* where aggregation has increased across the whole film. Between days 3-6 of culture, *M. smegmatis* mc^2 155 and *ΔMSMEG4722*-C develop reticulation and ridging, but for *ΔMSMEG4722,* the pellicle biofilm remains as large clusters of bacterial aggregates. By day five and six of culture, *M. smegmatis* mc^2 155 and *ΔMSMEG4722*-C pellicle biofilms had sunk below the air-liquid interface in the well, obscuring the pellicle biofilms from clear imaging (Figure 3.14).

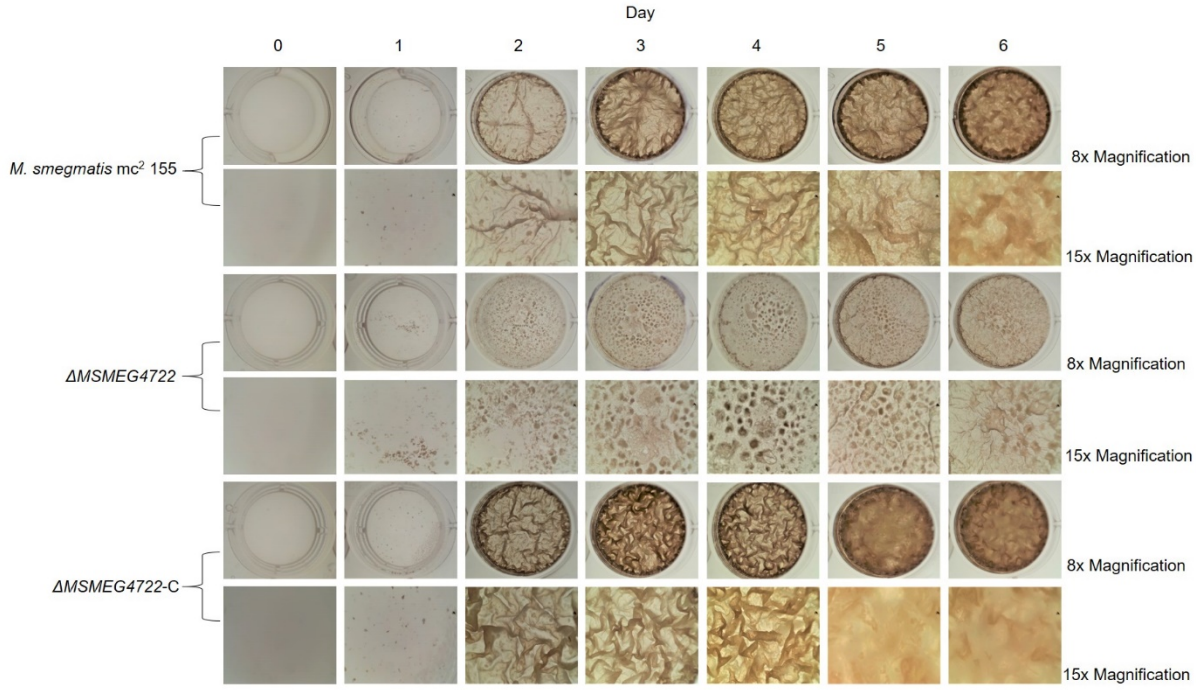


Figure 3.14: Imaging pellicle biofilm development over time.

Seven independent 24-well plates were inoculated with *M. smegmatis* mc^2 155, *ΔMSMEG4722* and *ΔMSMEG4722*-C in Sauton's 40 and one was microscopically imaged each day from inoculation to day six. Representative microscopic photographs of pellicle biofilms at 8x and 15x magnification.

3.2.7 *ΔMSMEG4722* pellicle biofilms do not mature and reticulate after prolonged incubation

To determine whether *ΔMSMEG4722* were delayed in pellicle biofilm formation, three biological replicates of either *M. smegmatis* mc^2 155, *ΔMSMEG4722* and *ΔMSMEG4722*-C were cultured, static at 37ºC in Sauton's 40 for sixteen days (methods section 7.1).

Increasing the incubation period did not result in *ΔMSMEG4722* forming reticulated pellicle biofilms as still observed for *M. smegmatis* mc^2 155 and *ΔMSMEG4722*-C, which had developed from a creamy colour to amber, still with the characteristic reticulation and ridging observed for mature pellicle biofilms. *ΔMSMEG4722* pellicle

biofilm formation remained as a film as seen after six days of culture but interspersed with large filamentous bacterial aggregates and small dark spots of aggregation (Figure 3.15).

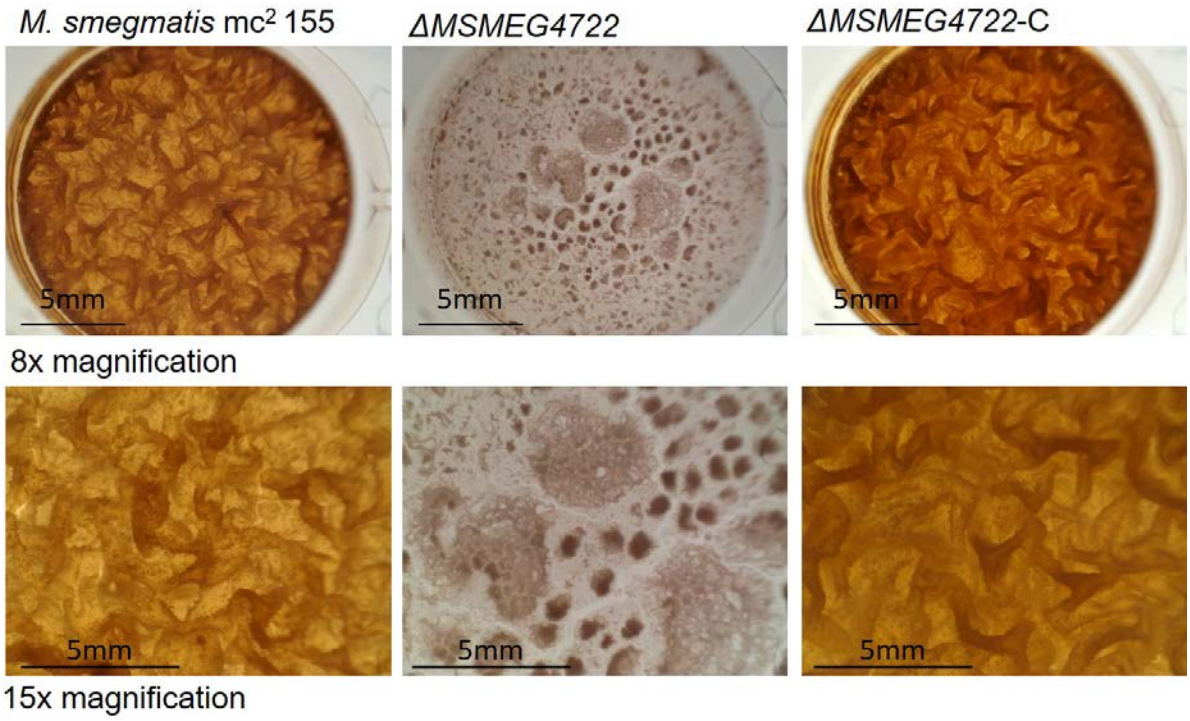


Figure 3.15: Prolonged pellicle biofilm development of *M. smegmatis* mc² 155, *ΔMSMEG4722* and *ΔMSMEG4722*-C.

Pellicles were imaged after sixteen days of incubation. Representative microscopic photographs of pellicle biofilms at 8x and 15x magnification.

3.2.8 Scanning Electron Microscopy to determine the topographical characteristics of *M. smegmatis* mc² 155, *ΔMSMEG4722* and *ΔMSMEG4722*-C shaking planktonic cultures and pellicle biofilms

To image the overall structure of shaking planktonic cultures and pellicle biofilms in microscopic detail, Scanning Electron Microscopy (SEM) was performed on planktonic cultures and the air and liquid interfaces of pellicle biofilms (Figure 3.16) for *M. smegmatis* mc² 155, *ΔMSMEG4722* and *ΔMSMEG4722*-C (methods section 7.23).

SEM was performed by Howard Tolley and Katherine Davies, Electron Microscopy Department, PHE-Porton.

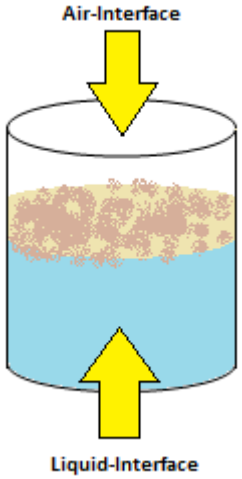


Figure 3.16: Schematic of an *M. smegmatis* pellicle biofilm on the air-liquid interface in a well.

3.2.8.1 Planktonic *ΔMSMEG4722* are more dispersed than *M. smegmatis* mc^2 155

Imaging the planktonic cultures by SEM, *M. smegmatis* mc^2 155 and *ΔMSMEG7422*-C bacteria primarily formed small clumps with a small number of holes/channels and a low quantity of visible extracellular material (ECM) (bacterial outlines still visible), but bacteria also exist as singular entities in the culture. *ΔMSMEG4722* formed fewer clumps and instead appeared under SEM as a sheet of bacteria with again a low amount ECM (Figure 3.17 and Figure 3.18).

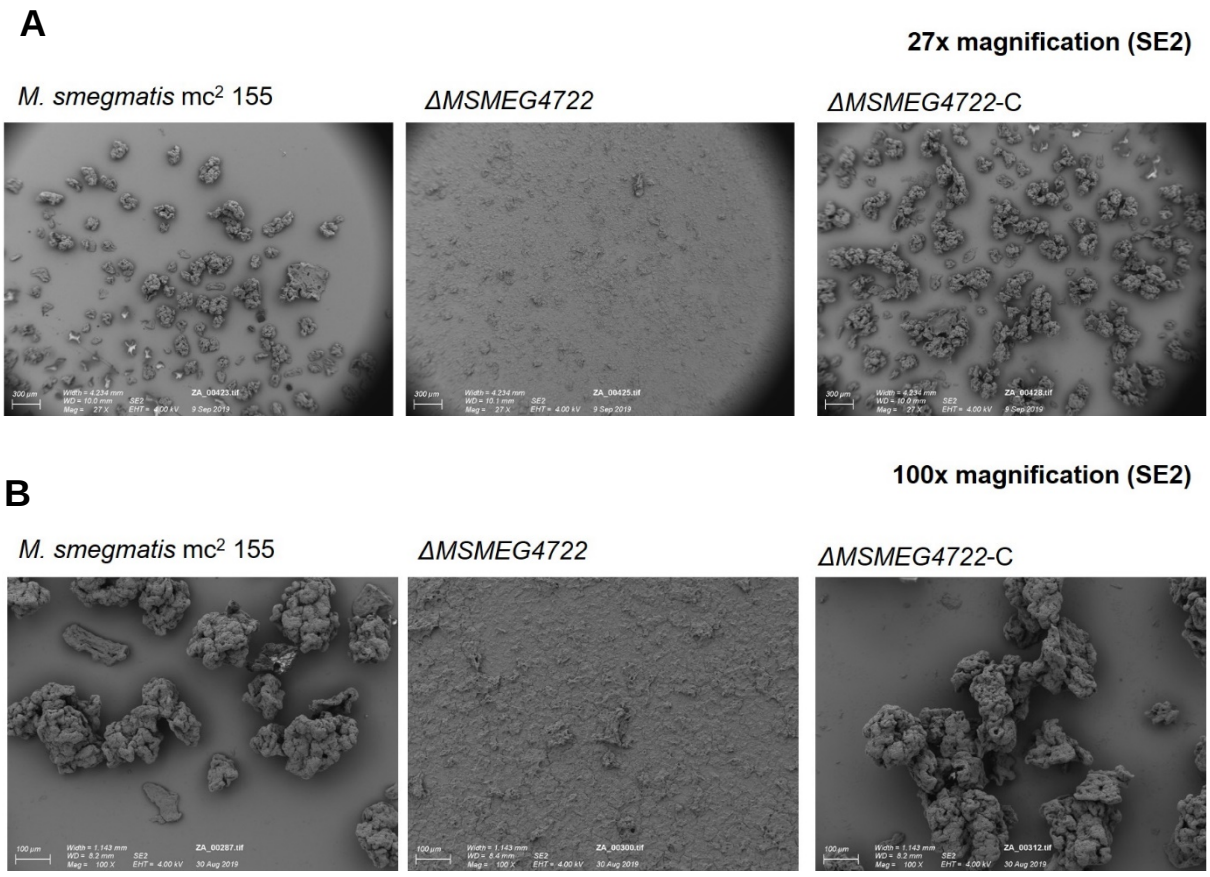


Figure 3.17: Scanning electron micrographs of shaking planktonic culture *M. smegmatis* mc² 155, *ΔMSMEG4722* and *ΔMSMEG4722*-C.

Samples prepared by air drying. (A) 27x magnification and (B) 100x magnification.

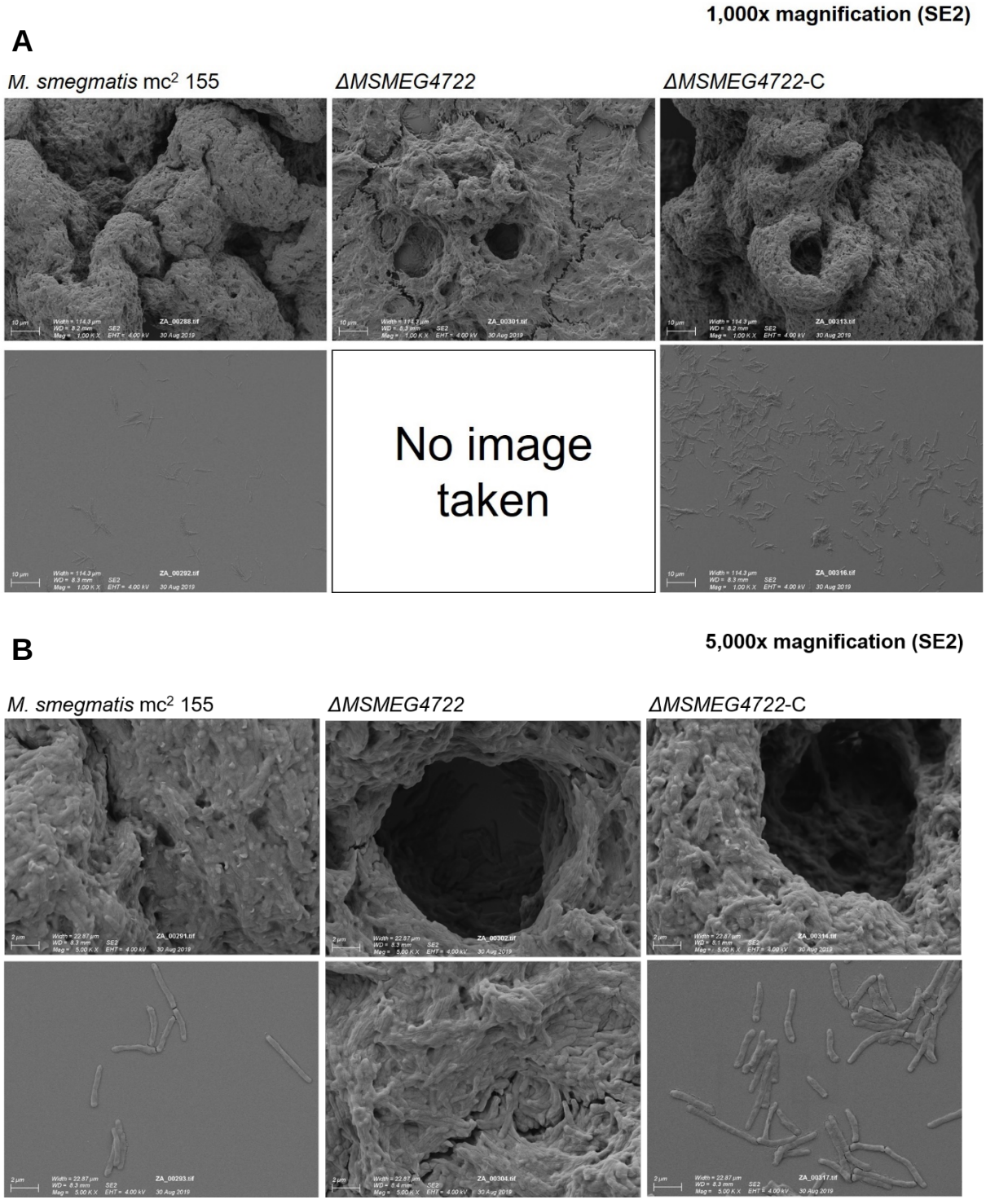


Figure 3.18: Scanning electron micrographs of shaking planktonic culture *M. smegmatis* mc² 155, *ΔMSMEG4722* and *ΔMSMEG4722*-C.

Samples prepared by air drying. (A) 1,000x magnification and (B) 5,000x magnification.

3.2.8.2 *ΔMSMEG4722* pellicle biofilms are significantly flatter with less extracellular material

SEM analysis of *M. smegmatis* mc^2 155, *ΔMSMEG7422* and *ΔMSMEG7422*-C pellicle biofilms' air-interfaces show that all three strains form a sheet of confluent growth, but *ΔMSMEG4722* is flat compared to *M. smegmatis* mc^2 155 and *ΔMSMEG7422*-C that have ridge-like interfaces with tendril projections. For all three strains, there is significant ECM present, so it was not possible to determine whether the bacteria were arranged pole-to-pole or as an un-orientated mass. At the liquid-interface for *M. smegmatis* mc^2 155 and *ΔMSMEG7422*-C, a ridged structure covered in ECM is present with holes/channels, but no tendrils were visible. For *ΔMSMEG7422,* there was minimal ECM, and the bacteria clusters form an interwoven cord-like structure with holes/channels (Figure 3.19 and Figure 3.20).

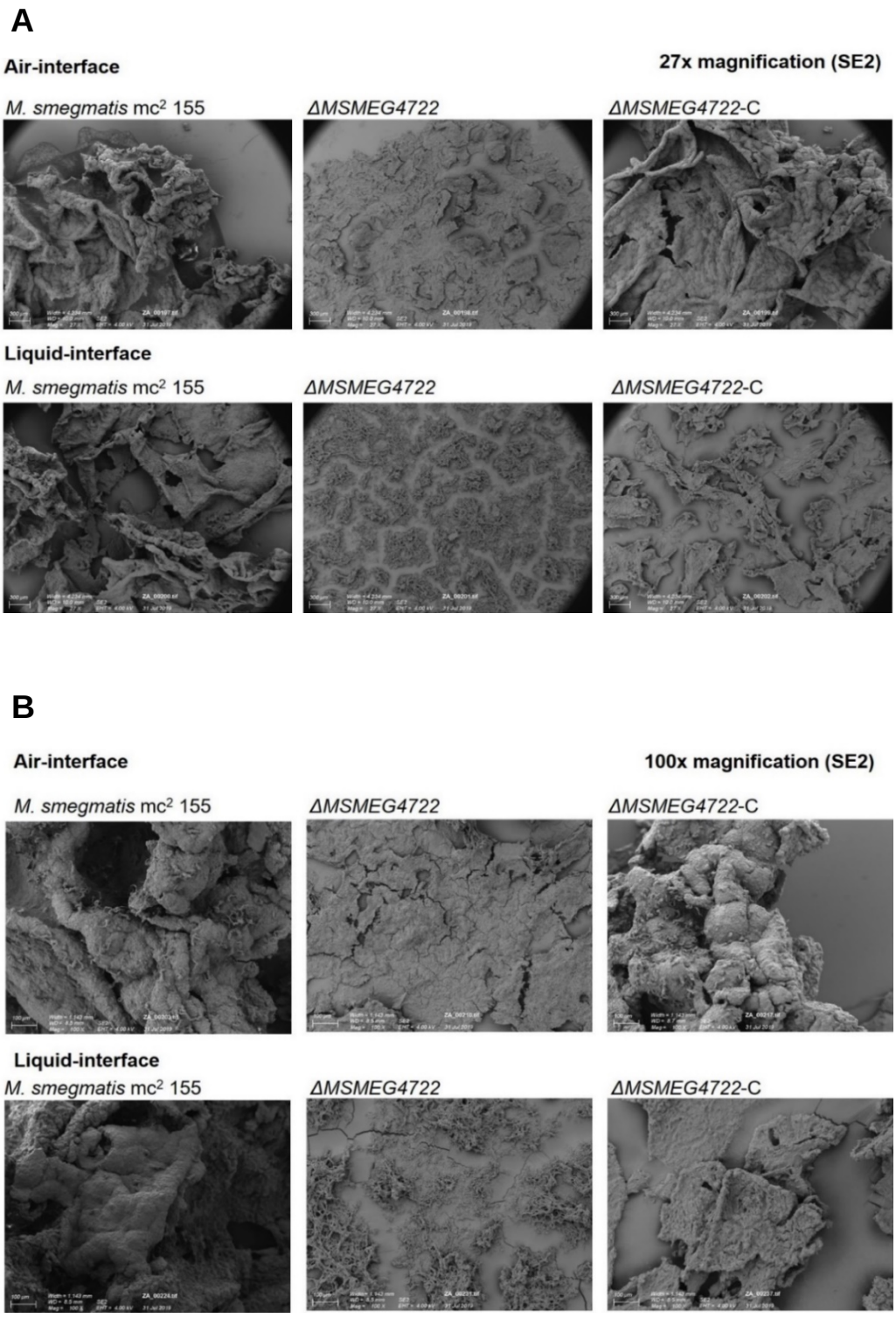


Figure 3.19: Scanning electron micrographs of air- and liquid-interface pellicle biofilms of *M. smegmatis* mc² 155, *ΔMSMEG4722* and *ΔMSMEG4722*-C.

Samples prepared by air drying. (A) 27x magnification and (B) 100x magnification.

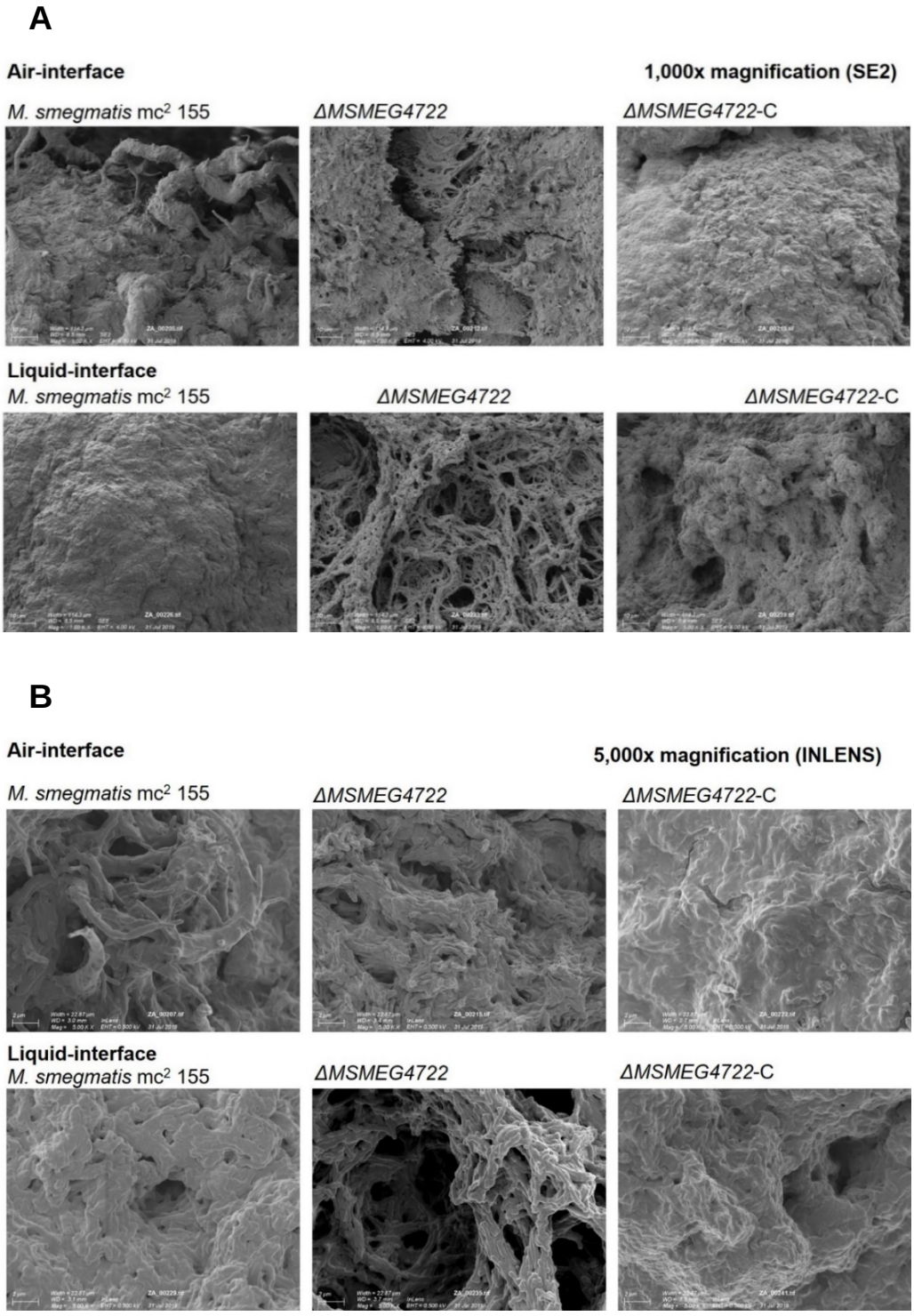


Figure 3.20: Scanning electron micrographs of air- and liquid-interface pellicle biofilms of *M. smegmatis* mc² 155, *ΔMSMEG4722* and *ΔMSMEG4722*-C.

Samples prepared by air drying. (A) 1,000x magnification and (B) 5,000x magnification.

3.3 Discussion

3.3.1 Pellicle biofilm development is inhibited in *ΔMSMEG4722*

At 30ºC, *M. smegmatis* pellicle biofilms grow as a uniform film over days 1-3, ridging and troughing begins at day four, and maturation is complete by day seven (Ojha *et al.*, 2005). Under the culture conditions of this thesis, including incubation at 37ºC, *M. smegmatis* mc^2 155 maturation appears to be accelerated, with ridging and troughing appearing by day two and phenotypic maturation appearing complete between days 4-5. Culture at 37ºC may better represent *in situ* conditions within cavities in the lungs, where biofilm-like structures have been observed (Nyka, 1963, 1967; Hunter *et al.*, 2006; Chakraborty *et al.*, 2021).

M. smegmatis mc^2 155 formed a thin film with bacterial aggregates on the air-liquid interface before reticulating, whereas *ΔMSMEG4722* continued to build up bacterial aggregates on a thin film and did not reticulate even under a prolonged incubation. *MSMEG4722* is the furthest gene along the mycolic acid biosynthesis pathway (Marrakchi, Lanéelle and Daffé, 2014). Losing the reduction of the β-oxo to a hydroxyl group on the mycolic motif inhibits pellicle biofilm maturation.

3.3.1.1 The inability to progress past surface aggregation could be an inability to accumulate unreduced free mycolate

In the wider literature, an inability to progress to reticulation has been observed for mutants with gene knockouts in the FAS I and FAS II pathway involved in the *de novo* synthesis and elongation of fatty acids prior to condensation and reduction of the mycolic motif (Marrakchi, Lanéelle and Daffé, 2014). The mutants display either

alterations to total mycolate content or changes to the ratio of mycolate subclasses within the cell wall (Ojha *et al.*, 2005; Jamet *et al.*, 2015; Lefebvre *et al.*, 2018).

GroEL is a Hsp60 chaperone protein proposed to be involved in the transition from early biofilm formation to maturation via regulating mycolic acid synthesis through association to kasA, a component of the FAS-II complex. Up to day three of culture, phenotypically, the *ΔGroEL* mutant aggregated on the air-liquid interface comparable to *M. smegmatis* mc^2 155, but development diverged from days 4-7 failing to reticulate. TLC analysis showed that the biosynthesis of all mycolates was reduced, but only under pellicle biofilm conditions. This is proposed to be through the destabilisation of GroEL interactions with kasA. Using MS, from day four of biofilm culture, *ΔGroEL* failed to increase production of shorter chain mycolic acids (C_{56}–C_{68} chains) from long-chain mycolic acids (C_{70} to C_{90}), which was observed in the wild-type strain. These shorter chain mycolic acids are predicted to correspond to short-chain mycolates or meromycolate precursors of α-mycolates (Ojha *et al.*, 2005).

KasA is involved in both condensation and elongation steps of meromycolate extension. KasA overexpression alters mycolate content, with a reduction in α'-mycolate and an increase in α- and epoxy-mycolates (Kremer *et al.*, 2002). When cultured as a pellicle biofilm, the KasA overexpression strain showed a delayed pellicle biofilm development but had comparable reticulation by day seven (Ojha *et al.*, 2005).

inhA is an enoyl-acyl carrier protein reductase proposed to be involved in the processing of fatty acids between FAS I and FAS II. A thermal sensitive mutant could not produce mycolates and accumulated FAS I end products (Vilchèze *et al.*, 2000).

ΔInhA could aggregate and form a thin layer at the air-liquid interface, but was unable to reticulate after seven days of culture (Ojha *et al.*, 2005).

The dehydratases of FAS-II, HadA, HadB and HadC, form heterodimers (HadA-HadB, HadB-HadC). HadA and HadC are proposed to bind substrates, and HadB provides catalytic activity. HadB (*MSMEG4341*) is an essential gene in *M. smegmatis* and *M. tuberculosis*. A *ΔHadC* mutant (*MSMEG4342*) displayed an inability to produce mature pellicle biofilm formation after four days producing aggregates only on the air-liquid interface. After seven days of culture, the pellicle biofilm was phenotypically thinner and less reticulated compared to *M. smegmatis* mc^2 155. A *ΔHadA* mutant (*MSMEG4340*) produced a poorly reticulated pellicle biofilm at days four and seven. When a double mutant was assessed *(ΔHadAC*), no aggregation was observed at day four and at day seven, *ΔHadAC* had developed a thin pellicle biofilm with minimal reticulation. The authors propose that *ΔHadA* exacerbates the *ΔHadC* phenotype in *ΔHadAC*. Lipids from stationary phase Middlebrook 7H9 cultures showed Δ*HadA* had a comparable mycolate profile to *M. smegmatis* mc^2 155, but *ΔHadC* displayed a decrease in epoxy-mycolates and the appearance of an unknown mycolate. Analysed by MALDI-TOF/MS, the unknown mycolate appeared to have lost the mycolic motif. Mycolate profiles from pellicle biofilms were not explored (Jamet *et al.*, 2015). Neither mutants nor complemented strains produced fully reticulated pellicle biofilms akin to *M. smegmatis* mc^2 155. Another dehydratase mutant, *ΔHadD* (*MSMEG0948),* displayed minimal aggregation on the air-liquid interface after six days, and complementation did not restore reticulation. From Middlebrook 7H9 cultured bacteria, the mycolic acid lipid content remained constant compared to wild-type, but TLC and MALDI-TOF/MS demonstrated the mutant only produced α'-mycolic acids. The change

affected all mycolates in the cell wall, including those esterified to trehalose (Lefebvre *et al.*, 2018).

In *M. smegmatis* all mycolate subclasses appear to contribute to pellicle biofilm development. For *ΔMSMEG4722*, mycolate production should not be reduced or the ratio of mycolate subclasses altered, as the mutation affects the terminal stage of mycolate production. The inability to progress past surface aggregation could be an inability to accumulate unreduced free mycolate.

3.3.1.2 Failure to reticulate could be related to the mycolate change in other mycolate-containing cell wall components

Mutants without altered mycolate classes but alterations to other mycolate-containing lipids can also not form pellicle biofilms (Chen *et al.*, 2006; Pacheco *et al.*, 2013). Characterisation of an lsr2 mutant (*MSMEG8444*), a gene of unknown function, saw the loss of two apolar lipid spots by TLC analysis. MS identified these as mycolyl-diacylglycerols (MDAGs), in which a mycolic acid (α- or α′-mycolate) is esterified to glycerol. The *Δlsr2* mutant could not produce pellicle biofilms on the air-liquid interface, hypothesised due to a loss in cell surface hydrophobicity (Chen *et al.*, 2006). A mutant of the mmpL11 transporter had delayed pellicle biofilm development that could not fully reticulate over prolonged culture. By SEM of the pellicle biofilm (air-interface), the ECM of *ΔmmpL11* was reduced compared to *M. smegmatis* mc^2 155. They did not observe a change in profile to the free mycolates or GPLs by TLC and MS, but they did observe the loss of monomeromycolyl diacylglycerols (MMMDAGs) and mycolate ester wax (Pacheco *et al.*, 2013).

3.3.1.3 Failure to reticulate could be influenced by structural changes to mycolates

M. tuberculosis mycolic acid mutants demonstrate chemical modifications to meromycolate chains provide a structural contribution in biofilm formation. *mmA3* is involved in the biosynthesis of methoxy-mycolates, the primary mycolate of *M. tuberculosis* pellicle biofilms. In an *ΔmmA3* mutant, pellicle biofilm reticulation was only slightly reduced compared to *M. tuberculosis.* This was also observed when knocking out the gene *pcaA,* involved in the synthesis of α-mycolates. In contrast, knocking out *mmA4,* a gene involved in the synthesis of both methoxy- and keto-mycolates (a minor free mycolate), inhibited pellicle biofilm formation (Sambandan *et al.*, 2013). In *M. tuberculosis,* methoxy-, keto- and hydroxy-mycolates are oxygenated in the distal portion of the meromycolate chain, and α-mycolates are not (Marrakchi, Lanéelle and Daffé, 2014). Sambandan *et al.*, (2013) propose that the stable 'W' folding of keto-mycolates is essential for pellicle biofilm development by providing organisation of the mycobacterial outer membrane and the free electrons on the oxygen moiety could anchor other cell wall components during pellicle biofilm development.

M. smegmatis mc^2 155 contain different mycolate subclasses to *M. tuberculosis*, oxygenated epoxy-mycolates and non-oxygenated α- and α'-mycolates (Marrakchi, Lanéelle and Daffé, 2014) with all three mycolates mycolic motifs affected in *ΔMSMEG4722*. When performing sodium borohydride reduction of delipidated *ΔMSMEG4722* cells where arabinogalactan esterified mycolates are still present, Bhatt *et al.*, (2008) observed that sodium borohydride access was restricted to epoxy mycolates. The author's hypothesis that epoxy-mycolates may fold in a 'W' conformation similar to oxygenated mycolates of *M. tuberculosis* and *M. bovis* BCG

and the hydroxyl group on the mycolic motif may not be essential for 'W' folding. Whether epoxy mycolates can form a 'W' conformation is still to be elucidated.

The results of this study show that mycolate maturation is important for pellicle biofilm formation but cannot distinguish if a single mycolate subclass is a deciding factor for pellicle biofilm development. Even if the mycolates are 'folded' correctly, losing the mature mycolic motif could result in the bacterial cell walls inability to organise into a structure that allows the interactions of free oxygens on the epoxy-meromycolate chain to interact with other cell wall components facilitating pellicle biofilm formation, as suggested by Sambandan *et al.*, (2013) for keto-mycolates. It would be interesting to identify and knockout the genes involved in specific mycolate production in *M. smegmatis* to determine the importance of oxygenated mycolates in *M. smegmatis* mc^2 155 pellicle biofilm formation.

3.3.2 *ΔMSMEG4722* pellicle biofilms produce less extracellular material

Using both SEM and crystal violet staining, a fundamental reduction in biomass present in *ΔMSMEG4722* compared to *M. smegmatis* mc^2 155 pellicle biofilms was observed, along with a changed overall topographical structure of the *ΔMSMEG4722* pellicle biofilms. Visually this could be attributed to the loss of ECM, especially apparent on the liquid-interface. To the best of my knowledge, the liquid-interface of *M. smegmatis* pellicle biofilms has not been imaged previously. A phenotypic difference is also observed between the strains cultured under planktonic conditions, with *M. smegmatis* mc^2 155 and *ΔMSMEG4722*-C forming small clumps, compared to *ΔMSMEG4722* which remained as single bacteria even without the presence of a

detergent in the culture medium. The loss of clumping of mutant strains where mycolic acids are affected has previously been reported in growth curves and sedimentation experiments (Jamet *et al.*, 2015; Lefebvre *et al.*, 2018; Chen *et al.*, 2020).

Pellicle biofilms formed on the air-liquid interface have opposing nutrient gradients (from the liquid-interface) and oxygen gradients (from the air-interface) (Sochorová *et al.*, 2014). Using SEM, due to these gradients, more holes/ channels on the liquid-interfaces of *M. smegmatis* mc^2 155 and *ΔMSMEG4722*-C were expected compared to the air-interfaces, but this was not apparent with the SEM images taken. The air-interfaces were more ridged, which could be a developmental process to increase surface area for oxygen diffusion, as observed for *P. aeruginosa* biofilms (Dietrich *et al.*, 2013), or a technical implication of how the liquid-interfaces were exposed (by gently pressing down a sticky carbon disk onto the air-interface). For the *ΔMSMEG4722* mutant, there is a contrast between the two interfaces; the air-interface was relatively flat with a small amount of ECM, compared to the liquid interface, which was also relatively flat, but the bacteria were visible as an interwoven cord-like structure with holes and channels. A reduction in ECM on the air-interface of *ΔmmpL11* was previously observed. The mutant lost MMMDAGs and mycolate ester wax (Pacheco *et al.*, 2013).

3.3.3 The growth rate of *ΔMSMEG4722* and *ΔMSMEG4722*-C was comparable to *M. smegmatis* mc^2 155

A change in the culture characteristics of *ΔMSMEG4722* compared to *M. smegmatis* mc^2 155 had been observed by Bhatt *et al.*, (2008). In TSB liquid culture, “a slightly slower growth rate than the parental mc^2 155 strain; the OD_{600} values at 24h

correspond to 2 × 10^8 and 10^7 colony forming units mL^{-1} for mc^2 155 and *ΔMSMEG4722*, respectively" was observed. Although cultured in a different medium, the TVC analysis agrees that *ΔMSMEG4722* enters and remains in stationary phase at around 1 log_{10} CFU mL^{-1} lower than *M. smegmatis* mc^2 155, but was restored by complementation of the *MSMEG4722* gene. The significant difference in OD measurements between *ΔMSMEG4722 and M. smegmatis* mc^2 155 seen in this chapter (again restored by complementation of *MSMEG4722*) were not reported by Bhatt *et al*., (2008), which could be attributed to previous OD readings being plotted as $log10OD600_{nm}$. Despite a 1 log_{10} CFU mL^{-1} reduction in growth by stationary phase, the doubling times, calculated from the exponential growth phase, were comparable between all three strains by both $OD540_{nm}$ and TVC.

OD measurements rely on cell size, sedimentation and light scattering (Peñuelas-Urquides *et al.,* 2013). With the homologue gene knockout strain *of C. glutamicum ΔNCgl2385*, Lea-Smith *et al.,* (2007) observed smaller colonies when grown on a solid medium. Bhatt *et al.,* (2008) observed that *ΔMSMEG4722* colonies had irregular convoluted surfaces compared to the smooth surfaces of *M. smegmatis* mc^2 155 when cultured on TSB ± Tween-80. This may be due to the changes observed in mycolate-containing cell wall components, as the lipid spots had altered TLC mobilities (Bhatt *et al.,* 2008). Lipids constitute up to 40% of mycobacterial dry cell envelope weight and mycolic acids; unbound, esterified to mAGP and as a constituent of glycolipids, are the most abundant components (Marrakchi, Lanéelle and Daffé, 2014). A small change to the most abundant cell wall components could alter the characteristics fundamental for OD measurements, resulting in a substantial drop in $OD540_{nm}$ readings of *ΔMSMEG4722* compared to *M. smegmatis* mc^2 155.

3.4 Technical Discussion

3.4.1 Culturing planktonic cells and pellicle biofilms with selective antibiotics

Selective antibiotics had an overall inhibitory effect in Middlebrook 7H9 cultures and pellicle biofilm cultures of *ΔMSMEG4722* and *ΔMSMEG4722*-C. *ΔMSMEG4722*-C cultured with kanamycin saw a drop in CFU mL^{-1} compared to antibiotic-free culture and by $OD540_{nm}$ had a slightly delayed growth curve profile, despite a comparable doubling time. *ΔMSMEG4722,* although phenotypically comparable, had decreased biomass when cultured as a pellicle biofilm with hygromycin. *ΔMSMEG4722*-C expresses a kanamycin resistance cassette via the pMV261 plasmid, but the presence of antibiotic in Sauton's 40 pellicle biofilm culture completely inhibits pellicle biofilm formation. For the complementation of *ΔHadC* and *ΔHadD*, the selective antibiotics kanamycin (37.5µg mL^{-1}) and gentamycin (5µg mL^{-1}) were present in the Sauton's pellicle biofilm media. This may be why poor phenotypic complementation was observed for both. *ΔHadC*-C was complemented with a plasmid containing a kanamycin resistance cassette, and was able to produce a poorly reticulated pellicle biofilm on the air-liquid interface, but *ΔHadD*-C which was complemented with a plasmid containing a gentamycin resistance cassette barely aggregated on the air-liquid interface (Jamet *et al.*, 2015; Lefebvre *et al.*, 2018). The inability to complement the gene loss may not be due to the complementation itself, but the culture of pellicle biofilms with selective antibiotics. The presence of selective antibiotics should be considered when interpreting the pellicle biofilm-forming capabilities of mutants.

3.4.2 Limitations of Middlebrook 7H9 growth analysis for comparing planktonic and pellicle biofilm culture

This thesis explores in chapter 5 the specific interactions of human complement system proteins with pellicle biofilms, which is compared to exponential phase shaking cultures (planktonic) grown in the same medium. For planktonic cultures' growth rates, a second growth curve would ideally have been performed in the same minimal media as used to culture pellicle biofilms; Sauton's 40. As observed by SEM, *M. smegmatis* mc^2 155 planktonic cultures in Sauton's 40 produced cellular clumps, whereas *ΔMSMEG4722* was a homogeneous culture, so $OD540_{nm}$ and TVC readings over a time course would have been incomparable between the strains. Including a detergent in the culture could have broken up the cellular clumps, but their presence inhibits biofilm formation (Kulka, Hatfull and Ojha, 2012). As Tween-80 can be utilised as a carbon source by providing oleic acid after hydrolysation (de Carvalho *et al.*, 2010), its addition would be a conflicting variable in any comparisons between planktonic cultures and pellicle biofilms. The use of nutrient-rich Middlebrook 7H9 + 10% OADC + 0.05% Tween-80 allowed us to characterise the *ΔMSMEG4722* mutant growth rate compared to *M. smegmatis* mc^2 155 and identify the exponential phase as between 15-24 hours for both strains. This was then extrapolated to planktonic culture in Sauton's 40. Culturing the planktonic cultures until the late exponential phase observed in the nutrient-rich culture (24-hours) was due to Sauton's 40 being a minimal media with an additional reduction in glycerol from 6% to 4% based on pellicle biofilm development observed in chapter 2.

4 Analysis of the outermost lipids of planktonic and pellicle biofilm *ΔMSMEG4722*

4.1 Introduction

4.1.1 Summary of progress in earlier chapters

In chapter 3, *ΔMSMEG4722* was demonstrated to have a similar growth rate to *M. smegmatis* mc^2 155. However, viable counts plateaued at a lower level of 1 log CFU mL^{-1} and had a significantly lower optical density when entering stationary phase in Middlebrook 7H9 culture. When cultured as pellicle biofilms, *M. smegmatis* mc^2 155 produced robust, reticulated pellicles on the air-liquid interface. In comparison, *ΔMSMEG4722* formed a flat thin layer interspersed with bacterial aggregates. The mutant also grew differently as planktonic culture, forming a homogeneous culture instead of small bacterial aggregates observed for *M. smegmatis* mc^2 155.

4.1.2 The lipid profile of *ΔMSMEG4722* in liquid culture

Characterising esterified mycolates from *ΔMSMEG4722* grown in TSB using Thin Layer Chromatography (TLC), Bhatt *et al.*, (2008) observed the loss of alpha (α)-, alpha prime (α')- and epoxy-mycolic acid methyl esters (MAMEs). MAMEs were replaced by a product with a higher retardation factor migrating above the fatty acid methyl esters (FAMEs). Using MALDI-TOF/MS and ^{1}H-NMR, this product resolved to be composed of unsaturated long-chain ketones. These are the degradation products of α-alkyl, β-oxo mycolate intermediates/ pre-mycolates (mycolic acid intermediates). When *ΔMSMEG4722* underwent alkaline hydrolysis, mycolate precursors produced unstable β-oxo acids. Through spontaneous decarboxylation, unstable β-oxo acids lose carbon dioxide to produce unsaturated long-chain ketones. The replacement of mature

mycolates for the mycolic acid intermediates (observed by the presence of unsaturated ketones on TLC graphs) was also observed in the outer cell envelope for free mycolic acids (FMA), trehalose dimycolate (TDM) and trehalose monomycolate (TMM), with mycolate-containing lipids having altered mobilities in *ΔMSMEG4722.* The loss of the *MSMEG4722*-encoded β-keto mycolate reductase affects the biosynthesis of all mycolates throughout the cell envelope (Bhatt *et al.*, 2008). The lipid profile of *ΔMSMEG4722* pellicle biofilms has not been evaluated previously.

4.1.3 Analyses of the lipid profiles of mycobacterial pellicle biofilms

M. smegmatis and *M. tuberculosis* pellicle biofilm lipid profiles have been described briefly previously. A hallmark of pellicle biofilm formation observed for *M. smegmatis,* and *M. tuberculosis* is the accumulation of FMA (Ojha *et al.*, 2008, 2010). Methoxy- and α-mycolate are the most abundant component of *M. tuberculosis* pellicle biofilms (Ojha *et al.*, 2008). However, the ability of *M. tuberculosis* pellicles to fully reticulate is dictated by the presence of oxygenated keto-mycolates (Sambandan *et al.*, 2013), which make up around 10% of pellicle FMA (Ojha *et al.*, 2008). For *M. tuberculosis,* a decrease in triacylglycerols (TAG) in pellicles at five weeks of growth has been observed (Ojha *et al.*, 2008). TDM concentrations extracted from clinical *M. tuberculosis* isolates cultured as pellicle biofilms are positively associated with spreading on the air-liquid interface and reticulation (Arora *et al.*, 2016).

For *M. smegmatis* TDM production decreased in early pellicle biofilm development between days 2-4, hypothesised to be due to cleavage of newly synthesised TDM to produce FMA by a cutinase-like serine carboxylesterase (*MSMEG1529*). Total TDM between 4-day pellicle biofilms and planktonic bacteria was comparable. Another lipid

change observed by TLC analysis in *M. smegmatis* pellicle biofilms was an increase in TAG compared to planktonic cultures (Ojha *et al.*, 2010).

4.1.4 TLC solvent systems to characterise lipids

A series of solvent systems to resolve the range of lipids found in the mycobacterial cell envelope into distinct lipid species has been developed based on increasing polarity (methods section 7.17, Table 7.6) (Dobson *et al.*, 1985; Habermehl, 2012). There is no comprehensive lipid profile established for *M. smegmatis* cultured in Middlebrook 7H9. There is also no comprehensive lipid profile established for planktonic cultures or pellicle biofilms cultured in Sauton's medium. Annotations of solvent-extractable cell wall lipid fractions (outer apolar, inner apolar, polar and FAMEs and MAMEs) characterised in detail are primarily based on *M. tuberculosis* (Table 4.1) (Dobson *et al.*, 1985; Besra, 1998), and this has been used as a basis to annotate the TLC plates in this chapter.

Table 4.1: Mycobacterial lipid profile using the solvent system combinations

1) Solvent systems developed by Dobson *et al.,* (1985) (A-D) and FAMEs and MAMEs (Habermehl, 2012). Solvent systems A-D are 2D-TLC. FAMEs and MAMEs is a 1D-TLC system. 2) Stains: MPA = Molybdophosphoric acid (visualises alkylated lipids) and α-naphthol (visualises carbohydrate containing lipids).

Solvent system[1]	Lipid fraction tested/stain	Selection of mycobacterial lipids observed in *M. tuberculosis*
A	Outer apolar and inner apolar (MPA[2])	Menaquinones Phthiocerol dimycocerosates Triacylglycerols
B	Outer apolar and inner apolar (MPA)	Trehalose mycolipenates
C	Outer apolar and inner apolar (MPA)	Glycosyl phenolphthiocerols Free fatty acids, including Free mycolic acids
D	Outer apolar, inner apolar and polar (MPA and α-naphthol)	Trehalose dimycolate Sulpholipids
FAMEs and MAMEs	FAMES and MAMES (MPA)	Esterified mycolic acids Esterified fatty acids

4.1.5 Aims

Applying Thin-layer chromatography to extracted lipid fractions, this chapter aims to:

1) Build on previous work by confirming the lipid profile of *ΔMSMEG4722* in optimal liquid culture conditions (Middlebrook 7H9). Extracted lipid fractions will be used in downstream analyses to determine the impact of altered cell wall lipids on host-pathogen interactions, specifically complement, in chapter 5.

2) Expand the lipid profile analyses to compare planktonic cultures and pellicle biofilms. *ΔMSMEG4722* and *M. smegmatis* mc^2 155 phenotypes will be compared to understand the effect of altered cell wall lipids on planktonic culture and pellicle biofilm formation. Extracted lipid fractions will be used in downstream analyses to

determine the impact of pellicle biofilm growth on complement activation in chapter 5.

4.1.6 Hypotheses

1) Compared to *M. smegmatis* mc^2 155, *ΔMSMEG4722* will display an altered lipid profile when cultured in Middlebrook 7H9. Specifically, cell wall bound and trehalose conjugated mycolates will be altered in the mutant (consistent with previously published findings when cultured in TSB (Bhatt *et al.,* (2008)).

2) Pellicle biofilm *M. smegmatis* mc^2 155 will have a distinct lipid profile to planktonic *M. smegmatis* mc^2 155, grown in an identical minimal medium (Sauton's 40). Differences in phenotypic lipid profiles observed in *M. smegmatis* mc^2 155 will be altered between planktonic and pellicle biofilm *ΔMSMEG4722*.

3) Free mycolic acid (FMA) accumulation will be observed in *M. smegmatis* mc^2 155 pellicle biofilms compared to planktonic cells. *ΔMSMEG4722* pellicles will not accumulate unsaturated ketones (decarboxylated mycolic acid intermediates/ pre-mycolates).

4.2 Results

Representative TLC plates are shown in this chapter stained with Molybdophosphoric acid (MPA) to visualises alkylated lipids or α-naphthol to visualise carbohydrate containing lipids. All TLC solvent system analyses (A to FAMEs and MAMEs) of the lipid fractions tested with three biological replicates are appendix 2 Figure A.2.1-Figure A.2.12 when comparing *M. smegmatis* mc^2 155, *ΔMSMEG4722* and *ΔMSMEG4722*-C. TLCs of three biological replicates for *M. smegmatis* mc^2 155, *ΔMSMEG4722* and *ΔMSMEG4722*-C planktonic and pellicle biofilm lipid comparisons are appendix 2 Figure A.2.13-Figure A.2.25.

4.2.1 Analysis of apolar, polar and FAMEs and MAMEs lipids comparing *M. smegmatis* mc^2 155 and *ΔMSMEG4722*

Three independent biological replicates of *M. smegmatis* mc^2 155, *ΔMSMEG4722* and *ΔMSMEG4722*-C were grown in Middlebrook 7H9 supplemented with OADC, Tween-80 and the appropriate selective antibiotics (methods section 7.1). From dried, heat-inactivated biomass (methods section 7.3), solvent-extractable lipid fractions; outer apolar, inner apolar and polar lipids, were extracted as described in methods sections 7.16.1-7.16.3. Esterified FAMEs and MAMEs were extracted as described in methods section 7.16.4. Lipid fractions were analysed by one dimensional (1D) or two dimensional (2D)-TLC using a range of solvent systems and were stained with either MPA (visualises alkylated lipids) or α-naphthol (visualises carbohydrate containing lipids) as described in methods section 7.17. Densitometry analysis of lipid spots present at a high enough concentration on TLC plates was performed as described in methods section 7.18.

ΔMSMEG4722-C had comparable TLC lipid profiles and densitometry analysis to *M. smegmatis* mc^2 155 throughout. A summary of all lipid changes between *M. smegmatis* mc^2 155 and *ΔMSMEG4722* in each lipid fraction can be found at the end of section 4.2.1. The results below focus on mycolates and changes in cell wall glycolipids with known immunomodulatory effects (Spargo *et al.*, 1991; Borders *et al.*, 2005; Axelrod *et al.*, 2008; Dao *et al.*, 2008; Welsh *et al.*, 2008; Ishikawa *et al.*, 2009).

4.2.1.1 *ΔMSMEG4722* has unreduced free mycolic acid intermediates that replace mature free mycolic acids

The outer and inner apolar lipid fractions were analysed using solvent system A and stained with MPA (Figure 4.1A). Present in *ΔMSMEG4722,* but not *M. smegmatis* mc^2 155 was a spot identified previously by Bhatt *et al.*, (2008) as unsaturated ketones. Unsaturated ketones are the decarboxylation products of free mycolic acid intermediates/ pre-mycolates with an altered TLC migration profile due to the loss of a hydroxyl group for a β-oxo group on the mycolic motif. Unsaturated ketones are present at a significantly lower density in the inner apolar lipid fraction compared to the outer apolar lipid fraction (P = 0.001) (Figure 4.1B).

When the outer apolar lipid fractions were analysed using solvent system C and stained with MPA (Figure 4.2), FMA was present in *M. smegmatis* mc^2 155 and not *ΔMSMEG4722.* However, FMA was not present in the inner apolar lipid fraction of *M. smegmatis* mc^2 155.

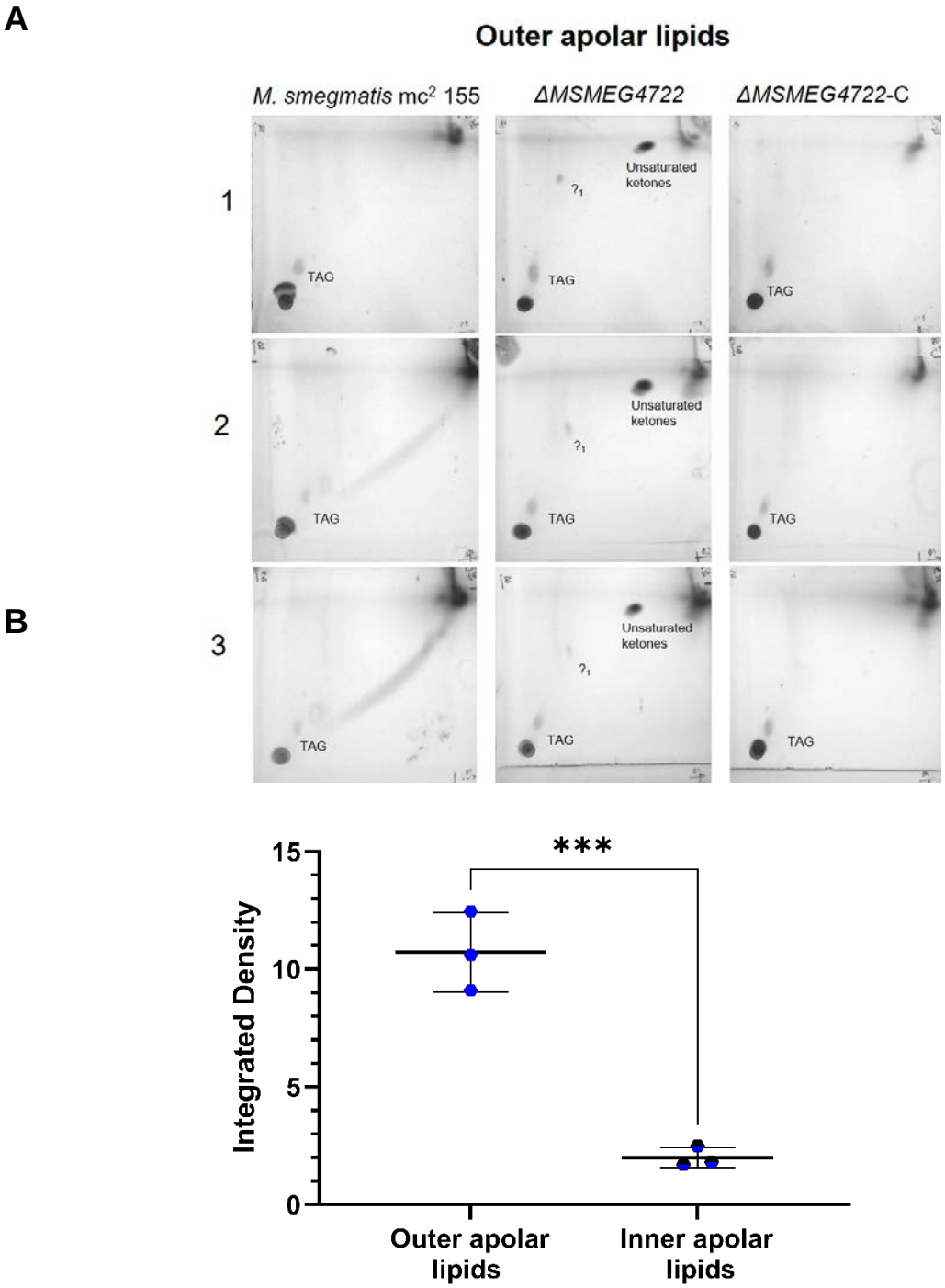


Figure 4.1: Outer and inner apolar lipid analysis of *M. smegmatis* mc² 155, *ΔMSMEG4722* and *ΔMSMEG4722*-C (solvent system A).

(A) Representative 2D-TLC plates of outer and inner apolar lipid fractions. Developed in petroleum ether 60-80ºC: ethyl acetate (98:2 v/v) x3 and petroleum ether 60-80ºC: acetone (98:2 v/v) x1 and stained with MPA. Triacylglycerol (TAG), unsaturated ketones, unidentified lipid 1 ($?_1$) unidentified lipid 2 ($?_2$). (B) Densitometry analysis of unsaturated ketones from *ΔMSMEG4722.* Densitometry was performed on three biological replicate lipid spots. Error bars = standard deviation. Statistical analysis by unpaired t-test, *** P = 0.001.

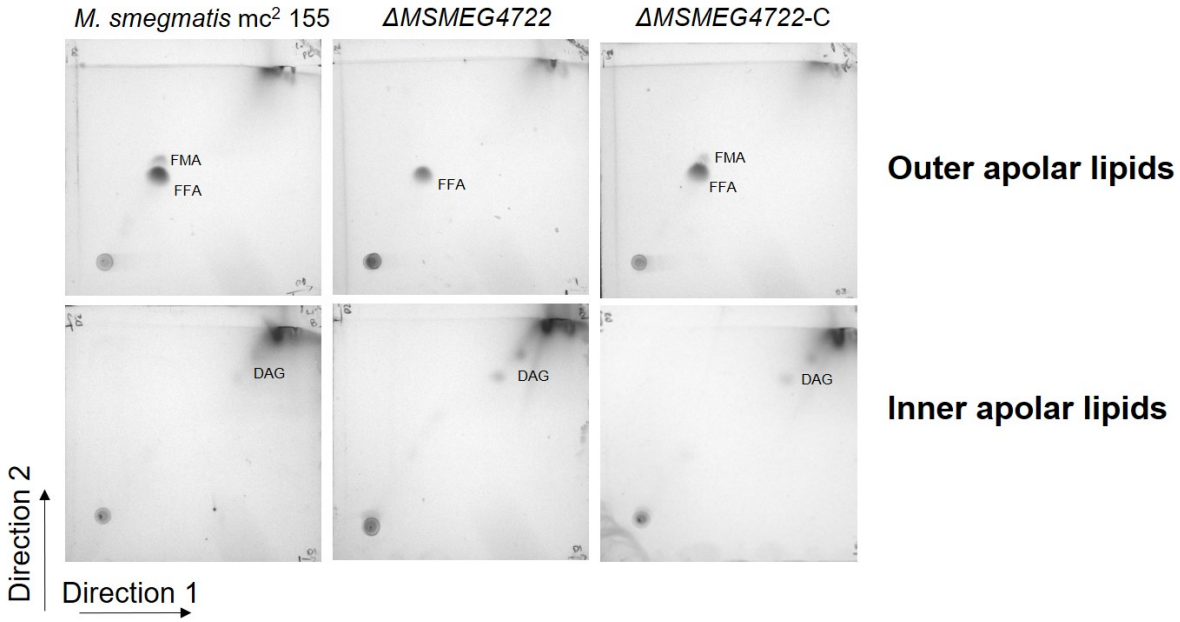


Figure 4.2: Outer and inner apolar lipid analysis of *M. smegmatis* mc² 155, *ΔMSMEG4722* and *ΔMSMEG4722*-C (solvent system C).

Representative 2D-TLC plates of outer and inner apolar lipid fractions. Developed in chloroform: methanol (96:4 v/v) x1 and toluene: acetone (80:20 v/v) x1 and stained with MPA. Free mycolic acids (FMA), free fatty acids (FFA), diacylglyceride (DAG).

4.2.1.2 TDM and GMM are present in *ΔMSMEG4722* in both the outer and inner apolar lipid fractions, but only the outer apolar lipid fraction of *M. smegmatis* mc² 155

The glycolipids were analysed in the outer and inner apolar lipid fractions using solvent system D and staining specifically for carbohydrate containing lipids with α-naphthol (Figure 4.3A).

In the outer apolar lipids, TDM, TMM and glucose monomycolate (GMM) were identified in both *M. smegmatis* mc² 155 and *ΔMSMEG4722*. TDM and GMM have altered mobilities in *ΔMSMEG4722* compared to *M. smegmatis* mc² 155 (Bhatt *et al.*, 2008). By densitometry analysis, there was significantly more TDM present in *ΔMSMEG4722* compared to *M. smegmatis* mc² 155 (P=0.0078) (Figure 4.3B).

TMM and GMM were too faint for densitometry. Visually, more TMM and GMM was present in *ΔMSMEG4722* compared to *M. smegmatis* mc^2 155. In *M. smegmatis* mc^2 155, a range of unidentified lipids migrate above GMM that is not present in *ΔMSMEG4722*.

For the inner apolar lipid fractions, TMM is present in both *M. smegmatis* mc^2 155 and *ΔMSMEG4722*. However, TDM and GMM were only present in *ΔMSMEG4722*, and TDM is present at a significantly lower density in the inner apolar lipid fraction compared to the outer apolar lipid fraction (P = 0.0039) (Figure 4.3C).

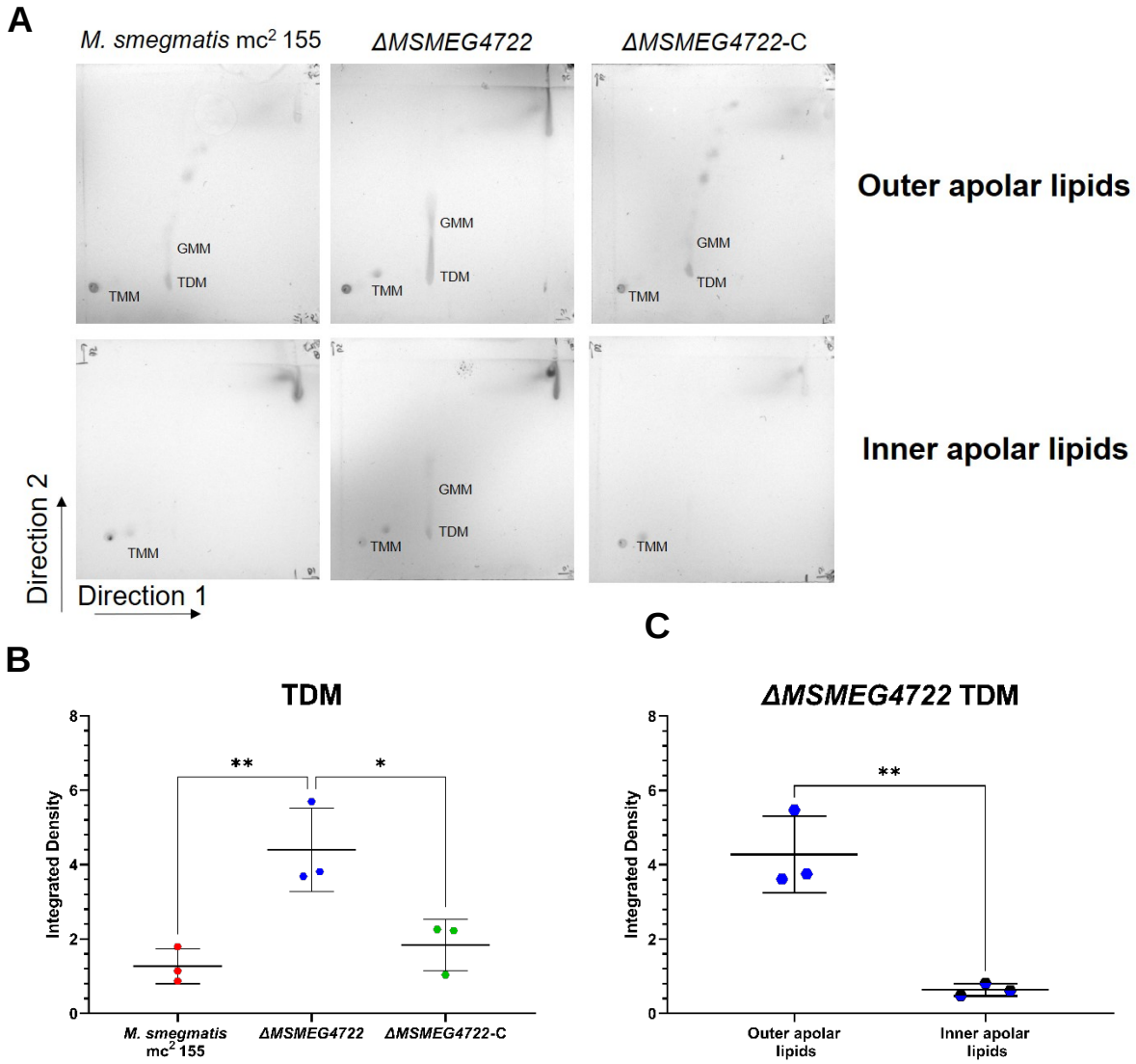


Figure 4.3: Outer and inner apolar lipid fraction analysis of *M. smegmatis* mc² 155, *ΔMSMEG4722* and *ΔMSMEG4722*-C (solvent system D).

(A) Representative 2D-TLC plates of the outer and inner apolar lipid fractions. Developed in chloroform: methanol: deionised water (100:14:0.8 v/v/v) x1 and chloroform: acetone: methanol: deionized water (50:60:2.5:3 v/v/v/v) x1 and stained with α-naphthol. Trehalose monomycolate (TMM), trehalose dimycolate (TDM), glucose monomycolate (GMM). Densitometry analysis of (B) TDM in the outer apolar lipid fractions of *M. smegmatis* mc² 155 (red), *ΔMSMEG4722* (blue) and *ΔMSMEG4722*-C (green) and (C) TDM in *ΔMSMEG4722* outer apolar and inner apolar lipid fractions. Densitometry performed on three biological replicate lipid spots. Error bars = standard deviation. Statistical analysis by (B) one-way ANOVA with Tukey's multiple comparison correction, * P = 0.0197, ** P = 0.0078, or (C) unpaired t-test, ** P = 0.0039.

4.2.1.3 No differences were observed in the polar lipid fractions

Examining the polar lipids using solvent system D and staining with α-naphthol (Figure 4.4), the only discernible lipid present is one unidentified lipid ($?_3$) present in both *M. smegmatis* mc^2 155 and *ΔMSMEG4722*, but at too low a concentration to perform densitometry analysis.

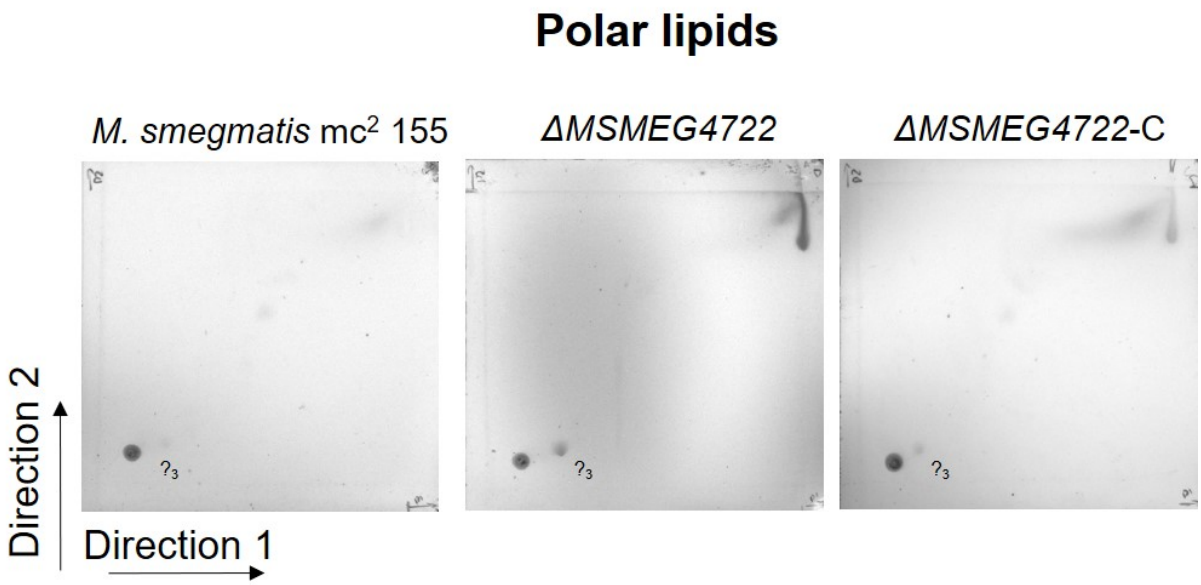


Figure 4.4: Polar lipid analysis of *M. smegmatis* mc^2 155, *ΔMSMEG4722* and *ΔMSMEG4722*-C (solvent system D)

Representative 2D-TLC plates of polar lipid fractions. Developed in chloroform: methanol: deionized water (100:14:0.8 v/v/v) x1 and chloroform: acetone: methanol: deionised water (50:60:2.5:3 v/v/v/v) x1 stained with MPA. Unidentified lipid 3 ($?_3$).

4.2.1.4 Mycolic acid intermediates were esterified to arabinogalactan in *ΔMSMEG4722,* replacing α, α' and epoxy mycolates

Esterified mycolic acids and fatty acids were extracted from the cell wall and analysed by 1D-TLC using a FAMEs and MAMEs specific solvent system and stained with MPA (Figure 4.5). In *M. smegmatis* mc^2 155, MAMEs resolved into α, α' and epoxy-

mycolates. In *ΔMSMEG4722*, a single lipid moved with the solvent front, previously identified by Bhatt *et al.*, (2008) as esterified unsaturated ketones.

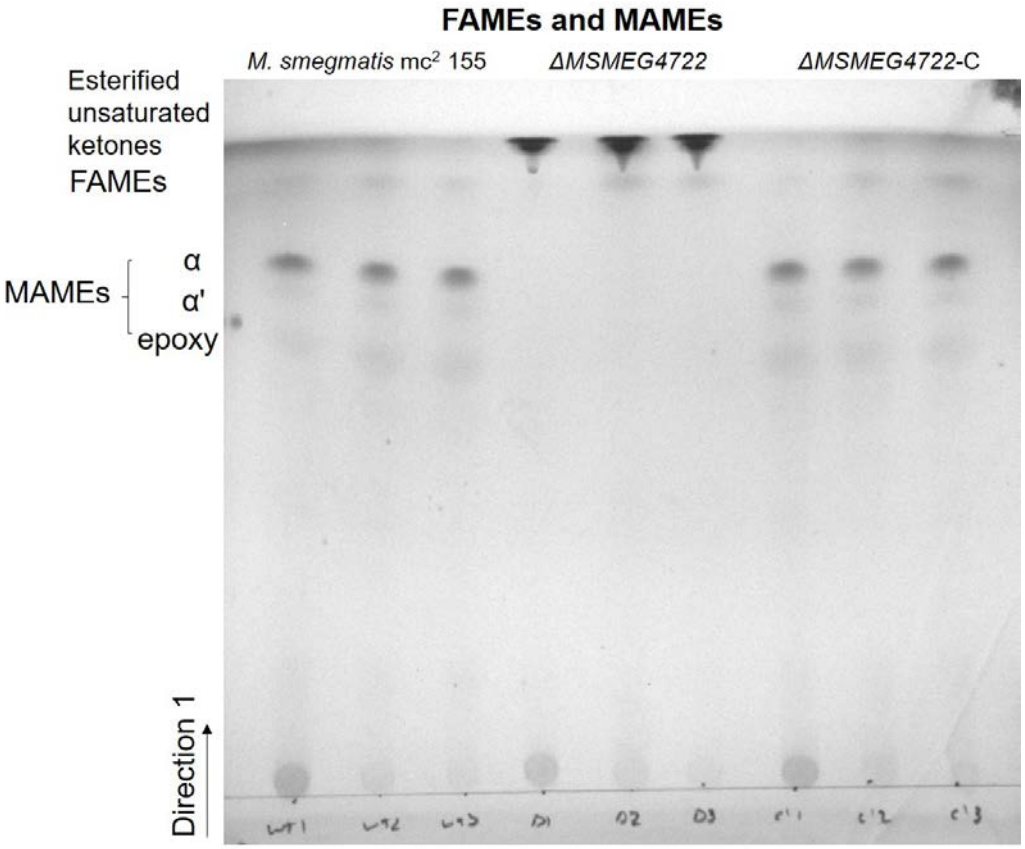


Figure 4.5: FAMEs and MAMEs analysis of *M. smegmatis* mc² 155, *ΔMSMEG4722* and *ΔMSMEG4722*-C.

1D-TLC plate of FAMEs and MAMEs. Developed in petroleum ether 60-80ºC: acetone (95:5 v/v) x3 and stained with MPA. Three independent biological replicates. Esterified unsaturated ketones, fatty acid methyl esters (FAMEs), Mycolic acid methyl esters (MAMEs); alpha (α), alpha prime (α') and epoxy.

Table 4.2: Changes to lipids in *ΔMSMEG4722* when *M. smegmatis* mc^2 155 is used as the control lipid profile.

Outer apolar lipids	***ΔMSMEG4722***
TAG	=^{ns}
FMA	WTO^1
Unsaturated ketones	ΔO^1
FFA	↓ p = 0.0473
TDM	↑ p = 0.0078
TMM	↑ ND
GMM	↑ ND
?$_1$	ΔO
Inner apolar lipids	
TAG	=^{ns}
DAG	=ND
FMA	WTO^1
Unsaturated ketones	ΔO^1
FFA	↓ ND
TDM	↑ ND
TMM	=ND
GMM	↑ ND
?$_2$	ΔO
Polar Lipids	
?$_3$	=ND
FAMEs and MAMEs	
MAMEs (α, α' and epoxy)	WTO^1
Esterified unsaturated ketones	ΔO^1
FAMEs	=ND
KEY ON NEXT PAGE	

ΔMSMEG4722-C is represented by *M. smegmatis* mc^2 155 as the complemented strain show comparable lipid profiles throughout TLC and densitometry analysis.

1. Expected lipid change in *ΔMSMEG4722*. Unsaturated ketones are decarboxylated α-alkyl, β-oxo mycolate intermediates/ pre-mycolates in *ΔMSMEG4722* that have an altered TLC migration profile due to the loss of a hydroxyl group for a β-oxo group on the mycolic motif (Bhatt *et al.*, 2008).

KEY	
WTO	Lipid present in *M. smegmatis* mc^2 155 only
ΔO	Lipid present in *ΔMSMEG4722* only
↑	More
=	Comparable
↓	Less
ND	Not concentrated enough for densitometry analysis. Symbol to the left (↑=↓) is a visual conclusion of lipid change.
ns	Densitometry was performed with no statistical difference.
P =	Densitometry performed, statistical p-value.

Lipids: triacylglycerols (TAG), free mycolic acid (FMA), unsaturated ketones, free fatty acid (FFA), TDM (trehalose dimycolate), TMM (trehalose monomycolate), glucose monomycolate (GMM), Mycolic acid methyl esters (MAMEs); alpha (α), alpha prime (α') and epoxy, esterified unsaturated ketones, fatty acid methyl esters (FAMEs).

4.2.2 Analysis of apolar, polar and FAMEs and MAMEs lipids comparing planktonic and pellicle biofilm cultures of *M. smegmatis* mc^2 155 and *ΔMSMEG4722*

M. smegmatis mc^2 155 planktonic and pellicle biofilm lipid profiles were compared to establish the differential expression of lipids between phenotypes. Then, the planktonic and pellicle biofilm lipid profiles of *ΔMSMEG4722* were compared to each other and their corresponding *M. smegmatis* mc^2 155 phenotypes to evaluate the effect of the mycolic motif alteration on planktonic and pellicle biofilm lipid profiles when cultured in minimal media.

Three independent biological replicates of *M. smegmatis* mc^2 155, *ΔMSMEG4722* and *ΔMSMEG4722*-C planktonic cells and pellicle biofilms were grown in Sauton's 40 (methods section 7.1), harvested, and evaporated to dryness (methods section 7.3). Lipid fractions; outer apolar, inner apolar, polar and FAMEs and MAMEs were extracted as described in methods sections 7.16.1-7.16.4. Lipid fractions were analysed by 1D- or 2D-TLC using a range of solvent systems and were stained with either MPA or α-naphthol as described in methods section 7.17. Densitometry analysis of lipid spots present at a high enough concentration on TLC plates was performed as described in methods section 7.18.

ΔMSMEG4722-C had comparable TLC lipid profiles and densitometry analysis to *M. smegmatis* mc^2 155 for both phenotypes. A summary of lipid changes in pellicle biofilms compared to planktonic cultures for both strains (Table 4.3) and changes between *ΔMSMEG4722* and *M. smegmatis* mc^2 155 for both phenotypes (Table 4.4) can be found in section 4.2.6.

The results below will focus on mycolates, which are a hallmark of pellicle biofilm formation, and cell wall glycolipids that have known immunomodulatory effects and may also play a role in pellicle biofilm formation (Middlebrook, Dubos and Pierce, 1947; Spargo *et al.*, 1991; Borders *et al.*, 2005; Hunter *et al.*, 2006; Hunter, Venkataprasad and Olsen, 2006; Axelrod *et al.*, 2008; Dao *et al.*, 2008; Welsh *et al.*, 2008; Ishikawa *et al.*, 2009).

4.2.2.1 *ΔMSMEG4722* pellicle biofilms accumulate unreduced free mycolate in the apolar lipid fractions

The outer and inner apolar lipid fractions were analysed using solvent system A and staining with MPA (Figure 4.6A). Unsaturated ketones (decarboxylated α-alkyl, β-oxo mycolate intermediates/ pre-mycolates) were not present in either phenotype of *M. smegmatis* mc^2 155. In *ΔMSMEG4722,* there was an accumulation of unsaturated ketones in pellicle biofilm compared to planktonic-derived lipids when analysed by densitometry for both lipid fractions ($P = 0.0038$ outer and $P = 0.032$ inner). Unsaturated ketones were present in both phenotypes at a lower density in the inner compared to outer apolar lipids ($P = 0.0141$ for planktonic and $P = 0.0019$ for pellicle biofilm) (Figure 4.6B).

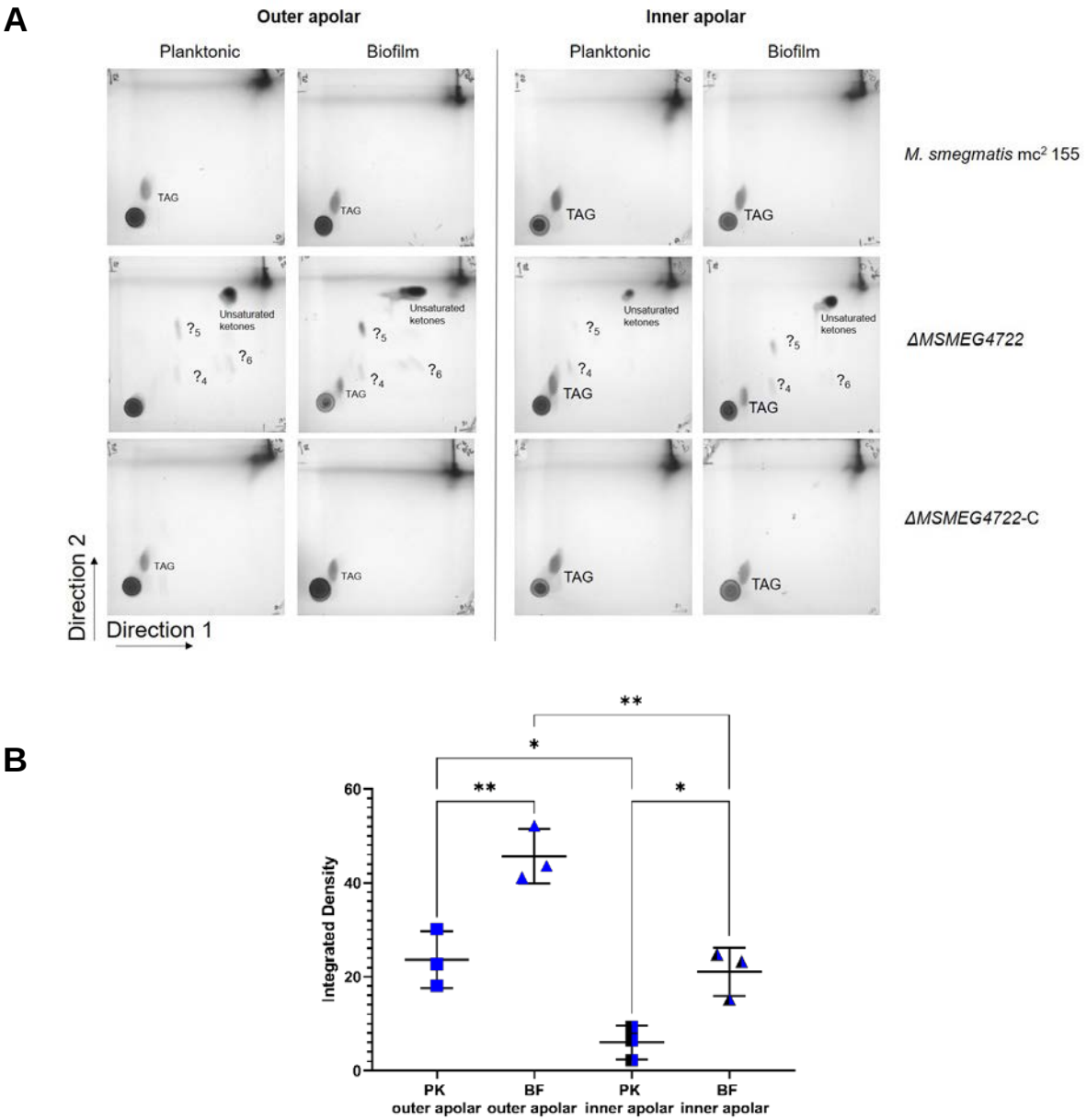


Figure 4.6: Outer and Inner apolar lipid analysis of planktonic and pellicle biofilm *M. smegmatis* mc² 155, *ΔMSMEG4722* and *ΔMSMEG4722*-C (solvent system A)

(A) Representative 2D-TLC plates of outer and inner apolar lipid fractions. Developed in petroleum ether 60-80ºC: ethyl acetate (98:2 v/v) x3 and petroleum ether 60-80ºC: acetone (98:2 v/v) x1 and stained with MPA. Triacylglycerol (TAG), Unsaturated ketones, unidentified lipid 4 ($?_4$), unidentified lipid 5 ($?_5$), unidentified lipid 6 ($?_6$). (B) Densitometry analysis of *ΔMSMEG4722* unsaturated ketones (both apolar lipid fractions). Planktonic (PK) (squares), pellicle biofilm (BF) (triangles). Densitometry performed on three biological replicate lipid spots. Error bars = standard deviation. Statistical analysis by one-way ANOVA with Tukey's multiple comparison correction. * P = 0.0141 (PK outer apolar vs inner apolar), * P = 0.032 (PK inner apolar vs BF inner apolar), ** P = 0.0038 (PK outer apolar vs BF outer apolar), ** P = 0.0019 (BF outer apolar vs BF inner apolar).

4.2.2.2 FMA accumulates in *M. smegmatis* mc^2 155 pellicle biofilms compared to planktonic cells

The outer and inner apolar lipid fractions were assessed using solvent system C and staining with MPA (Figure 4.7A). FMA is present in both phenotypes of *M. smegmatis* mc^2 155, but not *ΔMSMEG4722*. In *M. smegmatis* mc^2 155, FMA levels are comparable between pellicle biofilms and planktonic cells in the outer apolar lipid fraction but accumulate in pellicle biofilms compared to planktonic cells in the inner apolar lipid fraction (P = 0.0001). There was an increase in FMA in the *M. smegmatis* mc^2 155 pellicle biofilm inner apolar lipid fraction compared to outer apolar lipid fraction, but this was not statistically significant (Figure 4.7B).

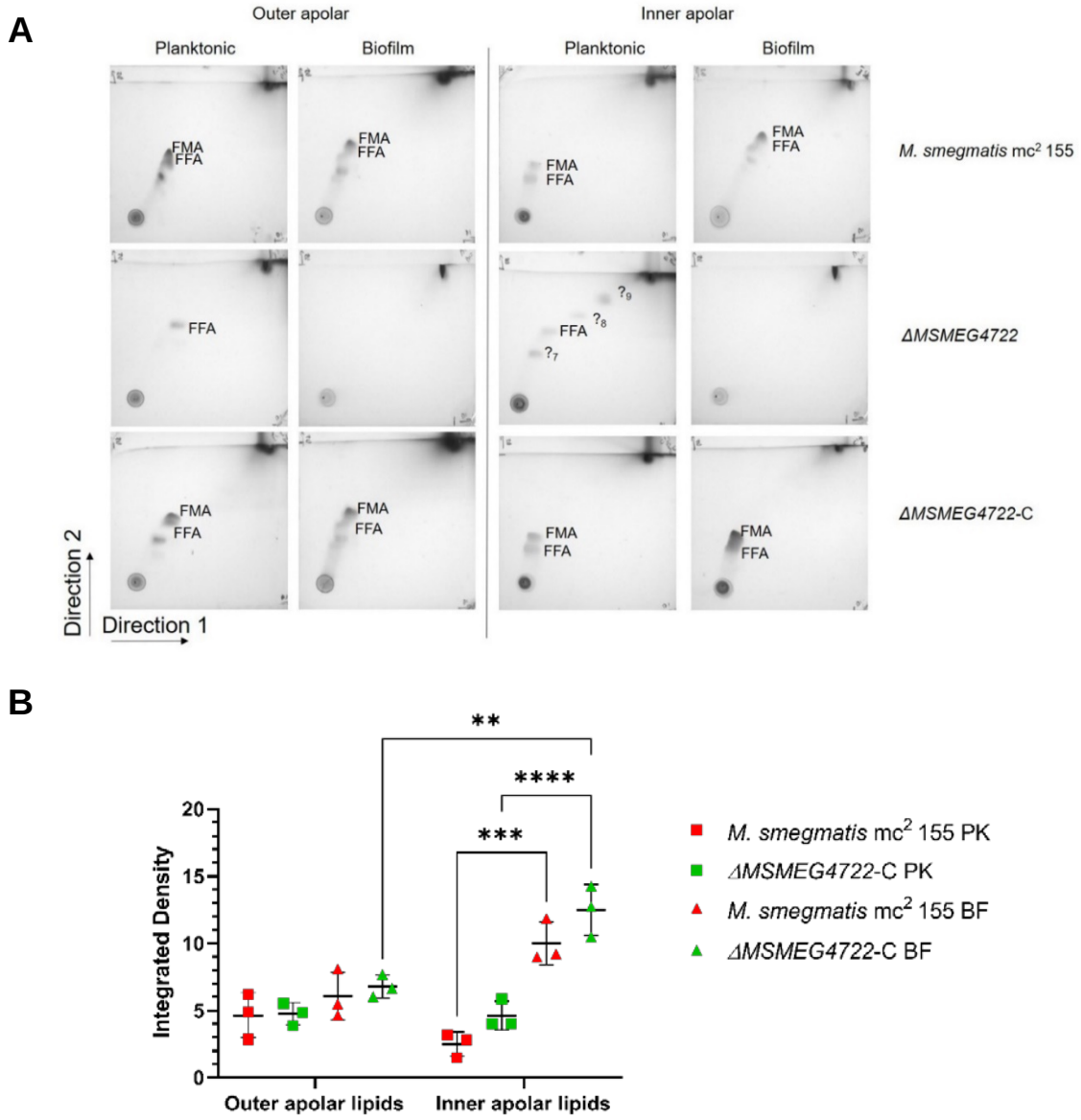


Figure 4.7: Outer and Inner apolar lipid analysis of planktonic and pellicle biofilm *M. smegmatis* mc² 155, *ΔMSMEG4722* and *ΔMSMEG4722*-C (solvent system C)

(A) Representative 2D-TLC plates of outer and inner apolar lipid fractions. Developed in chloroform: methanol (96:4 v/v) x1 and toluene: acetone (80:20 v/v) x1 and stained with MPA. Free fatty acid (FFA), free mycolic acid (FMA), unidentified lipid 7 ($?_7$), unidentified lipid 8 ($?_8$), unidentified lipid 9 ($?_9$). (B) Densitometry analysis of FMA in outer and inner apolar lipid fractions of planktonic (PK) (squares) and pellicle biofilm (BF) (triangle) *M. smegmatis* mc² 155 (red) and *ΔMSMEG4722*-C (green). Densitometry was performed on three biological replicate lipid spots. Error bars = standard deviation. Statistical analysis by two-way ANOVA with Tukey's multiple comparison correction, ** P = 0.0025, *** P = 0.0001, **** P < 0.0001.

4.2.2.3 TDM is distributed differently between the apolar lipid fractions of planktonic and pellicle biofilm *ΔMSMEG4722*

The outer and inner apolar lipid fractions were analysed for glycolipids using solvent system D and α-naphthol staining (Figure 4.8).

By densitometry, in the outer apolar lipid fraction, TDM levels were comparable between planktonic and pellicle biofilm *M. smegmatis* mc^2 155. There was significantly less TDM in pellicle biofilm *ΔMSMEG4722* compared to planktonic *ΔMSMEG4722* ($P < 0.0001$). Comparing planktonic *M. smegmatis* mc^2 155 and *ΔMSMEG4722*, there is significantly more TDM present in *ΔMSMEG4722* compared to *M. smegmatis* mc^2 155 ($P = 0.0007$). The opposite is observed in pellicle biofilms, and less TDM is present in *ΔMSMEG4722* than *M. smegmatis* mc^2 155, but this was not statistically significant (Figure 4.9A).

TDM was too faint in both phenotypes of *M. smegmatis* mc^2 155 for densitometry in the inner apolar lipid fraction. There was still a quantifiable concentration of TDM in planktonic and pellicle biofilm *ΔMSMEG4722.* There was significantly more TDM present in *ΔMSMEG4722* pellicle biofilms compared to *ΔMSMEG4722* planktonic cells ($P = 0.0052$). For *ΔMSMEG4722* in the inner apolar lipids compared to the outer apolar lipids, there was significantly less TDM present in planktonic *ΔMSMEG4722* ($P < 0.0001$), but significantly more TDM in pellicle biofilm *ΔMSMEG4722* ($P = 0.0003$) (Figure 4.9B).

TMM is too faint for densitometry analysis in both *M. smegmatis* mc^2 155 and *ΔMSMEG4722* in both phenotypes. Visually, the most noticeable observations are that in the outer apolar lipids, for both *M. smegmatis* mc^2 155 and *ΔMSMEG4722,* there is

less TMM in pellicle biofilms compared to planktonic cells. In the inner apolar lipids, TMM is present in both phenotypes of *ΔMSMEG4722,* but only present in planktonic *M. smegmatis* mc^2 155 (Figure 4.8).

GMM was observable in both strains in both phenotypes in the outer apolar lipids but at too low a concentration for quantification. In the inner apolar lipids, GMM is more visible in both phenotypes of *ΔMSMEG4722* compared to *M. smegmatis* mc^2 155. (Figure 4.8).

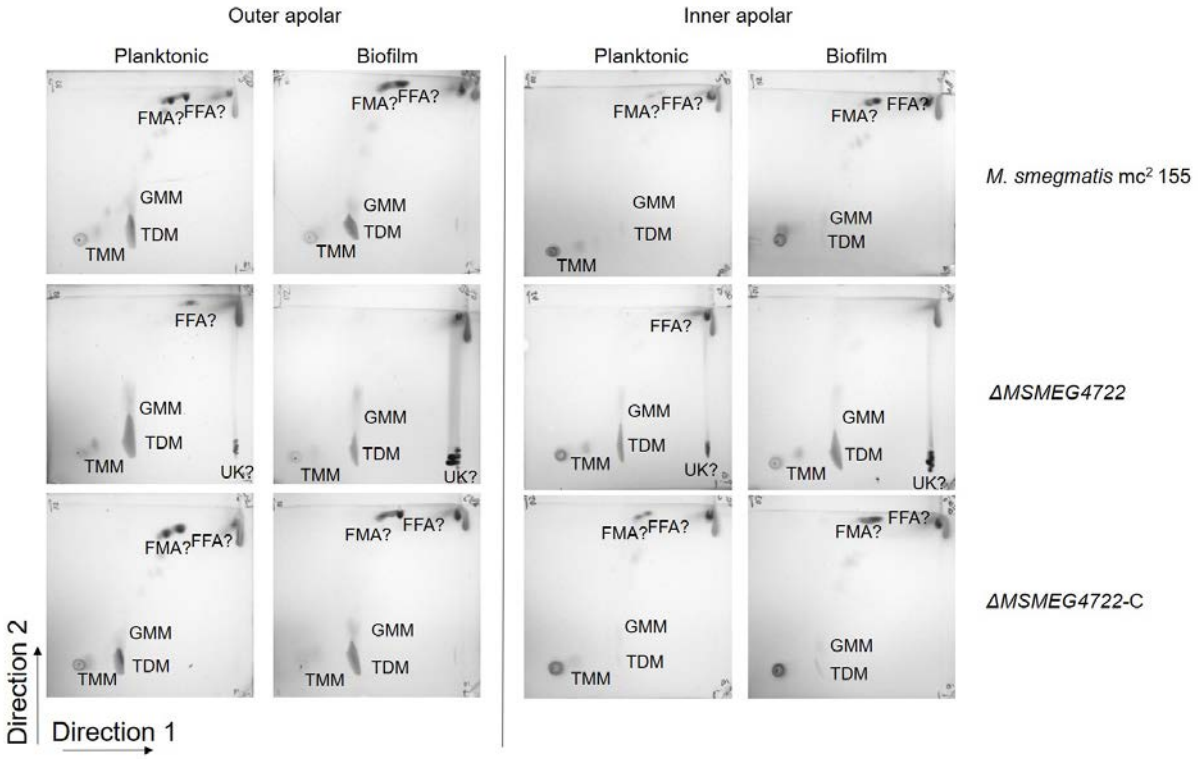


Figure 4.8: Outer and inner apolar lipid analysis of planktonic and pellicle biofilm *M. smegmatis* mc^2 155, *ΔMSMEG4722* and *ΔMSMEG4722*-C (solvent system D).

Representative 2D-TLC plates of outer and inner apolar lipid fractions. Developed in chloroform: methanol: deionised water (100:14:0.8 v/v/v) x1 and chloroform: acetone: methanol: deionised water (50:60:2.5:3 v/v/v/v) x1 and stained with α-naphthol. Trehalose monomycolate (TMM), trehalose dimycolate (TDM), glucose monomycolate (GMM), free fatty acid (FFA), free mycolic acid (FMA) and unsaturated ketones (UK).

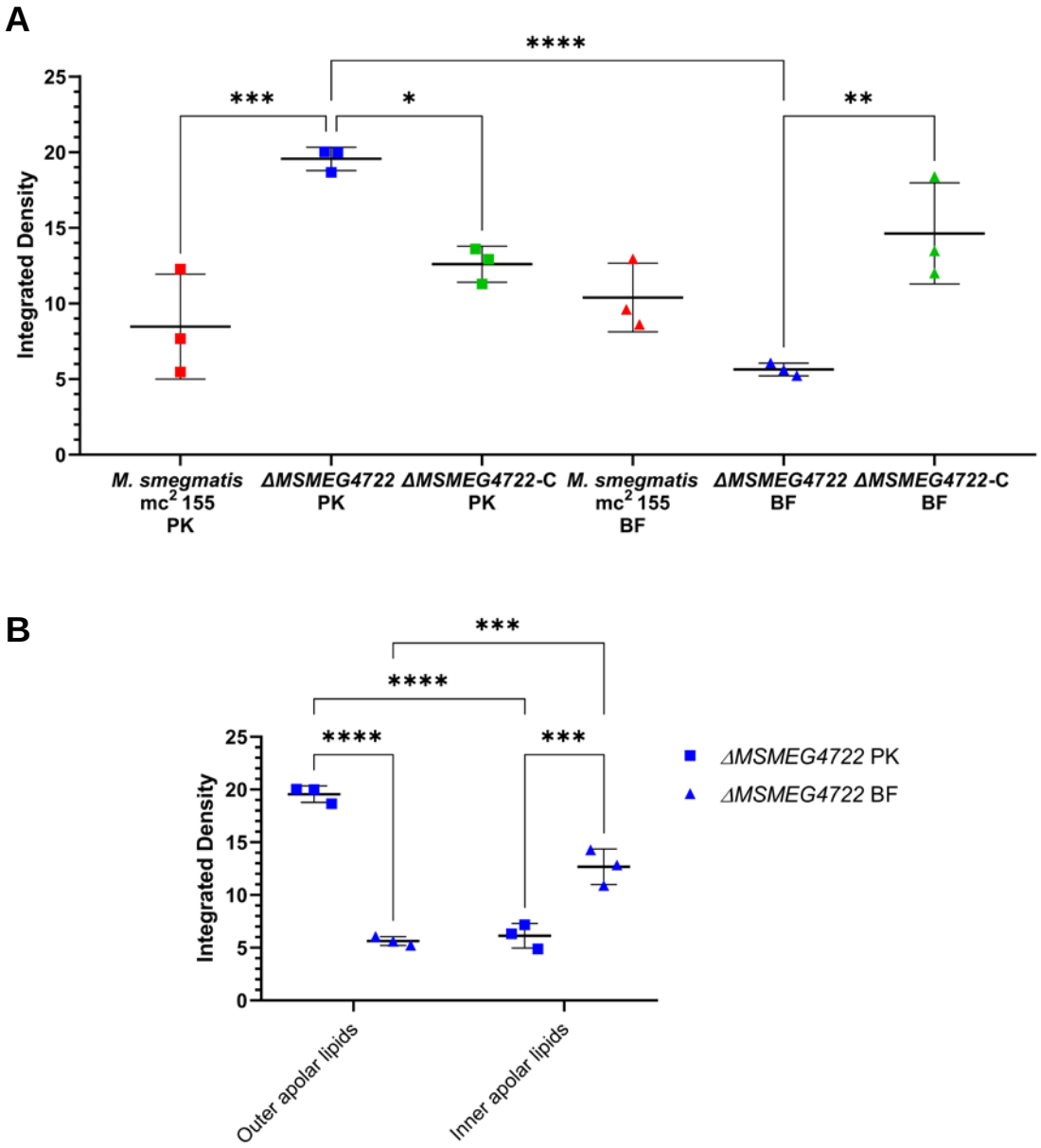


Figure 4.9: Outer and inner apolar lipid analysis of planktonic and pellicle biofilm *M. smegmatis* mc² 155, *ΔMSMEG4722* and *ΔMSMEG4722*-C (solvent system D).

Densitometry analysis of (A) TDM from planktonic (PK) (squares) and pellicle biofilm (BF) (triangles) outer apolar lipids for *M. smegmatis* mc² 155 (red), *ΔMSMEG4722* (blue) and *ΔMSMEG4722*-C (green). (B) TDM in the outer and inner apolar lipid fractions of PK and BF *ΔMSMEG4722*. Densitometry performed on three biological replicate lipid spots. Error bars = standard deviation. (A) Statistical analysis by one-way ANOVA with Tukey's multiple comparison correction, * P = 0.0247, ** P = 0.0039, *** = 0.0007, **** P < 0.0001. (B) Statistical analysis by two-way ANOVA with Tukey's multiple comparison correction **** P < 0.0001, *** P = 0.0003 (*ΔMSMEG4722* BF outer apolar vs *ΔMSMEG4722* BF inner apolar), *** P = 0.0004 (*ΔMSMEG4722* PK inner apolar vs *ΔMSMEG4722* BF inner apolar).

4.2.2.4 Polar lipids displayed a plethora of unidentified lipid spots in both phenotypes of *M. smegmatis* mc² 155, lost in *ΔMSMEG4722*.

The polar lipids were examined using solvent system D staining with MPA (Figure 4.10). In planktonic and pellicle biofilm *M. smegmatis* mc² 155, there was a range of unidentified lipids. Unidentified lipids were positioned primarily near the solvent front in *ΔMSMEG4722* pellicle biofilm TLC analyses. A single lipid spot was present in *ΔMSMEG4722* planktonic extracts.

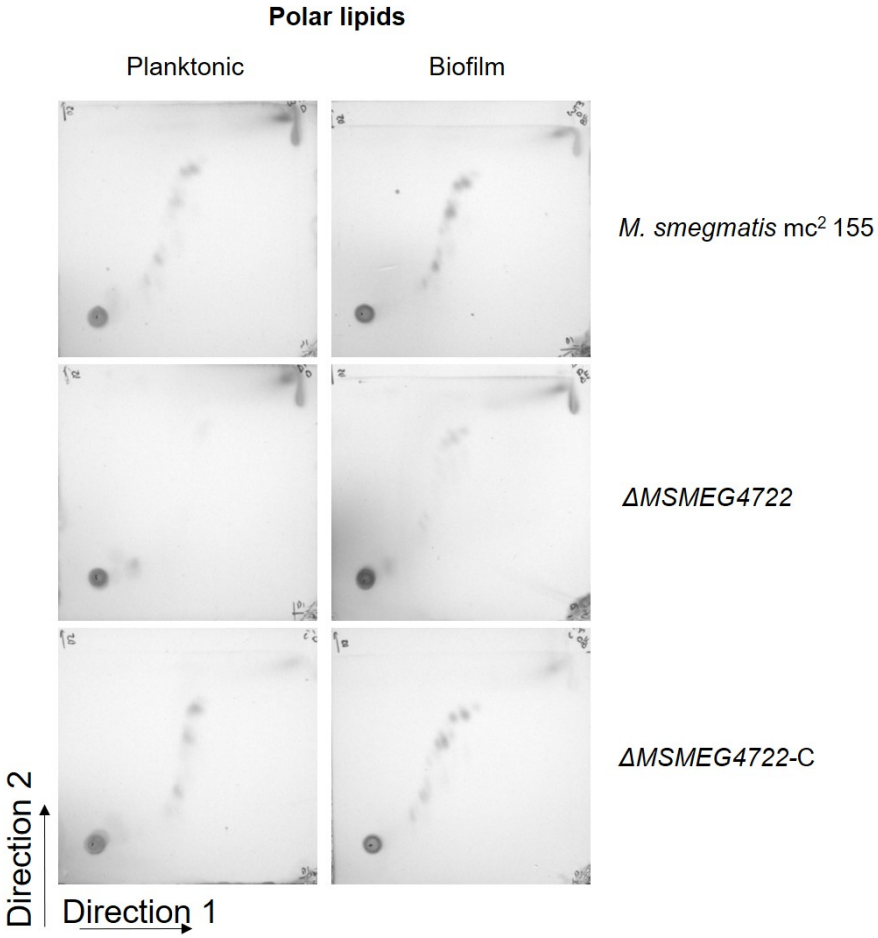


Figure 4.10: Polar lipid analysis of planktonic and pellicle biofilm culture *M. smegmatis* mc² 155, *ΔMSMEG4722* and *ΔMSMEG4722*-C (solvent system D)

Representative 2D-TLC plates of polar lipid fractions. Developed in chloroform: methanol: deionised water (100:14:0.8 v/v/v) x1 and chloroform: acetone: methanol: deionised water (50:60:2.5:3 v/v/v/v) x1 and stained with MPA.

4.2.2.5 Unreduced MAMEs are esterified to arabinogalactan for both phenotypes.

Esterified mycolic acids and fatty acids were extracted from the mAGP complex and assessed with a FAMEs and MAMEs specific solvent system (Figure 4.11A). Mycolic acids were absent from *ΔMSMEG4722*, replaced by esterified unsaturated ketones. In *M. smegmatis* mc^2 155, the MAMEs resolved into; α-, α'- and epoxy-mycolates. For both phenotypes, α-MAMEs were the most abundant, followed by α'- then epoxy. There was no difference in MAMEs composition between phenotypes (Figure 4.11B).

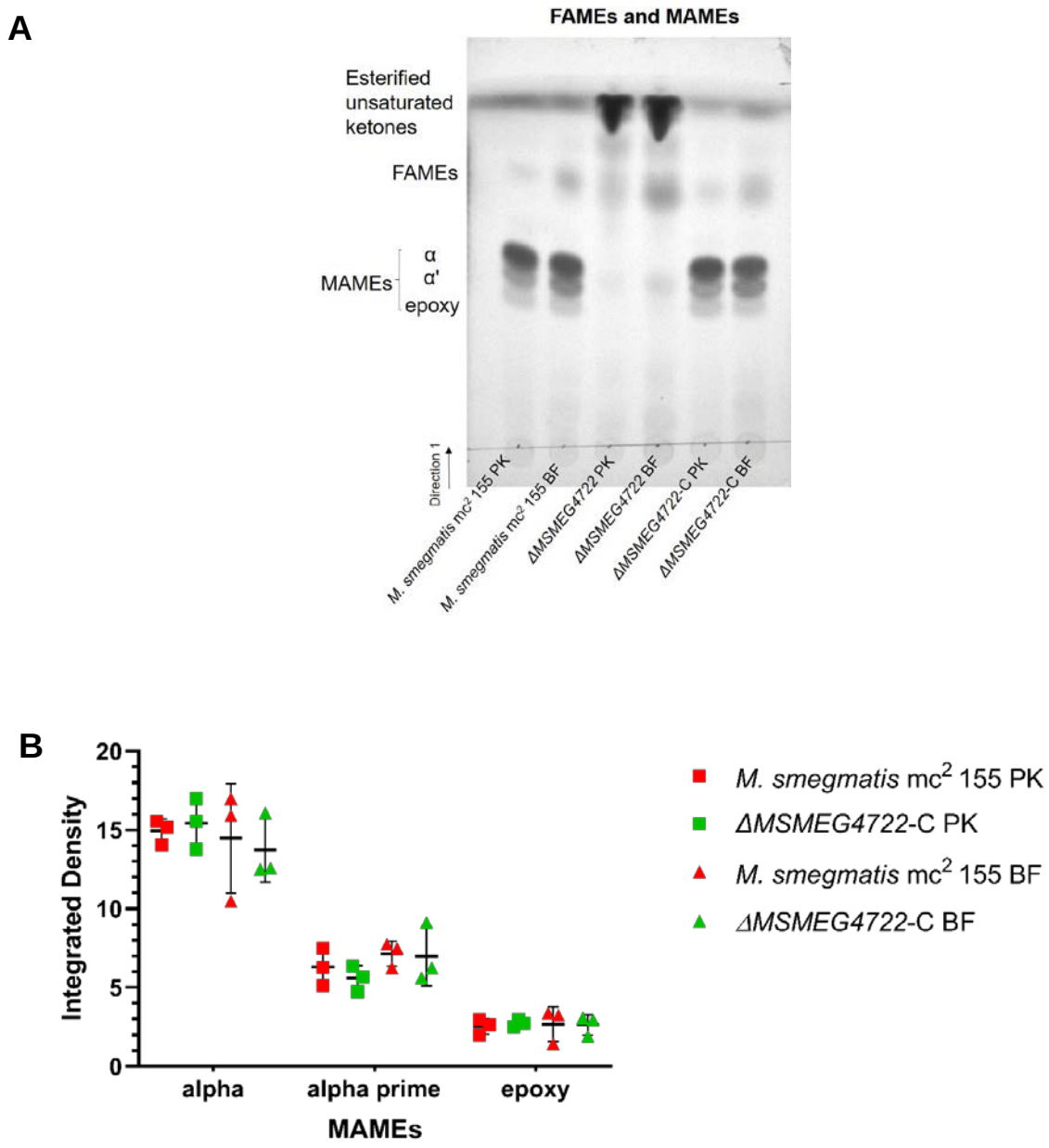


Figure 4.11: FAMEs and MAMEs analysis of planktonic and pellicle biofilm *M. smegmatis* mc² 155, *ΔMSMEG4722* and *ΔMSMEG4722*-C.

(A) Representative 1D-TLC of FAMEs and MAMEs. Developed in petroleum ether 60-80ºC: acetone (95:5) x3 and stained with MPA. Esterified unsaturated ketones, MAMEs; alpha (α), alpha prime (α') and epoxy, and FAMEs. (B) MAMEs from planktonic (squares) and pellicle biofilm (triangles) *M. smegmatis* mc² 155 (red) and *ΔMSMEG4722*-C (green).

4.2.2.6 Summary tables of lipid changes observed between strains and phenotypes

Table 4.3: Lipid changes in pellicle biofilms compared to planktonic for both *M. smegmatis* mc² 155 and *ΔMSMEG4722* (planktonic used as the control).

Lipid Fraction	Lipid	Pellicle Biofilm	
		***M. smegmatis* mc² 155**	***ΔMSMEG4722***
outer apolar	TAG	= ns	↑ BFO
	FMA	= ns	WTO[1]
	Unsaturated ketones	ΔO[1]	↑ P = 0.0038
	FFA	= ns	↓ PKO
	TDM	= ns	↓ p < 0.0001
	TMM	↓ ND	↓ ND
	GMM	= ND	= ND
	Unidentified lipids (?₄-?₆)	ΔO	= ND
inner apolar	TAG	= ns	↓ P = 0.0157
	FMA	↑ P=0.0001	WTO[1]
	Unsaturated ketones	ΔO[1]	↑ P = 0.032
	FFA	= ns	↓ PKO
	TDM	= ND	↑ P = 0.0052
	TMM	↓ ND	= ND
	GMM	= ND	= ND
	Unidentified lipids (?₄-?₆)	ΔO	= ND
	Unidentified lipids (?₇-?₉)	ΔO	↓ PKO
polar	A plethora of unidentified lipids	A comparable plethora of unidentified lipids	More unidentified lipids in pellicle biofilm
FAMEs and MAMEs	MAMEs: α	= ns	WTO[1]
	MAMEs: α'	= ns	WTO[1]
	MAMEs: epoxy	= ns	WTO[1]
	Esterified unsaturated ketones	ΔO[1]	= ND
	FAMEs	↑ NS	↑ P = 0.0089
KEY ON NEXT PAGE			

ΔMSMEG4722-C is represented by *M. smegmatis* mc^2 155 as they showed comparable lipid profiles throughout TLC analysis.

1. Expected lipid change in *ΔMSMEG4722*. Unsaturated ketones are decarboxylated α-alkyl, β-oxo mycolate intermediates/ pre-mycolates in *ΔMSMEG4722* that have an altered TLC migration profile due to the loss of a hydroxyl group for a β-oxo group on the mycolic motif (Bhatt *et al.*, 2008).

KEY	
WTO	Lipid present in *M. smegmatis* mc^2 155 only
ΔO	Lipid present in *ΔMSMEG4722* only
↑	More
=	Comparable
↓	Less
PKO	Lipid present in planktonic only
BFO	Lipid present in pellicle biofilm only
ND	Not concentrated enough for densitometry analysis. The symbol to the left (↑=↓) is a visual conclusion of lipid change.
ns	Densitometry was performed with no statistical difference.
P =	Densitometry performed, statistical p-value.

Lipids: triacylglycerols (TAG), free mycolic acid (FMA), unsaturated ketones, free fatty acid (FFA), TDM (trehalose dimycolate), TMM (trehalose monomycolate), glucose monomycolate (GMM), Mycolic acid methyl esters (MAMEs); alpha (α), alpha prime (α') and epoxy, esterified unsaturated ketones fatty acid methyl esters (FAMEs).

Table 4.4: Lipid changes between *ΔMSMEG4722* and *M. smegmatis* mc² 155 (*M. smegmatis* mc² 155 phenotypes used as the control).

Lipid Fraction	Lipid	*ΔMSMEG4722*	
		Planktonic	**Pellicle Biofilm**
outer apolar	TAG	↓ WTO	↓ ns
	FMA	WTO[1]	WTO[1]
	Unsaturated ketones	ΔO[1]	ΔO[1]
	FFA	= ns	↓ WTO
	TDM	↑ P = 0.0007	↓ ns
	TMM	= ND	= ND
	GMM	= ND	= ND
	Unidentified lipids (?$_4$-?$_6$)	↑ ΔO	↑ ΔO
inner apolar	TAG	= ns	↓ P = 0.0461
	FMA	WTO[1]	WTO[1]
	Unsaturated ketones	ΔO[1]	ΔO[1]
	FFA	= ns	↓ WTO
	TDM	↑ ΔO	↑ ΔO
	TMM	= ND	↑ ND
	GMM	↑ ΔO	↑ ΔO
	Unidentified lipids (?$_4$-?$_6$)	↑ ΔO	↑ ΔO
	Unidentified lipids (?$_7$-?$_9$)	↑ ΔO	X
polar	A plethora of unidentified lipids	More unidentified lipids in WT	More unidentified lipids in WT
FAMEs and MAMEs	MAMEs: α	WTO[1]	WTO[1]
	MAMEs: α'	WTO[1]	WTO[1]
	MAMEs: epoxy	WTO[1]	WTO[1]
	Esterified unsaturated ketones	ΔO[1]	ΔO[1]
	FAMEs	↑ ND	↑ P = 0.0089

KEY ON NEXT PAGE

ΔMSMEG4722-C is represented by *M. smegmatis* mc^2 155 as they showed comparable lipid profiles throughout TLC analysis.

1. Expected lipid change in *ΔMSMEG4722*. Unsaturated ketones are decarboxylated α-alkyl, β-oxo mycolate intermediates/ pre-mycolates in *ΔMSMEG4722* that have an altered TLC migration profile due to the loss of a hydroxyl group for a β-oxo group on the mycolic motif (Bhatt *et al.*, 2008).

KEY

WTO	Lipid present in *M. smegmatis* mc^2 155 only
ΔO	Lipid present in *ΔMSMEG4722* only
X	Present in neither strain
↑	More
=	Comparable
↓	Less
ND	Not concentrated enough for densitometry analysis, the symbol to the left (↑=↓) is a visual conclusion of lipid change.
ns	Densitometry was performed with no statistical difference.
P =	Densitometry performed, statistical p-value.

Lipids: triacylglycerols (TAG), free mycolic acid (FMA), unsaturated ketones, free fatty acid (FFA), TDM (trehalose dimycolate), TMM (trehalose monomycolate), glucose monomycolate (GMM), esterified unsaturated ketones, mycolic acid methyl esters (MAMEs); alpha (α), alpha prime (α') and epoxy, fatty acid methyl esters (FAMEs).

4.3 Discussion

4.3.1 Mature mycolates are required for pellicle biofilm maturation

The loss of mature mycolic acids throughout the cell envelope, in *ΔMSMEG4722*, has a cause-or-effect influence on cell wall composition changes observed in both planktonic and pellicle biofilm cultures of *ΔMSMEG4722* for apolar and polar lipids. Mycolic acids are the most abundant lipid of the cell envelope and have been implicated in the cell wall structure, integrity and impermeability. When covalently attached to mono or disaccharide glycoconjugates (GMM, TMM, TDM or Ara linked), mycolic acids are proposed to form a monolayer known as the mycomembrane. Due to the long-short branch conformation of mycolate chains, this creates an asymmetric bilayer in which other free lipids can intercalate. Mycolic acid chain modifications are evenly distributed within the monolayer and spaced in specific ways that facilitate their folding within the mycobacterial cell envelope giving rise to mycobacteria's hydrophobic, impermeable and well-organised cell wall structure (Marrakchi, Lanéelle and Daffé, 2014). The three-dimensional topology of the mAGP complex is still to be elucidated, but the Minnikin model, first proposed in 1982, still stands up to experimental scrutiny (Minnikin, 1982; Alderwick *et al.*, 2015). The arabinogalactan esterification to mycolate is via the carboxyl group of the mycolic motif (Marrakchi, Lanéelle and Daffé, 2014).

Accumulation of FMA has been observed previously in both *M. tuberculosis* and NTM pellicle biofilms (Ojha *et al.*, 2008, 2010; Totani *et al.*, 2017; Vega-Dominguez *et al.*, 2020) and was observed in *M. smegmatis* mc^2 155 pellicle biofilms in this chapter. Therefore, this chapter hypothesised that *ΔMSMEG4722* aggregation on the air-liquid

interface and inability to reticulate into mature pellicles could have been due to an inability to accumulate α-alkyl, β-oxo intermediates/ pre-mycolates. However, in *ΔMSMEG4722* pellicles, their accumulation was observed.

The generation of FMA in *M. smegmatis* mc^2 155 pellicle biofilm development is facilitated by a cutinase-like serine carboxylesterase encoded by the *MSMEG1529* gene, which hydrolyses mycolate from newly synthesised TDM (Ojha *et al.*, 2010). The mycolic acid residues present in TDM are esterified to trehalose at the mycolic motif, but at a distinct location from the β-oxo reduced by the *MSMEG4722* reductase (Noll *et al.*, 1956; Basso and Santos, 2005). If the *ΔMSMEG4722* mutant had been unable to accumulate α-alkyl, β-oxo mycolate intermediates/ pre-mycolates it could have been because the serine carboxylesterase was unable to cleave the altered mycolic motif, releasing mycolate.

This study highlights that maturation of the mycolic motif is necessary for pellicle biofilm formation when free mycolic acids can accumulate. As previously discussed in chapter 3, using *M. tuberculosis* mycolic acid mutants, it has been demonstrated that only oxygenated keto mycolates are essential to initiate reticulation of pellicles (Sambandan *et al.*, 2013). In contrast, for *M. smegmatis*, by TLC analysis, alterations to all mycolate classes have been implicated in producing pellicles that are unable to reticulate (Ojha *et al.*, 2005; Jamet *et al.*, 2015). In *ΔMSMEG4722*, all mycolate classes are affected, so whether a change to the mycolic motif of all mycolates or a specific mycolate class (α, α' or epoxy) determines the inability of *ΔMSMEG4722* to form mature pellicle biofilms is still to be explored.

4.3.2 TDM, TMM (and GMM) were found in the inner apolar lipids of *ΔMSMEG4722* regardless of phenotype

The most striking change to the cell envelope lipid composition observed through TLC analysis is that the glycolipids TDM, TMM, and GMM were found in the freely extractable outer apolar lipid fraction of *ΔMSMEG4722* and *M. smegmatis* mc^2 155, but in *ΔMSMEG4722* only, they were also extracted in abundance in the less freely extractable inner apolar lipid fraction. This was observed when the bacteria were cultured in Middlebrook 7H9 and in Sauton's 40 minimal media as planktonic cells and pellicle biofilms. This was not reported in the TLC analysis by Bhatt *et al.*, (2008) because lipids were extracted as total apolar lipids and not as two separate apolar lipid fractions.

TDM and TMM are the most abundant conserved non-covalently bound lipid in the mycobacterial envelope, making up to 1.5-3% of the dry cell weight of *M. smegmatis* (Woodruff *et al.*, 2004; Yang *et al.*, 2013). For *M. tuberculosis*, TDM is a well-established virulence factor that can; inhibit phospholipid vesicle fusion (speculated to inhibit phagosome-lysosome fusion) (Spargo *et al.*, 1991), delay macrophage phagosome maturation and acidification (Axelrod *et al.*, 2008), bind the Mincle receptor activating macrophage production of proinflammatory cytokines and NO (Ishikawa *et al.*, 2009), and induce granuloma formation in mice (Borders *et al.*, 2005; Welsh *et al.*, 2008; Ishikawa *et al.*, 2009). In addition, synthetic TDM has adjuvant properties and can induce a strong humoral and $CD4^+$ T cell response against mycobacterial subunit vaccines, providing protection against *M. tuberculosis* challenge in mice (Davidsen *et al.*, 2005; Khader *et al.*, 2007; Agger *et al.*, 2008).

As TDM and TMM have been characterised in both pathogenic and non-pathogenic species of mycobacteria, their intercalation into the mycomembrane has been implicated as being essential for cell wall integrity and low permeability (Draper, 1998).

In a model mimicking the mycobacterial membrane consisting of a fluid, TDM-monolayer leaflet and a non-fluid hydrophobic leaflet, TDM monolayers maintained integrity through de- and rehydration. In a mixed model with phospholipids, TDM protected the membrane lipids from desiccation (Harland *et al.*, 2008). *M. smegmatis* glycolipids have been demonstrated to be relatively immobile during growth through metabolic labelling with FITC-trehalose analogues. Labelled trehalose glycolipids were excluded from newly synthesised pole cell wall growth, demonstrating a lack of fluidity in the mycomembrane (Rodriguez-Rivera *et al.*, 2017).

TDM has been shown to be important for cell wall organisation and permeability through disruption of TDM synthesis using a small molecule Ag85C inhibitor (I3-AG85) (Warrier *et al.*, 2012). Ag85C belongs to the Ag85 complex proteins that possess enzymatic mycolyl-transferase activity. They cleave mycolate from TMM, providing mycolate for TDM esterification to arabinogalactan (Kremer *et al.*, 2002). When incubated with I3-AG85, the TDM/TMM balance in *M. tuberculosis* was disrupted with a reduction of TDM and an accumulation of TMM. MAMEs were not affected. Significantly more radiolabelled glycerol accumulated in *M. tuberculosis* incubated with I3-AG85 compared to an untreated control (Warrier *et al.*, 2012). SQ109, an anti-TB candidate in clinical trials, is implicated in inhibiting the efflux of TMM across the plasma membrane, potentially via the membrane transporter mmpL3. *M. tuberculosis* exposed to the drug accumulated TMM, but lost TDM from the apolar lipids and

esterified mycolates. The treated cell surface became ruffled, as observed in isoniazid treated cells where the target is mycolic acid synthesis (Tahlan *et al.*, 2012).

MAR1, a mutant isolated from a transposon library, has a stop codon insertion into *fbpA*, a gene of the Ag85C complex proteins in *M. smegmatis.* The mutant displays a 45% decrease in TDM in extracted apolar lipids, but MAMEs were not altered. Overall, MAR1 colony morphology was smoother than *M. smegmatis* mc^2 155 and became more hydrophilic. The mutant was 12-fold more susceptible to the lipophilic antibiotics rifampicin, erythromycin and imipenem (Nguyen, Chinnapapagari and Thompson, 2005).

Glycolipids of *ΔMSMEG4722* were previously demonstrated to have altered mobilities by TLC due to the esterification of the unreduced mycolic acid(s) to trehalose and glucose moieties (Bhatt *et al.*, 2008), which was also observed in this chapter. Hypothetically, replacing a hydroxyl group with a β-oxo group on the mycolic motif may have affected both the glycolipids and esterified mycolate of arabinogalactan, altering the rigidity of mycolate anchoring. A consequence of this could be a change in the distribution of glycolipids within the cell wall.

4.3.3 Changes to TDM distribution may affect *ΔMSMEG4722* pellicle biofilm development

In 6-day mature *M. smegmatis* mc^2 155 pellicle biofilms, comparable TDM levels to planktonically cultured cells were observed. This agrees with Ojha *et al.*, (2010), who observed comparable TDM in 4-day pellicle biofilms compared to planktonically cultured cells, in concurrence with a significant increase in FMA. An observation from the apolar lipid fractions is that *ΔMSMEG4722* had significantly less TDM in the pellicle

biofilm fraction compared to planktonic cells in the outer apolar lipids, but an accumulation of TDM in the inner apolar lipid fraction compared to planktonic cells. Thus, a change in TDM distribution within *ΔMSMEG4722* could affect pellicle biofilm formation.

Historically, when first characterising TDM, the biomass used for lipid extraction by petroleum ether was from 'early stage' *M. tuberculosis* pellicle biofilms, described as being composed of bacillary cords on the air-liquid interface (Bloch, 1950; Noll *et al.*, 1956). Cording was heavily implicated in forming pellicle biofilms by virulent strains of *M. tuberculosis,* producing a thin veil with serpentine cords, compared to avirulent strains that produced discrete, unstable islands. It was noted that fast-growing non-pathogenic mycobacteria also produced phenotypically similar pellicles to virulent strains (Middlebrook, Dubos and Pierce, 1947).

TDM is hypothesised to play a structural role during pellicle biofilm formation (Hunter, Venkataprasad and Olsen, 2006). Modelling on an air-liquid interface, TDM dissolved in hexane-ethanol forms a highly organised pattern of concentric circles as the solvent evaporates. These crystalline monolayers were stable enough to build up with more layers of TDM (Behling *et al.*, 1993). Hunter, Venkataprasad and Olsen, (2006) hypothesise that the release of TDM from the surface of mycobacteria facilitates early pellicle biofilm formation by spreading on the air-liquid interface. This is based on observations that TDM in the crystalline monolayers could spread across liquid media and support surface liquid when put under increasing surface tension. Biologically, this was demonstrated with a low TDM producing avirulent strain and a high TDM producing virulent strain of *M. tuberculosis*. At the air-liquid interface, the avirulent

strain formed small islands with serpentine cords of organisms present on top. In contrast, the virulent strain produced a pellicle consisting entirely of cords in a series of interconnected, overlapping loops. During early pellicle biofilm formation, the virulent strain produced concentric circles characteristic of the TDM monolayers, and immunostaining for TDM was stronger in the spaces between the interconnected loops. In contrast, TDM immunostaining on the avirulent strain was stronger on the serpentine cords.

TDM production and a positive correlation to pellicle biofilm formation have also been observed from patient isolates. *M. tuberculosis* Beijing isolates from sputum, associated with cavity necrosis, have been compared to extrapulmonary Beijing isolates (granulomas) for pellicle production and TDM content. Beijing isolates from pulmonary sites typically displayed faster pellicle initiation, earlier cord formation, spreading growth across the air-liquid interface and climbing of the well walls. When TDM was extracted from 4-week pellicle biofilms, Beijing pulmonary isolates produced more TDM than extrapulmonary isolates (Arora *et al.*, 2016).

A change to the distribution of TDM and other glycolipids in *ΔMSMEG4722*, possibly facilitated by the change in cell wall integrity due to the loss of mature mycolic acids, could, in addition to altering stability and ability to form mature pellicle biofilms, alter cell wall interactions with the immune system, including the human complement system.

4.4 Technical Discussion

4.4.1 Radiolabelling lipids

Densitometry analyses was used to quantify differences in lipids between strains and phenotypes. However, only lipids present in abundance are dense enough to be measured using traditional densitometry analysis. More lipid could be loaded onto the TLC plates to overcome faint spots, but the potential for overloading must be considered as this can result in streaking or merged lipid spots. Another technique with improved sensitivity for quantifying lipids is incorporating ^{14}C labelled glycerol to radiolabel the lipids. This may have allowed the quantification of lipids visible by TLC but too light to quantify, e.g. TMM in solvent system D, and improved the understanding of the TDM distribution change in *ΔMSMEG4722*. This could further tease out strain and phenotype differences between *ΔMSMEG4722* and *M. smegmatis* mc^2 155.

4.4.2 Deciphering polar lipid spots

In *M. smegmatis* mc^2 155 and *ΔMSMEG4722*-C planktonic and pellicle biofilm polar lipid fractions, there was a range of lipids over the TLC plate that have not previously been characterised that appeared lost in *ΔMSMEG4722*. It will be important to characterise this altered lipid profile to determine which polar lipids may be lost in *ΔMSMEG4722.* This could be achieved using solvent system E; chloroform: methanol: deionised water (60:30:6 v/v/v) (D1) and chloroform: acetic acid: methanol: deionised water (40:25:3:6 v/v/v/v) (D2) (Habermehl, 2012). System E is a polar solvent system that resolves a large plethora of phospholipids and glycolipids, including the acetylated phosphatidylinositol mannosides (PIMs).

5 Complement activation by *ΔMSMEG4722*

5.1 Introduction

5.1.1 Summary of progress in earlier chapters

In chapter 2, IgM induced complement activation resulting in C3b/iC3b and C5b-9 deposition onto both planktonic and pellicle biofilm-derived *M. smegmatis* mc^2 155. However, after removing IgM from the complement source, *M. smegmatis* mc^2 155 could still mediate complement activation through innate host-cell interactions.

In chapter 3, *ΔMSMEG4722* formed a thin, flat, pellicle biofilm on the air-liquid interface with a reduction in ECM compared to fully reticulated pellicle biofilms by *M. smegmatis* mc^2 155.

In chapter 4, biochemical changes in the cell wall of *ΔMSMEG4722* included the loss of mature mycolic acids for unsaturated ketones (decarboxylation products of free mycolic acid intermediates/ pre-mycolates). There was also a change to the distribution of solvent-extractable non-covalently bound glycolipids (TDM, TMM and GMM) in the apolar lipid fractions, occurring in bacteria cultured in Middlebrook 7H9 and as planktonic cells and pellicle biofilms. In pellicle biofilms, mature free mycolic acids and unsaturated ketones accumulated in the apolar lipid fractions for *M. smegmatis* mc^2 155 and *ΔMSMEG4722*, respectively.

5.1.2 Complement pathway activation by mycobacteria

The human complement system, when activated, plays multiple roles in host defence. These include; opsonising pathogens (C3b/iC3b deposition) for phagocytosis via

complement receptors (CR), total activation of the cascade resulting in the formation of the membrane attack complex (C5b-9 deposition), which can lyse gram-negative bacteria, and anaphylatoxin generation and release (C3a and C5a) to trigger inflammation and crosstalk with the adaptive immune system. The system can be activated via three pathways; classical pathway activation by C1q, lectin pathway activation by mannose binding lectin (MBL), ficolin-1, ficolin-2, ficolin-3, collectin-10 and collectin-11, and the alternative pathway that 'ticks over' through spontaneous hydrolysis of C3 to generate C3b (Figure 5.1). The alternative pathway maintains a low level of constitutive activation, amplifying upon response to a pathogen (Merle *et al.*, 2015).

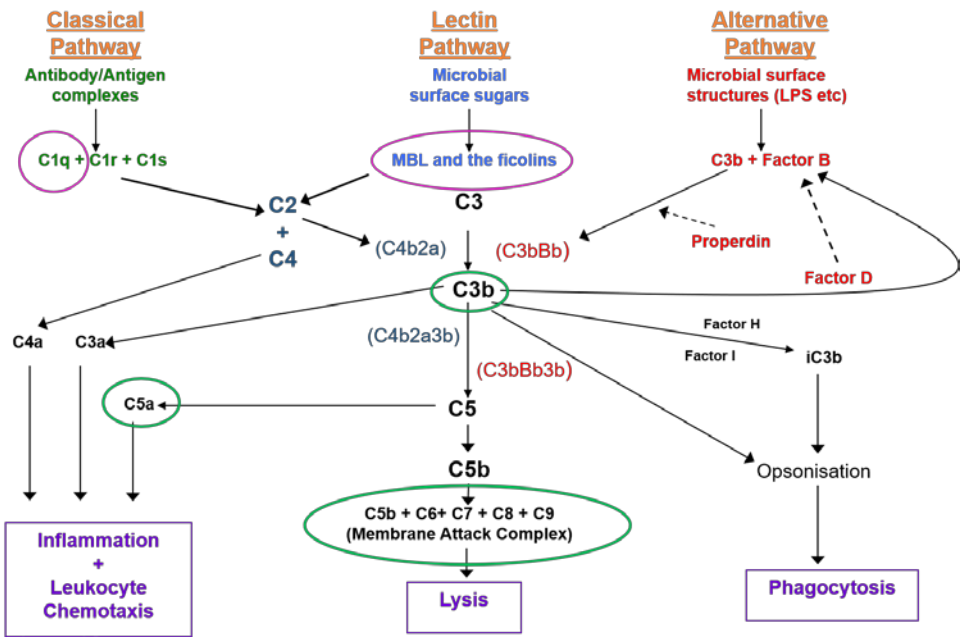


Figure 5.1: Overview of the complement cascade with components measured in this chapter highlighted.

The three pathways; classical, lectin and alternative, all lead to the formation of C5b-9 via cleavage of the central component of complement, C3. Highlighted in magenta are the complement activators investigated for binding in this chapter. Highlighted in green are the activation products investigated in this chapter. Complement cascade image created by and reproduced with permission from Stephen Taylor, PHE, adapted.

The human complement system is an innate part of the defence against *M. tuberculosis* with multifaceted and diverse consequences, but the innate host-pathogen interactions are not well understood. All three pathways of complement have been implicated in activation by mycobacteria (Schlesinger *et al.*, 1990; Ferguson *et al.*, 2004; Bartlomiejczyk *et al.*, 2014).

Pathogenic mycobacteria, including *M. tuberculosis* and *M. leprae,* enter phagocytic cells, including mycobacteria's intracellular niche, the macrophages via CR. Opsonisation with C3b/iC3b increases bacterial adherence to CR (Schlesinger *et al.*, 1990; L S Schlesinger and Horwitz, 1991; Hirsch *et al.*, 1994; Zimmerli, Edwards and Ernst, 1996) and accelerates phagocytosis (Hu *et al.*, 2000; Melo *et al.*, 2000). Entry via CR has been observed not to activate macrophage intracellular Ca^{2+} signalling, which is important for the activation of cellular defence signalling (Malik, Denning and Kusner, 2000).

Deposition of the terminal product of the cascade, C5b-9, has been observed on gram-positive bacteria but can only lyse gram-negative bacteria (Berends *et al.*, 2013). Mycobacteria have a cell wall intermediate between gram-positive and gram-negative (Jarlier and Nikaido, 1994; Jackson, 2014; Rodriguez-Rivera *et al.*, 2017). C5b-9 deposition on *M. bovis* BCG was first observed by Hetland *et al.*, (1998), but the resulting lysis has not been confirmed.

Concurrent with cleavage of C5 to generate C5b is the generation of the potent anaphylatoxin C5a, which could play a significant biological role in TB pathogenesis. Mice deficient in C5a under a range of *M. tuberculosis* doses have displayed

exacerbated disease, an increased bacterial burden in the lungs, faster onset of death and faster disease re-activation with the removal of isoniazid treatment (Jagannath *et al.*, 2000). In addition, mice could not form distinct pulmonary granulomas, replaced by interstitial inflammation and widening, an unstructured infiltration of lymphocytes and bacteria within the interstitium by day 12 post-infection (Jagannath *et al.*, 2000; Actor *et al.*, 2001). TDM induces pulmonary granuloma formation in mice, but mice defective in C5a or C5aR, when injected with TDM, cannot form cohesive granulomas (Borders *et al.*, 2005; Welsh *et al.*, 2008).

5.1.3 Identified mycobacterial cell wall ligands of complement activators

Binding of complement activators onto whole-cell mycobacteria has been demonstrated, including C1q, MBL and ficolin-2 for *M. bovis* BCG (Carroll *et al.,* 2009), MBL for *M. avium* (Polotsky *et al.*, 1997) and MBL, ficolin-1, ficolin-2 and ficolin-3 for *M. tuberculosis* and (weakly) *M. smegmatis* (Bartlomiejczyk *et al.*, 2014).

Despite observations of complement activation and direct binding of activators to whole-cell mycobacteria, there are few identified ligands from the mycobacterial cell wall. Research has focused primarily on activators of the lectin pathway. Recombinant MBL has been observed to bind purified ManLAM from *M. tuberculosis* H37Rv as well as showing weak binding to LM (“rapidly growing Mycobacterium species”), non-capped LAM (AraLAM) (“rapidly growing Mycobacterium species”) and the PIMs (*M. tuberculosis* Erdman) (Polotsky *et al.*, 1997). The proteins Ag85A and Ag85B of the Ag85 complex primarily binds to another set of lectin pathway activators, the ficolins (rficolin-2 > rficolin-3 > rficolin-1), but can also bind rMBL (Swierzko *et al.*, 2016). *M.*

tuberculosis H37Rv ManLAM functionally activates the lectin pathway via rMBL binding (Bartlomiejczyk *et al.*, 2014; Świerzko *et al.*, 2016). The virulence factor TDM and its related mycolate donor TMM also functionally activate the complement cascade, but the activator was not identified (Ramanathan, Curtis and Turk, 1980; Yasuda, 1999).

5.1.4 Biofilms and complement activation

Existing as part of a biofilm lifestyle alters interactions with the human complement system compared to planktonic cells, facilitated in part by accumulated extracellular material. For *M. tuberculosis,* which accumulates free mycolic acids when cultured as a pellicle biofilm, pellicle biofilm-derived bacteria have reduced C3b/iC3b and C5b-9 deposition. C1q, MBL and ficolin-3 activator binding were also reduced on pellicle biofilm bacilli (Keating *et al.*, 2021). Disaggregated biofilm bacteria associated with ECM could represent the aerosolised expectorate that facilitate *M. tuberculosis* transmission (Orme, 2014).

Domenech *et al.*, (2013) showed that disaggregated biofilm-derived *Streptococcus pneumoniae* had decreased binding of C1q and pentraxin (a C-reactive protein that increases C1q binding) and an increase in the regulator Factor H binding compared to planktonic cells. In addition, C3b deposition was reduced on disaggregated biofilm cells, and opsonophagocytosis was reduced. Jensen *et al.*, (1993) showed for *P. aeruginosa* that intact biofilms could activate the complement cascade (detection of C3b, iC3b and C3c), but activation was submaximal compared to planktonic cells. C5b-9 detection was lower, but C5a levels were comparable. When examining disaggregated biofilms compared to planktonic cells, complement activation, C5b-9

detection and C5a generation were decreased compared to planktonic cells (Jensen *et al.*, 1993).

Protection from complement-induced opsonophagocytosis and PMN lysis when existing as part of a biofilm has been reported for *P. aeruginosa* (Anwar, Strap and William Costerton, 1992; Meluleni *et al.,* 1995), *Mycoplasma pulmonis* (Simmons and Dybvig, 2007) and *S. epidermidis* (Cerca *et al.,* 2006; Kristian *et al.,* 2008). Intact biofilms of *S. epidermidis* were reported to have reduced C3b deposition, but generated more C3a compared to planktonic cells (Kristian *et al.,* 2008).

5.1.5 Aims

There is a limited understanding of the role of mycolic acids in innate mycobacterial interactions with the complement cascade. *ΔMSMEG4722* has a β-oxo group instead of a hydroxyl group on the mycolic motif, which results in altered, full-length mycolic acids throughout the cell envelope.

1) The first aim was to evaluate how this mycolate alteration would affect innate activation of the complement cascade by comparing Middlebrook 7H9 cultured *M. smegmatis* mc^2 155 and *ΔMSMEG4722*.

Free mycolic acid accumulation is a hallmark of pellicle biofilm formation, but its role in altering pellicle biofilm interactions with complement activation is unknown.

2) The second aim was to determine the role of mycolic acids and mycolate-containing lipids in complement interactions with pellicle biofilms. This was assessed through comparisons of planktonic and pellicle biofilm *M. smegmatis* mc^2 155. The effect of

losing mature mycolate in pellicle biofilms on complement interactions was assessed by comparing *M. smegmatis* mc^2 155 to their *ΔMSMEG4722* counterparts.

For aims one and two, activation of the complement cascade was assessed by evaluating the binding of activators (C1q, MBL, ficolin-1 or ficolin-2) and the progression of the complement cascade (C3b/iC3b deposition, C5a release and C5b-9 deposition) onto live bacteria (Figure 5.1). The extracted, characterised lipid fractions from chapter 4 were analysed to determine if the change to lipid profile influences complement activation via measuring C3b/iC3b deposition. Extracted carbohydrates/lipoglycans were also assessed for complement activation via C3b/iC3b deposition. *ΔMSMEG4722*-C was included as a control in all experiments and was comparable to *M. smegmatis* mc^2 155.

3) The third aim was to broaden the knowledge of mycobacterial cell envelope components that can activate the complement system. Purified mycobacterial cell envelope components sourced from BEI Resources were evaluated for complement activation via C3b/iC3b deposition using ELISA.

5.1.6 Hypotheses

1) Live *ΔMSMEG4722* will show altered activator binding and complement activation compared to *M. smegmatis* mc^2 155.

2) Pellicle biofilm-derived bacteria will have decreased activator binding and complement activation compared to planktonically-derived bacteria. Bacteria

derived from a pellicle that did not reticulate and mature (*ΔMSMEG4722*) will not display alterations to complement activation.

3) Purified cell envelope components will display a range of complement activation.

5.2 Results Aim 1: Functional activation of the complement cascade by *ΔMSMEG4722* and *M. smegmatis* mc^2 155

The first aim of this chapter was to evaluate how altered mycolates in *ΔMSMEG4722* affect activation of the complement cascade.

5.2.1 Complement protein deposition and C5a generation onto *M. smegmatis* mc^2 155 and *ΔMSMEG4722*

5.2.1.1 Increased C3b/iC3b deposition was observed on *ΔMSMEG4722* compared to *M. smegmatis* mc^2 155

Five or six biological replicates of live *M. smegmatis* mc^2 155, *ΔMSMEG4722* and *ΔMSMEG4722*-C and the positive control zymosan were incubated with either 10% (all three pathways active) or 2% (classical and lectin pathway activity only) IgG- and IgM-depleted complement. Bacteria were labelled with the appropriate fluorescent antibodies to measure complement activation via deposition of C3b/iC3b and C5b-9 by flow cytometry (methods section 7.10).

There was significantly more C3b/iC3b deposition on *ΔMSMEG4722* compared to *M. smegmatis* mc^2 155, only when all three pathways were active (P = 0.0176) (Figure 5.2A). For C5b-9, there was a trend towards increased deposition on *ΔMSMEG4722* compared to *M. smegmatis* mc^2 155, only when all three pathways were active. This was not statistically significant (Figure 5.2B).

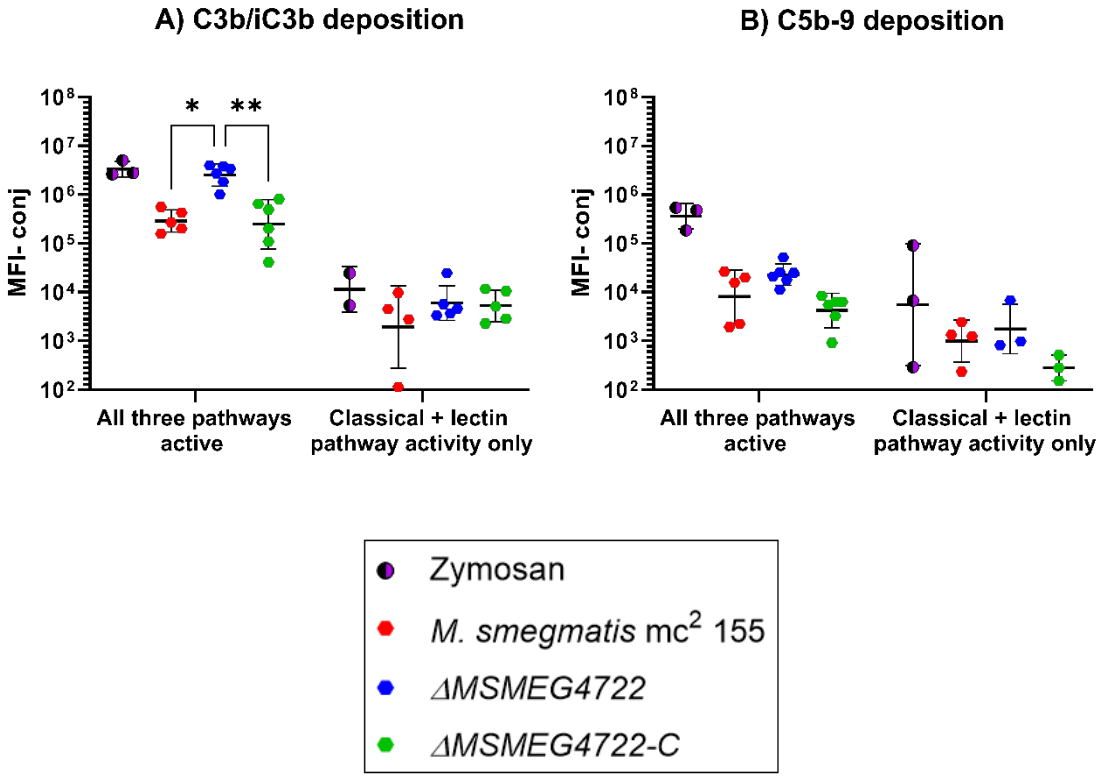


Figure 5.2: C3b/iC3b and C5b-9 deposition on *M. smegmatis* mc² 155, *ΔMSMEG4722* and *ΔMSMEG4722*-C.

Median fluorescence intensity – conjugate only fluorescence (MFI-conj) corresponding to (A) C3b/iC3b deposition or (B) C5b-9 deposition, measured by flow cytometry. Bacteria were incubated with 10% complement (all three pathways) or 2% complement (classical and lectin pathways only). Zymosan (black/purple circles) was used as a positive control. At 2% complement, MFI-conj correlating to C5b-9 deposition was negative for one biological replicate of *M. smegmatis* mc² 155 (red) and three biological replicates of *ΔMSMEG4722* (blue) and *ΔMSMEG4722*-C (green). Error bars show the standard deviation of ≥ five biological replicates. For statistical analysis, data were log10 transformed before performing a two-way ANOVA with Tukey's multiple comparison correction. (A) * P 0.0176, ** P 0.0063.

5.2.1.2 C5a generation was comparable between *M. smegmatis* mc² 155 and *ΔMSMEG4722*

The potent immunomodulatory anaphylatoxin C5a is a complement protein produced after deposition of C3b and formation of the C5-convertase, which cleaves C5 to produce C5a and C5b (Merle *et al.*, 2015).

The generation of C5a by the activated complement cascade was measured using ELISA. The supernatants of three biological replicates of *M. smegmatis* mc^2 155, *ΔMSMEG4722* and *ΔMSMEG4722*-C incubated with 10% IgG- and IgM-depleted complement (all three pathways active) was added to a commercial C5a ELISA kit (Abcam). Fluorescence readings were interpolated from a C5a standard curve to give C5a concentrations in pg mL^{-1} (Figure 5.3A). Zymosan and *Neisseria meningitidis* (± positive serum) were added as positive controls for C5a generation as both are potent activators of the complement system through to C5b-9 deposition (Taylor *et al.*, 2008) (methods section 7.24).

The results showed comparable concentrations of generated C5a in the supernatants of *M. smegmatis* mc^2 155 and *ΔMSMEG4722* (Figure 5.3B).

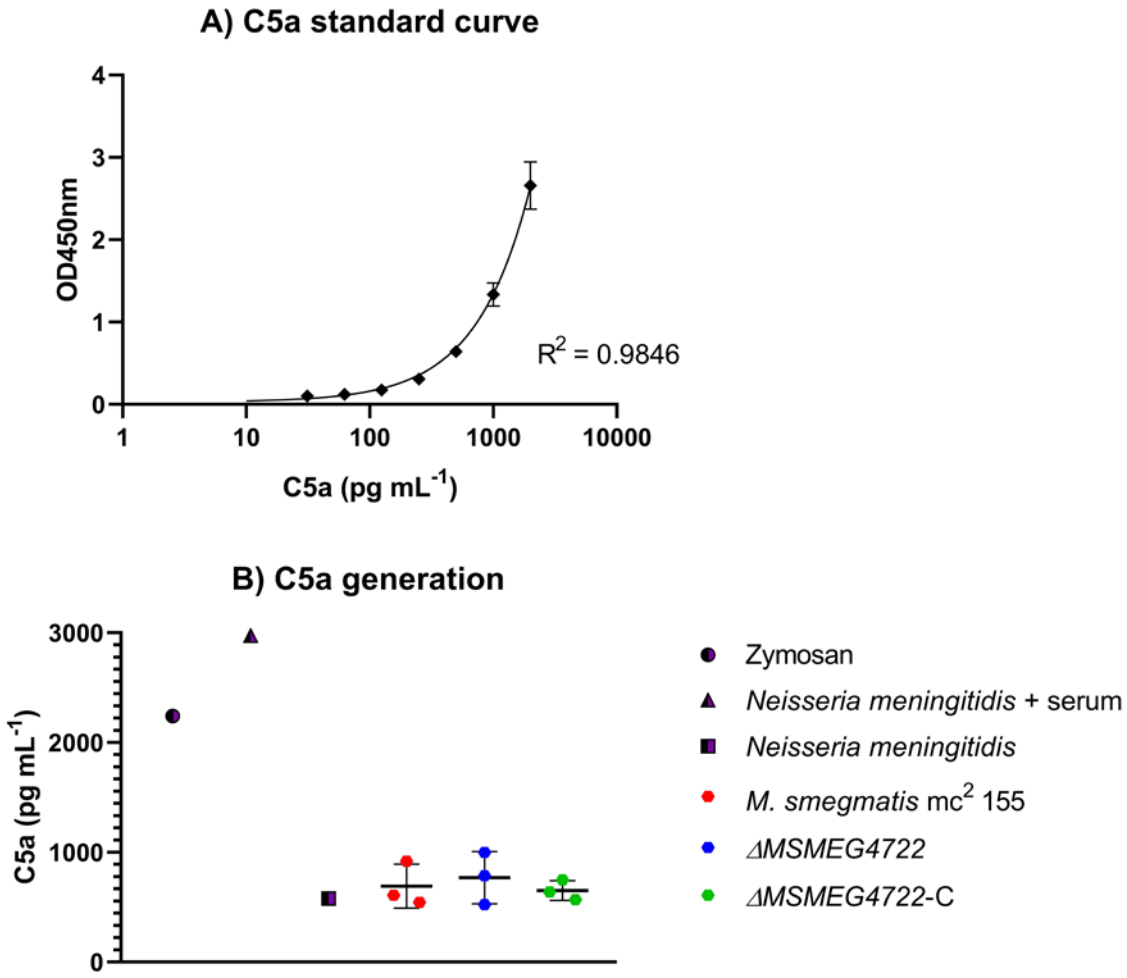


Figure 5.3: C5a anaphylatoxin generation in the supernatant of *M. smegmatis* mc² 155, *ΔMSMEG4722* and *ΔMSMEG4722*-C incubated with complement.

Bacteria were incubated with 10% complement (all three pathways active), and the supernatant was measured for C5a generation by ELISA. (A) 8-point 1:2 C5a Standard Curve (Abcam). (B) Fluorescence was interpolated from a C5a standard curve to give C5a concentration in pg mL^{-1}. Error bars = standard deviation of three biological replicates. Statistical analysis performed was a one-way ANOVA with Tukey's multiple comparison correction.

5.2.2 Activator binding to *M. smegmatis* mc^2 155 and *ΔMSMEG4722*

5.2.2.1 Activator binding screen to identify positive controls

The complement cascade is initiated by activators binding to pathogen-associated molecular patterns, either directly or via antibodies (Merle *et al.*, 2015). To establish positive controls, activator binding (C1q, MBL, ficolin-1 and ficolin-2) was screened for on a range of bacteria and zymosan. Positive controls allowed us to confirm the functionality of activators and primary antibodies. Binding was assessed by flow cytometry. *Salmonella enterica* Minnesota R595 bound C1q, NTHi BV749 bound ficolin-2 and zymosan bound MBL and ficolin-1 (appendix 3 Figure A.3.1).

5.2.2.2 Ficolin-1 was the only activator to show increased binding to *ΔMSMEG4722* compared to *M. smegmatis* mc^2 155

To assess activator binding to *M. smegmatis* mc^2 155 and *ΔMSMEG4722*, three biological replicates of *M. smegmatis* mc^2 155, *ΔMSMEG4722* and *ΔMSMEG4722*-C and the positive controls for each activator were incubated with either C1q, MBL, ficolin-1 or ficolin-2. Primary antibodies for each activator were used to label binding, followed by a FITC-fluorescent secondary antibody for detection by flow cytometry (methods section 7.11).

Overall, activator binding on *M. smegmatis* mc^2 155 and *ΔMSMEG4722* was low compared to the positive controls. Ficolin-1 showed significantly greater binding to *ΔMSMEG4722*, compared to *M. smegmatis* mc^2 155 ($P = 0.0025$) (Figure 5.4C). C1q, MBL and ficolin-2 binding were comparable between *M. smegmatis* mc^2 155 and *ΔMSMEG4722* (Figure 5.4A, B and D, respectively).

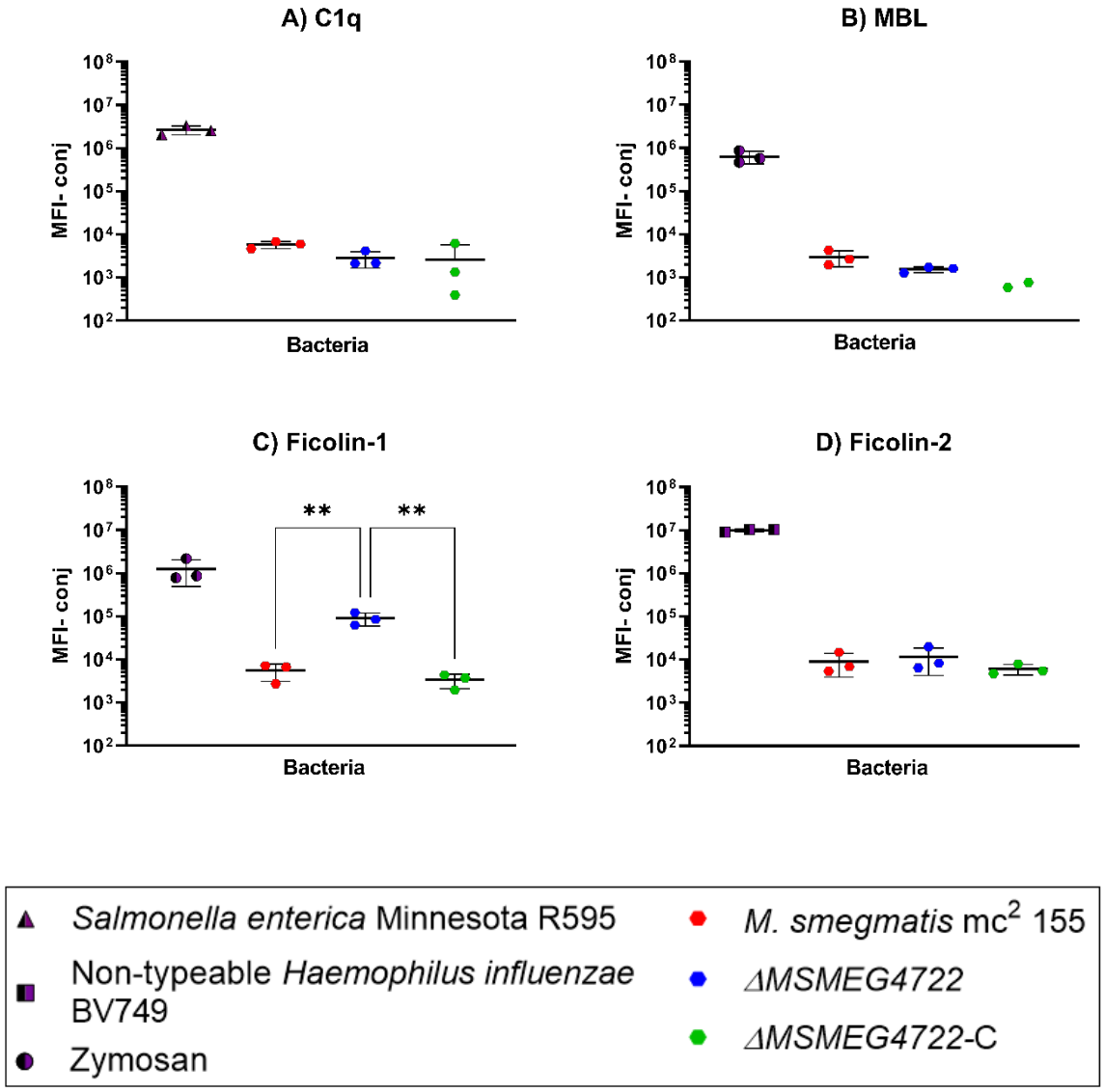


Figure 5.4: Complement activator binding to *M. smegmatis* mc² 155, *ΔMSMEG4722* and *ΔMSMEG4722*-C.

Median fluorescence intensity – conjugate only fluorescence (MFI-conj) corresponding to binding of (A) C1q (B) MBL (C) ficolin-1 or (D) ficolin-2, measured by flow cytometry. Positive controls used were *Salmonella enterica* Minnesota R595 (C1q), Non-typeable *Haemophilus influenzae* BV749 (ficolin-2) and zymosan (MBL and ficolin-1). One biological replicate of *ΔMSMEG4722*-C incubated with MBL produced a negative MFI-conj. Error bars = standard deviation of three biological replicates. Statistical analysis performed was one-way ANOVA with Tukey's multiple comparison correction. (C) ** P = 0.0025 (*M. smegmatis* mc² 155 vs *ΔMSMEG4722),* ** P = 0.0022 (*ΔMSMEG4722* vs *ΔMSMEG4722*-C).

5.2.3 C3b/iC3b deposition onto lipid fractions extracted from *M. smegmatis* mc^2 155 and *ΔMSMEG4722*

ΔMSMEG4722 has an altered lipid profile compared to *M. smegmatis* mc^2 155, including the loss of mature mycolates for mycolic acid intermediates and redistribution of glycolipids through the cell envelope (results chapter 4, Table 4.2). To evaluate whether these changes in lipid profile can explain or account for whole-cell differences in complement activation and ficolin-1 binding on *ΔMSMEG4722*, the lipid fractions characterised in chapter 4 were assessed for C3b/iC3b deposition by ELISA.

5.2.3.1 Development of a lipid-based C3b/iC3b ELISA

A lipid-based ELISA was developed to evaluate complement activation via C3b/iC3b deposition by mycobacterial lipid fractions. This was based on a carbohydrate-based C3b/iC3b ELISA (Keating *et al.*, 2021) and lipid-based ELISAs for antibody-binding from the literature, summarised by Julián *et al.*, (2001).

The ELISA was developed by; 1) identifying a solvent composition to resuspend and dilute lipids (2:1 chloroform: methanol diluted in ethanol), 2) identifying a preferentially coated plate for lipid-binding (Nunc™ Microplate, Immuno Polysorp), 3) identifying a suitable positive control (cholesterol), 4) evaluating the effect of 0.05% Tween-20 in the blocking buffer (removed), 5) optimising blocking conditions (5% Foetal Calf Serum, 1.5 hours), 6) optimising the coating concentration (50µg mL^{-1}) and 7) evaluating the effect of adding barbitone during complement incubation and anti-C3c HRP binding (barbitone not included in final assay) (appendix 3 Figure A.3.2-Figure A.3.6). A carbohydrate-based C3 standard curve was generated to interpolate

fluorescence values into ng of C3 deposition (C3 = C3b/iC3b deposition) (methods section 7.20 appendix 3 Figure A.3.7).

5.2.3.2 Only the outer apolar lipids displayed increased C3b/iC3b binding to *ΔMSMEG4722* compared to *M. smegmatis* mc^2 155

Lipid fractions (outer apolar, inner apolar, polar and FAMEs and MAMEs) extracted from three biological replicates of *M. smegmatis* mc^2 155, *ΔMSMEG4722* and *ΔMSMEG4722*-C (methods section 7.16) were incubated with 10% (all three pathways active) or 2% complement (classical and lectin pathway activation only) IgG- and IgM-depleted complement, and assessed for complement activation via C3b/iC3b deposition by ELISA (methods section 7.21).

The only lipid fraction of *ΔMSMEG4722* that showed altered complement activation was the outer apolar lipids. When all three pathways were active and when only the classical and lectin pathways were active, there was statistically more C3b/iC3b deposition on *ΔMSMEG4722* compared to *M. smegmatis* mc^2 155 (P = 0.0322 and P = 0.0104 respectively) (Figure 5.5A).

For the inner apolar lipids, polar lipids and FAMEs and MAMEs, there was no difference in C3b/iC3b deposition between *M. smegmatis* mc^2 155 and *ΔMSMEG4722* using either complement condition (Figure 5.5B- Figure 5.5D).

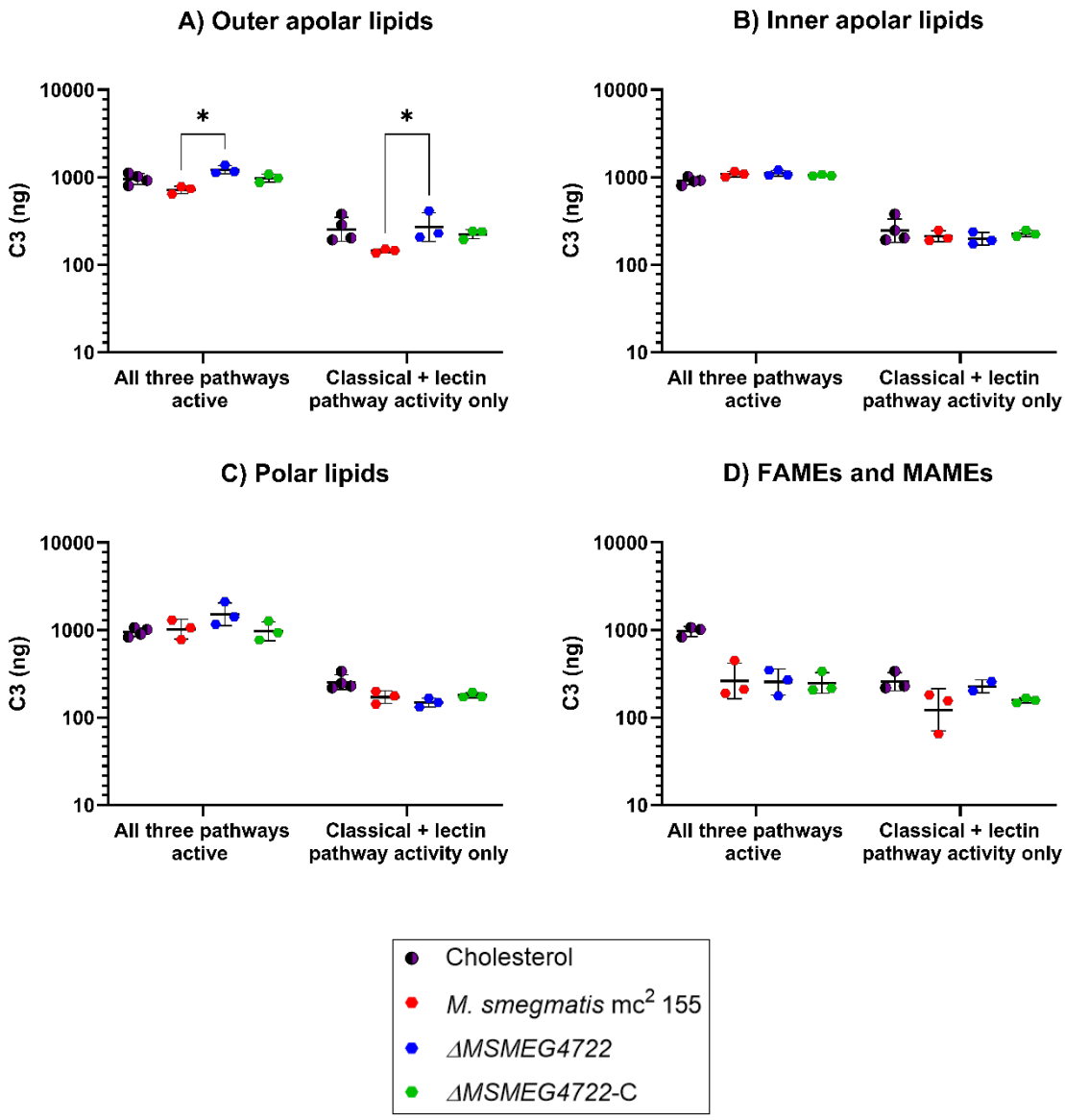


Figure 5.5: C3b/iC3b deposition on *M. smegmatis* mc^2 155, *ΔMSMEG4722* and *ΔMSMEG4722*-C lipid fractions.

C3b/iC3b deposition measured by ELISA. Lipid fractions were incubated with 10% complement (all three pathways active) or 2% complement (classical and lectin pathway activity only). (A) Outer apolar lipids (B) Inner apolar lipids (C) Polar lipids (D) FAMEs and MAMEs. Fluorescence values (minus complement only background) were log10 transformed and interpolated from the C3 standard curve to give C3b/iC3b deposition in ng. C3 = C3b/iC3b deposition. Error bars = standard deviation of three biological replicates. Statistical analysis performed were two-way ANOVA with Tukey's multiple comparison correction. (A) * P = 0.0322 (*M. smegmatis* mc^2 155 10% vs *ΔMSMEG4722* 10%), * P = 0.0104 (*M. smegmatis* mc^2 155 2% vs *ΔMSMEG4722* 2%).

5.2.4 C3b/iC3b deposition onto *M. smegmatis* mc^2 155 and *ΔMSMEG4722* carbohydrate fractions

The loss of the reductase function for maturation of the mycolic motif should not chemically alter the carbohydrates/lipoglycans of *ΔMSMEG4722,* and therefore should not alter their activation of complement. The outermost carbohydrates/lipoglycans were extracted from *M. smegmatis* mc^2 155, *ΔMSMEG4722* and *ΔMSMEG4722*-C and analysed for complement activation to investigate this. This fraction should primarily consist of a mixture of Lipomannan, Lipoarabinomannan and PIMs.

5.2.4.1 Development of a carbohydrate-based ELISA

To evaluate complement activation via C3b/iC3b deposition onto mycobacterial carbohydrate/lipoglycan, the lipid-based C3b/iC3b ELISA conditions were re-evaluated. The ELISA was adapted by; 1) identifying an appropriate carbohydrate-binding plate (Nunc, MaxiSorp™), 2) re-evaluating the effect of adding barbitone to the binding buffer during complement incubation and anti-C3c HRP binding (added), 3) identifying a positive control (zymosan), 4) optimising blocking conditions (1% BSA, 1.5 hrs) and 5) optimising the coating concentration (12.5µg mL^{-1}) (appendix 3 Figure A.3.8-Figure A.3.10). A C3 standard curve was used to interpolate fluorescence values into ng of C3 deposition (C3 = C3b/iC3b deposition) (method section 7.20). The final ELISA method can be found in methods section 7.22.

5.2.4.2 Comparable C3b/iC3b deposition levels were observed between *M. smegmatis* mc^2 155 and *ΔMSMEG4722* extracted lipoglycans

Carbohydrate/lipoglycans extracted from *M. smegmatis* mc^2 155, *ΔMSMEG4722* and *ΔMSMEG4722*-C (methods section 7.19) were incubated with 10% (all three pathways

active) or 2% (classical and lectin pathway activation only) IgG- and IgM-depleted complement and assessed for complement activation via C3b/iC3b deposition by ELISA (methods section 7.22).

High, comparable C3b/iC3b deposition levels were observed on *M. smegmatis* mc^2 155 and *ΔMSMEG4722* when all three pathways were active. Comparable C3b/iC3b deposition levels were also observed on *M. smegmatis* mc^2 155 and *ΔMSMEG4722* when the alternative pathway was inhibited (Figure 5.6).

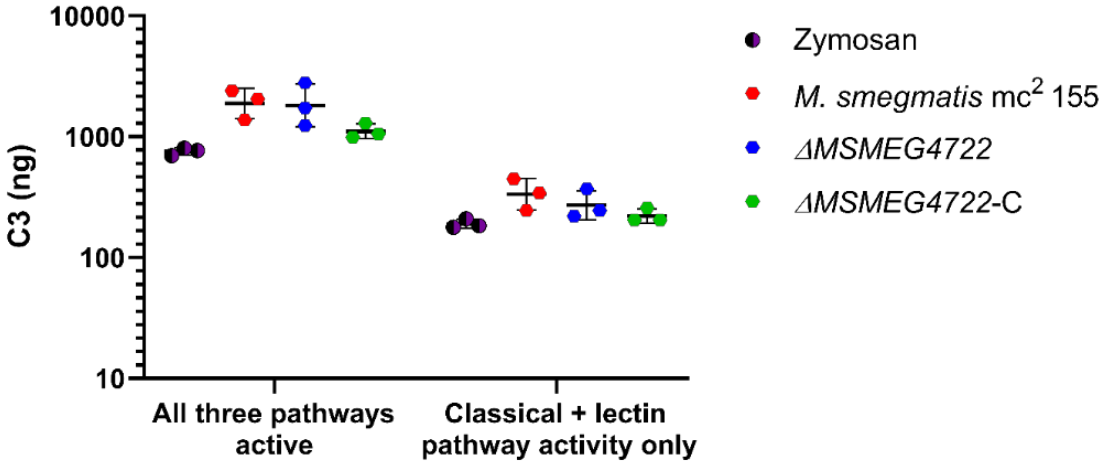


Figure 5.6: C3b/iC3b deposition on *M. smegmatis* mc^2 155, *ΔMSMEG4722* and *ΔMSMEG4722*-C carbohydrate/ lipoglycan extractions.

C3b/iC3b deposition measured by ELISA. Carbohydrate/lipoglycan fractions were incubated with 10% complement (all three pathways active) or 2% complement (classical and lectin pathway activation only). C3 = C3b/iC3b deposition. Error bars = standard deviation of three biological replicates. Fluorescence values (minus complement only background) were log10 transformed and interpolated from the C3 standard curve to give C3/iC3b deposition in ng. Statistical analysis performed was two-way ANOVA with Tukey's multiple comparison correction. Error bars = standard deviation of three biological replicates.

5.2.5 Summary of Aim 1 results

When all three complement pathways are active, more C3b/iC3b and C5b-9 deposition was observed on *ΔMSMEG4722* than *M. smegmatis* mc^2 155. Ficolin-1 was the only activator to show increased binding to *ΔMSMEG4722* compared to *M. smegmatis* mc^2 155. The outer apolar lipid fraction was the only lipid fraction with more significant C3b/iC3b deposition on *ΔMSMEG4722* than *M. smegmatis* mc^2 155. There was no difference in C3b/iC3b deposition on the extracted carbohydrates/ lipoglycans between strains.

5.3 Results Aim 2: Functional activation of the complement cascade by planktonic and pellicle biofilm *M. smegmatis* mc^2 155 and *ΔMSMEG4722*

The next aim was to determine the impact of pellicle biofilm growth on complement activation and whether being unable to produce mature reticulated pellicle biofilms (*ΔMSMEG4722*) affects these complement interactions.

5.3.1 Complement protein deposition and C5a generation onto planktonic and pellicle biofilm mycobacteria

5.3.1.1 Increased C3b/iC3b deposition was observed on both phenotypes of *ΔMSMEG7422* compared to *M. smegmatis* mc^2 155

Six biological replicates of either live planktonic or pellicle biofilm *M. smegmatis* mc^2 155, *ΔMSMEG4722* and *ΔMSMEG4722*-C and the positive control zymosan were incubated with either 10% (all three pathways active) or 2% (classical and lectin pathway only) IgG- and IgM-depleted complement. Bacteria were then labelled with the appropriate fluorescent antibodies to measure complement activation via C3b/iC3b and C5b-9 deposition by flow cytometry (methods section 7.10).

A significant increase in C3b/iC3b deposition was observed on planktonic *ΔMSMEG4722* compared to planktonic *M. smegmatis* mc^2 155, only when all three complement pathways were active (P = 0.0195). Increased C3b/iC3b deposition was also observed on pellicle biofilm *ΔMSMEG4722* compared to pellicle biofilm *M. smegmatis* mc^2 155, only when all three pathways were active, but this was not statistically significant. Between the phenotypes of *M. smegmatis* mc^2 155 or *ΔMSMEG4722*, there was no difference in C3b/iC3b deposition in either complement condition (Figure 5.7A).

A trend of increased C5b-9 deposition was observed on both planktonic and pellicle biofilm *ΔMSMEG4722* compared to their *M. smegmatis* mc^2 155 counterparts, only when all three pathways were active. These were not statistically significant. Between the phenotypes of *M. smegmatis* mc^2 155 or *ΔMSMEG4722*, there was no difference in C5b-9 deposition in either complement condition (Figure 5.7B).

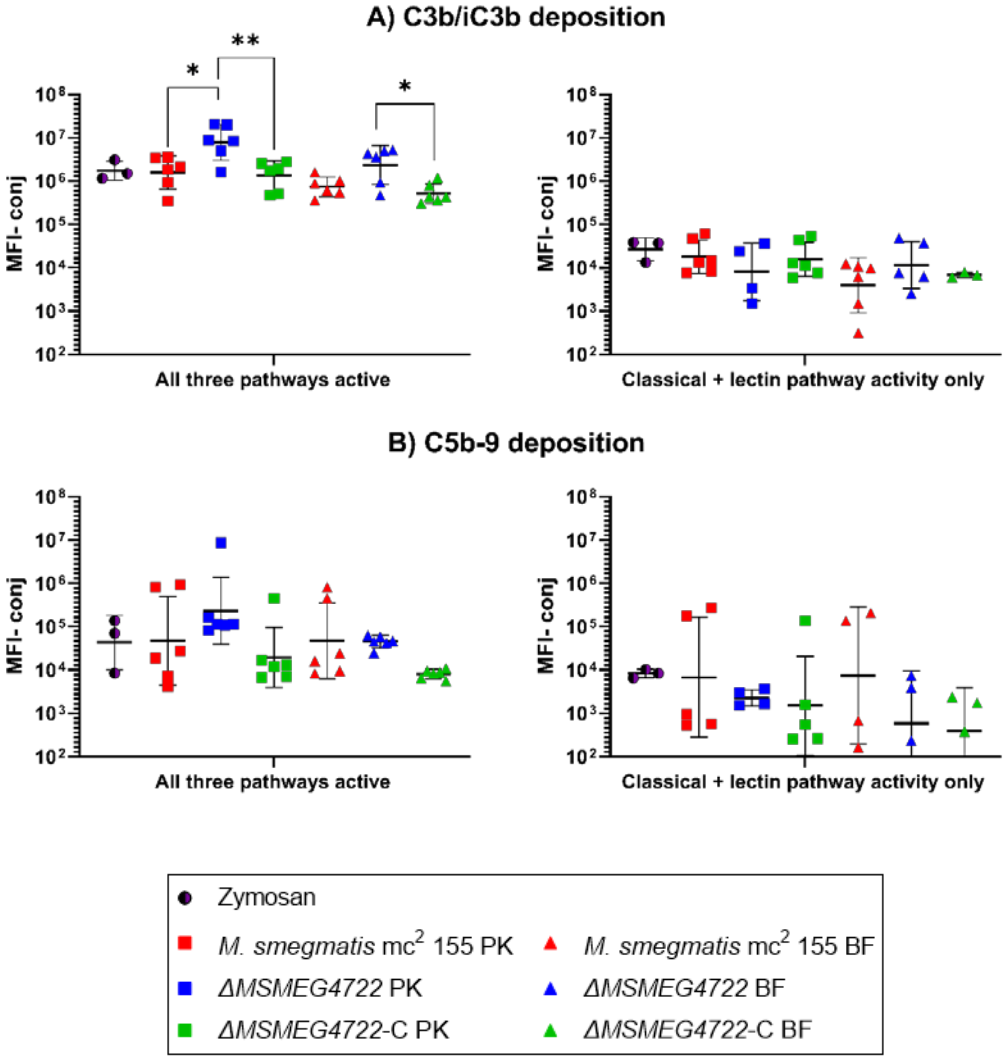


Figure 5.7: C3b/iC3b and C5b-9 deposition on planktonic and pellicle biofilm *M. smegmatis* mc² 155, *ΔMSMEG4722* and *ΔMSMEG4722*-C.

Median fluorescence intensity – conjugate only fluorescence (MFI-conj) corresponds to (A) C3b/iC3b deposition or (B) C5b-9 deposition, measured by flow cytometry. Bacteria were incubated with either 10% complement (all three pathways active) or 2% complement (classical and lectin pathway activity only). Zymosan (black/purple circles) was used as a positive control. Planktonic (PK) (squares), pellicle biofilm (BF) (triangles). Using 2% complement, MFI-conj correlating to C5b-9 deposition was negative for one biological replicate of planktonic *ΔMSMEG4722* (blue), two biological replicates of planktonic *ΔMSMEG4722*-C (green), one biological replicate of pellicle biofilm *M. smegmatis* mc² 155 (red) and three biological replicates of pellicle biofilm *ΔMSMEG4722* and *ΔMSMEG4722*-C. For statistical analysis, data were log10 transformed before performing a two-way ANOVA with Tukey's multiple comparison correction. (A) * P = 0.0195 (*M. smegmatis* mc² 155 PK vs *ΔMSMEG4722* PK), * P = 0.0319 (*ΔMSMEG4722* BF vs *ΔMSMEG4722*-C BF), ** P = 0.0083. Error bars = standard deviation of six biological replicates.

5.3.1.2 C5a generation was increased in the supernatant of planktonic and pellicle biofilm *ΔMSMEG4722* compared to *M. smegmatis* mc² 155

To measure C5a anaphylatoxin generation from the activated complement cascade, either live planktonic or pellicle biofilm *M. smegmatis* mc^2 155, *ΔMSMEG4722* and *ΔMSMEG4722*-C were incubated with 10% IgG- and IgM-depleted complement (all three pathways active) and the supernatants added to a C5a commercial ELISA kit (Abcam) (methods section 7.24).

There was significantly more C5a generated in the supernatants of planktonic and pellicle biofilm *ΔMSMEG4722* compared to their *M. smegmatis* mc^2 155 counterparts (P = 0.0078 and P = 0.0175 respectively). Between the phenotypes of *M. smegmatis* mc^2 155 or *ΔMSMEG4722*, there was no difference in C5a in the supernatant (Figure 5.8).

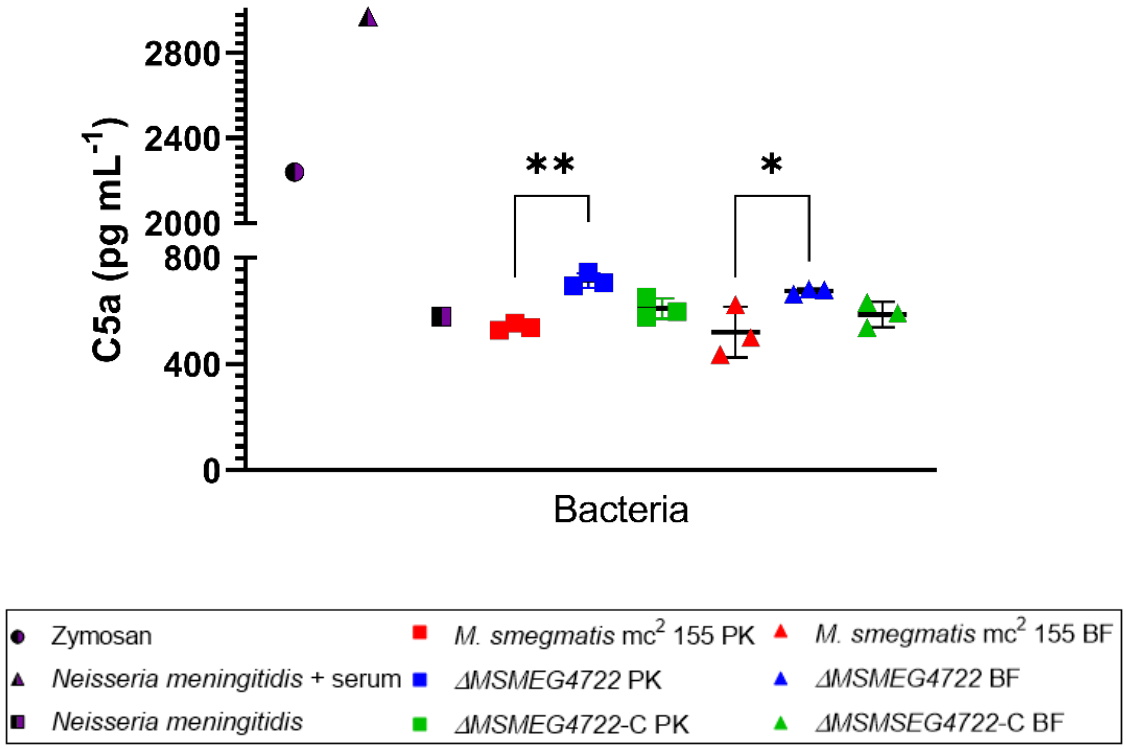


Figure 5.8: C5a anaphylatoxin generation in the supernatant of planktonic and pellicle biofilm *M. smegmatis* mc² 155, *ΔMSMEG4722* or *ΔMSMEG4722*-C incubated with complement.

Bacteria were incubated with 10% complement (all three pathways active), and the supernatant was tested for the generation of C5a by ELISA. Planktonic (PK) (squares) and pellicle biofilm (BF) (triangles). Fluorescence was interpolated from a C5a standard curve to give C5a concentration in pg mL^{-1}. Error bars = standard deviation of three biological replicates. Statistical analysis by one-way ANOVA with Tukey's multiple comparison correction, ** P = 0.0078, * P = 0.0175.

5.3.2 Activator binding to planktonic and pellicle biofilm mycobacteria

Activator binding was assessed to determine if activator affinities differ between *M. smegmatis* mc^2 155 phenotypes. Another aim was to understand which activators facilitated increased complement activation by *ΔMSMEG4722* and whether this differed between phenotypes.

Three biological replicates of either planktonic or pellicle biofilm *M. smegmatis* mc^2 155, *ΔMSMEG4722* and *ΔMSMEG4722*-C and the positive controls for each activator were incubated with either C1q, MBL, ficolin-1 or ficolin-2. Primary antibodies for each activator were used to label binding, followed by a FITC-fluorescent secondary antibody for detection by flow cytometry (methods section 7.11). The range of activator binding onto the same strain and phenotype (e.g. *M. smegmatis* mc^2 155 planktonic) can be found in appendix 3 Figure A.3.11.

5.3.2.1 C1q binding decreases on pellicle biofilm-derived *M. smegmatis* mc^2 155 compared to planktonic *M. smegmatis* mc^2 155

Between the phenotypes of *M. smegmatis* mc^2 155, there was a significant decrease in C1q binding on pellicle biofilm compared to planktonic cells (P = 0.0006) (Figure 5.9A). There was also a decrease in ficolin-1 and ficolin-2 binding on pellicle biofilm compared to planktonic cells, but not statistically significant (Figure 5.9C and D).

5.3.2.2 *ΔMSMEG4722* pellicle biofilm-derived bacteria bind more ficolin-1 and ficolin-2 than planktonic *ΔMSMEG4722*

There were comparable levels of C1q binding between planktonic and biofilm *ΔMSMEG4722* (Figure 5.9A). However, the binding of ficolin-1 and ficolin-2 was significantly increased on the biofilm cells (P = 0.257 and P < 0.0001 respectively) (Figure 5.9C and D).

5.3.2.3 C1q binding is lower on planktonic *ΔMSMEG4722* compared to planktonic *M. smegmatis* mc^2 155

Between *M. smegmatis* mc^2 155 and *ΔMSMEG4722*, on planktonic cells, there was a significant decrease in C1q binding to *ΔMSMEG4722* compared to *M. smegmatis* mc^2

155 (P = 0.0013) (Figure 5.9A). Ficolin-1 and ficolin-2 binding were comparable (Figure 5.9C and D).

Comparing pellicle biofilm-derived bacteria, there was more C1q binding onto *ΔMSMEG4722* compared to *M. smegmatis* mc^2 155, but this was not statistically significant (Figure 5.9A). Ficolin-1 and ficolin-2 showed statistically greater binding to *ΔMSMEG4722* compared to *M. smegmatis* mc^2 155 (P = 0.015 and P < 0.0001 respectively) (Figure 5.9C and D).

MBL binding was comparable between phenotypes for both *M. smegmatis* mc^2 155 and *ΔMSMEG4722*. There was no difference in MBL binding between strains for either planktonic cells or pellicle biofilm cells (Figure 5.9B).

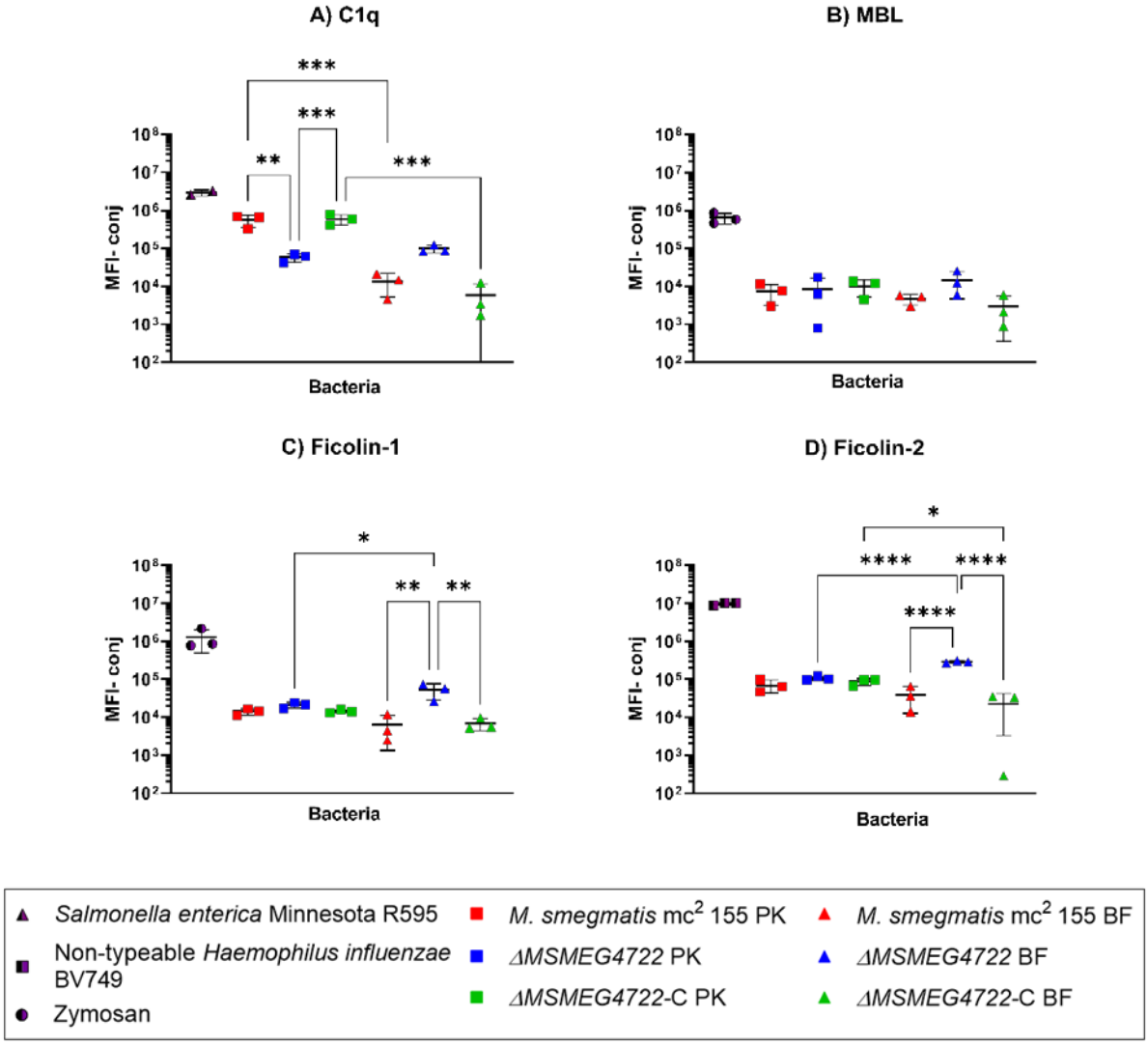


Figure 5.9: Complement activator binding to planktonic and pellicle biofilm *M. smegmatis* mc² 155, *ΔMSMEG4722* and *ΔMSMEG4722*-C.

Median fluorescence intensity – conjugate only fluorescence (MFI-conj) corresponds to binding of (A) C1q (B) MBL (C) ficolin-1 or (D) ficolin-2, measured by flow cytometry. Planktonic (PK) (squares), pellicle biofilm (BF) (triangles). Positive controls used were *Salmonella enterica* Minnesota R595 (C1q), Non-typeable *haemophilus influenzae* BV749 (ficolin-2) and zymosan (MBL and ficolin-1). Error bars = standard deviation of three biological replicates. Statistical analysis performed were one-way ANOVA with Tukey's multiple comparison correction. (A) ** P = 0.0013 (*M. smegmatis* mc² 155 PK vs *ΔMSMEG4722* PK), *** P = 0.0007 (*ΔMSMEG4722* vs *ΔMSMEG4722*-C), *** P = 0.0006 (*M. smegmatis* mc² 155 PK vs *M. smegmatis* mc² 155 BF), *** P = 0.0003 (*ΔMSMEG4722*-C PK vs *ΔMSMEG4722*-C BF) (C) * P = 0.0257, ** P = 0.0015 (*M. smegmatis* mc² 155 vs *ΔMSMEG4722),* ** P = 0.0016 (*ΔMSMEG4722* vs *ΔMSMEG4722*-C), (D) * P = 0.0230, **** P < 0.0001.

5.3.3 C3b/iC3b deposition measured onto lipid fractions from extracted planktonic and pellicle biofilm mycobacteria

M. smegmatis mc^2 155 accumulated FMA in pellicle biofilms compared to planktonic cells. *ΔMSMEG4722* also accumulated unsaturated ketones (decarboxylated α-alkyl, β-oxo mycolate intermediates/ pre-mycolates) in pellicle biofilms and had different distributions of glycolipids between phenotypes lipid fractions. Both phenotypes of *ΔMSMEG4722* had altered glycolipid distribution compared to their *M. smegmatis* mc^2 155 counterparts (results chapter 4, Table 4.4). To evaluate whether these changes in lipid profile can explain or account for phenotypic differences observed in both complement deposition and activator binding, the lipid fractions (outer apolar, inner apolar, polar, and FAMEs and MAMEs) extracted from three biological replicates of either planktonic or pellicle biofilm *M. smegmatis* mc^2 155, *ΔMSMEG4722* and *ΔMSMEG4722*-C (methods section 7.16) were assessed for complement activation via C3b/iC3b deposition by ELISA (methods section 7.21). Comparing phenotypes for *M. smegmatis* mc^2 155 or *ΔMSMEG4722* is summarised in chapter 4 Table 4.4. Comparing *ΔMSMEG4722* and *M. smegmatis* mc^2 155 for both phenotypes is summarised in chapter 4 Table 4.3.

5.3.3.1 *M. smegmatis* mc^2 155 pellicle biofilm-derived apolar lipid fractions have lower C3b/iC3b deposition compared to planktonic cells

Comparing the planktonic and pellicle biofilm-derived lipids of *M. smegmatis* mc^2 155, for the outer and inner apolar lipid fractions, when all three pathways were active, there was significantly less C3b/iC3b deposition onto pellicle biofilm-derived lipids compared to planktonic ($P < 0.0001$ and $P = 0.0017$ respectively) (Figure 5.10A and B). For the outer apolar lipid fraction only, this pattern was also observed when only the classical

and lectin pathways were active (P < 0.0001) (Figure 5.10A). For the polar lipid fraction, increased deposition on pellicle biofilm-derived lipids compared to planktonic derived lipids was observed only when all three pathways were active (P = 0.0086) (Figure 5.10C).

5.3.3.2 For all lipid fractions of *ΔMSMEG4722*, C3b/iC3b deposition was comparable between planktonic and pellicle biofilm lipids

For planktonic and pellicle biofilm derived lipids of *ΔMSMEG4722* when comparing within a lipid fraction (outer apolar, inner apolar and polar), under both complement conditions, no statistical differences in C3b/iC3b deposition were observed (Figure 5.10A-C).

5.3.3.3 Decreased C3b/iC3b deposition was observed on the outer apolar lipids of both phenotypes of *ΔMSMEG4722* compared to *M. smegmatis* mc^2 155

Between phenotypes of *M. smegmatis* mc^2 155 and *ΔMSMEG4722*, on the outer apolar lipids, there was a significant decrease in C3b/iC3b deposition on planktonic *ΔMSMEG4722* (P < 0.0001) and pellicle biofilm *ΔMSMEG4722* (P < 0.0001) lipids when all three pathways were active. This was also observed when only the classical and lectin pathways were active (P < 0.0001 planktonic and P = 0.033 pellicle biofilm) (Figure 5.10A).

For the inner apolar and polar lipid fractions when all three pathways are active, as a consequence of the phenotypic changes in *M. smegmatis* mc^2 155, increased C3b/iC3b deposition was observed on *ΔMSMEG4722* pellicle biofilm inner apolar lipids compared to pellicle biofilm *M. smegmatis* mc^2 155 (P = 0.033) and more C3b/iC3b

deposition onto *ΔMSMEG4722* planktonic polar lipids compared to planktonic *M. smegmatis* mc^2 155 (P = 0.0016).

There was minimal C3b/iC3b deposition onto all FAMEs and MAMEs lipid extracts tested (Figure 5.10D).

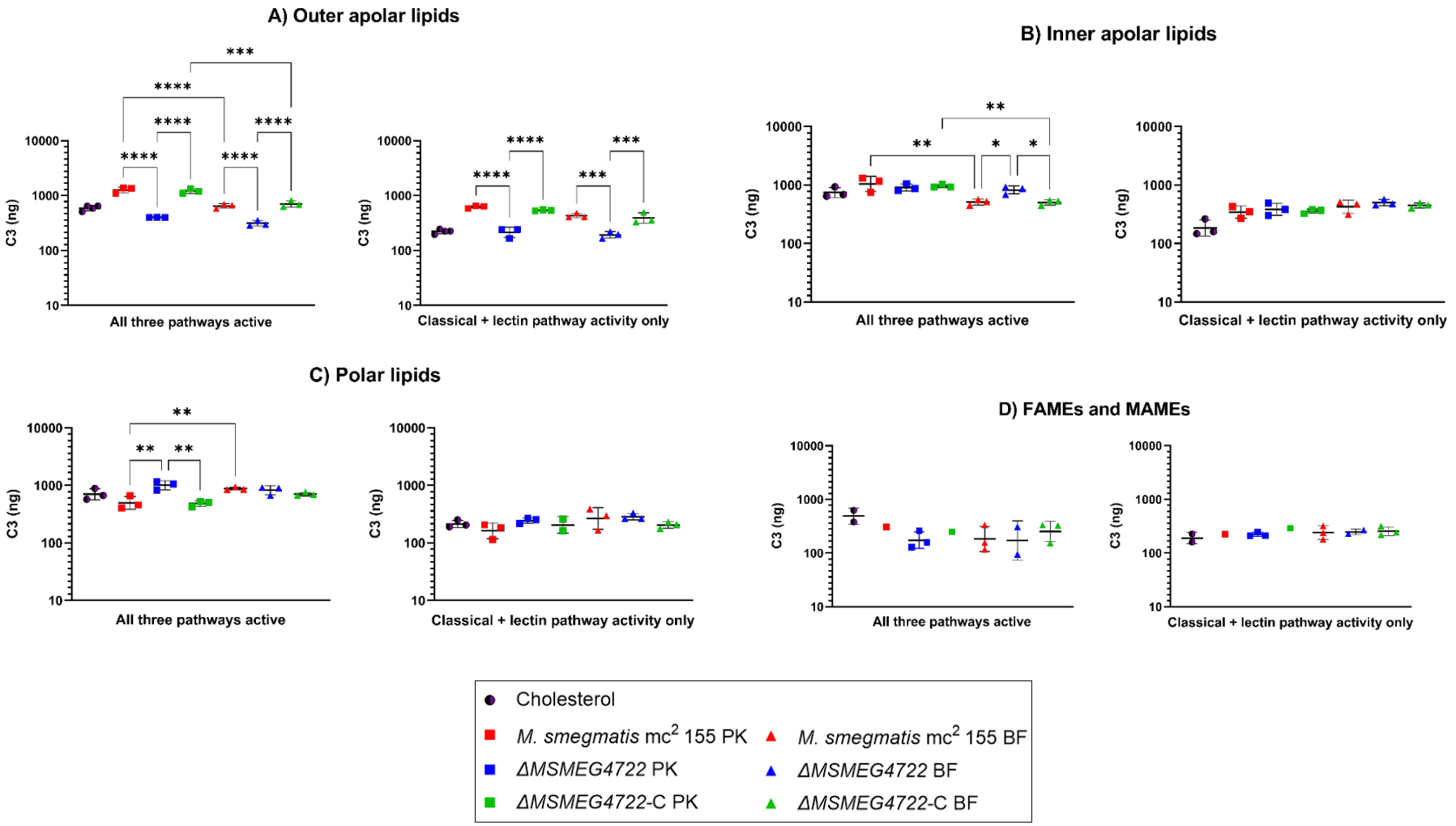

A) Outer apolar lipids
B) Inner apolar lipids
C) Polar lipids
D) FAMEs and MAMEs
C3 (ng)
All three pathways active
Classical + lectin pathway activity only
Cholesterol
M. smegmatis mc2 155 PK
M. smegmatis mc2 155 BF
ΔMSMEG4722 PK
ΔMSMEG4722 BF
ΔMSMEG4722-C PK
ΔMSMEG4722-C BF

Figure 5.10: C3b/iC3b deposition on lipid extracts from planktonic and pellicle biofilm *M. smegmatis* mc^2 155, *ΔMSMEG4722* and *ΔMSMEG4722*-C.

C3b/iC3b deposition measured by ELISA. Lipids were incubated with 10% complement (all three pathways active) or 2% complement (classical and lectin pathway activity only). (A) Outer apolar lipids (B) Inner apolar lipids (C) Polar lipids (D) FAMEs and MAMEs. C3 = C3b/iC3b deposition. Planktonic (PK) (squares), pellicle biofilm (BF) (triangles). Error bars = standard deviation of three biological replicates. Fluorescence values (minus complement only background) were log10 transformed and interpolated from the C3 standard curve to give C3b/iC3b deposition in ng. Statistical analysis performed were two-way ANOVA with Tukey's multiple comparison correction. (A) All three pathways active: *** P = 0.0004, **** P < 0.0001. Classical and lectin pathways only: *** P = 0.0002 (*M. smegmatis* mc^2 155 BF vs *ΔMSMEG4722* BF), *** P = 0.0008 (*ΔMSMEG4722* BF vs *ΔMSMEG4722*-C BF), **** P < 0.0001. (B) ** P = 0.0017 (*M. smegmatis* mc^2 155 PK vs *M. smegmatis* mc^2 155 BF), ** P = 0.0043 (*ΔMSMEG4722*-C PK vs *ΔMSMEG4722*-C BF), * P = 0.033 (*M. smegmatis* mc^2 155 BF vs *ΔMSMEG4722* BF), * P = 0.0292 (*ΔMSMEG4722* BF vs *ΔMSMEG4722*-C BF) (C) ** P = 0.0016 (*M. smegmatis* mc^2 155 PK vs *ΔMSMEG4722* PK), ** P = 0.0012 (*ΔMSMEG4722* PK vs *ΔMSMEG4722*-C PK), ** P = 0.0086 (*M. smegmatis* mc^2 155 PK vs *M. smegmatis* mc^2 155 BF).

Table 5.1: C3b/iC3b deposition onto extracted lipid fractions comparing pellicle biofilms and planktonic cells for both *M. smegmatis* mc² 155 and *ΔMSMEG4722* (planktonic used as the control).

Complement condition	Lipid Fraction	Pellicle Biofilm	
		***M. smegmatis* mc² 155**	***ΔMSMEG4722***
All three pathways active	Outer apolar	↓ P < 0.0001	=
	Inner apolar	↓ P = 0.0017	=
	Polar	↑ P = 0.0086	=
	FAMEs and MAMEs	=	=
Classical and lectin pathway activity only	Outer apolar	=	=
	Inner apolar	=	=
	Polar	=	=
	FAMEs and MAMEs	=	=

Table 5.2: C3b/iC3b deposition onto extracted lipid fractions comparing *ΔMSMEG4722* and *M. smegmatis* mc² 155 (*M. smegmatis* mc² 155 phenotype used as the control).

Complement condition	Lipid fraction	*ΔMSMEG4722*	
		Planktonic	**Pellicle Biofilm**
All three pathways active	Outer apolar	↓ P < 0.0001	↓ P < 0.0001
	Inner apolar	=	↑ P = 0.033
	Polar	↑ P = 0.0016	=
	FAMEs and MAMEs	=	=
Classical and lectin pathway activity only	Outer apolar	↓ P <0.0001	↓ P = 0.0002
	Inner apolar	=	=
	Polar	=	=
	FAMEs and MAMEs	=	=

5.3.4 Minimal C3b/iC3b deposition was observed onto both planktonic and pellicle biofilm lipoglycans of *M. smegmatis* mc² 155 and *ΔMSMEG4722*

It is unknown whether an inability to reticulate into a mature pellicle biofilm will have a knock-on consequence on carbohydrates/lipoglycans in *ΔMSMEG4722* during pellicle biofilm formation. However, it has previously been shown for *M. tuberculosis* that

pellicle biofilm formation modulates the carbohydrates constituent sugars which are important for complement activation (Keating *et al.*, 2021).

Carbohydrate/lipoglycans extracted from three biological replicates of either planktonic or pellicle biofilm *M. smegmatis* mc^2 155, *ΔMSMEG4722* and *ΔMSMEG4722*-C (methods section 7.19) were incubated with 10% (all three pathways active) or 2% (classical and lectin pathway activation only) IgG- and IgM-depleted complement and assessed for complement activation via C3b/iC3b deposition by ELISA (methods section 7.22).

Analysing the planktonic and pellicle biofilm carbohydrate/lipoglycan extracts, there was low-level deposition of C3b/iC3b onto both *M. smegmatis* mc^2 155 and *ΔMSMEG4722* cultured as either phenotype at both concentrations of complement (Figure 5.11).

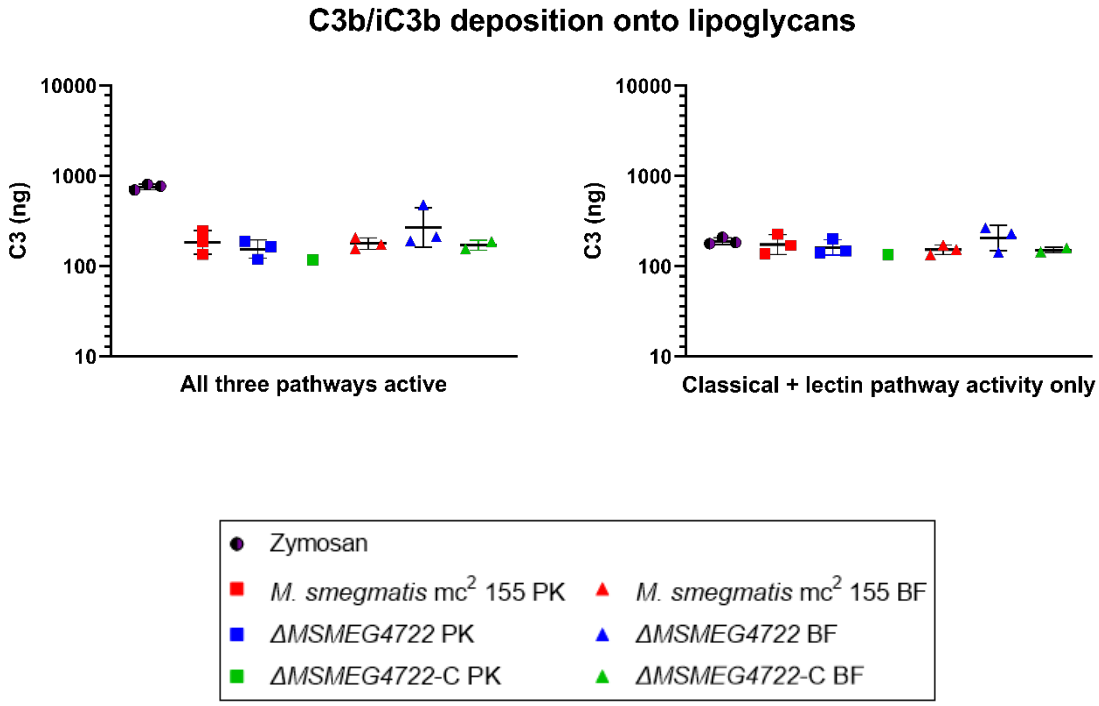


Figure 5.11: C3b/iC3b deposition on planktonic and pellicle biofilm *M. smegmatis* mc² 155, *ΔMSMEG4722* and *ΔMSMEG4722*-C carbohydrate/lipoglycan extractions.

C3b/iC3b deposition measured by ELISA. Carbohydrate/lipoglycan fractions were incubated with 10% complement (all three pathways active) or 2% complement (classical and lectin pathway activity only). Fluorescence values (minus complement only background) were log10 transformed and interpolated from the C3 standard curve to give C3 concentration in ng. C3 = C3b/iC3b deposition in ng. Planktonic (PK) (squares) and pellicle biofilm (BF) (triangles). Two planktonic *ΔMSMEG4722*-C extractions and one *ΔMSMEG4722*-C pellicle biofilm extraction fell below conjugate only fluorescence at both 10% and 2% complement so could not be interpolated. Error bars = standard deviation of three biological replicates. Statistical analysis performed was two-way ANOVA with Tukey's multiple comparison correction.

5.3.5 Summary of Aim 2 results

Comparable C3b/iC3b deposition, C5b-9 deposition and C5a generation was observed between planktonic and pellicle biofilm *M. smegmatis* mc² 155. There was a significant decrease in activator C1q binding on pellicle biofilm compared to planktonic cells. Although not statistically significant, a decrease was observed in ficolin-1 and ficolin-2 binding on pellicle biofilms compared to planktonic cells. For the outer and inner apolar

lipid fractions, when all three pathways were active, there was significantly less C3b/iC3b deposition onto pellicle biofilm-derived lipids compared to planktonic-derived lipids. This pattern was also observed for the outer apolar lipid fraction only when the alternative pathway of complement was inhibited. On the polar lipid fraction, increased deposition on pellicle biofilm-derived lipids compared to planktonic-derived lipids was observed when all three pathways were active. Low, comparable deposition of C3b/iC3b was observed on both planktonic and pellicle biofilm extracted carbohydrates/lipoglycans.

Comparable C3b/iC3b deposition, C5b-9 deposition and C5a generation was observed between planktonic and pellicle biofilm *ΔMSMEG4722.* For the activators, there was a comparable binding of C1q but increased binding of ficolin-1 and ficolin-2 on pellicle biofilms compared to planktonic cells. For all planktonic and pellicle biofilm derived lipids when comparing within a lipid fraction, no statistical differences in C3b/iC3b deposition are observed. Low, comparable deposition of C3b/iC3b was observed on both planktonic and pellicle biofilm extracted carbohydrates/lipoglycans.

More C3b/iC3b deposition, C5b-9 deposition and C5a generation was observed on both planktonic and pellicle biofilm *ΔMSMEG4722* compared to their *M. smegmatis* mc^2 155 counterparts when all three pathways were active. There was a significant decrease in C1q binding onto planktonic *ΔMSMEG4722* compared to planktonic *M. smegmatis* mc^2 155. For the activators C1q, ficolin-1 and ficolin-2, there was more deposition onto pellicle biofilm *ΔMSMEG4722* compared to pellicle biofilm *M. smegmatis* mc^2 155. The outer apolar lipids had reduced C3b/iC3b deposition on *ΔMSMEG4722* compared to *M. smegmatis* mc^2 155 on both phenotypes. More

C3b/iC3b deposition was observed onto *ΔMSMEG4722* pellicle biofilm-derived inner apolar lipids compared to *M. smegmatis* mc^2 155 pellicle biofilms, and more C3b/iC3b deposition was observed on *ΔMSMEG4722* planktonic derived polar lipids compared to *M. smegmatis* mc^2 155. There was low comparable deposition onto both phenotypes of carbohydrates/lipoglycans extracted from *ΔMSMEG4722* compared to *M. smegmatis* mc^2 155.

5.4 Results Aim 3: Purified *Mycobacterium* spp. cell envelope components show a range of C3b/iC3b deposition

Few mycobacterial cell wall components are identified activators of the complement cascade. Purified cell envelope components from a range of *Mycobacterium* spp. sourced from BEI Resources (Table 5.3) were evaluated for complement activation via C3b/iC3b deposition. All solvent-soluble cell wall components were evaluated using the lipid-based ELISA (methods section 7.21). All water-soluble cell wall components were evaluated using the carbohydrate-based ELISA (method section 7.22).

Table 5.3: Purified mycobacterial cell wall components.

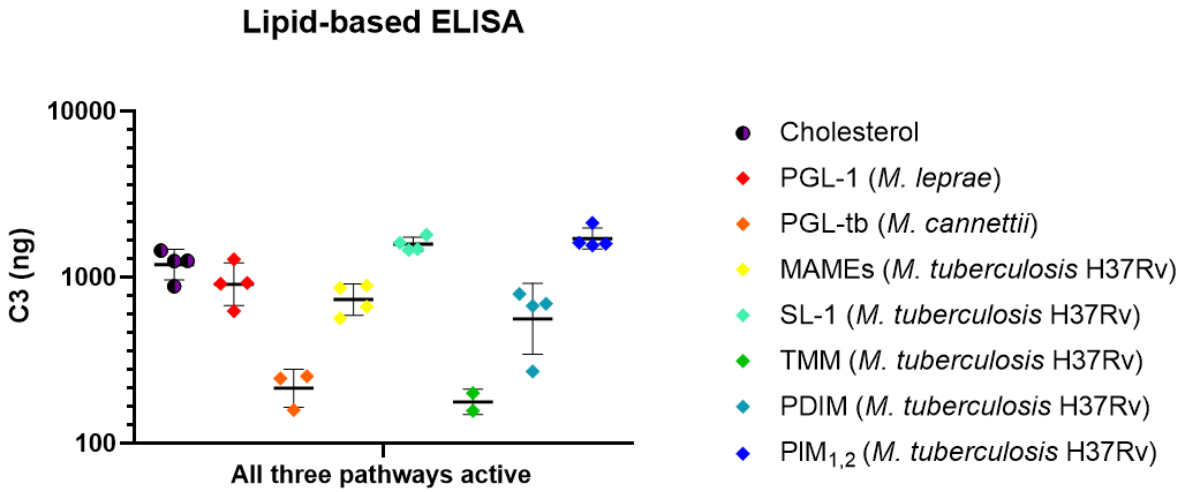
Lipid	Mycobacterial species
Arabinogalactan	*M. tuberculosis* H37Rv
Lipoarabinomannan (LAM)	*M. smegmatis*
Lipomannan (LM)	*M. tuberculosis* H37Rv
Mycolic acid methyl esters (MAMEs)	*M. tuberculosis* H37Rv
Mannosylated LAM (ManLAM)	*M. tuberculosis* H37Rv
Mannosylated LAM (ManLAM)	*M. leprae*
Phthiocerol dimycocerosates (PDIM)	*M. tuberculosis* H37Rv
Phenolic glycolipid-1 (PGL-1)	*M. leprae*
Phenolic glycolipid (PGL-tb)	*M. canetti*
Phosphatidylinositol mannoside 1,2 ($PIM_{1,2}$)	*M. tuberculosis* H37Rv
Phosphatidylinositol mannoside 6 (PIM_6)	*M. tuberculosis* H37Rv
Sulfolipid-1 (SL-1)	*M. tuberculosis* H37Rv
Trehalose monomycolate (TMM)	*M. tuberculosis* H37Rv

5.4.1 C3b/iC3b deposition on solvent-soluble cell envelope components

Evaluating solvent-soluble cell wall components with the lipid-based ELISA, statistically lower deposition of C3b/iC3b was observed on *M. tuberculosis* H37Rv TMM and *Mycobacterium canetti* PGL-tb compared to all other purified cell wall

components. There was a moderate level of deposition on *M. tuberculosis* H37Rv MAMEs and PDIM. Statistically higher C3b/iC3b deposition was observed on *M. tuberculosis* H37Rv SL-1 and $PIM_{1,2}$ compared to the other purified cell wall components, excluding PGL-1. There was species-specific variation between PGL complement activation, with significantly more C3b/iC3b deposition observed on *M. leprae* PGL-1, compared to *M. canetti* PGL-tb ($P < 0.0001$) (Figure 5.12).

A



B

	PGL-1	PGL-tb	MAMEs	SL-1	TMM	PDIM
PGL-tb	**** P < 0.0001					
MAMEs	ns	*** P = 0.0003				
SL-1	ns	**** P < 0.0001	* P = 0.0147			
TMM	**** P < 0.0001	ns	*** P = 0.0002	**** P < 0.0001		
PDIM	ns	** P = 0.0040	ns	*** P = 0.0009	** P = 0.0024	
$PIM_{1,2}$	ns	**** P < 0.0001	** P = 0.0064	ns	**** P < 0.0001	*** P = 0.0004

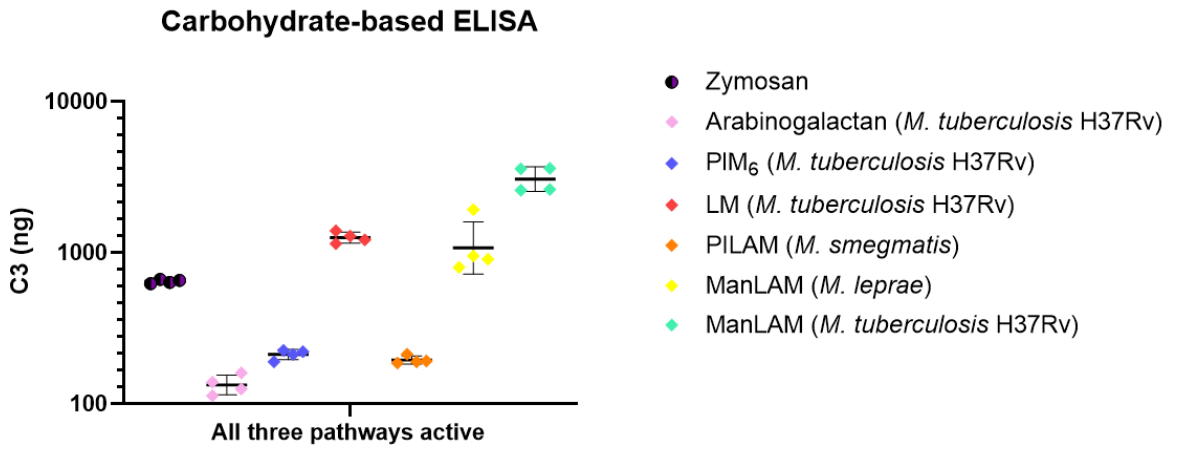
Figure 5.12: C3b/iC3b deposition on purified mycobacterial spp. cell wall components using the lipid-based ELISA.

(A) Cell wall components were incubated with 10% complement (all three pathways active). Error bars = standard deviation of four technical repeats. $OD450_{nm}$ fluorescence values (minus complement background) were log10 transformed and interpolated from the C3 standard curve to give C3 concentration in ng. C3 = C3b/iC3b deposition. One replicate of PGL-tb and two replicates of TMM had fluorescence below conjugate only levels. (B) Table of statistical comparisons for complement activation. Statistical analysis by one-way ANOVA with Tukey's multiple comparison correction.

5.4.2 C3b/iC3b deposition onto water-soluble cell envelope components

Evaluating water-soluble cell wall components with the carbohydrate ELISA conditions, significantly less C3b/iC3b deposition was observed on *M. tuberculosis* arabinogalactan compared to all other cell wall components excluding PILAM. LM and ManLAM from *M. tuberculosis* are biosynthetically related lipoglycans (Mishra *et al.*, 2011). There was significantly more C3b/iC3b deposition onto *M. tuberculosis* ManLAM compared to LM ($P < 0.0001$). PIM_6, which is a terminal PIM not used as a substrate for LM and LAM biosynthesis (Nigou, Gilleron and Puzo, 2003), had significantly lower C3b/iC3b deposition than *M. tuberculosis* LM ($P < 0.0001$) and ManLAM ($P < 0.0001$). There was also species-specific variation in C3b/iC3b deposition for LAM. PILAM from *M. smegmatis* had significantly lower C3b/iC3b deposition than ManLAM from *M. tuberculosis* H37Rv and ManLAM from *M. leprae* (both $P < 0.0001$). *M. tuberculosis* H37Rv ManLAM had significantly higher C3b/iC3b deposition than *M. leprae* ManLAM ($P < 0.0001$) (Figure 5.13).

A



B

	Arabinogalactan	**PIM_6**	**LM**	**PILAM**	**ManLAM (*M. tuberculosis*)**
PIM_6	* P = 0.0365				
LM	**** P < 0.0001	**** P < 0.0001			
PILAM	ns	ns	**** P < 0.0001		
ManLAM (*M. tuberculosis*)	**** P < 0.0001	**** P < 0.0001	**** P < 0.0001	**** P < 0.0001	
ManLAM (*M. leprae*)	**** P < 0.0001	**** P < 0.0001	ns	**** P < 0.0001	**** P < 0.0001

Figure 5.13: C3b/iC3b deposition on purified mycobacterial spp. cell wall components using the carbohydrate-based ELISA.

(A) Cell wall components were incubated with 10% complement (all three pathways active). Error bars = standard deviation of four technical repeats. $OD450_{nm}$ fluorescence values (minus complement background) were log10 transformed and interpolated from the C3 standard curve to give C3 concentration in ng. C3 = C3b/iC3b deposition. (B) Table of statistical comparisons for complement activation. Statistical analysis by one-way ANOVA with Tukey's multiple comparison correction.

5.5 Discussion Aim 1

5.5.1 Increased activation of the complement cascade was observed on *ΔMSMEG4722*

Previous studies have demonstrated that opsonisation with C3b/iC3b is a main mode of entry for *M. tuberculosis* to gain access to its intracellular niche via CR *in vitro* (Schlesinger *et al.*, 1990; Schlesinger, 1993; Hirsch *et al.*, 1994).

Mycolic acids and glycolipids are at the interface between mycobacteria and the immune system. However, their role or contribution in innate complement activation to facilitate opsonised entry is unknown. The *ΔMSMEG4722* mutant has an unreduced mycolic motif, where a β-oxo group on the mycolic motif has not been reduced to a hydroxyl group by the *MSMEG4722*-encoded reductase (Bhatt *et al.*, 2008). This small change to all the mycolate containing components of the cell envelope resulted in increased activation of the complement cascade observed through increased deposition of cascade products C3b/iC3b and C5b-9 when the bacteria were cultured in Middlebrook 7H9.

From examining total activation of the cascade, it is not possible to directly determine if the classical or lectin pathway facilitates increased innate activation on *ΔMSMEG4722*. One of the alternative pathway's traditional functions is the amplification of C3b generation after initial C3b generation via the classical or lectin pathways. Increased C3b/iC3b deposition could be driven by this positive feedback amplification loop of the alternative pathway as differences between *ΔMSMEG4722,* and *M. smegmatis* mc^2 155 were not observed when the alternative pathway was inhibited.

Increased deposition of C5b-9 on *ΔMSMEG4722* when all three pathways were active could be a consequence of increased C3b deposition. The alternative pathway C5 convertase (C3bBbC3b) has six to nine-fold weaker cleavage activity than the classical C5 convertase (C4b2a3b), but to compensate, it is stabilised by properdin which increases the half-life of the convertase 10-fold. This, along with the alternative pathway amplification loop, drives the alternative pathway C5 convertase to generate the most significant contribution to C5b-9 formation of the three pathways (Merle *et al.*, 2015). Properdin has been identified as a direct activator of the alternative pathway (Harboe and Mollnes, 2008) and has been observed to directly bind to zymosan (Ferreira, Cortes and Pangburn, 2010) and *Chlamydia pneumoniae* (Cortes, Ferreira and Pangburn, 2011). Whether properdin can directly bind to mycobacteria could be explored.

5.5.2 Mycolic acids (mature and unreduced) are unlikely to facilitate complement activation

For *ΔMSMEG4722,* Bhatt *et al.*, (2008) demonstrated that the loss of the hydroxyl groups altered the cell wall permeability as it became more susceptible to the lipophilic antibiotic rifampicin compared to *M. smegmatis* mc^2 155. Thus, increased complement activation by *ΔMSMEG4722* could be facilitated by the altered mycolic acids. However, no direct conclusions can be drawn on whether free mycolic acids or free mycolic acids with an unreduced mycolic motif (present as unsaturated ketones within the lipid extractions) can directly bind activators and activate the complement system, as the lipid fractions were tested as a whole.

In the lipid fraction consisting of esterified mycolic acids (MAMEs), with esterified fatty acids (FAMEs), for both *M. smegmatis* mc^2 155 and *ΔMSMEG4722,* minimal complement activation occurred. Although different mycolate classes, this agrees with Yasuda, (1999), who observed that none of the *M. tuberculosis* mycolic acid subclasses, α-, keto- and methoxy (extracted as MAMEs) activated the complement system. MAMEs were derived from pellicle biofilms. This was measured by lysis of sensitised sheep erythrocytes with the supernatant of guinea pig sera that had been incubated with *M. tuberculosis* H37Rv MAMEs (residual complement activity after complement consumption). In contrast, this study also observed complement activation of purified *M. tuberculosis* MAMEs (BEI Resources) by ELISA. Therefore, mycolic acids (mature and unreduced) potential to directly activate the complement system will have to be explored further.

While mycolic acids are the major cell surface component of *M. smegmatis,* the major cell surface components of *M. avium* are glycopeptidolipids (GPLs). Strains not producing GPLs (strain 2151 Rg3) or producing only the lipopeptide portion of GPLs (serovar strain 2 2151 RgO) demonstrated greater MBL binding compared to a strain with intact GPLs (serovar 2 strain 2151 SmO). The authors hypothesised that GPLs themselves were not the major ligand of MBL in *M. avium*, and their presence may block access to MBL activating cell wall moieties (Polotsky *et al.*, 1997). Mycolic acids could play a similar role to the GPLs of *M. avium*, reducing access of complement activators to cell wall moieties that can activate the complement system, which potentially include the glycolipids. In *ΔMSMEG4722*, the ‘blocking’ effect of mycolic acids may be lost due to the altered mycolic motif.

5.5.3 Redistributed glycolipids in *ΔMSMEG4722* may facilitate increased activation of the complement cascade

On *M. smegmatis* mc^2 155, positive binding of all four activators was observed, with ficolin-1 and ficolin-2 showing overall more binding than C1q and MBL. On *ΔMSMEG4722,* there was an increase in ficolin-1 binding, an activator of the lectin pathway.

Ficolin-1 binds *M. tuberculosis* H37Rv, *M. bovis* BCG, *M. kansasii* and weakly, *M. smegmatis* and *M. gordonae*. Compared to MBL, it weakly activates the lectin pathway on these mycobacteria (Bartlomiejczyk *et al.,* 2014). Ficolin-1 avidly recognises patterns of acetyl groups (Gout *et al.,* 2010; Bidula, Sexton and Schelenz, 2019) and *N*-Acetylglucosamine and ficolin-1 interactions have been observed to directly activate the lectin pathway (Frederiksen *et al.,* 2005; Matsushita *et al.,* 2005). The binding repertoire of ficolin-1 is underexplored as Świerzko *et al.,* (2016) observed that rAg85B (an Ag85 complex protein) could bind all three ficolins. rAg85B had not undergone any posttranslational modification, including glycosylation or acetylation.

Increased binding of ficolin-1 mirrored increased C3b/iC3b deposition on whole-cell bacteria and the outer apolar lipids of *ΔMSMEG4722*. The main characterised differences in this lipid fraction between *ΔMSMEG4722* and *M. smegmatis* mc^2 155 were the presence of unreduced free mycolate (unsaturated long-chain ketones in the lipid fractions), significantly less free fatty acid and an increase in TDM, TMM and GMM (summarised in chapter 4, Table 4.2).

The most likely candidates for increased complement activation within the outer apolar lipid fraction are the carbohydrate-containing mycolate esters TDM and TMM. As

discussed in chapter 4, TDM is an established virulence factor of *M. tuberculosis* (Spargo *et al.*, 1991; Borders *et al.*, 2005; Axelrod *et al.*, 2008; Welsh *et al.*, 2008; Ishikawa *et al.*, 2009).

Both TDM and TMM have been shown to activate the complement system. Guinea pig sera lacked residual complement activity after incubation with *M. tuberculosis* H37Rv TDM, and TMM derived from pellicle biofilms (Ramanathan, Curtis and Turk, 1980; Yasuda, 1999). Interestingly, *M. tuberculosis* H37Rv TMM from BEI resources exhibited positive, but very low-level complement activation by ELISA. TDM has previously been shown to exhibit very low binding to MBL, but this may be a consequence of experimental set up as it was coated to the ELISA plate resuspended in carbonate-buffer (Polotsky *et al.*, 1997). In a competition ELISA, increasing concentrations of free purified trehalose inhibited lectin pathway activation, indicating it is a functional ligand of the lectin pathway. As the study used the Weislab-style ELISA, the lectin pathway competition ligand was likely mannose and the activator MBL (Ilyas *et al.*, 2011). The orientation of all cell wall components likely plays a critical role in complement activation. *In situ,* TDM and TMM mycolates intercalate into the mycomembrane, exposing their trehalose moiety to the external environment (Garcia-Vilanova, Chan and Torrelles, 2019).

Both Ramanathan, Curtis and Turk, (1980) and Yasuda, (1999) concluded that TDM complement activation was via the alternative pathway. They saw equal 'consumption of complement activity' in normal and C4-depleted guinea pig sera. Depleting C4 will inactivate the classical and lectin pathways, as it is part of the classical and lectin C3-convertase (C4b2a) (Merle *et al.*, 2015). Although the primary activation of the

complement cascade by MBL is via the traditional C3-convertase (C4b2a), MBL-driven activation of the alternative pathway in a C2 and C4-independent manner has been observed using O antigen-specific *Salmonella* oligosaccharides. However, the underlying mechanisms are still to be elucidated (Selander *et al.*, 2006). Whether the ficolins also activate the alternative pathway using this alternative mechanism has not been explored. C2a recruitment to the cell wall of pathogenic mycobacteria to form a C3-convertase has been demonstrated previously, but the binding ligand is unidentified (Schorey, Carroll and Brown, 1997).

5.5.4 Changes in distribution to cell wall components other than lipids may facilitate increased activation on *ΔMSMEG4722*

A mutation to the mycolic motif should not alter the chemical nature of the lipoglycans within the mycobacterial cell wall. However, as the cell wall has altered permeability, this may be a factor in increased ficolin-1 binding. As the mycobacterial cell surface is carbohydrate-rich, lectin pathway activation may increase if the overall distribution of lipoglycans and carbohydrates is altered. Complement activation was observed on the extracted outermost lipoglycans and carbohydrates of both *M. smegmatis* mc^2 155 and *ΔMSMGE4722*, but whether the proportion of lipoglycans in the extractable fraction was altered between *M. smegmatis* mc^2 155 and *ΔMSMGE4722* was not determined.

Extracted lipoglycans from *M. smegmatis* have not been assessed for complement activation in the literature, but purified LAM from BEI Resources showed positive innate complement activation. *M. tuberculosis* ManLAM strongly binds MBL and, to a weaker extent, ficolin-1, ficolin-2 and ficolin-3 (Świerzko *et al.*, 2016).

On the whole-cell *ΔMSMEG4722* bacteria, as increased ficolin-1 binding was observed, increased ficolin-2 binding may also have been expected due to the proteins high amino acid similarity at 79% (Garred *et al.*, 2016). Ficolin-2 has been previously demonstrated to bind to *M. bovis* BCG (depletion from sera after incubation) and could activate the lectin pathway in response to *M. bovis* BCG in the absence of MBL through measuring MASP activity (Carroll *et al.*, 2009).

Unexplored in this thesis, acetylated proteins must be considered as potential complement activators on whole bacteria. Acetylated proteins account for approximately 16% of all proteins in *M. tuberculosis* (1028 acetylation sites on 658 proteins) (Xie *et al.*, 2015). Proteins are interspersed throughout the cell envelope participating in various functions, including cell wall assembly and regulation of cell wall synthesis (Dulberger, Rubin and Boutte, 2020). Proteins without modifications, demonstrated by Ag85B, also have to be considered in complement activation (Świerzko *et al.*, 2016).

5.6 Discussion Aim 2

5.6.1 Comparable complement activation was observed on planktonic and pellicle biofilm *M. smegmatis* mc^2 155

Although there is histological evidence that *M. tuberculosis* can persist in an extracellular state in biofilm-like structures within human cavities (Nyka, 1963, 1967, 1977; Nyka and O'Neill, 1970; Hunter *et al.*, 2006; Hunter, 2011; Chakraborty *et al.*, 2021) and surrounding lung tissue (Shaler *et al.*, 2013), the importance of the biofilm phenotype in complement activation is relatively unknown. Within primary necrotic lesions of guinea pig granulomas, auramine-rhodamine staining has detected mycolic acids (Hoff *et al.*, 2011), which are a feature typical of mycobacterial pellicle biofilm extracellular material (Ojha *et al.*, 2008).

Cavities are associated with an increased risk of person-to-person transmission due to a higher bacterial load in the sputum (Urbanowski *et al.*, 2020). This higher bacterial load could be through the dispersal of small clumps of bacteria from biofilms. Viable *M. tuberculosis* aerosols from active TB patients have an estimated particle size of 0.65 to 4.7μm aerodynamic diameter (Fennelly *et al.*, 2012), so disaggregated biofilm bacteria associated with ECM could represent the aerosolised expectorate that facilitate transmission (Orme, 2014). Sputum contains heterogeneous populations of bacteria ranging from metabolically active to dormant non-replicating bacteria (Garton *et al.*, 2008; Mukamolova *et al.*, 2010; Dusthackeer *et al.*, 2019). Biofilms also contain a phenotypically heterogeneous population of bacteria, facilitated by exposure to heterogeneous microenvironments (Costerton *et al.*, 1999; Islam, Richards and Ojha, 2012). A heterogeneous population of bacteria may modulate complement interactions.

A hypothesis of this chapter was that complement activation would be reduced on disaggregated *M. smegmatis* mc^2 155 pellicle biofilm bacteria compared to bacteria in a planktonic state. However, the results in this chapter disagree with this hypothesis and contrast to the published literature; there was comparable activation of the complement cascade on *M. smegmatis* mc^2 155 from pellicle biofilm-derived bacilli compared to their planktonic counterparts, while C3b/iC3b deposition has previously been observed to be reduced on disaggregated biofilm cells compared to planktonic bacteria for *S. pneumoniae* (Domenech *et al.*, 2013), *P. aeruginosa* (Jensen *et al.*, 1993) and *M. tuberculosis* (Keating *et al.*, 2021).

5.6.2 Activator binding decreases on pellicle biofilm-derived *M. smegmatis* mc^2 155 compared to planktonic cells

Despite no whole-cell changes to overall complement activation between phenotypes, a significant reduction in C1q binding was observed to the pellicle biofilm-derived bacteria when examining activator binding. This agrees with C1q binding being reduced on *M. tuberculosis* pellicle biofilm bacilli (Keating *et al.*, 2021). A decrease in C1q binding to disaggregated biofilm cells has also been observed on non-capsulated *S. pneumoniae* (Domenech *et al.*, 2013).

Of the activators tested, C1q was the most bound activator to *M. smegmatis* mc^2 155 planktonic bacilli. This indicates a cell wall component is altered, either in exposure, quantity or composition, on pellicle biofilm bacteria that on planktonic cells could be directly recognised by C1q. The globular head of C1q has a surface pattern of charged and hydrophobic residues, giving C1q a broad recognition spectrum (Gaboriaud *et al.*, 2003). C1q is primarily associated with activating in a complex with IgG or IgM.

However, antibody-independent bacterial ligands have been identified that include *S. pneumoniae* Endopeptidase O (Agarwal *et al.*, 2014), LPS of *Salmonella typhimurium* (Roumenina *et al.*, 2008) and *Klebsiella pneumoniae* porin OmpK36 (Albertí *et al.*, 1996). Direct binding of C1q to *M. bovis* BCG has been reported, but the ligand was not identified (Carroll *et al.*, 2009). Although not statistically significant, a decrease in lectin pathway activator binding was observed for ficolin-1 and ficolin-2 to disaggregated pellicle biofilm cells from *M. smegmatis* mc^2 155 compared to planktonic cells.

Strikingly, the decrease in C1q, ficolin-1 and ficolin-2 binding observed on pellicle biofilm-derived *M. smegmatis* mc^2 155 compared to planktonic cells mirrored a decrease in C3b/iC3b deposition on pellicle biofilm-derived lipids in both apolar lipid fractions. Based on the TLC analysis carried out in chapter 4 (summarised in Table 4.4), few changes in the apolar lipid profiles of *M. smegmatis* mc^2 155 planktonic cells compared to pellicle biofilms were observed. The main change observed was a reduction in TMM in *M. smegmatis* pellicle biofilms. In both apolar lipid fractions, TMM was present in the planktonic phenotype but reduced in pellicle biofilms. TMM has been observed to activate the complement system more potently than TDM as residual complement activity in guinea pig sera was abolished at a lower concentration of TMM compared to TDM (Yasuda, 1999). Decreased C3b/iC3b deposition on the pellicle biofilm inner apolar lipids where free mycolic acids accumulate, and minimal C3b/iC3b deposition onto FAMEs and MAMEs lipids suggest that mature mycolic acids do not appear to activate the complement system directly. Changes to one cell wall component is unlikely to be fully responsible for the reduction in complement activation by *M. smegmatis* mc^2 155 pellicle biofilms as the activators recognise a broad range

of ligands (Merle *et al.*, 2015). Reduced C3b/iC3b deposition directly onto pellicle biofilm carbohydrates was observed for *M. tuberculosis* compared to their planktonic counterparts. Sugar analysis demonstrated that constituent sugar ratios (arabinose, mannose, glucose) changed depending on the phenotype, with the proportion of glucose relative to arabinose and mannose lower in the pellicle biofilms compared to planktonic cells (Keating *et al.*, 2021). For *M. smegmatis,* a reduction of LAM content has been observed as bacteria enter stationary phase, associated with loss of acid fastness and clumping, despite the presence of 0.05% Tween-80 in the culture media (Dhiman *et al.*, 2011). On the carbohydrate fractions extracted from planktonic and pellicle biofilm *M. smegmatis* mc^2 155, there was minimal overall complement activation and C3b/iC3b deposition. A limitation of the extracted carbohydrates is that no carbohydrate/lipoglycan gel was achieved to confirm a reduction in LAM in pellicle biofilms.

5.6.3 *ΔMSMEG4722* phenotypes highlight that the picture of complement activation by mycobacteria is complicated and incomplete

Another hypothesis of this chapter was that bacteria derived from a pellicle biofilm that did not reticulate and mature (*ΔMSMEG4722*) would not display alterations to complement activation, previously observed between planktonic and pellicle biofilm *M. tuberculosis* (Keating *et al.*, 2021). For overall complement activation, comparable C3b/iC3b deposition, C5b-9 deposition and C5a generation was observed between planktonic and pellicle biofilm *ΔMSMEG4722,* which was higher than observed on the corresponding phenotypes of *M. smegmatis* mc^2 155. As greater complement deposition was observed on *ΔMSMEG4722* compared to *M. smegmatis* mc^2 155, it

would have been expected that overall activator binding would be greater on both phenotypes of *ΔMSMEG4722.* For *ΔMSMEG4722* pellicle biofilms, C1q, ficolin-1 and ficolin-2 binding were increased compared to pellicle biofilm *M. smegmatis* mc^2 155. However, no activator showed increased binding to *ΔMSMEG4722* planktonic cells, and for C1q, there was a significant reduction in binding.

Despite comparable complement activation between *ΔMSMEG4722* phenotypes, activator binding was variable with increased binding of ficolin-1 and ficolin-2 to pellicle biofilms compared to planktonic cells. *ΔMSMEG4722* phenotypically looks like a pellicle biofilm at the early stage of development (chapter 3 Figure 3.14 and Ojha *et al.*, (2005)), and very little is known about the adaptations to cell wall components going from a planktonic to sessile state and then through pellicle development. The sugar composition of cell wall components and ECM in early mycobacterial pellicle biofilms may facilitate complement activation, which decreases as pellicle biofilms mature.

Glycolipids appeared likely candidates for complement activation in the outer and inner apolar lipid fractions when analysing Middlebrook 7H9 cultured bacteria and comparing *M. smegmatis* mc^2 155 planktonic and pellicle biofilm phenotypes. Despite seeing alterations to the composition of glycolipids between planktonic and pellicle biofilm *ΔMSMEG4722* (chapter 4, Table 4.3), when the lipids were tested for complement activation, comparable levels were observed between phenotypes in all lipid fractions.

Additionally, in the outer apolar lipids, which had significantly more TDM in planktonic *ΔMSMEG4722* compared to planktonic *M. smegmatis* mc^2 155 and significantly less TDM in pellicle biofilm *ΔMSMEG4722* than pellicle biofilm *M. smegmatis* mc^2 155,

complement activation was lower on planktonic *ΔMSMEG4722* compared to *M. smegmatis* mc^2 155 and higher on pellicle biofilm *ΔMSMEG4722* compared to *M. smegmatis* mc^2 155.

The above observations highlight the complexity of complement interactions and activation within the mycobacterial cell wall and the potential spectrum of unidentified complement activating epitopes, which are likely modified throughout pellicle biofilm development. Multiple cell wall components- lipoglycans, carbohydrates, lipids and proteins– may have a synergistic role in complement activation, which may differ between *ΔMSMEG4722* phenotypes but cannot be fully deciphered from the current work.

5.7 Discussion Aim 3

5.7.1 Arabinogalactan does not activate the complement system

This chapter aimed to broaden the knowledge of cell envelope components that can innately functionally activate the complement system. This was done by measuring C3b/iC3b deposition onto purified mycobacterial cell envelope components. Cell envelope components currently identified as able to bind activators or activate the complement system are summarised in section 5.1.3.

There were very low levels of complement activation by purified arabinogalactan from *M. tuberculosis* H37Rv. Arabinogalactan provides a robust base for the support of the upper 'mycomembrane', including esterified mycolic acids and is primarily composed of arabinose and galactose. There are no know modulatory effects seen with mycobacterial arabinogalactan (Alderwick *et al.*, 2015). Minimal C3b deposition on arabinogalactan purified from *M. leprae* has been observed when incubated with non-immune serum (Larry S Schlesinger and Horwitz, 1991).

5.7.2 *M. leprae* PGL-1 is a more potent activator of the complement system than *M. canetti* PGL-tb

PGL exhibits species-specific activation of the complement system. Increased C3b/iC3b deposition occurred on *M. leprae* PGL-1 compared to *M. canetti* PGL-tb. PGL-1 is a surface-associated virulence factor of *M. leprae* that causes irreversible peripheral nerve damage, potentially mediated by macrophages in response to PGL-1 inducing demyelination and NO production (Madigan *et al.*, 2017). PGL-1 coated *Staphylococcus aureus* were protected from killing by macrophages and scavenges oxygen radicals (Neill and Klebanoff, 1988).

Initially identified in *M. canetti,* PGL-tb is associated with hypervirulent strains in mice and rabbits (Sinsimer *et al.*, 2008). However, only a few clinical isolates of Beijing descent *M. tuberculosis* produce PGL-tb, and it is not produced by the lab strains H37Rv and Erdman (Arbues *et al.*, 2014). PGL has a conserved lipid backbone with minor structural modifications but a species-specific trisaccharide domain. Both PGL-tb and PGL-1 contain two rhamnose sugar moieties, but the terminal sugars vary; fucose in PGL-tb and glucose in PGL-1. Structural differences between the trisaccharides include the position of methyl groups and the carbon position for the attachment of the subsequent sugar moieties to the first and second rhamnose (Tabouret *et al.*, 2010; Arbues *et al.*, 2014).

PGL-1 had activated complement in a classical pathway-dependent manner from fresh non-immune serum observed through the loss of complement activation when Ca^{2+} were chelated with EGTA-$MgCl_2$ (Larry S Schlesinger and Horwitz, 1991), but the lectin pathway could also play a role as Ca^{2+} are essential for lectin activator recognition (Garlatti *et al.*, 2007; Garred *et al.*, 2016). PGL-1 complement activation was determined by terminal saccharides, with C3 fixation decreasing over the sequential removal of the three saccharides to baseline. Acylation of the lipid core was also important, with the removal of the long-chain mycocerosyl fatty acyl groups resulting in background levels of C3 fixation despite the trisaccharide domain remaining (Larry S Schlesinger and Horwitz, 1991).

The glucose saccharide moiety of PGL-1 could contribute to activating the complement cascade via the lectin pathway. Competition binding has demonstrated that mannose recognition by MBL can be inhibited in increasing glucose concentrations and that

lectin pathway activation was also inhibited by increasing glucose concentrations (Ilyas *et al.*, 2011).

Fucose, the terminal saccharide for PGL-tb, has been identified as a ligand of both collectin-10 and ficolin-3 (Garred *et al.*, 2016) and activates the lectin pathway (Ilyas *et al.*, 2011). However, in this study, only low complement activity was observed. Thus, the structural differences of the saccharide moieties could contribute to PGL-1 inducing stronger activation of the complement system compared to PGL-tb.

The results presented here agree with Larry S Schlesinger and Horwitz, (1991) that PGL-1 is an activator of the complement system. Using a complement source depleted of both IgG and IgM, it has been further demonstrated here that PGL-1 can trigger innate activation of the complement system. The primary pathway of activation is still to be elucidated.

5.7.3 The biosynthetically related $PIM_{1,2}$, PIM_6, LM and ManLAM in *M. tuberculosis* H37Rv showed different activation of complement

Lipoglycan biosynthesis in *M. tuberculosis* H37Rv is simplistically PI → PIM → LM → LAM, which become increasingly glycosylated. ManLAM may arrest phagosome maturation through inhibiting calcium ion increase, while PIMs stimulate fusion with early endosomes to provide a source of nutrients to phagosome-residing mycobacteria, and both ManLAM and PIM_6 are ligands of the mannose receptor (Mishra *et al.*, 2011).

Lipoglycans have demonstrated a range of complement activation. PIMs are composed of a phosphatidyl-*myo*-inositol (PI) lipid anchor carrying one to six mannopyranose residues. PIM_2 is the foundation for LM and LAM biosynthesis (MPI anchor), compared to PIM_6, a terminal product (Mishra *et al.*, 2011). Mannose is a known ligand for MBL and complexed collectin-10/11 (Garred *et al.*, 2016; Howard, Farrar and Sacks, 2018), so both PIMs could be hypothesised to activate the complement system. PIM_6 contains terminal α(1→2)-linked mannosyl residues identical to the mannose cap on ManLAM (Driessen *et al.*, 2009), which is a known activator of the complement system (Bartlomiejczyk *et al.*, 2014).

Apolar $PIM_{1,2}$ showed strong complement activation, but polar PIM_6 showed poor activation. These observations contrast with previously published interactions of complement activators with PIMs. Using a Tris-buffer saline-based capture ELISA, Seiler *et al.*, (2019) observed MBL captured PIM_6, but not $PIM_{1,2}$. Hoppe *et al.*, (1997) assessed opsonised *M. tuberculosis* H37Rv and *M. smegmatis* attachment to CHO cells with a range of *M. tuberculosis* H37Rv whole cell-specific monoclonal-antibodies and found mAb 1D1 was able to block attachment efficiently. The mAb-specific antigen, when purified, was identified as an apolar PIM (PIM_5 or PIM_6), which could bind rMBL.

Studies of *M. tuberculosis* and *M. bovis* BCG strains have demonstrated that PIMs are heterogeneous with different degrees of acylation; mono-, di-, tri-, and tetra-. Mono-acylated forms, $AcPIM_2$ and $AcPIM_6$, are the most prominent PIMs found in mycobacteria (Gilleron *et al.*, 2001; Gilleron, Quesniaux and Puzo, 2003; Mishra *et al.*, 2011). Acylation was previously demonstrated to be essential for PGL-1 activation of

complement (Schlesinger and Horwitz, 1990). The distribution of 'acyl isoforms' within each of the purified lipid fractions from BEI Resources is unknown, but this may contribute to the difference in complement activation observed.

LM consists of the MPI anchor, with an elongated mannopyranose backbone (30-35 residues) that contains α(1→2)-linked mannosyl branches, and the final structure in the synthetic pathway LAM has the addition of an arabinan domain (60 arabinofuranose units) that branches with 'caps' (Nigou, Gilleron and Puzo, 2003).

rMBL binding to *M. tuberculosis* ManLAM has been previously documented (Polotsky *et al.*, 1997; Bartlomiejczyk *et al.*, 2014; Świerzko *et al.*, 2016). Lectin pathway activation (C4c-deposition) by cell lysate ManLAM (30–35 kDa fractions) and purified ManLAM from *M. tuberculosis* Aoyama-B has also been demonstrated (Bartlomiejczyk *et al.*, 2014; Świerzko *et al.*, 2016). *M. tuberculosis* H37Rv LM showed lower levels of complement activation than ManLAM, which may be due to the lack of mannose caps.

Although individual pathways were not explored, this study confirms quantifiably that LM and ManLAM can innately activate the complement system. This is likely via the lectin pathway when using an antibody-depleted complement source. Additionally, $PIM_{1,2}$ was observed to strongly activate the complement system, which has not previously been reported.

Due to different polarities, $PIM_{1,2}$ was tested using the carbohydrate-based ELISA, compared to PIM_6, which was tested using the lipid-based ELISA. The orientation of lipoglycan binding could influence differences in complement activation to the ELISA plates. For the lipid-based ELISA, likely, fatty acid acyl groups of molecules will

preferentially bind to the plate, keeping the carbohydrate moieties free. In comparison, on a carbohydrate-specific ELISA plate, where the binding will occur by the carbohydrates present. This may not be as visually impactful on highly glycosylated molecules, but for PIMs, this may explain why PIM_6 showed minimal complement activation.

5.7.4 Species-specific differences in C3b/iC3b deposition onto LAM was observed

The primary variation between LAM species is capping; mannose caps (ManLAM) are seen on pathogenic mycobacteria including *M. tuberculosis* and *M. leprae*, phosphoinositol capping (PILAM) has been identified on rapidly growing mycobacteria including *M. smegmatis,* and AraLAM has been identified on *M. chelonae* (Nigou, Gilleron and Puzo, 2003).

M. smegmatis PILAM showed low-level complement activation, which may be due to a lack of mannose capping. Virulent *M. tuberculosis* and *M. leprae* share mannose capping, but *M. tuberculosis* H37Rv is estimated to have seven caps per molecule compared to *M. leprae,* which has an estimated one cap per molecule (Nigou, Gilleron and Puzo, 2003). Thus, the degree of mannose capping could correlate to the activating capacity of ManLAM. This has been demonstrated by lower C3b/iC3b deposition on purified *M. leprae* ManLAM compared to *M. tuberculosis* H37Rv ManLAM in the carbohydrate-based ELISA. However, this would have to be confirmed with an adaptation of the carbohydrate-based ELISA that probes for MBL binding.

Schlesinger and Horwitz, (1991) saw minimal C3 fixation to ManLAM from *M. leprae* by ELISA, but this could be because a very low concentration of human sera was used

as the complement source (2.5%), meaning any amplification by the alternative pathway would not be observed. Luo *et al.*, (2013) hypothesised that ManLAM is also a ligand of ficolin-2, based on the observation that in a competition assay, co-incubation of *M. tuberculosis* H37Rv, ManLAM and rficolin-2 resulted in lower binding of rficolin-2 to *M. tuberculosis* H37Rv compared to *M. tuberculosis* H37Rv and rficolin-2 incubation alone by flow cytometry. Bartlomiejczyk *et al.*, (2014) observed very weak binding of C4c to the ManLAM cell lysate fraction after treating serum with mannan-agarose via western blot, hypothesising that the ficolins could be involved. Western blot interactions of ManLAM with recombinant ficolins by Świerzko *et al.*, (2016) did not observe any binding. Adapting the ELISA to probe for ficolin binding to the purified cell wall ManLAM would explore this hypothesis.

M. tuberculosis H37Rv LM activated the complement cascade to a similar level as *M. leprae* LAM despite having no mannose caps indicating multiple features of the lipoglycans that influence complement activation, which may include acylation and mannose branching. This is also highlighted by the high level of activation seen on *M. tuberculosis* H37Rv $PIM_{1,2}$.

5.7.5 Sulpholipid-1 and PDIM were potent activators of the complement system

Sulpholipid-1 (SL-1) is a tetra-acylated trehalose based glycolipid virulence factor of pathogenic mycobacteria located on the outer membrane. No direct role in virulence has been established, but multiple, sometimes conflicting roles have been proposed for SL-1, including macrophage ‘swelling’ and altered phagosome-lysosome fusion (Goren *et al.*, 1976), regulating intracellular growth in macrophages (Gilmore *et al.*,

2012) and inhibition of macrophage IFN-γ priming resulting in reduced production of superoxide ions, reduced phagocytosis and reduced IL-1 release when macrophages are stimulated (Pabst *et al.*, 1988). In contrast, Zhang *et al.*, (1988) observed that IFN-γ primed monocytes had an enhanced oxidative response (superoxide anion production) to SL-1. They also observed that SL-1 enhanced neutrophil production of superoxide anions and primed neutrophils for enhanced superoxide production when stimulated with a range of agonists. Neither Pabst *et al.*, (1988) or Zhang *et al.*, (1988) studied SL-1 effects directly on *M. tuberculosis* survival.

Strongly activating the complement system could highlight another potential role of SL-1 in *M. tuberculosis* infection or could be a consequence of being composed of acyl groups and trehalose, which have both been described to either activate or play a role in complement activation (Larry S Schlesinger and Horwitz, 1991; Ilyas *et al.*, 2011).

PDIM is another abundant surface-associated virulence factor of *M. tuberculosis* whose function is not well understood. PDIM is structurally related to PGL through a common lipid backbone with minor structural variations, but lacks the glycosylation observed on PGL (Arbues *et al.*, 2014). PDIM plays both a structural role in cell wall permeability (Camacho *et al.*, 2001) and has been implicated in immunomodulatory roles, including non-opsonised macrophage invasion via CR3, arresting phagosome maturation (Astarie-Dequeker *et al.*, 2009) and masking PAMPs from TLRs, preventing recruitment of inducible nitric oxide expressing macrophages (Cambier *et al.*, 2014). In macrophage survival screens of 1,500 *M. bovis* BCG non-essential gene mutants, three mutants with insertions into genes associated with PDIM synthesis or transport were in the top twenty most attenuated mutants (Stewart *et al.*, 2005).

PDIM can also innately activate the complement cascade, potentially giving this virulence factor another role and highlighting the importance of acylation of the lipid core first observed on PGL-1 for complement activation (Larry S Schlesinger and Horwitz, 1991).

6 General Discussion

There is an urgent need for more effective vaccines and antibiotics against *M. tuberculosis* (WHO, 2020a). Currently, there are no immune correlates of protection against TB and vaccine research focuses on eliciting $CD4^+$ T cell responses. The authors of the MVA85A TB subunit vaccine clinical trial highlighted in their conclusions that the lack of immune correlates of protection makes the parameters for selecting TB vaccine candidates difficult and potentially incomplete (Tameris *et al.,* 2013). A major challenge for antibiotic development is understanding the biological mechanisms behind latency/bacterial 'persistence' and identifying novel mechanisms of action against these 'persistent' bacteria (Ginsberg and Spigelman, 2007).

To develop effective vaccines and antibiotics, a better understanding of host-pathogen interactions and the phenotypes of *M. tuberculosis* during disease is needed. In this thesis, the role of mature mycolic acids in pellicle biofilm formation and innate cell wall interactions with the human complement system were explored using *M. smegmatis* mc^2 155 and the mycolic acid biosynthesis reductase mutant *ΔMSMEG4722.*

The loss of mature mycolic acids for mycolic acid intermediates resulted in *ΔMSMEG4722* pellicle biofilms that could form on the air-liquid interface but could not mature or reticulate. The pellicles also produced significantly less ECM. Mycolic acids have previously been implicated in pellicle biofilm formation (Ojha *et al.*, 2005; Chen *et al.*, 2006; Pacheco *et al.*, 2013; Sambandan *et al.*, 2013; Jamet *et al.*, 2015; Lefebvre *et al.*, 2018), but this thesis demonstrated their maturation is also essential for pellicle biofilm development. Thus, biofilms may be an important phenotype that facilitates bacterial survival within lung cavities (Nyka, 1963, 1967; Hunter *et al.*, 2006), or reflect

the phenotype of 'persistent' bacteria difficult to treat with conventional antibiotic regimes (Orme, 2014).

As well as the loss of mature mycolic acids for mycolic acid intermediates, other biochemical changes in the cell wall of *ΔMSMEG4722* included the redistribution of solvent-extractable non-covalently bound glycolipids (TDM, TMM and GMM) in the apolar lipid fractions, occurring in bacteria cultured in Middlebrook 7H9 and when cultured as planktonic and pellicle biofilm phenotypes. In pellicle biofilms, mature free mycolic acids and free mycolic acid intermediates (decarboxylated to unsaturated ketones) accumulated in the apolar lipid fractions for *M. smegmatis* mc^2 155 and *ΔMSMEG4722*, respectively. A hallmark of pellicle biofilms is the accumulation of free mycolic acids (Ojha *et al.*, 2010). The loss of pellicle biofilm maturation and reticulation was not due to an inability to accumulate unreduced free mycolic acids by *ΔMSMEG4722,* highlighting that multiple cell wall components are essential in pellicle biofilm development. TDM levels positively correlate to pellicle biofilm formation in clinical strains of *M. tuberculosis* isolated from cavities and may play a structural role in pellicle development (Hunter *et al.*, 2006; Arora *et al.*, 2016). The structural contribution of TDM may have been altered in *ΔMSMEG4722*.

The removal of IgM from the complement source was essential for studying innate cell-wall interactions with the human complement system for planktonic and pellicle biofilm-derived *M. smegmatis.* On *ΔMSMEG4722* compared to *M. smegmatis* mc^2 155, when cultured in Middlebrook 7H9, *ΔMSMEG4722* showed increased complement activation, increased ficolin-1 binding and increased complement activation on the outer apolar lipids. *M. smegmatis* mc^2 155 innately activated the complement cascade

but losing the full anchoring of the mycolic acids within the cell envelope highlights that mycobacteria are composed of cell wall components that can potently innately activate the complement system. Complement (C3b/iC3b) opsonisation is a main mode of entry via opsonophagocytosis for *M. tuberculosis* to gain access to alveolar macrophages (Schlesinger, 1993; Hirsch *et al.*, 1994). TDM, which was at an increased concentration in the outer apolar lipid fractions of *ΔMSMEG4722* compared to *M. smegmatis* mc^2 155, is a potent virulence factor in *M. tuberculosis* implicated in a wide range of immune functions, including complement activation (Ramanathan, Curtis and Turk, 1980; Yasuda, 1999) and granuloma formation in association with the anaphylatoxin C5a and its receptor C5aR (Borders *et al.*, 2005; Welsh *et al.*, 2008).

Comparable complement activation was observed between planktonic and pellicle biofilm *M. smegmatis* mc^2 155, but there was a decrease in activator binding (C1q, ficolin-1 and ficolin-2) on pellicle biofilm compared to planktonic cells. This was also reflected in decreased complement activation by the apolar lipid fractions of pellicle biofilms compared to planktonic cells. The main observed apolar lipid change was a decrease in TMM between planktonic and pellicle biofilm bacteria. TMM has previously been demonstrated to activate the complement cascade (Yasuda, 1999). Decreases in ficolin binding may be due to alterations in carbohydrate/lipoglycan sugar composition within biofilms compared to planktonic cells (Dhiman *et al.*, 2011; Keating *et al.*, 2021). During chronic infection, opsonophagocytosis and replication in macrophages are likely less important than during the initial establishment of infection, but inducing minimal activation of the complement cascade as a pellicle biofilm (demonstrated by low activator binding) minimises anaphylatoxin generation and recruitment of new immune cells to the site of infection/ inflammation which may aid

the clearance of *M. tuberculosis*. Pellicle biofilms could also offer phenotypic protection from these immune responses. These persistent bacteria could then form a reservoir for re-activation or spread, as hypothesised by Orme (2014).

Non-reticulated *ΔMSMEG4722* pellicle biofilms showed comparable complement activation to planktonic *ΔMSMEG4722*, which was increased compared to their *M. smegmatis* mc^2 155 counterparts. *ΔMSMEG4722* pellicle biofilms overall demonstrated greater lectin activator binding (ficolin-1 and ficolin-2) than planktonic *ΔMSMEG4722* and *M. smegmatis* mc^2 155 pellicle biofilms. *ΔMSMEG4722* pellicle biofilms are phenotypically similar to early pellicle biofilms of *M. smegmatis* mc^2 155. However, little is known about cell wall composition and cell wall changes from the early to mature stages of *M. smegmatis* pellicle development. Activator interactions of the complement system over pellicle biofilm development have not been explored but may decrease with cell wall adaptations to sugar or carbohydrate moieties as the biofilms reach maturity.

Despite differences in apolar lipid composition, including the glycolipids, between planktonic and pellicle biofilm *ΔMSMEG4722*, and increased TDM in planktonic *ΔMSMEG4722* compared to planktonic *M. smegmatis* mc^2 155, complement activation was comparable between *ΔMSMEG4722* phenotypes and significantly lower than that observed on the outer apolar lipids of both planktonic and biofilm *M. smegmatis* mc^2 155. This indicates that complement interactions and activation by the mycobacterial cell wall, including the glycolipids, are highly complex. There is still a potential spectrum of unidentified activating epitopes that may vary between the planktonic and pellicle biofilm phenotypes and potentially the stage of pellicle biofilm development.

Examining purified cell envelope components sourced from BEI resources demonstrated that numerous cell envelope components innately activate the complement cascade to varying degrees. Previously identified activators *M. leprae* PGL-1 (Larry S Schlesinger and Horwitz, 1991) and *M. tuberculosis* ManLAM (Bartlomiejczyk *et al.*, 2014; Świerzko *et al.*, 2016) were confirmed to have innate complement activating capabilities. In addition, new potential ligands were identified, including *M. tuberculosis* SL-1 and PDIM.

The discussion below will look at the results of this thesis in the broader context of the immune response to *M. tuberculosis* and vaccine and drug evaluation. Areas of future work will also be addressed.

6.1 Do biofilms aid the dissemination of *M. tuberculosis* to a new host?

Decreased complement activator binding to disaggregated pellicle biofilm cells of *M. smegmatis* mc^2 155 was observed in chapter 5. The form that bacilli are aerosolised and transmitted as is still not fully understood, and dispersal from a biofilm may aid transmission.

The aerosol dose of *M. tuberculosis* during transmission is unknown, with animal research aiming towards single-cell low aerosol challenge (<30 dispersed bacteria) (Laddy *et al.*, 2018). In cynomolgus macaques, low dose challenge has been demonstrated to induce the spectrum of disease observed in humans (Capuano III *et al.*, 2003; Sharpe *et al.*, 2016).

In expelled aerosol transmissions from individuals with active TB, particle sizes vary, containing variable numbers of culturable *M. tuberculosis*. Aerosols are likely combinations of single bacteria and small aggregates (Todar, 2006; Patterson *et al.*, 2017). The effect of adapted bacilli expelled by a patient with (re)active TB is not considered in animal challenge models. Aerosolised sputum harbours *M. tuberculosis* that cannot be cultured conventionally but could be detected after culturing with exogenous *M. tuberculosis* culture filtrate (Chengalroyen *et al.*, 2016) or 'resuscitation-promoting factors' (Mukamolova *et al.*, 2010) or were detected through PCR (Patterson *et al.*, 2017). Extracellular *M. tuberculosis* in lung tissue (Ulrichs *et al.*, 2005) and biofilm-like structures of *M. tuberculosis* (Nyka, 1967; Nyka and O'Neill, 1970) are often not detected with conventional Zeihl-Neelsen staining as the bacteria are either acid-fast negative or weakly acid-fast.

Bacteria disseminated from biofilms in cavities could aid transmission of *M. tuberculosis* to a new host by facilitating survival during initial contact with host defences. One host defence is surfactant hydrolases secreted by type II alveolar epithelial cells. *M. tuberculosis* exposed to hydrolases in human alveolar lavage had a reduction in cell envelope sugar components arabinose, mannose, myo-inositol and glucose, which translated to reduced ManLAM and TDM. Hydrolase-treated bacteria had lower binding to human macrophages and increased phagosome-lysosome fusion when macrophages were infected without serum (Arcos *et al.*, 2011). ECM could protect disseminated bacilli from environmental immune pressures such as hydrolases, or the ECM itself would be modulated by the hydrolase function. Bacteria may still have cell envelopes that can activate the complement system via lipoglycans (Bartlomiejczyk *et al.*, 2014; Świerzko *et al.*, 2016) and glycolipids including TDM and

TMM (Ramanathan, Curtis and Turk, 1980; Yasuda, 1999), facilitating opsonised interactions with CR on alveolar macrophages.

6.2 Do biofilms protect *M. tuberculosis* from antibody-mediated complement activation and killing by immune cells?

In chapter 2, IgM in the complement source significantly increased complement activation on both planktonic and pellicle biofilm-derived *M. smegmatis* mc^2 155 compared to an antibody-depleted complement source.

Whether antibodies and the humoral immune response are important for TB disease progression or protection against *M. tuberculosis* has renewed interest (Jacobs *et al.*, 2016; Li and Javid, 2018). Antibodies against LAM correlate with less severe forms of TB disease (pulmonary vs disseminated) in children (de L. Costello *et al.*, 1992). In low (Denmark), intermediate (Brazil) and high (Ethiopia) TB incidence countries, TB positive individuals had higher anti-ESAT-6 antibody levels (secretory antigenic protein specific to *M. tuberculosis*) compared to community control subjects. In Ethiopia, overall antibody levels were higher in all three groups, but there were significantly more anti-ESAT-6 antibodies in latent and active TB individuals compared to the controls (Hoff *et al.*, 2007).

Antibody functions include enhancing phagocytosis, enhancing phagolysosome formation, neutralisation, enhancing inflammasome activation and enhancing cytotoxic NK cell activity. Although not currently known, antibodies may help coordinate phagocyte and $CD4^+$ T cells in response to *M. tuberculosis* by enhancing antigen

processing and presentation to $CD4^+$ T cells, which will enhance the overall adaptive immune response (Li and Javid, 2018).

An interesting next step would be to determine which cell wall components from planktonic and pellicle biofilm *M. smegmatis* IgM antibodies have avidity to and whether there are differences despite comparably activating the complement system. A complement source not depleted of IgG could also be assessed.

Existing as part of a biofilm may protect *M. tuberculosis* from antibody-mediated immune responses. For *S. epidermis*, biofilm-cells enhance polysaccharide intracellular adhesin (PNAG) production, a major component of its EPS. PNAG can act as an 'antibody sink', binding antibodies away from the surface of bacteria within biofilms, preventing complement-mediated phagocytic killing (Cerca *et al.*, 2006). The phagocytic killing of *P. aeruginosa* requires complement-mediated opsonophagocytosis. *P. aeruginosa* biofilms have an EPS rich in mucoid exopolysaccharide (MEP). The MEP did not prevent penetration of phagocytes into the biofilm structure or activation of the complement cascade, but the authors' hypothesis that reduced phagocytic killing was observed because the rich MEP EPS interfered with bound complement opsonins on bacterial cells interacting with complement receptors on the phagocytes (Meluleni *et al.*, 1995).

The development of monoclonal IgG antibodies (mAbs) could be an effective therapeutic to target biofilm-encased bacteria. The mAbs 17H12 and 8F12 bind whole and oligosaccharide epitopes of the capsular polysaccharide of carbapenem-resistant *K. pneumoniae. In vitro,* compared to a non-specific IgG control, the mAbs prevented

biofilm formation, prevented replication in serum, increased classical pathway-mediated complement activation via C3b/iC3b and C5b-9 deposition, increased opsonophagocytosis and increased neutrophil killing via ROS production and excreted neutrophil extracellular traps. *In vivo,* mice treated with the mAbs had significantly lower bacterial burdens in the lungs, liver and spleen and had overall lower inflammatory cell recruitment to the lungs (Diago-Navarro *et al.*, 2018).

An *M. tuberculosis* mAb against the arabinomannan moiety of LAM, SMITB14, has shown protection against *M. tuberculosis* in a mouse model. SMITB14, when administered intravenously or through pre-opsonising *M. tuberculosis* Harlingen, demonstrated reduced weight loss, reduced mortality and reduced bacterial burden in the lung and spleen (Hamasur *et al.*, 2004).

For *M. tuberculosis*, mAbs could be developed that target conserved regions of cell wall components, like the mycolic motif. This may prevent the development of biofilms and increase neutrophil-mediated killing. Ideally, the mAbs should be non-functional for complement activation as *M. tuberculosis* utilises this immune interaction to gain access to its intracellular niche via CR (Schlesinger, 1993).

6.3 Could complement aid anti-Tuberculosis drug evaluation through synergy?

Treatment for TB requires long-term therapy using multiple antibiotics due to genotypic and phenotypic resistance mechanisms (Connolly, Edelstein and Ramakrishnan, 2007). The current 6-month regime for drug-susceptible TB includes rifampicin, isoniazid, ethambutol and pyrazinamide. For drug-resistant TB, treatment lasts up to

20 months and involves using an expanded antibiotic regime including second-line injectables (aminoglycosides and capreomycin). Three of the four first-line drugs are most effective when *M. tuberculosis* replicate*s* (WHO, 2020a). Rifampicin, introduced as an anti-Tuberculosis in the 1960s, binds RNA polymerase disrupting RNA transcription (Marriner *et al.*, 2011). Isoniazid was introduced in the 1940s and targets *inhA*, which encodes a reductase of the FAS-II fatty acid elongation system, inhibiting mycolic acid synthesis and is only effective against replicating *M. tuberculosis* (Marrakchi, Lanéelle and Quémard, 2000). Ethambutol was introduced in the 1960s and is a bacteriostatic agent. It targets arabinan synthesis, affecting both the mAGP complex and LAM formation within the cell wall (Mikusova *et al.*, 1995). Pyrazinamide anti-TB properties were discovered in 1952. Its target is not fully defined but may include mRNA translation and energy production. Pyrazinamide only works under acidic pH conditions, is effective against *M. tuberculosis* persisters, and shows minimal activity against actively growing bacteria (Zhang *et al.*, 2014).

Mycobacteria's lipid and carbohydrate-rich outer permeability barrier acts as a pseudo-outer membrane with a periplasmic space akin to the outer membrane (OM) of gram-negative bacteria (Jarlier and Nikaido, 1994; Jackson, 2014). The OM of gram-negative bacteria functions as a physical barrier to many antibiotics, but when C5b-9 deposits, it can rapidly perforate the gram-negative OM. Inner membrane (IM) damage, which is required for complement-mediated killing, is substantially slower (Heesterbeek *et al.*, 2019).

C5b-9 deposition on *M. smegmatis* mc^2 155 was observed in this thesis (chapter 5), and C5b-9 deposition was previously reported for *M. bovis* BCG (Hetland *et al.*, 1998).

Its role in the immune response against *M. tuberculosis* and its effect *in vivo* on the mycobacterial cell wall is still unknown.

Complement in human sera can synergistically sensitise gram-negative bacteria to antibiotics that previously were only effective against gram-positive bacteria. Using a range of 53 clinical isolates across six bacterial species, serum and nisin (a broad-spectrum gram-positive antibiotic), bactericidal synergy was observed for 22 strains by SYTOX staining. An MDR strain of *K. pneumonia* was also killed by the synergy between serum and the gram-positive antibiotics nisin and ceftazidime, with antibiotics individually having no bactericidal effect (Heesterbeek *et al.*, 2019).

Dutcher *et al.*, (1978) demonstrated the synergistic effects of complement activation and streptomycin or tetracycline for the improved killing of several strains of *E. coli*. Streptomycin was one of the first anti-Tuberculosis drugs introduced in 1944, but antibiotic resistance in *M. tuberculosis* developed within a couple of years of administration (Crofton and Mitchison, 1948). Despite the fast onset of drug resistance, streptomycin is an emergency second-line drug against MDR-TB (WHO, 2020b).

Dutcher *et al.*, (1978) also showed that complement-antibiotic synergy could overcome drug resistance using an *E. coli* strain with a tetracycline and streptomycin resistance plasmid. Antibiotics alone did not produce any bactericidal activity against the strain, but in combination with serum, bactericidal activity significantly increased.

Synergy with complement has also been demonstrated for novel synthetic antimicrobial peptides (peptidomimetic 1) against a range of gram-positive and gram-negative bacteria, including *E. coli*, *S. aureus*, *P. aeruginosa* and *S. epidermidis*. For

several bacteria, the presence of non-heat inactivated plasma or serum potentiated peptide activity with reductions in the minimum inhibitory concentration and minimum bactericidal concentrations compared to antibiotic only conditions (Citterio *et al.*, 2016).

Having a better understanding of the innate immune interactions and the phenotypic state of bacteria *in vivo* will aid the development and evaluation of more effective anti-Tuberculosis drugs. Testing antibiotics in more physiologically relevant settings could improve accuracy in determining their efficacy. As *M. tuberculosis* is primarily a pulmonary disease but can disseminate and cause extrapulmonary disease, as well as testing serum and plasma which contain complement proteins, antibiotic efficacy could be explored with BALF, which contains complement proteins and other immune components, including the surfactants (Watford *et al.*, 2000; Vogt *et al.*, 2020) and hydrolases (Arcos *et al.*, 2011).

6.4 What role do anaphylatoxins play in TB disease, and could changes to the cell wall alter the innate and adaptive immune response to *M. tuberculosis*?

C5a generation was observed in the supernatant of both *M. smegmatis* cultured planktonically and as pellicle biofilms incubated with complement (chapter 5).

C3a and C5a are potent proinflammatory polypeptides, and their receptors (C3aR, C5aR and C5L2) are expressed on many cells, including neutrophils, monocytes, macrophages and dendritic cells. Anaphylatoxins play a role in innate and adaptive immunity (Köhl, 2001; Klos *et al.*, 2009). C3a and C5a help induce a localised inflammatory response during infection as they are potent chemoattractants for macrophages, neutrophils, activated B cells and activated T cells. C5a binding can

trigger the oxidative burst in macrophages and oxidative burst/degranulation of neutrophils, killing intracellular bacteria. For the adaptive immune response, the role of complement is less well-defined. Observed functions include C5a priming of dendritic cells, enhancing the production of proinflammatory cytokines including IL-1β, IL-12, IL-23, IL-6 and TGF-β, which mediate either Th2 T cell responses, associated with stimulating the humoral immune response including B cell proliferation and inducing antibody production, or Th17 T cell responses which are associated with cell-mediated inflammation. Anaphylatoxins also directly influence Th1 T cell responses via autocrine signalling through C3aR and C5aR. T-cell-APC interactions stimulate the production and secretion of complement proteins. Extracellular C3 and C5-convertases form, cleaving C3 and C5 to produce anaphylatoxins. T-cells and APCs concurrently upregulate C5aR and C3aR to which the extracellular anaphylatoxins bind, generating IFN-γ and driving Th1 induction (Köhl, 2001; Klos *et al.*, 2009).

Studying the role of terminal phase complement (functions of the complement cascade beyond C5) in pulmonary TB has been carried out in mouse models (Jagannath *et al.*, 2000; Actor *et al.*, 2001; Moulton *et al.*, 2007; Welsh *et al.*, 2008) and has posed the question, is terminal phase complement activation beneficial or harmful to TB disease outcome?

Mice lacking C7, when aerosol challenged with *M. tuberculosis* Erdman have reduced lung immunopathology, smaller granulomas and reduced bacterial dissemination to the liver. T-cell induction by macrophages may also be affected as bone-marrow-derived macrophages, when infected with *M. tuberculosis,* produced less IL12-p40 and

more TGF-β. The authors suggest that C7 could play a role in developing lung immunopathology (Welsh *et al.*, 2012).

In contrast, C5a has been demonstrated to be essential for granuloma formation and controlling bacterial burden in the lungs (Jagannath *et al.*, 2000; Actor *et al.*, 2001). Lacking C5a could alter adaptive immune activation in response to *M. tuberculosis.* C5a-deficient mice DCs produced less IL-12p70 and were less successful at priming naïve T cells to develop into IFN-γ producing Th1 T cells as well as their expansion over a prolonged period. IL-12p70 secretion was driven by C5a, demonstrated by blocking C5aR in C5-sufficient mice. C5-deficient mice had a higher bacterial burden in the lungs and, in the initial infection, a lower infiltration of $CD4^+$ and $CD8^+$ T cells. Overall all T cells in the lungs of C5-deficient mice secreted less IFN-γ (Moulton *et al.*, 2007).

The role of anaphylatoxins in human pulmonary TB disease has not been studied but has been studied in Tuberculosis Pleural Effusion (TPE), a common form of extrapulmonary TB (Luo *et al.*, 2019). TPE can be difficult to diagnose from sputum by acid-fast bacillus smear test and culture, with the most effective diagnostic tool being pleural biopsy (Conde *et al.*, 2003). TPE is associated with an abundant inflammatory cell infiltration and high levels of cytokines and chemokines in the pleural space. In pleural effusion from TPE patients, “nonclassical” $CD14^+$ $CD16^+$ monocytes accumulated, accompanied with the transcriptional upregulation of chemokines as well as C3a and C5a from pleural mesothelial cells, the initial cells to encounter *M. tuberculosis* in the pleural space. Numerous complement proteins, including C1q, MBL, Factor B, C3a, C5a and C5b-9, were detected during staining of pleurisy tissue.

For ‘nonclassical’ monocytes, C3a and C5a enhanced migration, induced upregulation of C3aR and C5aR receptors on the cell surface and induced increased production of proinflammatory cytokines (IL-1β, lL-17, and IL-27). The authors suggest that the high levels of cytokine production from nonclassical monocytes could help facilitate immunopathology during chronic *M. tuberculosis* infection (Luo *et al.*, 2019).

High anaphylatoxin concentrations have been shown to correlate with disease severity in other chronic diseases that cause lung damage, including Cystic Fibrosis (Sass *et al.*, 2015; Hair *et al.*, 2017) and COPD (Marc *et al.*, 2004). Terminal complement cascade functions are rarely considered in TB disease, but the generation of anaphylatoxins could influence TB disease outcome. Do the anaphylatoxins help drive inflammation and play a role in the recruitment of immune cells, including macrophages for bacterial replication, that facilitates *M. tuberculosis* reaching a high extracellular (biofilm) bacterial burden within granulomas and cavities?

ΔMSMEG4722, with an altered cell envelope demonstrated through altered cell wall morphology and permeability to the lipophilic antibiotic rifampicin (Bhatt *et al.*, 2008), could represent the phenotype of *M. tuberculosis* present in the host whose cell walls has been disrupted by antibiotic therapy before killing. *ΔMSMEG4722*, cultured both planktonically and as a pellicle biofilm that could not mature and reticulate (chapter 3), induced increased activation of the complement system and generation of C5a compared to *M. smegmatis* mc^2 155 (chapter 5). Through SEM, no differences in cell wall morphology were observed, but *ΔMSMEG4722* did not clump akin to *M. smegmatis* mc^2 155 when cultured planktonically (chapter 3).

Treatment with isoniazid (mycolic acid synthesis inhibition) or the novel anti-Tuberculosis SQ109 (prevents TMM transport) visibly alter the cell wall of *M. tuberculosis* (Takayama, Wang and Merkal, 1973; Tahlan *et al.*, 2012). Using SEM, isoniazid treatment for 24 hours prior to killing resulted in *M. tuberculosis* cells which developed a wrinkled surface, then overall cell morphology becoming rough and ragged (Takayama, Wang and Merkal, 1973). By SEM analysis, *M. tuberculosis* treated with SQ109 had a ruffled surface. By TEM, SQ109 and isoniazid treated *M. tuberculosis,* accumulated dense material between the plasma membrane and the cell wall (Tahlan *et al.*, 2012). Could patients that have undergone antibiotic therapy have *M. tuberculosis* with altered cell walls that can facilitate increased levels of complement activation and anaphylatoxin generation? Could this contribute to the difficulty to resolve TB infection through anaphylatoxins extensive immune cross-talk?

6.5 Further assessment of the role of mycolic acids and other cell envelope components in pellicle biofilm development

Despite a comparable concentration of TDM in the apolar lipids between planktonically cultured cells and mature pellicle biofilms, previously it has been shown that TDM is reduced in *M. smegmatis* mc^2 155 pellicle biofilms as they develop, with newly synthesised TDM being the precursor for FMA release (Ojha *et al.*, 2010). It is also hypothesised that the release of TDM from the surface of mycobacteria facilitates early pellicle biofilm formation through spreading on the air-liquid interface (Hunter, Venkataprasad and Olsen, 2006). In this thesis, only the lipid profiles of ‘mature’ six-day cultured *M. smegmatis* mc^2 155 and *ΔMSMEG4722* pellicles were examined, so any lipid changes over the development of pellicle biofilms were not quantified.

Visually, pellicle biofilm development of *M. smegmatis* mc^2 155 and *ΔMSMEG4722* diverged from early pellicle formation (chapter 3). Harvesting at each time point (day one to day six) and quantifying the lipids present (including FMA and TDM) could determine when the lipid profiles diverge and whether this reflects an inability to develop mature reticulated pellicle biofilms.

Understating the composition of lipids and other cell wall components in the ECM, including carbohydrates, lipoglycans, and (potentially) eDNA of *M. smegmatis* mc^2 155 and *ΔMSMEG4722* may also decipher why *ΔMSMEG4722* could not form mature, reticulated pellicles. Confocal Laser Scanning Microscopy (CLSM) has been used to determine bacterial distribution within ECM of adherent biofilms of *M. tuberculosis, M. smegmatis, and M. abscesses* via imaging GFP-fluorescing bacteria (Ojha *et al.*, 2005; Hall-Stoodley *et al.*, 2006), but Trivedi *et al.*, (2016) have also analysed ECM composition through combining GFP-expressing *M. tuberculosis* and dyes that can stain different components, e.g. eDNA, proteins, polysaccharides and carbohydrates. The images are overlaid to determine the distribution of ECM components and bacteria. Reconstruction of *ΔMSMEG4722* to express GFP, combined with a range of ECM dyes, could determine which ECM components have either altered production or redistribution in *ΔMSMEG4722* pellicles compared to *M. smegmatis* mc^2 155. This could give some insight into the overarching impact of losing mature mycolic acids for mycolic acid intermediates on pellicle biofilm formation. The staining profile could also be applied to planktonic cultures.

A better understanding of ECM composition of pellicle biofilms and the surface of planktonically-cultured cells would help decipher the cell wall changes that lead to

decreased activator binding (C1q, ficolin-1 and ficolin-2) to *M. smegmatis* mc^2 155 pellicles compared to planktonic cells and why *ΔMSMEG4722* pellicle biofilms demonstrated increased ficolin-1 and ficolin-2 binding compared to *ΔMSMEG4722* planktonic cells.

6.6 Further assessment of the cell envelope components that activate the complement system

To understand complement activation on mycobacteria, including *M. tuberculosis,* a broader knowledge of cell envelope components that can activate the complement system is still required. This was observed directly for purified SL-1 and PDIM from *M. tuberculosis* H37Rv and could be inferred for TDM and TMM using the lipid extracts of *M. smegmatis* mc^2 155 and *ΔMSMEG4722* (chapter 5). Activating capacities can then be explored in the context of whole bacteria where cell wall components are in their natural configuration within the cell envelope, potentially using monoclonal antibodies that block complement interactions against specific cell envelope components.

Surface binding of antibodies by physical absorption can affect their orientation which can then affect the ability of antibodies to capture their corresponding antigens (Wiseman and Frank, 2012; Welch *et al.*, 2017). Physical absorption was applied in the ELISA using plates that preferentially bound either lipids or carbohydrates to study complement activation by mixtures of lipids, carbohydrates and purified cell envelope components. There may have been ligand-binding orientation bias of complement activation, demonstrated by $PIM_{1,2}$, but not PIM_6 activating the complement cascade (chapter 5).

An alternative technique to study complement-cell wall interactions that would eliminate orientation bias is pull-down immunoassays. Pull-down immunoassays are not widely utilised in studying complement-bacterial cell wall component interactions but have been used to demonstrate C1q binding to *S. aureus* virulence adhesin molecules, 'Cna-like family of collagen-binding microbial surface components recognising adhesive matrix molecules' (MSCRAMMs). Utilising pull-down immunoassays with other methods demonstrated that MSCRAMMs bound C1q and inhibited classical pathway complement activation, presenting a secondary function of the virulence factor (Kang *et al.*, 2013). Pull-down immunoassays have also shown that an uncharacterised *Staphylococcal* superantigen-like protein (SSL), SSL10, competes for C1q binding against IgG. Through haemolysis of IgG-sensitised sheep erythrocytes is was demonstrated that SSL10 inhibited classical pathway complement activation (Itoh *et al.*, 2010).

Pull-down immunoassays usually probe for protein-protein interactions but could be adapted for protein-lipid or protein-lipoglycan interactions, with complement activators immobilised directly to beads or anti-activator antibodies 'pulling out' activator-ligand complexes. This could help resolve questions such as, do cell wall components cultured as pellicle biofilms have altered binding to cell wall activators compared to planktonic cells? This would include interactions of the lipoglycans and lectin pathway activators, as lipoglycans have altered sugar compositions in *M. tuberculosis* pellicle biofilms (Keating *et al.*, 2021). Does the modification to mycolate-containing components alter their ability to bind activators, e.g. TDM? This may resolve why, despite alterations to TDM concentrations between phenotypes of *ΔMSMEG7422*, comparable complement activation was observed in the outer apolar lipid fractions.

Once activator-ligands have been identified, activator or complement protein binding affinity could be studied by surface plasmon resonance (SPR). The technique can be used to determine the affinity of ligand: molecule interactions through measuring association and dissociation kinetics. Using SPR, the virulence factor S*taphylococcus aureus* binder of IgG (Sbi) proteins have been demonstrated to have stable binding to C3 degradation products C3b and C3d (strong association and slow dissociation), whereas C3 binding was unstable (strong association, but fast dissociation). It also characterised the formation of Sbi:C3d:Factor H complexes, demonstrating that Factor H stably bound to a Sbi:C3d complex, which could aid the survival of *S. aureus* through inhibiting complement activation on the pathogen surface (Haupt *et al.*, 2008). Interestingly, SPR binding bias was demonstrated in the *S. aureus* adhesin study when studying C1q-MSCRAMM affinities. The binding affinity was around 1000-fold higher for C1q-MSCRAMM when the MSCRAMM was immobilised than C1q (Kang *et al.*, 2013).

Understanding the binding kinetics of activators and cell envelope components and stability of complement protein deposition may help decipher which cell envelope components are potent activators of the complement cascade, may facilitate opsonophagocytosis into alveolar macrophages, or induce the generation of anaphylatoxins, which all play a role in the immune response to *M. tuberculosis*.

6.7 Concluding Statement

The results presented in this thesis have demonstrated that the maturation of mycolic acids is essential for pellicle biofilm formation. When pellicles can mature, there is overall decreased innate complement activator binding (and therefore potentially

complement activation) to the *M. tuberculosis* surrogate organism *M. smegmatis.* Biofilm establishment could dampen the inflammatory response to *M. tuberculosis* during chronic infection and contribute to the difficulty faced by our immune system and therapeutics in resolving TB disease. The *ΔMSMEG4722* mutant demonstrated a plethora of complement activating cell envelope components are present at the host-pathogen interface that mycolic acids may obscure. The physiological state of *M. tuberculosis in vivo* during the establishment of infection is unknown, so these cell envelope components could play an important role in TB pathogenesis, from inducing opsonophagocytosis by alveolar macrophages to inflammation and granuloma establishment. More research is needed to fully understand and evaluate the relevance of individual mycobacterial cell envelope component interactions with the complement cascade and the effect of biofilm formation on these interactions.

7 Materials and Methods

7.1 *M. smegmatis* Middlebrook 7H9 and Sauton's 40 planktonic and pellicle biofilm culture

M. smegmatis mc^2 155, *ΔMSMEG4722* and *ΔMSMEG4722*-C strains were cultured on Middlebrook 7H10 + 10% OADC (+50µg mL^{-1} hygromycin or 50µg mL^{-1} hygromycin and 50µg mL^{-1} kanamycin for *ΔMSMEG4722* and *ΔMSMEG4722*-C respectively) for three days at 37°C. The resulting bacteria were then cultured in Middlebrook 7H9 + 10% OADC + 0.05% Tween-80 (with the appropriate selective antibiotics) at 37°C, aerated, shaking at 200RPM for 16-18 hours. Bacteria were pelleted and washed with 20mL PBS (3000RPM, 10 minutes) and resuspended in PBS.

For planktonic and pellicle biofilm cultures, resuspended bacteria were used to inoculate Sauton's medium (Parish and Stoker, 2015), modified with a reduction in glycerol from 6% to 4% (Sauton's 40) (Table 7.1), to an $OD540_{nm}$ of 0.05. 400mL planktonic cultures were grown in 1L aerated flasks at 37°C, shaking at 200RPM for 24 hours. Pellicle biofilms were grown in non-TC culture-treated 24-well microplates (2mL per well), remaining static for six days at 37°C, inside an airtight box lined with a damp tissue.

Table 7.1: Sauton's 40 media defined composition

Ingredient	To make 1L
KH_2PO_4 (potassium phosphate monobasic)	0.5g
$MgSO_4.7H_20$ (magnesium sulphate heptahydrate)	0.5g
Citric Acid	2.0g
Ferric Ammonium citrate	0.05g
L-Asparagine	4.0g
Glycerol	40mL
1% zinc sulphate solution	0.1mL
Water (H_2O)	Make up to 1L

7.2 Alternative culture of *M. smegmatis* mc^2 155, *M. tuberculosis* H37Rv and non-mycobacterial bacteria for use in various assays

M. tuberculosis H37Rv was harvested from a CMM MOD2 steady-state chemostat culture. Cultures were treated with 4% (v/v) formaldehyde in water for 1 hour at room temperature (RT), washed with PBS (3000RPM, 10 minutes), then resuspended in PBS and frozen in 1mL aliquots at -80^{o}C until required.

M. smegmatis mc^2 155 was cultured on Middlebrook 7H10 + 10% OADC for three days, then cultured for 24 hours in CMM MOD2 media at 37^{o}C, shaking at 200RPM. NTHi BV749 and BV793 were streaked onto Chocolate Agar + PolyViteX plates and incubated overnight at 37^{o}C + 5% CO_2 before inoculating Supplemented Brain Heart Infusion Broth to an $OD620_{nm}$ of 0.08. The cultures were grown shaking at 180RPM, 37^{o}C to an $OD620_{nm}$ of 0.5. *S. agalactiae* serotype III (GBS) was streaked onto Columbian Blood agar and incubated overnight at 37^{o}C + 5% CO_2 before inoculating Todd Hewitt broth to an $OD600_{nm}$ of 0.1. The culture was grown shaking at 180RPM, 37^{o}C to an $OD620_{nm}$ of 1.0. *Salmonella enterica* sv. Minnesota Re deep rough mutant (strain R595) was streaked onto Luria-Bertani (LB) agar plates and incubated overnight at 37^{o}C + 5% CO_2 before inoculating LB broth to an $OD600_{nm}$ of 0.1. The culture was grown shaking at 180RPM, 37^{o}C to an $OD600_{nm}$ of 1.0.

Cultures of *M. smegmatis*, NTHi, GBS, or *S. enterica* Minnesota R595 were either (A) treated with 4% (v/v) formaldehyde in water at RT for 1 hour, washed with PBS (3000RPM, 5 minutes), then resuspended in PBS or (B) diluted in 50% glycerol (final

concentration 15% glycerol) (live). 1mL aliquots of both conditions were frozen at -80^{o}C until required.

7.3 Preparation of heat-inactivated biomass

Pellicle biofilms (methods section 7.1) were scraped into glass universals using disposable spatulas and resuspended in 20mL PBS. Planktonic cultures were split and pelleted (3000RPM, 10 minutes) in 250mL falcon tubes, the supernatant removed before being consolidated in 20mL PBS and transferred into glass universals. Biomass was heat-killed at 80^{o}C for 2 hours before being transferred into pre-weighed glass tubes and evaporated to dryness using a Genevac EZ-2 Plus evaporator on the aqueous setting at 37^{o}C (Genevac Ltd, UK). The glass tubes were re-weighed then frozen at -80^{o}C until required.

7.4 Preparation of single-cell *M. smegmatis* stocks

Pellicle biofilms (methods section 7.1) were scraped into pre-weighed 50mL falcon tubes using disposable spatulas. Planktonic cultures were split and pelleted (3000RPM, 10 minutes) in pre-weighed 250mL falcon tubes, and the supernatant was removed. 4mm glass beads were added at a ratio of 5g beads: 1g mycobacterial mass. Biomass was vortexed for 30 seconds, resuspended in PBS and left to sediment for 30 minutes before the supernatant was transferred to a new 50mL falcon tube. The supernatants containing dispersed single-cell mycobacteria were then either (A) fixed with 4% (v/v) formaldehyde in water for 1 hour at RT and washed with PBS (3000RPM, 10 minutes) or (B) resuspended in 50% glycerol (final concentration 15% glycerol) (live). 1mL aliquots of both conditions were frozen at -80^{o}C until required.

7.5 Crystal Violet staining and imaging of pellicle biofilms

Liquid underneath the pellicle biofilms was removed using a P200 pipette and the biomass dried overnight. 1mL of 1% crystal violet in water was added to each well and incubated at RT for 10 minutes. The crystal violet was removed, and the biomass was washed three times with 1mL water. The biomass was de-stained with 1mL 95% ethanol for 10 minutes at RT. A 10-fold dilution in 95% ethanol of the eluted crystal violet stain in each well was performed in a new 24-well microplate and measured on a spectrometer at $A595_{nm}$. An average was taken from 16-points measured across the area of each well. Biological replicates and technical replicates varied across experiments but consisted of at least two biological replicates with a minimum of four technical replicates/ biological replicate. All data were log10 transformed, and statistical analysis performed was one-way ANOVA with Tukey's multiple comparison correction. Photographs of pellicle biofilms were taken with a Canon Ixus 115HS camera. Microscopic photographs were taken with an Olympus SZ61 microscope and a Digi-Pad Microscope Tablet camera attachment at 8x and 15x magnification.

7.6 Visualisation of *M. smegmatis* mc^2 155 with nucleic acid stains

Three biological replicates of 4% (v/v) formaldehyde-treated Middlebrook 7H9 cultured *M. smegmatis* mc^2 155 were diluted to an $OD540_{nm}$ of 0.05. 100µl of bacterial culture was added to 96-well plates (technical triplicate per biological replicate per stain condition) and pelleted (3000RPM, 5 minutes) before the supernatant was removed and the plate was washed with 2% BSA in PBS. SYTO 40, SYTOX BLUE and DAPI were each diluted to 5, 10 or 20µM in filter sterilised PBS, and 100µl added to the

appropriate wells. To unstained controls, 100µl filter sterilised PBS was added. On a Cytoflex S flow cytometer (Beckman Coulter® Life Sciences), bacterial populations were broadly gated using an FSC-A vs SSC-A scatter plot. The population was displayed on a PB450-A vs FSC-A scatter plot, and quadrant gates were applied to define unstained populations from the stained bacterial populations (Figure 7.1).

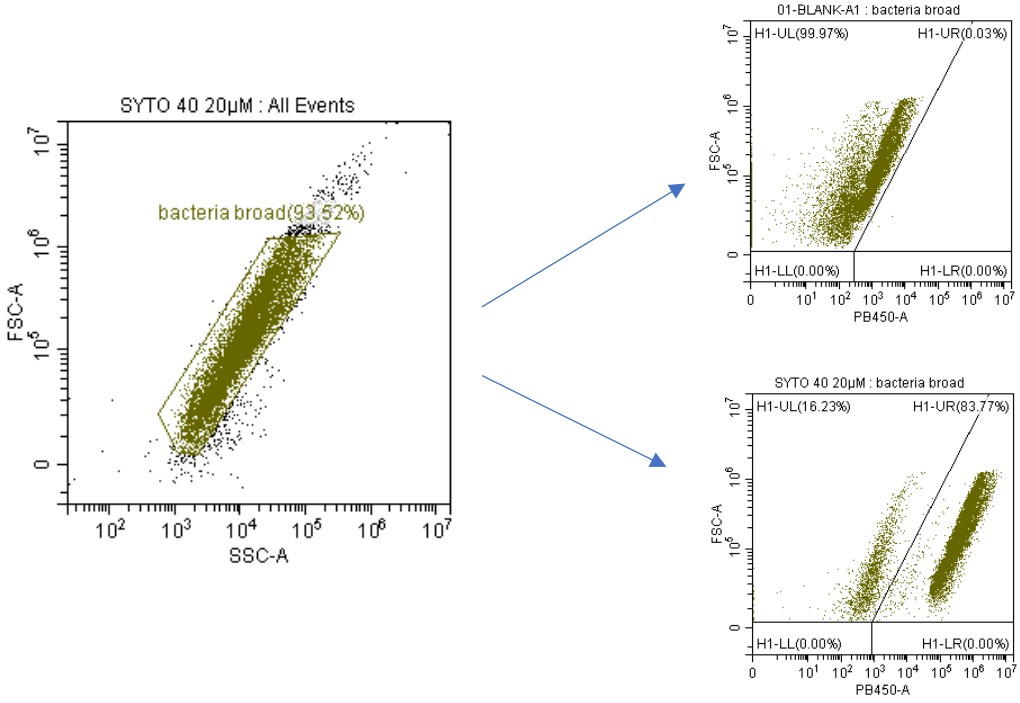


Figure 7.1: Channel and gating strategy for separating *M. smegmatis* mc² 155 events from unstained background events by flow cytometry.

(Left) Representative Forward Scatter (FSC-A) and Side Scatter (SSC-A) plot gated to define the broader bacterial population of *M. smegmatis* mc² 155. (Top right) Representative unstained bacterial population providing quadrant gating to separate bacterial events from background noise. (Bottom right) Representative stained *M. smegmatis* mc² 155 population separated from unstained background events.

The mean fluorescence intensity was calculated and averaged for the three technical replicates per biological replicate per stain based on the events in the positive bacterial gate. Between each stain, the flow cytometer was washed with water and Decon 90 to

minimise stain spill over. The Z-Factor (Table 7.2) was calculated for the difference in mean fluorescence intensity between the averages of stained and unstained populations for statistical analysis. Overlay scatter plots and histograms were generated in CytExpert Software v2.2.

Table 7.2: Z-factor ranges.

Z-Factor ranges defined from Zhang, Chung and Oldenburg, (1999).

Definition	Score
Ideal	1.0
Excellent	0.5-1.0
Marginal	0-0.5
Positive/negative overlap	<0

7.7 Gating strategy and compensation matrix for flow cytometry

Figure 7.2 demonstrates the gating strategy employed to analyse flow cytometry data. A compensation matrix for the FITC and APC fluorochromes was generated using formaldehyde-treated *Neisseria meningitides* H44/76 and a strong positive serum.

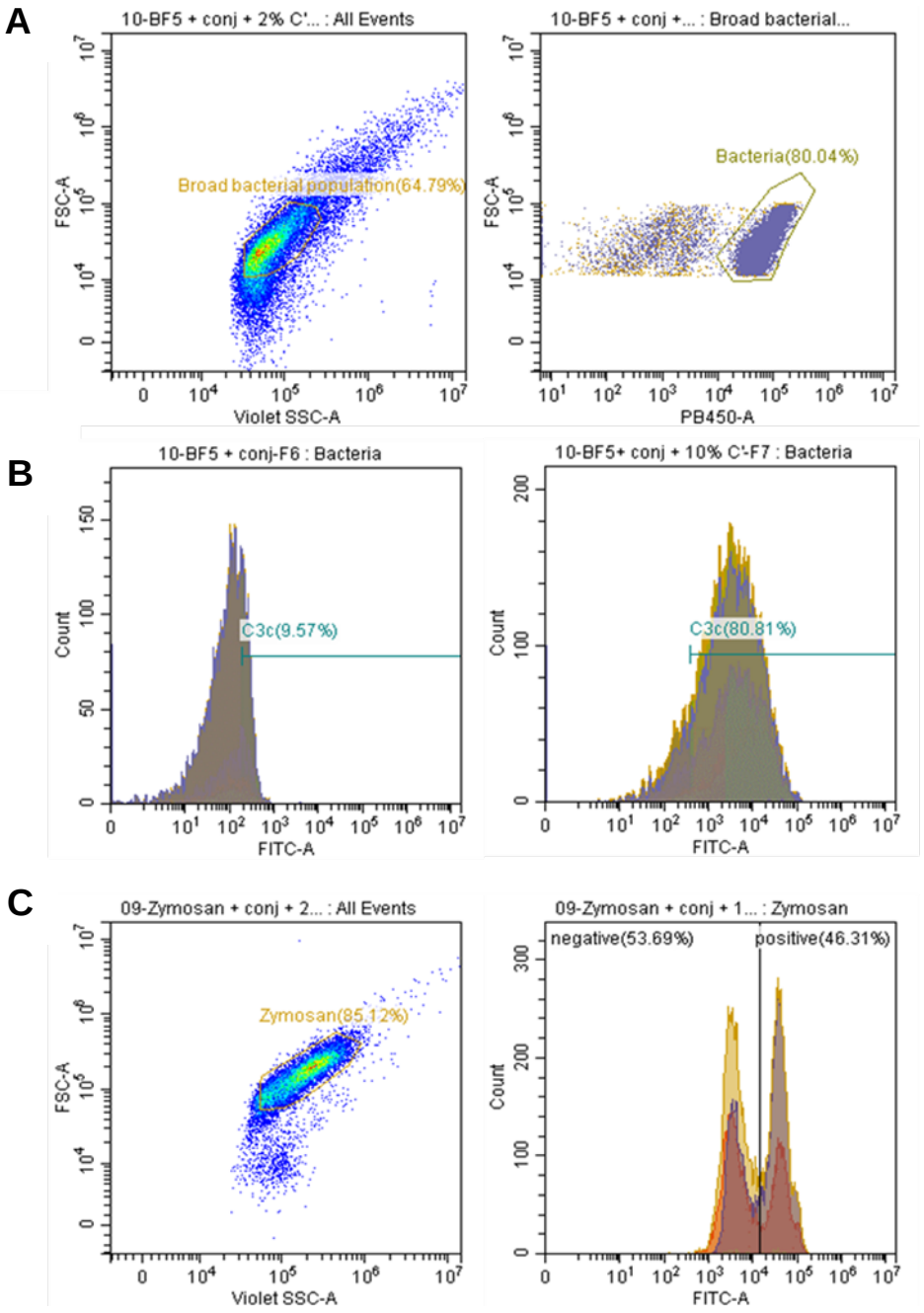


Figure 7.2: Gating strategy for flow cytometry assays.

(A) (Left) Forward Scatter (FSC-A) vs Side Scatter (SSC-A) pseudocolour plot for *M. smegmatis* mc^2 155 with a gate set around the 'single' cell events. (Right) Based on the 'single-cell events' gate, the bacterial population separated using a stain from background events and gated using an FCS-A vs PB450-A fluorescent channel. (B) Both populations are gated off the stained bacterial population (Left) *M. smegmatis* mc^2 155 + conjugate only (background fluorescence control) (Right) *M. smegmatis* mc^2 155 + exogenous human complement + conjugate (positive sample). (C) Gating strategy for the zymosan control with exogenous human complement.

7.8 Calculating bacterial stock concentrations

Bacterial stocks were diluted 10-fold in HBSS. 10µl of diluent was then mixed with 100µl Flow-Count™ Fluorospheres and 890µl 10µM SYTO 40-HBSS in polypropylene flow cytometry tubes. An FSC-A vs APC-A fluorescent channel was used to visualise the fluorescent bead population. This population was gated, and the acquisition set to 1,000 events based on this gate. For gating the bacterial population, an FSC-A vs PB450-A fluorescent channel was used. The number of bacteria mL^{-1} was calculated:

(Bacteria count/ bead count) * bead concentration (~1000 μl^{-1}) * dilution factor (100) * 1000 (µl→mL) = bacteria mL^{-1}

7.9 IgM deposition flow cytometry assays

For the initial experiment, three biological replicates of 4% (v/v) formaldehyde-treated stocks of *M. smegmatis* mc^2 155 cultured in Middlebrook 7H9, CMM MOD2-chemostat cultured *M. tuberculosis* H37Rv, NTHi BV793 and GBS (methods section 7.2) were diluted to an $OD540_{nm}$ of 0.1 and 90µl mixed with 10µl IgG-depleted human exogenous complement. All bacteria were tested in technical triplicate.

For the serial dilution assay, three biological replicates of 4% (v/v) formaldehyde-treated stocks of CMM MOD2-cultured *M. smegmatis* mc^2 155, CMM MOD2-chemostat culture *M. tuberculosis* H37Rv and NTHi BV793 (methods section 7.2) were diluted to an $OD540_{nm}$ of 0.1. To the starting well of each serial dilution, 20µl IgG-depleted human exogenous complement was added. To all other wells, 10µl BB was added. 10µl complement was serial-diluted from 10% to 0.3125%. To each well, 90µl of the relevant bacteria was added. All bacteria were tested in technical triplicate.

For both assays, the plates were incubated at 37ºC, shaking 900RPM for 45 minutes before being centrifuged (3060g, 5 minutes) and washed with 200µl BB. The bacterial pellets were resuspended in either 200µl (1:500) Goat anti-human IgM (FITC) pAb (Jackson ImmunoResearch) or 200µl BB (bacteria only wells) and incubated at 4ºC for 20 minutes. The plates were centrifuged (3060g, 5 minutes) and washed with 200µl BB. All wells were stained with 10µM SYTO 40-HBSS and analysed by flow cytometry.

The compensation and gating strategy are shown in Figure 7.2. The acquisition was set to 10,000 events in the stained bacteria gate. Deposition of IgM was measured by calculating the median fluorescence intensity (median fluorescence * % positive cells) for each sample (average of technical replicates). Background fluorescence (bacteria + conjugate control) was subtracted from each sample. For statistical analysis, data was log10 transformed and a two-way ANOVA with Tukey's multiple comparison correction performed in GraphPad Prism 9.

7.10 Complement deposition flow cytometry assays determining C3b/iC3b and C5b-9 deposition

In complement deposition assays bacterial stocks used were (A) three biological replicates of 4% (v/v) formaldehyde-treated planktonic or pellicle biofilm cultured *M. smegmatis* mc^2 155 (B) six biological replicates of live Middlebrook 7H9 cultured *M. smegmatis* mc^2 155, *ΔMSMEG4722* and *ΔMSMEG4722*-C or (C) six biological replicates of live planktonic or pellicle biofilm cultured *M. smegmatis* mc^2 155, *ΔMSMEG4722* and *ΔMSMEG4722*-C (methods section 7.1 and 7.4). All bacteria were tested in technical triplicate.

Bacteria were diluted to $1x10^7$ bacteria mL^{-1} in BB (methods section 7.8). Pre-activated zymosan ($5.14x10^7$ particles mL^{-1} in PBS) (CompTech, B400) was used as a positive control. To both bacteria only and bacteria + conjugate only control wells, 10µl BB was added. To 10% complement wells, 10µl of the appropriate human complement (IgG- or IgG- and IgM- depleted) was added. To 2% complement wells, 10µl of the appropriate human complement (IgG- or IgG- and IgM-depleted) diluted 1:5 in BB was added. To all wells, 90µl of the appropriate bacteria was added. The plates were then incubated at 37°C for 45 minutes, shaken at 900RPM before being centrifuged (3060g, 5 minutes) and washed with 200µl BB (3060g, 5 minutes) with the supernatant removed. For determining C3b/iC3b and C5b-9 deposition, 200µl (1:500) Rabbit anti-human C3c (FITC) pAb (Abcam, ab4212) and (1:4,000) Alexafluor 647nm conjugated mouse anti-human SC5b-9 (Quidel, A239) was added. For 4% (v/v) formaldehyde-treated planktonic or pellicle biofilm cultured *M. smegmatis* mc^2 155 only, IgM binding was labelled using 200µl (1:500) Goat anti-human IgM (FITC) pAb (Jackson ImmunoResearch). The plates were incubated for 20 minutes at 4°C, then centrifuged (3060g, 5 minutes) and washed with 200µl BB (3060g, 5 minutes). Live bacteria were then fixed with 200µl 4% (v/v) formaldehyde at RT for 30 minutes. All bacteria containing wells were stained with 200µl 10µM SYTO 40-HBSS. Zymosan only wells were resuspended in 200µl HBSS.

Gating, compensation and data analysis was performed as described in methods sections 7.7 and 7.9. For statistical analysis, data were log10 transformed before performing a one-way or two-way ANOVA with Tukey's or Šidák multiple comparison corrections using GraphPad Prism 9 software.

7.11 C1q, MBL, ficolin-1 and ficolin-2 flow cytometry binding assay

Three biological replicates of live *M. smegmatis* mc^2 155*, ΔMSMEG4722* and *ΔMSMEG4722*-C cultured in (A) Middlebrook 7H9 or (B) as planktonic or pellicle biofilm cultures in Sauton's 40 (methods section 7.1) dispersed into single-cell suspensions (methods section 7.4), were diluted to $1x10^7$ bacteria mL^{-1} (methods section 7.8) in Complement Binding Buffer (Barbitone Buffered Saline 5X concentrate (VB100, TCS Bioscience Ltd) in 2% BSA in PBS (CBB)).

Pre-activated zymosan (CompTech, B400) diluted in PBS to $5.14x10^7$ particles mL^{-1} was used as a positive control for MBL and ficolin-1 binding, NTHi BV749 was used as a positive control for C1q binding and *S. enterica* Minnesota strain R595 was used as a positive control for ficolin-2 binding (methods section 7.2). All bacteria were run in technical duplicate.

The activators; C1q (CompTech, A099), rMBL (R&D Systems, 9086-MB-050), rFicolin-1 (R&D Systems, 4209-FC-050) and rFicolin-2 (R&D Systems, 2428-FC-050) were diluted to 25µg mL^{-1} in CBB and 20µl was added to the appropriate wells (final concentration 5µg mL^{-1}). To the bacteria/zymosan only and bacteria/zymosan + conjugate only wells, 20µl CBB was added. To each well, 80µl of bacteria or zymosan were added and mixed well. All samples were tested in technical duplicate. The plate was sealed and incubated at 37^{o}C for 45 minutes, shaking at 900RPM.

The plates were centrifuged at 3060g for 5 minutes and washed with 200µl BB (3060g, 5 minutes) before being resuspended in either 200µl; CBB (bacteria/ zymosan only),

mouse anti-C1q (Hycult, HM1096), mouse anti-MBL (Hycult, HM2061), mouse anti-FCN1/M-Ficolin (Abcam, ab112476) or mouse anti-Ficolin 2 (Abcam, ab56225).

The plate was incubated for 20 minutes at 4°C. The plates were then centrifuged at 3060g for 5 minutes before being washed with 200µl BB (3060g, 5 minutes) and resuspended in either 200µl CBB or 200µl Anti-Mouse IgG (H+L) Fluorescein (FITC)-AffiniPure F(ab')2 Fragment antibody (Stratech, 115-096-062-JIR). Plates were incubated for 20 minutes at 4°C. Plates were then centrifuged at 3060g for 5 minutes before being washed with 200µl BB (3060g, 5 minutes) and resuspended in 4% (v/v) formaldehyde and left at RT for 1 hour. Plates were centrifuged at 3060g for 5 minutes, the formaldehyde removed and washed with 200µl BB (3060g, 5 minutes) before being resuspended in 10µM SYTO 40-HBSS (zymosan- HBSS only) and analysed by flow cytometry. Gating, compensation and data analysis was performed as described in methods sections 7.7 and 7.9. Statistical analysis was performed using one-way ANOVA with Tukey's multiple comparison correction using GraphPad Prism 9 software.

7.12 DNA extraction

DNA was isolated from two biological replicates of Middlebrook 7H9 cultured *M. smegmatis* mc^2 155, *ΔMSMEG4722* and *ΔMSMEG4722*-C grown as described in methods section 7.1. DNA from NTHi BV793, cultured as described in methods section 7.2, was also isolated as a negative bacterial control. Defrosted bacterial pellets were resuspended in 450µl GTE solution before being incubated with 50µl 10mg mL^{-1} lysozyme solution at 37ºC overnight. This was mixed with 150µl 10% SDS and 20mg mL^{-1} proteinase K (2:1) and incubated at 55°C for 2 hours. 3.5µl of 10mg mL^{-1} DNase

free RNaseA was added and incubated at 37°C for 45 minutes before 200µl of 5M sodium chloride was added. 160µl of CTAB solution was added and incubated at 65°C for 10 minutes. 500µl of the sample was mixed with 500µl chloroform: Isoamyl alcohol (24:1), shaken vigorously and microcentrifuged at 13000RPM for 5 minutes. The aqueous phase was transferred to a new tube containing 700µl isopropanol and mixed gently until DNA had precipitated, then microcentrifuged at 13000RPM for 10 minutes before being washed in 1mL 70% ethanol (13000RPM, 5 minutes). The supernatant was removed, and the DNA pellet was left to air dry before being resuspended in 100µl nuclease-free water. 1µl of DNA was quantified for yield and purity using a Nanodrop™ 2000 spectrophotometer (Thermo Fisher Scientific).

7.13 Polymerase Chain Reaction

Two sets of primers were designed for confirmation of the presence and deletion of the *MSMEG4722* gene. The first primer set amplified the *MSMEG4722* gene, and the second primer set amplified the *MSMEG4722* gene and part of the *SacB* gene of the *SacB-Hyg*^{R} cassette integrated after allelic exchange to delete the *MSMEG4722* gene (Table 7.3).

KAPA Taq LongRange PCR Kit was used following the manufacturer's instructions (KAPA Biosystems, USA). DMSO was added to a final concentration of 5%, and each PCR reaction made up to 25µl. The thermocycler conditions for both primer sets (1 and 2) are described in Table 7.4, with conditions identical except for the extension time.

Table 7.3: Primer pairs.

Set	Primers	Sequence	Description	Size
1	MSMEG4722_F	5' AGA ACA TCG GCG AAG CGT T 3'	Within the remaining 84bp sequence at the start of the *MSMEG4722* gene.	*M. smegmatis* mc^2 155 and *ΔMSMEG4722*-C = 636bp *ΔMSMEG4722* and *ΔMSMEG4722*-C = 3772bp
	MSMEG4722_R	5' TCT TGT TGT GCT CCA AGC CA 3'	Within the remaining 174bp sequence at the end of the *MSMEG4722* gene.	
2	MSMEG4722_F	5' AGA ACA TCG GCG AAG CGT T 3'	Within the remaining 84bp sequence at the start of the *MSMEG4722* gene.	*M. smegmatis* mc^2 155 =N/A *ΔMSMEG4722* and *ΔMSMEG4722*-C = 1238bp
	MSMEG4722_SacB_R	5' AGC CGT GAT AGT TTG CGA CA 3'	Within the *SacB* gene of the *SacB-Hyg^R* cassette.	

Table 7.4: Thermocycler conditions.

Step	Temperature	Duration	Cycles
Initial denaturation	95ºC	5:00	1
Denaturation	95ºC	0:30	35
Annealing	56.9ºC	0:30	
Extension	72ºC	4:00 (1) / 1:30 (2)	
Final extension	72ºC	5:00	1
Hold	4ºC	∞	1

To the PCR products, loading dye was added to a final concentration of 1x (v/v). 2-5µl of PCR products were visualised by gel electrophoresis on a 1% (w/v) TAE (4.84 g Tris, 1.14 ml acetic acid, 2 ml EDTA pH 8.0, per litre) agarose gel containing 1x (v/v) SYBR® Safe DNA Gel Stain (Invitrogen) in 1x TAE buffer at 80V for 90 minutes. 5µl TrackIt™ 1kb Plus DNA ladder (Invitrogen) was run alongside the samples. The gels

were visualised on an UVIdoc (UVITECH, Cambridge) gel documentation imaging system.

7.14 Testing the stability of the *ΔMSMEG4722* and *ΔMSMEG4722*-C *MSMEG4722* gene deletion and complementation

Three independent cultures of *M. smegmatis* mc^2 155, *ΔMSMEG4722* and *ΔMSMEG4722*-C were set up for planktonic culture as described in methods section 7.1. After setting up the planktonic shaking cultures, the remaining Middlebrook 7H9 culture was pelleted (3000RPM, 5 minutes) and frozen at -80ºC. After 24 hours of planktonic culture, 25mL of culture was removed from each replicate, pelleted (3000RPM, 5 minutes) and frozen at -80ºC. The planktonic culture was continued for another five days before 2mL of culture was pelleted (3000RPM, 5 minutes) and frozen at -80ºC. A single biological replicate of pellicle biofilms of either *M. smegmatis* mc^2 155, *ΔMSMEG4722* and *ΔMSMEG4722*-C were scraped into a falcon and frozen at -80ºC. The bacteria were defrosted, and DNA was extracted as described in methods 7.12. PCR was performed as described in methods section 7.13.

7.15 *M. smegmatis* mc^2 155, *ΔMSMEG4722* and *ΔMSMEG4722*-C optical density and total viable count growth curves

Three biological replicates of *M. smegmatis* mc^2 155, *ΔMSMEG4722* and *ΔMSMEG4722*-C strains were cultured in Middlebrook 7H9 + 10% OADC + 0.05% Tween-80 with various antibiotic conditions (Table 7.5).

Table 7.5: Antibiotic conditions for $OD540_{nm}$ and total viable count growth curves.

Strain	No antibiotic	50µg mL^{-1} hygromycin	50µg mL^{-1} kanamycin	50µg mL^{-1} hygromycin and kanamycin
M. smegmatis mc^2 155	Yes	Yes	Yes	No
ΔMSMEG4722	Yes	Yes	Yes	No
ΔMSMEG4722-C	Yes	Yes	Yes	Yes

The flasks were incubated at 37ºC, shaking 200RPM for 56 hours with a time point taken approximately every 4 hours. At each time point, $OD540_{nm}$ and total viable counts were taken. If the $OD540_{nm}$ was >0.5, a 1:10 dilution was performed in PBS and the $OD540_{nm}$ re-measured. For total viable counts, 20µl of flask culture was serially diluted into 180µl PBS over the range 10^0-10^6. 20µl of each dilution was plated onto Middlebrook 7H10 + 10% OADC in triplicate. The number of colonies in the three spots was averaged and adjusted for dilution to give a CFU mL^{-1} (Miles and Misra method). The limit of detection (LOD) was calculated as 50 colonies mL^{-1}. To calculate the doubling time for each strain, the curve was logarithmic scale transformed on the x-axis (time), and the exponential portion of the curve was plotted. The 'exponential curve fitting function' was used to generate the equation; $y= Ae^{\wedge Bx}$. In2 = (0.693) was divided by B. Statistical analysis was performed by a matched two-way ANOVA ($OD540_{nm}$) or matched mixed effect analysis (CFU mL^{-1}) using the Geisser-Greenhouse Correction.

7.16 Full lipid extraction of *M. smegmatis* mc^2 155, *ΔMSMEG4722* and *ΔMSMEG4722*-C

A full lipid extraction of *M. smegmatis* mc^2 155, *ΔMSMEG4722* and *ΔMSMEG4722*-C was performed to separate the ‘layers’ of apolar (outer apolar and inner apolar) and

polar lipids and cell wall-bound fatty acid methyl esters (FAMEs) and mycolic acid methyl esters (MAMEs) (Figure 7.3).

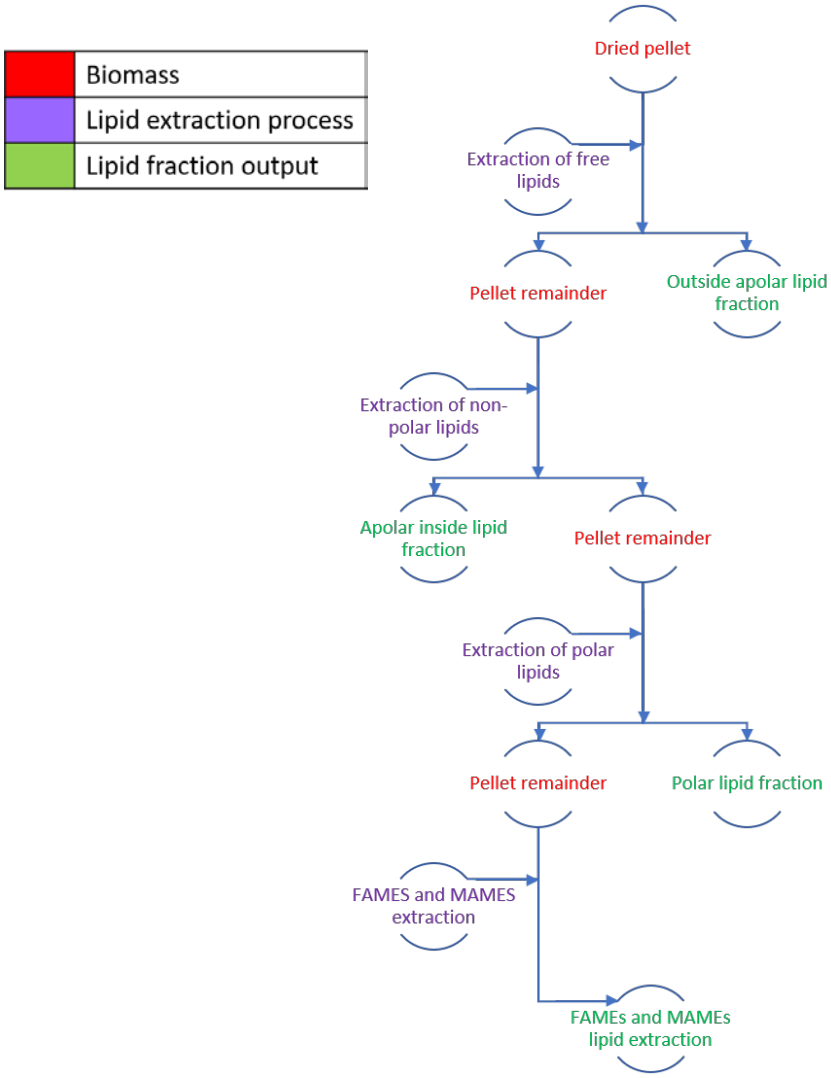


Figure 7.3: Flowchart of full lipid extraction.

A full lipid extraction from biomass of *M. smegmatis* mc^2 155, *ΔMSMEG4722*, and *ΔMSMEG4722*-C to separate the 'layers' of apolar and polar lipids along with cell wall-bound FAMEs and MAMEs.

7.16.1 Extraction of free lipids (outer apolar lipid fraction)

1g of heat-inactivated, dried biomass (methods section 7.3) of three biological replicates of (A) Middlebrook 7H9 culture or (B) planktonic and pellicle biofilm culture

M. smegmatis mc^2 155, *ΔMSMEG4722* and *ΔMSMEG4722*-C (methods section 7.1) were resuspended in 10mL petroleum ether 60-80^{o}C and each replicate split into four separate glass tubes, with the volume made up to 10mL in each and mixed for 1 hour. The suspensions were centrifuged (3000RPM, 10 minutes), and the supernatant was transferred to a new glass tube before 10mL of petroleum ether 60-80^{o}C was added to the pellets repeating the process. The supernatants were pooled and dried at 50^{o}C under airflow in a pre-weighed glass tube before being resuspended to 5 mg mL^{-1} in chloroform: methanol (2:1).

7.16.2 Extraction of non-polar lipids (inner apolar lipid fraction)

To the remaining biomass, 5mL methanol: 0.3% sodium chloride (10:1) and 5mL petroleum ether 60-80^{o}C were added and mixed for 15 minutes. The suspensions were centrifuged (3000RPM, 5 minutes), and the upper phase was transferred to a new glass tube. 5mL petroleum ether 60-80^{o}C was added to the resulting biomass, mixed for 15 minutes and centrifuged (3000RPM, 5 minutes). The upper phases were pooled into a pre-weighed glass tube and dried at 50^{o}C under airflow. The dried upper phase was resuspended to 5 mg mL^{-1} in chloroform: methanol (2:1).

7.16.3 Extraction of polar lipids (polar lipid fraction)

To the remaining biomass, 5.75mL chloroform: methanol: sodium chloride 0.3% (9:10:3) was added and mixed for 1 hour, then centrifuged (3000RPM, 15 minutes) with the supernatant transferred to a new glass tube. To the biomass, 1.875mL chloroform: methanol: sodium chloride 0.3% (5:10:4) was added, mixed for 30 minutes and centrifuged (3000 RPM, 15 minutes) and the supernatant pooled. The 1.875mL chloroform: methanol: sodium chloride 0.3% (5:10:4) step was repeated and the

supernatant pooled. To the pooled supernatant (all four biomass/ replicate), 13mL chloroform and 13mL 0.3% sodium chloride was added and mixed for 5 minutes before being split 10mL/ tube and centrifuged (3000RPM, 5 minutes). The lower phases were pooled and dried at 50^{o}C under airflow in a pre-weighed glass tube before being resuspended to 5 mg mL^{-1} in chloroform: methanol (2:1).

7.16.4 Extraction of FAMEs and MAMEs (FAMEs and MAMEs lipid fraction)

The biomass was resuspended in 2mL 5% tetrabutylammonium hydroxide and incubated at 95^{o}C overnight. 2mL water, 4mL dichloromethane and 500µl iodomethane was added and mixed for 30 minutes before being centrifuged (3000 RPM, 5 minutes). The lower phase was transferred to a new glass tube, and 4mL of water was added and mixed for 5 minutes before being centrifuged (3000RPM, 5 minutes), and the upper aqueous phase was discarded. This process was repeated a further two times. The lower phase was dried at 50^{o}C under airflow before being resuspended in 4mL diethyl ether. The tubes were sonicated for 5 minutes before being centrifuged (3000 RPM for 5 minutes) and the supernatant pooled in a pre-weighed glass tube. The supernatant was dried at 50^{o}C under airflow before being resuspended to 5 mg mL^{-1} in chloroform: methanol (2:1).

7.17 Thin-layer chromatography analysis of lipid extractions

Lipid extractions were analysed by either 1D-TLC or 2D-TLC and stained with 5% MPA to visualise alkylated lipids or α-naphthol-sulphuric acid to visualise carbohydrate containing lipids after charring with a heat-gun (Table 7.6). For the 2D-TLC, aluminium

backed silicon TLC sheets with the dimensions 6.6cm by 6.6cm were used. For 1D-TLC, the height of each sheet was 10cm.

Table 7.6: Solvent systems for TLC lipid analysis.

Solvent system	Lipid fractions tested	Direction 1 solvent	Direction 2 solvent	Stain
A	Outer apolar and inner apolar	Petroleum ether 60-80^{o}C: Ethyl acetate (98:2) x3	Petroleum ether 60-80^{o}C: acetone (98:2) x1	MPA
B	Outer apolar and inner apolar	Petroleum ether 60-80^{o}C: acetone (92:8) x3	Toluene: acetone (95:5) x1	MPA
C	Outer apolar and inner apolar	Chloroform: methanol (96:4) x1	Toluene: acetone (80:20) x1	MPA
D	Outer apolar, inner apolar and polar	Chloroform: methanol: deionised water (100:14:0.8) x1	Chloroform: acetone: methanol: deionised water (50:60:2.5:3) x1	α-naphthol and MPA
F	FAMES and MAMES	Petroleum ether 60-80^{o}C: acetone (95:5) x3	N/A	MPA

7.18 Densitometry analysis of TLC lipid spots

Densitometry analysis using scanned Greyscale TLC images was performed using ImageJ (Schneider, Rasband and Eliceiri, 2012). The background was subtracted before the images were inverted. The integrated density was measured by gating each lipid spot. Statistical analysis performed was one-way or two-way ANOVA with Tukey's multiple comparison correction or unpaired t-test in GraphPad Prism 9 software.

7.19 Lipoglycan extraction of *M. smegmatis* mc^2 155, *ΔMSMEG4722* and *ΔMSMEG4722*-C

Heat-inactivated biomass of three biological replicates of (A) Middlebrook 7H9 culture or (B) planktonic and pellicle biofilm culture *M. smegmatis* mc^2 155, *ΔMSMEG4722* and *ΔMSMEG4722*-C (methods section 7.1 and 7.3) were resuspended in 2mL 50% ethanol (50% (v/v) water) and incubated at 65^{o}C for 2 hours before being centrifuged (3000RPM, 5 minutes) and the supernatant transferred to a new glass tube. This process was repeated, the supernatant pooled and dried at 50^{o}C under airflow. 2mL PBS and 2mL phenol were added to the supernatant, incubated at 80^{o}C for one hour, and centrifuged (3000RPM, 5 minutes) to create a biphase. The upper phase was dialysed overnight in 3.5Da dialysis tubing against water, then for 2 hours against deionised water before being dried at 50^{o}C under airflow and resuspended to 5 mg mL^{-1} in deionised water.

7.20 C3 Standard Curve

A 12-point standard curve was performed (Table 7.7). Std1 (90281.25ng mL^{-1}) was generated by diluting 30.38µl of neat C3 (CompTech, A113) (1.07mg mL^{-1}) into 329.62µl of the carbonate-bicarbonate buffer. A 2:3 serial dilution was used to generate a range from 90281.25ng mL^{-1} to 1043.74ng mL^{-1}. A blank control was generated with carbonate-bicarbonate buffer only. 50µl of each standard was then added to a MaxiSorp™ high protein-binding capacity F96 plate in duplicate.

Table 7.7: 12-point 2:3 C3 standard curve dilution series.

	Lot 20a C3	Std1	Std2	Std3	Std4	Std5	Std6	Std7	Std8	Std9	Std 10	Std 11	Std 12	Blank
Conc. (ng mL^{-1})	1070000	90281.25	60187.5	40125	26750	17833	11888.8	7925.93	5283.95	3522.63	2348.42	1565.61	1043.74	0
µl to add	N/A	50	50	50	50	50	50	50	50	50	50	50	50	0
ng in well	N/A	4514	3009.375	2006.25	1337.5	891.6	594.4	396.26	264.18	176.13	117.42	78.28	52.187	0

Plates were washed three times with PBS before being blocked with 1% BSA in PBS at 25ºC, shaking 250RPM for 1.5 hours before being washed three times with PBS. 100µl pAb anti-C3c HRP (1:200) (Abcam, ab64684) in 2% BSA in PBS was added. The plate was incubated, shaking 250RPM for 1 hour at 25ºC before being washed three times with PBS. The plates were developed using 100µl Tetramethylbenzidine (TMB) as substrate (Abcam, ab171527) for 10 minutes (25ºC, shaking 250PRM), and the reaction stopped using 100µl Stop Solution (Abcam, ab171529). Absorbance was measured at $OD450_{nm}$ on a Tecan Sunrise plate reader. For analysis, the $OD450_{nm}$ fluorescence from the blank was taken away from the corresponding $OD450_{nm}$ fluorescence from the C3 containing wells to give a final $OD450_{nm}$. A standard curve was fitted using the Sigmoidal, 4PL, X is log(concentration) model in GraphPad Prism 9 software based on five replicate experiments (ng/well). The generated curve was used to interpolate $OD450_{nm}$ results to calculate C3b/iC3b deposition in ng.

7.21 C3b/iC3b lipid ELISA

Three biological replicates of (A) Middlebrook 7H9 culture or (B) planktonic and pellicle biofilm culture *M. smegmatis* mc^2 155, *ΔMSMEG4722* and *ΔMSMEG4722*-C lipid fractions (A) outer apolar, (B) inner apolar, (C) polar and (D) FAMEs and MAMEs (methods section 7.16) were assessed for C3b/iC3b deposition by ELISA. In addition,

purified cell envelope components (solvent-soluble) obtained through BEI Resources, NAID, NIH (Table 7.8) were assessed in four separate experiments for C3b/iC3b deposition. All lipids/ components tested were run in technical duplicate.

Table 7.8: Purified solvent-soluble cell wall components obtained through BEI Resources, NAID, NIH.

Product	Volume in vial	Reconstitution solvents	BEI Reference
M. tuberculosis H37Rv SL-1	250µg	2:1 chloroform: methanol	NR-14845
M. canetti PGL-tb	250µg	2:1 chloroform: methanol	NR-36510
M. tuberculosis H37Rv TMM	250µg	2:1 chloroform: methanol	NR-48784
M. tuberculosis H37Rv $PIM_{1,2}$	500µg	2:1 chloroform: methanol	NR-14846
M. tuberculosis H37Rv PDIM	500µg	2:1 chloroform: methanol	NR-20328
M. tuberculosis H37Rv MAMEs	1,000µg	Chloroform	NR-14854
M. leprae PGL-1	1,000µg	Ethanol	NR-19342

M. smegmatis mc^2 155, *ΔMSMEG4722* and *ΔMSMEG4722*-C lipid fractions were resuspended to 5mg mL^{-1} in 2:1 chloroform: methanol, heated in a water bath at 55ºC then diluted in 1mL ethanol to a final concentration of 50µg mL^{-1}. Purified solvent-soluble cell wall components from BEI Resources were reconstituted in 250µl of the recommended solvent (Table 7.7) before being diluted to 50µg mL^{-1} in ethanol. Cholesterol (Sigma Aldrich, C8503) was used as a positive control, resuspended to 40mg mL^{-1} in 2:1 chloroform: methanol then diluted to 50µg mL^{-1} in ethanol. Complement background binding controls were created by diluting the equivalent volumes of reconstitution solvent into ethanol required to reach 50µg mL^{-1} for lipid fractions, purified lipids and cholesterol, respectively. 100µl of resuspended

mycobacterial lipid fractions, purified lipids, cholesterol and controls were added to Nunc PolySorp™ high-affinity binding plates F96 in technical duplicate. Plates were blocked with 5% Foetal Calf Serum in PBS at 25^{o}C 250RPM for 1.5 hours before being washed three times with PBS. 100µl 2% BSA in PBS, 10% or 2% IgG- and IgM-depleted human complement diluted in 2% BSA in PBS was added to the appropriate wells in each plate. The plates were incubated for 1 hour at 37^{o}C, shaking at 400RPM before being washed three times with PBS. 100µl 2% BSA in PBS or pAb anti-C3c HRP (1:200) (Abcam, ab64684) in 2% BSA in PBS was added. The plates were incubated, shaking 250RPM for 1 hour at 25^{o}C before being washed three times with PBS. The plates were developed using 100µl TMB as the substrate for 10 minutes (25^{o}C shaking 250PRM), and the reaction stopped using 100µl Stop Solution.

Absorbance was measured at $OD450_{nm}$ on a Tecan Sunrise plate reader. For analysis, the $OD450_{nm}$ fluorescence from the complement background controls was taken away from the corresponding $OD450_{nm}$ fluorescence from the lipid and complement containing samples to give a final $OD450_{nm}$. $OD450_{nm}$ values were interpolated against the standard curve generated as described in methods 7.20. Statistical analysis performed was two-way ANOVA on the interpolated log(X) values with Tukey's multiple comparison correction using GraphPad Prism 9 software.

7.22 C3b/iC3b carbohydrate ELISA

Three biological replicates of (A) Middlebrook 7H9 culture or (B) planktonic and pellicle biofilm culture *M. smegmatis* mc^2 155, *ΔMSMEG4722* and *ΔMSMEG4722*-C extracted carbohydrates/lipoglycans (methods section 7.19) were assessed for C3b/iC3b deposition by ELISA. In addition, purified cell wall components (water-soluble) were

obtained through BEI Resources, NAID, NIH (Table 7.9) and measured under four separate experiments. All lipoglycans/cell wall components were run in technical duplicate.

Table 7.9: Purified water-soluble cell wall components obtained through BEI Resources, NAID, NIH.

Product	Volume in vial	Reconstitution liquid	BEI Reference
M. tuberculosis H37Rv Arabinogalactan	1,000µg	H_20	NR-14852
M. tuberculosis H37Rv LM	100µg	H_20	NR-14850
M. leprae ManLAM	100µg	H_20	NR-19348
M. tuberculosis H37Rv PIM_6	250µg	H_20	NR-14847
M. tuberculosis H37Rv ManLAM	500µg	H_20	NR-14848
M. smegmatis LAM	500µg	H_20	NR-14849

M. smegmatis mc^2 155, *ΔMSMEG4722* and *ΔMSMEG4722*-C carbohydrate/lipoglycan fractions were resuspended to 5mg mL^{-1} in water then diluted in 1mL carbonate-bicarbonate buffer (ThermoFisher, 18912-014) to a final concentration of 12.5µg mL^{-1}. Purified cell envelope components (water-soluble) from BEI Resources were resuspended in 250µl of water before being diluted to 12.5µg mL^{-1} in the carbonate-bicarbonate buffer. 10 mg mL^{-1} zymosan (CompTech, B400) was used as a positive control, diluted to 5mg mL^{-1} in PBS before being diluted to 12.5µg mL^{-1} in the carbonate-bicarbonate buffer. Complement background binding controls were carbonate-bicarbonate buffer. 100µl of resuspended mycobacterial carbohydrates/lipoglycans, purified cell envelope components, zymosan and controls were added to a Nunc MaxiSorp™ high protein-binding capacity F96 plates in technical duplicate. Plates were washed three times with PBS before being blocked with 1%

BSA in PBS at 25ºC 250RPM for 1.5 hours before being washed three times with PBS. Complement Binding Buffer (CBB) was made by diluting Barbitone Buffered Saline 5X concentrate (VB100, TCS Bioscience Ltd) in 2% BSA in PBS. 100µl CBB, 10% or 2% IgG- and IgM-depleted human complement diluted in CBB was added to the appropriate wells in each plate. The plates were incubated for 1 hour at 37ºC shaking 400RPM before being washed three times with PBS. 100µl 2% BSA in PBS or pAb anti-C3c HRP (1:200) (Abcam, ab64684) in 2% BSA in PBS was added. The plate was incubated, shaking 250RPM for 1 hour at 25ºC before being washed three times with PBS. The plates were developed using 100µl TMB as the substrate for 10 minutes (25ºC shaking 250PRM), and the reaction stopped using 100µl Stop Solution.

Absorbance was measured at $OD450_{nm}$ on a Tecan Sunrise plate reader. For analysis, the $OD450_{nm}$ fluorescence from the complement background controls was taken away from the corresponding $OD450_{nm}$ fluorescence from the lipoglycan/cell envelope component and complement containing samples to give a final $OD450_{nm}$. $OD450_{nm}$ values were interpolated using the standard curve generated as described in methods section 7.20. Statistical analysis performed was two-way ANOVA on the interpolated log(X) values with Tukey's multiple comparison correction using GraphPad Prism 9 software.

7.23 SEM of *M. smegmatis* planktonic cultures and pellicle biofilms

M. smegmatis mc^2 155, *ΔMSMEG4722* and *ΔMSMEG4722*-C planktonic cultures and pellicle biofilms were set up as described in methods section 7.1. To prepare planktonic cultures for SEM, the cultures were split into Nunc wide-mouth centrifuge tubes and

pelleted before being treated with 25mL of 4% (v/v) formaldehyde. Pellets were then washed with water and resuspended in 25mL water. Approximately 100µl of planktonic cultures were pipetted directly onto a sticky carbon disk mounted onto an SEM stub. To prepare the pellicle biofilms for SEM, using a thin-tipped pastette, the pellicles were gently detached from the sides of the wells, and the liquid from underneath was gently aspirated off. Under each pellicle, approximately 2mL of 4% (v/v) formaldehyde was added, and the pellicles were fixed for 24 hours. To image the air-interface, the formaldehyde was replaced with 2mL water. In each well, a 10mm 1.5 thickness round glass coverslip was slid down one side using thin metal tweezers, trying not to disturb the pellicle, then angled so that it sat at the bottom of the well. The liquid was gently aspirated off to settle the pellicle on top of the coverslip. The coverslip was removed from the bottom of the well using tweezers and placed on Whatmann™ filter paper to absorb any excess liquid before being attached to a sticky carbon disk mounted onto an SEM stub. To image the liquid interface, the formaldehyde was aspirated off using a thin-tipped pastette. Then, using an SEM specimen stub with a double-sided sticky carbon disk present, the carbon disk was gently pressed down onto the air-interface of the pellicle biofilm. The biomass attached to the sticky carbon disk was mounted onto an SEM stub exposing the liquid-interface. All samples were air-dried overnight before being processed for SEM by the Electron Microscopy Department, PHE-Porton. The samples were conductively coated with approximately 10nm thickness of gold using the AtomTech Z705 (ion beam) ultra-fine grain sputter coater. SEM was performed with a Zeiss Sigma 300VP Scanning Electron Microscope.

7.24 C5a ELISA

Three biological replicates of live (A) Middlebrook 7H9 culture or (B) planktonic or pellicle biofilm cultured *M. smegmatis* mc^2 155*, ΔMSMEG4722* and *ΔMSMEG4722*-C (methods section 7.1 and 7.4) were diluted to $1x10^7$ bacteria mL^{-1} in BB (methods section 7.8). Controls included bacteria only made up to the same volume as complement containing wells (100µl) using 10µl BB. Pre-activated zymosan ($5.14x10^7$ particles mL^{-1} in PBS), *N. meningitidis* H44/76 and *N. meningitidis* H44/76 + positive serum (NA7455/PIP027) (5µl) were used as positive controls. All conditions for each biological replicate were run in technical duplicate. 10µl of IgG- and IgM-depleted complement were added to the relevant wells for a final concentration of 10%. 90µl of the appropriate bacteria at $1x10^7$ bacteria mL^{-1} (85µl for *N. meningitidis* + positive serum) or 90µl $5.14x10^7$ particles mL^{-1} zymosan were added to the relevant wells and mixed well. The plate was sealed and incubated at 37ºC for 45 minutes, shaking 900RPM. The plates were centrifuged (3060g, 5 minutes), and 50µl of supernatant was transferred into a well containing 150µl C5a ELISA Assay Diluent A (1:4 dilution-final dilution of neat serum is 40-fold in the C5a ELISA plate). 100µl of samples were added to the C5a ELISA plate and the standards for a Human C5a standard curve according to the manufacturer's instructions (following a 1:2 serial dilution from 2000pg mL^{-1} to 32.5pg mL^{-1} plus a blank control).

The plate was incubated, shaking 250RPM at 4ºC overnight. The plate was washed four times with Wash Buffer (200µl), and 100µl biotinylated Human C5a Detection Antibody was added and incubated for 1 hour at RT, shaking at 250RPM. The plate was washed four times with Wash Buffer and 100µl HRP-Streptavidin solution added

and incubated for 45 minutes at RT, shaking at 250RPM. The plate was washed four times with Wash Buffer, and 100µl of TMB One-Step Substrate Reagent was added for 30 minutes, shaking at 250RPM. The reaction was stopped with 50µl of Stop Solution.

Absorbance was measured at $OD450_{nm}$ on a Tecan Sunrise plate reader. For analysis, the $OD450_{nm}$ fluorescence from the no complement controls was taken away from the corresponding $OD450_{nm}$ fluorescence from the bacteria and complement containing samples to give a final $OD450_{nm}$. $OD450_{nm}$ values were interpolated from the generated standard curve to give C5a in pg mL^{-1}. Statistical analysis was performed by one-way ANOVA with Tukey's multiple comparison correction using GraphPad Prism 9 software.

8 List of References

Actor, J. K. *et al.* (2001) 'A role for complement C5 in organism containment and granulomatous response during murine tuberculosis', *Scandinavian Journal of Immunology*. Wiley Online Library, 53(5), pp. 464–474.

Agarwal, V. *et al.* (2014) 'Binding of Streptococcus pneumoniae endopeptidase O (PepO) to complement component C1q modulates the complement attack and promotes host cell adherence', *Journal of biological chemistry*. Elsevier, 289(22), pp. 15833–15844.

Agger, E. M. *et al.* (2008) 'Cationic liposomes formulated with synthetic mycobacterial cordfactor (CAF01): a versatile adjuvant for vaccines with different immunological requirements', *PloS one*. Public Library of Science, 3(9), p. e3116.

Albertí, S. *et al.* (1996) 'Interaction between complement subcomponent C1q and the Klebsiella pneumoniae porin OmpK36.', *Infection and immunity*. Am Soc Microbiol, 64(11), pp. 4719–4725.

Alderwick, L. J. *et al.* (2015) 'The Mycobacterial cell wall—Peptidoglycan and arabinogalactan', *Cold Spring Harbor perspectives in medicine*. Cold Spring Harbor Laboratory Press, p. a021113.

Andersen, A. B. *et al.* (1986) 'Interspecies reactivity of five monoclonal antibodies to Mycobacterium tuberculosis as examined by immunoblotting and enzyme-linked immunosorbent assay.', *Journal of clinical microbiology*. Am Soc Microbiol, 23(3), pp. 446–451.

Andersen, P. and Doherty, T. M. (2005) 'The success and failure of BCG - implications for a novel tuberculosis vaccine.', *Nature reviews. Microbiology*, 3(8), pp. 656–62. doi: 10.1038/nrmicro1211.

Anwar, H., Strap, J. L. and William Costerton, J. (1992) 'Susceptibility of biofilm cells of Pseudomonas aeruginosa to bactericidal actions of whole blood and serum', *FEMS Microbiology letters*. Blackwell Publishing Ltd Oxford, UK, 92(3), pp. 235–241.

Arbues, A. *et al.* (2014) 'Playing hide-and-seek with host macrophages through the use of mycobacterial cell envelope phthiocerol dimycocerosates and phenolic glycolipids', *Frontiers in cellular and infection microbiology*. Frontiers, 4, p. 173.

Arcos, J. *et al.* (2011) 'Human lung hydrolases delineate Mycobacterium tuberculosis–macrophage interactions and the capacity to control infection', *The Journal of Immunology*. Am Assoc Immnol, 187(1), pp. 372–381.

Armitano, J., Méjean, V. and Jourlin-Castelli, C. (2014) 'G ram-negative bacteria can also form pellicles', *Environmental microbiology reports*. Wiley Online Library, 6(6), pp. 534–544.

Arora, R. *et al.* (2016) 'Association of pellicle growth morphological characteristics and clinical presentation of Mycobacterium tuberculosis isolates', *Tuberculosis*. Elsevier, 101, pp. S63–S68.

Astarie-Dequeker, C. *et al.* (1999) 'The mannose receptor mediates uptake of pathogenic and nonpathogenic mycobacteria and bypasses bactericidal responses in human macrophages', *Infection and immunity*. Am Soc Microbiol, 67(2), pp. 469–477.

Astarie-Dequeker, C. *et al.* (2009) 'Phthiocerol dimycocerosates of M. tuberculosis participate in macrophage invasion by inducing changes in the organization of plasma membrane lipids', *PLoS Pathog*. Public Library of Science, 5(2), p. e1000289.

Axelrod, S. *et al.* (2008) 'Delay of phagosome maturation by a mycobacterial lipid is reversed by nitric oxide', *Cellular microbiology*. Wiley Online Library, 10(7), pp. 1530–1545.

Bartlomiejczyk, M. A. *et al.* (2014) 'Interaction of lectin pathway of complement-activating pattern recognition molecules with Mycobacteria', *Clinical & Experimental Immunology*. Wiley Online Library, 178(2), pp. 310–319.

Basaraba, R. J. (2008) 'Experimental tuberculosis: the role of comparative pathology in the discovery of improved tuberculosis treatment strategies', *Tuberculosis*. Elsevier, 88, pp. S35–S47.

Basso, L. A. and Santos, D. S. (2005) 'Drugs that inhibit mycolic acid biosynthesis in Mycobacterium tuberculosis-an update', *Medicinal Chemistry Reviews-Online*. Bentham Science Publishers, 2(5), pp. 393–413.

Behling, C. A. *et al.* (1993) 'Development of a trehalose 6, 6'-dimycolate model which explains cord formation by Mycobacterium tuberculosis.', *Infection and immunity*. Am Soc Microbiol, 61(6), pp. 2296–2303.

Berends, E. T. M. *et al.* (2013) 'Distinct localization of the complement C5b-9 complex on Gram-positive bacteria', *Cellular Microbiology*, 15(12), pp. 1955–1968. doi: 10.1111/cmi.12170.

Besra, G. S. (1998) 'Preparation of cell-wall fractions from mycobacteria', in *Mycobacteria protocols*. Springer, pp. 91–107.

Bester, E. *et al.* (2011) 'Biofilm form and function: carbon availability affects biofilm architecture, metabolic activity and planktonic cell yield', *Journal of applied microbiology*. Wiley Online Library, 110(2), pp. 387–398.

Beveridge, N. E. R. *et al.* (2007) 'Immunisation with BCG and recombinant MVA85A induces long-lasting, polyfunctional Mycobacterium tuberculosis-specific CD4+ memory T lymphocyte populations', *European journal of immunology*. Wiley Online Library, 37(11), pp. 3089–3100.

Bhatt, A. *et al.* (2008) 'Loss of a mycobacterial gene encoding a reductase leads to an altered cell wall containing β-oxo-mycolic acid analogs and accumulation of ketones', *Chemistry & biology*. Elsevier, 15(9), pp. 930–939.

Bidula, S., Sexton, D. W. and Schelenz, S. (2019) 'Ficolins and the recognition of pathogenic microorganisms: an overview of the innate immune response and contribution of single nucleotide polymorphisms', *Journal of immunology research*. Hindawi, 2019.

Birch, H. L. *et al.* (2008) 'Biosynthesis of mycobacterial arabinogalactan: identification of a novel α (1→ 3) arabinofuranosyltransferase', *Molecular microbiology*. Wiley Online Library, 69(5), pp. 1191–1206.

Bloch, H. (1950) 'Studies on the virulence of tubercle bacilli: isolation and biological properties of a constituent of virulent organisms', *The Journal of experimental medicine*. Rockefeller University Press, 91(2), pp. 197–218.

Bohlson, S. S. *et al.* (2001) 'Role of complement in Mycobacterium avium pathogenesis: in vivo and in vitro analyses of the host response to infection in the absence of complement component C3.', *Infection and immunity*. American Society for Microbiology (ASM), 69(12), pp. 7729–35. doi: 10.1128/IAI.69.12.7729-7735.2001.

Borders, C. W. *et al.* (2005) 'Requisite role for complement C5 and the C5a receptor in granulomatous response to mycobacterial glycolipid trehalose 6, 6′-dimycolate', *Scandinavian Journal of Immunology*. Wiley Online Library, 62(2), pp. 123–130.

Brambilla, C. *et al.* (2016) 'Mycobacteria clumping increase their capacity to damage macrophages', *Frontiers in microbiology*. Frontiers, 7, p. 1562.

Brennan, P. J. and Nikaido, H. (1995) 'The envelope of mycobacteria.', *Annual review of biochemistry*. Annual Reviews 4139 El Camino Way, P.O. Box 10139, Palo Alto, CA 94303-0139, USA, 64, pp. 29–63. doi: 10.1146/annurev.bi.64.070195.000333.

Brookes, C. *et al.* (2013) 'Development of a large scale human complement source for use in bacterial immunoassays', *Journal of Immunological Methods*. Elsevier, 391(1–2), pp. 39–49. doi: 10.1016/J.JIM.2013.02.007.

Camacho, L. R. *et al.* (2001) 'Analysis of the Phthiocerol Dimycocerosate Locus ofMycobacterium tuberculosis: Evidence that this lipid is involved in the cell wall permeability barrier', *Journal of Biological Chemistry*. Elsevier, 276(23), pp. 19845–19854.

Cambier, C. J. *et al.* (2014) 'Mycobacteria manipulate macrophage recruitment through coordinated use of membrane lipids', *Nature*. Nature Publishing Group, 505(7482), pp. 218–222.

Capuano III, S. V *et al.* (2003) 'Experimental Mycobacterium tuberculosis infection of cynomolgus macaques closely resembles the various manifestations of human M. tuberculosis infection', *Infection and immunity*. American Society for Microbiology (ASM), 71(10), p. 5831.

Carroll, M. C. (2004) 'The complement system in regulation of adaptive immunity', *Nature immunology*. Nature Publishing Group, 5(10), pp. 981–986.

Carroll, M. V *et al.* (2009) 'Multiple routes of complement activation by Mycobacterium bovis BCG', *Molecular immunology*. Elsevier, 46(16), pp. 3367–3378.

Carter, G. *et al.* (2003) 'Characterization of biofilm formation by clinical isolates of Mycobacterium

avium', *Journal of medical microbiology*. Microbiology Society, 52(9), pp. 747–752.
de Carvalho, L. P. S. *et al.* (2010) 'Metabolomics of Mycobacterium tuberculosis reveals compartmentalized co-catabolism of carbon substrates', *Chemistry & biology*. Elsevier, 17(10), pp. 1122–1131.
Cerca, N. *et al.* (2006) 'Comparative antibody-mediated phagocytosis of Staphylococcus epidermidis cells grown in a biofilm or in the planktonic state', *Infection and immunity*. American Society for Microbiology (ASM), 74(8), p. 4849.
Chakraborty, P. *et al.* (2021) 'Biofilm formation in the lung contributes to virulence and drug tolerance of Mycobacterium tuberculosis', *Nature communications*. Nature Publishing Group, 12(1), pp. 1–17.
Chakraborty, P. and Kumar, A. (2019) 'The extracellular matrix of mycobacterial biofilms: could we shorten the treatment of mycobacterial infections?', *Microbial Cell*. Shared Science Publishers, 6(2), p. 105.
Chen, J. M. *et al.* (2006) 'Roles of Lsr2 in colony morphology and biofilm formation of Mycobacterium smegmatis', *Journal of bacteriology*. Am Soc Microbiol, 188(2), pp. 633–641.
Chen, S. *et al.* (2020) 'The aceE involves in mycolic acid synthesis and biofilm formation in Mycobacterium smegmatis', *BMC microbiology*. Springer, 20(1), pp. 1–11.
Chengalroyen, M. D. *et al.* (2016) 'Detection and quantification of differentially culturable tubercle bacteria in sputum from patients with tuberculosis', *American journal of respiratory and critical care medicine*. American Thoracic Society, 194(12), pp. 1532–1540.
Chiaradia, L. *et al.* (2017) 'Dissecting the mycobacterial cell envelope and defining the composition of the native mycomembrane', *Scientific reports*. Nature Publishing Group, 7(1), pp. 1–12.
Citterio, L. *et al.* (2016) 'Improved in vitro evaluation of novel antimicrobials: potential synergy between human plasma and antibacterial peptidomimetics, AMPs and antibiotics against human pathogenic bacteria', *Research in microbiology*. Elsevier, 167(2), pp. 72–82.
Cole, F. S. *et al.* (1983) 'Complement biosynthesis by human bronchoalveolar macrophages', *Clinical immunology and immunopathology*. Elsevier, 27(2), pp. 153–159.
Collins, C., Tsui, F. W. L. and Shulman, M. J. (2002) 'Differential activation of human and guinea pig complement by pentameric and hexameric IgM', *European journal of immunology*. Wiley Online Library, 32(6), pp. 1802–1810.
Conde, M. B. *et al.* (2003) 'Yield of sputum induction in the diagnosis of pleural tuberculosis', *American journal of respiratory and critical care medicine*. American Thoracic Society, 167(5), pp. 723–725.
Connolly, L. E., Edelstein, P. H. and Ramakrishnan, L. (2007) 'Why is long-term therapy required to cure tuberculosis?', *PLoS Med*. Public Library of Science, 4(3), p. e120.
Cortes, C., Ferreira, V. P. and Pangburn, M. K. (2011) 'Native properdin binds to Chlamydia pneumoniae and promotes complement activation', *Infection and immunity*. Am Soc Microbiol, 79(2), pp. 724–731.
Costerton, A. J. W. *et al.* (1999) 'Bacterial Biofilms : A Common Cause of Persistent Infections', *Science*. American Association for the Advancement of Science, 284(5418), pp. 1318–1322. doi: 10.1126/science.284.5418.1318.
Coulombe, F. *et al.* (2009) 'Increased NOD2-mediated recognition of N -glycolyl muramyl dipeptide', 206(8), pp. 1–8. doi: 10.1084/jem.20081779.
Crofton, J. and Mitchison, D. A. (1948) 'Streptomycin resistance in pulmonary tuberculosis', *British medical journal*. BMJ Publishing Group, 2(4588), p. 1009.
Cywes, C. *et al.* (1997) 'Nonopsonic binding of Mycobacterium tuberculosis to complement receptor type 3 is mediated by capsular polysaccharides and is strain dependent.', *Infection and immunity*. Am Soc Microbiol, 65(10), pp. 4258–4266.
Daffé, M. *et al.* (1999) 'The capsule of Mycobacterium tuberculosis and its implications for pathogenicity.', *Tubercle and lung disease : the official journal of the International Union against Tuberculosis and Lung Disease*. Elsevier, 79(3), pp. 153–169. doi: 10.1054/tuld.1998.0200.
Daffé, M. and Lanée, M.-A. (2001) 'Analysis of the Capsule of Mycobacterium tuberculosis',

Mycobacterium tuberculosis Protocols. Springer, pp. 217–227.
Daffé, M. and Marrakchi, H. (2019) 'Unraveling the structure of the mycobacterial envelope', *Gram-Positive Pathogens*. Wiley Online Library, pp. 1087–1095.
Dao, D. N. *et al.* (2008) 'Mycolic acid modification by the mmaA4 gene of M. tuberculosis modulates IL-12 production', *PLoS Pathog*. Public Library of Science, 4(6), p. e1000081.
Darzins and Fahr (1956) 'Cord-forming property, lethality and pathogenicity of Mycobacteria', *Diseases of the Chest*. Elsevier, 30(6), pp. 642–648.
Davidsen, J. *et al.* (2005) 'Characterization of cationic liposomes based on dimethyldioctadecylammonium and synthetic cord factor from M. tuberculosis (trehalose 6, 6′-dibehenate)—a novel adjuvant inducing both strong CMI and antibody responses', *Biochimica et Biophysica Acta (BBA)-Biomembranes*. Elsevier, 1718(1–2), pp. 22–31.
Dhiman, R. K. *et al.* (2011) 'Lipoarabinomannan localization and abundance during growth of Mycobacterium smegmatis', *Journal of bacteriology*. Am Soc Microbiol, 193(20), pp. 5802–5809.
Diago-Navarro, E. *et al.* (2018) 'Novel, broadly reactive anticapsular antibodies against carbapenem-resistant Klebsiella pneumoniae protect from infection', *MBio*. Am Soc Microbiol, 9(2), pp. e00091-18.
Dietrich, L. E. P. *et al.* (2013) 'Bacterial community morphogenesis is intimately linked to the intracellular redox state', *Journal of bacteriology*. American Society for Microbiology (ASM), 195(7), p. 1371.
Dillon, S. P. *et al.* (2009) *Systemic lupus erythematosus and C1q: A quantitative ELISA for determining C1q levels in serum*, *Biotechnology journal*. Wiley Online Library. doi: 10.1002/biot.200800273.
Dobson, G. *et al.* (1985) 'Systematic analysis of complex mycobacterial lipids', *Society for Applied Bacteriology. Technical Series*, (20), pp. 237–265.
Domenech, M. *et al.* (2013) 'Biofilm formation avoids complement immunity and phagocytosis of Streptococcus pneumoniae', *Infection and Immunity*, 81(7), pp. 2606–2615. doi: 10.1128/IAI.00491-13.
Donlan, R. M. (2002) 'Biofilms: microbial life on surfaces', *Emerging infectious diseases*. Centers for Disease Control and Prevention, 8(9), p. 881.
Douvas, G. S. *et al.* (1985) 'Gamma interferon activates human macrophages to become tumoricidal and leishmanicidal but enhances replication of macrophage-associated mycobacteria.', *Infection and immunity*. Am Soc Microbiol, 50(1), pp. 1–8.
Draper, P. (1998) 'The outer parts of the mycobacterial envelope as permeability barriers', *Front Biosci*, 3, pp. D1253–D1261.
Driessen, N. N. *et al.* (2009) 'Role of phosphatidylinositol mannosides in the interaction between mycobacteria and DC-SIGN', *Infection and immunity*. Am Soc Microbiol, 77(10), pp. 4538–4547.
Dulberger, C. L., Rubin, E. J. and Boutte, C. C. (2020) 'The mycobacterial cell envelope—a moving target', *Nature Reviews Microbiology*. Nature Publishing Group, 18(1), pp. 47–59.
Dusthackeer, A. *et al.* (2019) 'Differential culturability of Mycobacterium tuberculosis in culture-negative sputum of patients with pulmonary tuberculosis and in a simulated model of dormancy', *Frontiers in microbiology*. Frontiers, 10, p. 2381.
Dutcher, B. S. *et al.* (1978) 'Potentiation of antibiotic bactericidal activity by normal human serum', *Antimicrobial Agents and Chemotherapy*. American Society for Microbiology (ASM), 13(5), p. 820.
Esteban, J. and García-Coca, M. (2018) 'Mycobacterium biofilms', *Frontiers in microbiology*. Frontiers, 8, p. 2651.
Falkinham, J. O. (2010) 'Hospital water filters as a source of Mycobacterium avium complex', *Journal of medical microbiology*. Microbiology Society, 59(10), pp. 1198–1202.
Fedrizzi, T. *et al.* (2017) 'Genomic characterization of Nontuberculous Mycobacteria', *Nature Publishing Group*. Nature Publishing Group, (March), pp. 1–19. doi: 10.1038/srep45258.
Fennelly, K. P. *et al.* (2012) 'Variability of infectious aerosols produced during coughing by patients with pulmonary tuberculosis', *American journal of respiratory and critical care medicine*.

American Thoracic Society, 186(5), pp. 450–457.
Fennelly, K. P. *et al.* (2016) 'Biofilm Formation by *Mycobacterium abscessus* in a Lung Cavity', *American Journal of Respiratory and Critical Care Medicine*, 193(6), pp. 692–693. doi: 10.1164/rccm.201508-1586IM.
Ferguson, J. S. *et al.* (2004) 'Complement protein C3 binding to Mycobacterium tuberculosis is initiated by the classical pathway in human bronchoalveolar lavage fluid', *Infection and immunity*. Am Soc Microbiol, 72(5), pp. 2564–2573.
Ferreira, V. P., Cortes, C. and Pangburn, M. K. (2010) 'Native polymeric forms of properdin selectively bind to targets and promote activation of the alternative pathway of complement', *Immunobiology*. Elsevier, 215(11), pp. 932–940.
Flemming, H.-C. and Wingender, J. (2010) 'The biofilm matrix', *Nature reviews. Microbiology*. Nature Publishing Group, 8(9), p. 623.
Flynn, J. L. and Chan, J. (2001) 'Immunology of tuberculosis', *Annual review of immunology*. Annual Reviews 4139 El Camino Way, PO Box 10139, Palo Alto, CA 94303-0139, USA, 19(1), pp. 93–129.
Frederiksen, P. D. *et al.* (2005) 'M-ficolin, an innate immune defence molecule, binds patterns of acetyl groups and activates complement', *Scandinavian journal of immunology*. Wiley Online Library, 62(5), pp. 462–473.
Fu, L. M. and Fu-Liu, C. S. (2002) 'Is Mycobacterium tuberculosis a closer relative to Gram-positive or Gram– negative bacterial pathogens?', *Tuberculosis*, 82(2/3), pp. 85–90. doi: 10.1054/tube.328.
Gaboriaud, C. *et al.* (2003) 'The crystal structure of the globular head of complement protein C1q provides a basis for its versatile recognition properties', *Journal of Biological Chemistry*. Elsevier, 278(47), pp. 46974–46982.
Garcia-Vilanova, A., Chan, J. and Torrelles, J. B. (2019) 'Underestimated manipulative roles of Mycobacterium tuberculosis cell envelope glycolipids during infection', *Frontiers in immunology*. Frontiers, 10, p. 2909.
Garlatti, V. *et al.* (2007) 'Structural insights into the innate immune recognition specificities of L-and H-ficolins', *The EMBO journal*. John Wiley & Sons, Ltd Chichester, UK, 26(2), pp. 623–633.
Garred, P. *et al.* (2016) 'A journey through the lectin pathway of complement—MBL and beyond', *Immunological reviews*. Wiley Online Library, 274(1), pp. 74–97.
Garton, N. J. *et al.* (2008) 'Cytological and transcript analyses reveal fat and lazy persister-like bacilli in tuberculous sputum', *PLoS Med*. Public Library of Science, 5(4), p. e75.
Gaynor, C. D. *et al.* (1995) 'Pulmonary surfactant protein A mediates enhanced phagocytosis of Mycobacterium tuberculosis by a direct interaction with human macrophages.', *The Journal of Immunology*. Am Assoc Immnol, 155(11), pp. 5343–5351.
Gilleron, M. *et al.* (2001) 'Acylation state of the phosphatidylinositol mannosides from Mycobacterium bovis bacillus Calmette Guerin and ability to induce granuloma and recruit natural killer T cells', *Journal of Biological Chemistry*. Elsevier, 276(37), pp. 34896–34904.
Gilleron, M., Quesniaux, V. F. J. and Puzo, G. (2003) 'Acylation state of the phosphatidylinositol hexamannosides from Mycobacterium bovis bacillus Calmette Guerin and Mycobacterium tuberculosis H37Rv and its implication in Toll-like receptor response', *Journal of Biological Chemistry*. Elsevier, 278(32), pp. 29880–29889.
Gilmore, S. A. *et al.* (2012) 'Sulfolipid-1 biosynthesis restricts Mycobacterium tuberculosis growth in human macrophages', *ACS chemical biology*. ACS Publications, 7(5), pp. 863–870.
Ginsberg, A. M. and Spigelman, M. (2007) 'Challenges in tuberculosis drug research and development', *Nature medicine*. Nature Publishing Group, 13(3), pp. 290–294.
Gopalaswamy, R. *et al.* (2007) 'Mycobacterium smegmatis biofilm formation and sliding motility are affected by the serine/threonine protein kinase PknF', *FEMS microbiology letters*. Blackwell Publishing Ltd Oxford, UK, 278(1), pp. 121–127.
Goren, M. B. *et al.* (1976) 'Prevention of phagosome-lysosome fusion in cultured macrophages by sulfatides of Mycobacterium tuberculosis', *Proceedings of the National Academy of Sciences*. National Acad Sciences, 73(7), pp. 2510–2514.

Gout, E. *et al.* (2010) 'Carbohydrate recognition properties of human ficolins: glycan array screening reveals the sialic acid binding specificity of M-ficolin', *Journal of Biological Chemistry*. Elsevier, 285(9), pp. 6612–6622.

Guallar-Garrido, S. *et al.* (2020) 'Each Mycobacterium Requires a Specific Culture Medium Composition for Triggering an Optimized Immunomodulatory and Antitumoral Effect', *Microorganisms*. Multidisciplinary Digital Publishing Institute, 8(5), p. 734.

Guirado, E. and Schlesinger, L. S. (2013) 'Modeling the Mycobacterium tuberculosis granuloma - the critical battlefield in host immunity and disease', *Frontiers in Immunology*, 4(APR), pp. 1–7. doi: 10.3389/fimmu.2013.00098.

Habermehl, K.-O. (2012) *Rapid Methods and Automation in Microbiology and Immunology: Fourth International Symposium on Rapid Methods and Automation in Microbiology and Immunology, Berlin, June 7–10, 1984*. Springer Science & Business Media.

Hair, P. S. *et al.* (2017) 'Complement effectors, C5a and C3a, in cystic fibrosis lung fluid correlate with disease severity', *PLoS One*. Public Library of Science San Francisco, CA USA, 12(3), p. e0173257.

Hall-Stoodley, L. *et al.* (2006) 'Mycobacterium marinum biofilm formation reveals cording morphology', *FEMS microbiology letters*. Blackwell Publishing Ltd Oxford, UK, 257(1), pp. 43–49.

Hall-Stoodley, L., Costerton, J. W. and Stoodley, P. (2004) 'Bacterial biofilms: from the natural environment to infectious diseases', *Nature reviews. Microbiology*. Nature Publishing Group, 2(2), p. 95.

Hamasur, B. *et al.* (2004) 'A mycobacterial lipoarabinomannan specific monoclonal antibody and its F (ab′) 2 fragment prolong survival of mice infected with Mycobacterium tuberculosis', *Clinical & Experimental Immunology*. Wiley Online Library, 138(1), pp. 30–38.

Hanks, J. H. (1961) 'Significance of capsular components of Mycobacterium leprae and other mycobacteria.', *International journal of Leprosy*. Wash, 29(1), pp. 74–83.

Harboe, M. and Mollnes, T. E. (2008) 'The alternative complement pathway revisited', *Journal of cellular and molecular medicine*. Wiley Online Library, 12(4), pp. 1074–1084.

Harland, C. W. *et al.* (2008) 'The Mycobacterium tuberculosis virulence factor trehalose dimycolate imparts desiccation resistance to model mycobacterial membranes', *Biophysical journal*. Elsevier, 94(12), pp. 4718–4724.

Haupt, K. *et al.* (2008) 'The Staphylococcus aureus protein Sbi acts as a complement inhibitor and forms a tripartite complex with host complement Factor H and C3b', *PLoS Pathog*. Public Library of Science, 4(12), p. e1000250.

Heesterbeek, D. A. C. *et al.* (2019) 'Complement-dependent outer membrane perturbation sensitizes Gram-negative bacteria to Gram-positive specific antibiotics', *Scientific reports*. Nature Publishing Group, 9(1), pp. 1–10.

Hetland, G. *et al.* (1998) 'Involvement of antilipoarabinomannan antibodies in classical complement activation in tuberculosis', *Clinical and diagnostic laboratory immunology*. Am Soc Microbiol, 5(2), pp. 211–218.

Hetland, G. and Wiker, H. G. (1994) 'Antigen 85C on Mycobacterium bovis, BCG and M. tuberculosis promotes monocyte-CR3-mediated uptake of microbeads coated with mycobacterial products.', *Immunology*. Wiley-Blackwell, 82(3), p. 445.

Hickling, T. P. *et al.* (2004) 'Collectins and their role in lung immunity', *Journal of leukocyte biology*. Wiley Online Library, 75(1), pp. 27–33.

Hirsch, C. S. *et al.* (1994) 'Complement receptor-mediated uptake and tumor necrosis factor-alpha-mediated growth inhibition of Mycobacterium tuberculosis by human alveolar macrophages.', *The Journal of Immunology*. Am Assoc Immnol, 152(2), pp. 743–753.

Hoff, D. R. *et al.* (2011) 'Location of intra- and extracellular M. tuberculosis populations in lungs of mice and guinea pigs during disease progression and after drug treatment.', *PloS one*. Edited by L. Tailleux. Public Library of Science, 6(3), p. e17550. doi: 10.1371/journal.pone.0017550.

Hoff, S. T. *et al.* (2007) 'Evaluation of Mycobacterium tuberculosis-specific antibody responses in populations with different levels of exposure from Tanzania, Ethiopia, Brazil, and Denmark', *Clinical infectious diseases*. The University of Chicago Press, 45(5), pp. 575–582.

Hoppe, H. C. *et al.* (1997) 'Identification of phosphatidylinositol mannoside as a mycobacterial adhesin mediating both direct and opsonic binding to nonphagocytic mammalian cells.', *Infection and immunity*. Am Soc Microbiol, 65(9), pp. 3896–3905.

Howard, M., Farrar, C. A. and Sacks, S. H. (2018) 'Structural and functional diversity of collectins and ficolins and their relationship to disease', in *Seminars in immunopathology*. Springer, pp. 75–85.

Howard, S. T. *et al.* (2006) 'Spontaneous reversion of Mycobacterium abscessus from a smooth to a rough morphotype is associated with reduced expression of glycopeptidolipid and reacquisition of an invasive phenotype', *Microbiology*. Microbiology Society, 152(6), pp. 1581–1590. doi: 10.1099/mic.0.28625-0.

Hu, C. *et al.* (2000) 'Mycobacterium tuberculosis Infection in Complement Receptor 3-Deficient Mice', *The Journal of Immunology*. American Association of Immunologists, 165(5), pp. 2596–2602. doi: 10.4049/jimmunol.165.5.2596.

Hughes-Jones, N. C. (1977) 'Functional affinity constants of the reaction between 125I-labelled C1q and C1q binders and their use in the measurement of plasma C1q concentrations.', *Immunology*. Wiley-Blackwell, 32(2), p. 191.

Hunter, R. L. (2011) 'Pathology of post primary tuberculosis of the lung: An illustrated critical review', *Tuberculosis*, 91(6), pp. 497–509.

Hunter, R. L., Venkataprasad, N. and Olsen, M. R. (2006) 'The role of trehalose dimycolate (cord factor) on morphology of virulent M. tuberculosis in vitro', *Tuberculosis*. Elsevier, 86(5), pp. 349–356.

Hunter, R. R. L. *et al.* (2006) 'Multiple roles of cord factor in the pathogenesis of primary, secondary, and cavitary tuberculosis, including a revised description of the pathology of secondary disease', *Annals of Clinical & …*, 36(4), pp. 371–386.

Ilyas, R. *et al.* (2011) 'High glucose disrupts oligosaccharide recognition function via competitive inhibition: a potential mechanism for immune dysregulation in diabetes mellitus', *Immunobiology*. Elsevier, 216(1–2), pp. 126–131.

Ishikawa, E. *et al.* (2009) 'Direct recognition of the mycobacterial glycolipid, trehalose dimycolate, by C-type lectin Mincle', *Journal of experimental medicine*. The Rockefeller University Press, 206(13), pp. 2879–2888.

Islam, M. S., Richards, J. P. and Ojha, A. K. (2012) 'Targeting drug tolerance in mycobacteria: a perspective from mycobacterial biofilms'. doi: 10.1586/eri.12.88.

Itoh, S. *et al.* (2010) 'Staphylococcal superantigen-like protein 10 (SSL10) binds to human immunoglobulin G (IgG) and inhibits complement activation via the classical pathway', *Molecular immunology*. Elsevier, 47(4), pp. 932–938.

Jackson, M. (2014) 'The Mycobacterial Cell Envelope—Lipids', *Cold Spring Harbor perspectives in medicine*. Cold Spring Harbor Laboratory Press, 4(10), p. a021105.

Jacobs, A. J. *et al.* (2016) 'Antibodies and tuberculosis', *Tuberculosis*. Elsevier, 101, pp. 102–113.

Jagannath, C. *et al.* (2000) 'Hypersusceptibility of A/J mice to tuberculosis is in part due to a deficiency of the fifth complement component (C5)', *Scandinavian journal of immunology*. Wiley Online Library, 52(4), pp. 369–379.

James, B. W., Williams, A. and Marsh, P. D. (2000) 'The physiology and pathogenicity of Mycobacterium tuberculosis grown under controlled conditions in a defined medium', *Journal of applied microbiology*. Wiley Online Library, 88(4), pp. 669–677.

Jamet, S. *et al.* (2015) 'The non-essential mycolic acid biosynthesis genes hadA and hadC contribute to the physiology and fitness of Mycobacterium smegmatis', *PloS one*. Public Library of Science San Francisco, CA USA, 10(12), p. e0145883.

Jankute, M. *et al.* (2015) 'Assembly of the Mycobacterial Cell Wall.', *Annual review of microbiology*, 69, pp. 405–23. doi: 10.1146/annurev-micro-091014-104121.

Jarlier, V. and Nikaido, H. (1994) 'Mycobacterial cell wall: structure and role in natural resistance to antibiotics', *FEMS microbiology letters*. The Oxford University Press, 123(1–2), pp. 11–18.

Javid, A. *et al.* (2020) 'The mycolic acid reductase Rv2509 has distinct structural motifs and is essential for growth in slow-growing mycobacteria', *Molecular microbiology*. 2019/12/17. John Wiley and

Sons Inc., 113(2), pp. 521–533. doi: 10.1111/mmi.14437.
Jensen, E. T. *et al.* (1993) 'Complement activation by Pseudomonas aeruginosa biofilms', *Microbial pathogenesis*. Elsevier, 15(5), pp. 377–388.
Julián, E. *et al.* (2001) 'An ELISA for five glycolipids from the cell wall of Mycobacterium tuberculosis:: Tween 20 interference in the assay', *Journal of immunological methods*. Elsevier, 251(1–2), pp. 21–30.
Kang, M. *et al.* (2013) 'Collagen-binding microbial surface components recognizing adhesive matrix molecule (MSCRAMM) of Gram-positive bacteria inhibit complement activation via the classical pathway', *Journal of biological chemistry*. Elsevier, 288(28), pp. 20520–20531.
Kang, P. B. *et al.* (2005) 'The human macrophage mannose receptor directs Mycobacterium tuberculosis lipoarabinomannan-mediated phagosome biogenesis.', *The Journal of experimental medicine*, 202(7), pp. 987–99. doi: 10.1084/jem.20051239.
Keating, T. *et al.* (2021) 'Mycobacterium tuberculosis modifies cell wall carbohydrates during biofilm growth with a concomitant reduction in complement activation', *bioRxiv*. Cold Spring Harbor Laboratory.
Khader, S. A. *et al.* (2007) 'IL-23 and IL-17 in the establishment of protective pulmonary CD4+ T cell responses after vaccination and during Mycobacterium tuberculosis challenge', *Nature immunology*. Nature Publishing Group, 8(4), pp. 369–377.
Kieser, K. J. and Rubin, E. J. (2014) 'How sisters grow apart: mycobacterial growth and division', *Nat Rev Micro*. Nature Publishing Group, a division of Macmillan Publishers Limited. All Rights Reserved., 12(8), pp. 550–562. Available at: http://dx.doi.org/10.1038/nrmicro3299.
Kishore, U. *et al.* (2004) 'Structural and functional anatomy of the globular domain of complement protein C1q', *Immunology letters*. Elsevier, 95(2), pp. 113–128.
Klos, A. *et al.* (2009) 'The role of the anaphylatoxins in health and disease', *Molecular immunology*. Elsevier, 46(14), pp. 2753–2766.
Knechel, N. A. (2009) 'Tuberculosis: Pathophysiology, clinical features, and diagnosis', *Critical Care Nurse*, 29(2), pp. 34–43. doi: 10.4037/ccn2009968.
Koch, R. (1882) 'The etiology of tuberculosis.', *Berl. Klin. Wochenschr.*, 15, pp. 221–30.
Köhl, J. (2001) 'Anaphylatoxins and infectious and non-infectious inflammatory diseases', *Molecular immunology*. Elsevier, 38(2–3), pp. 175–187.
Kohler, P. *et al.* (2015) 'Healthcare-associated prosthetic heart valve, aortic vascular graft, and disseminated *Mycobacterium chimaera* infections subsequent to open heart surgery', *European Heart Journal*. Oxford University Press, 36(40), pp. 2745–2753. doi: 10.1093/eurheartj/ehv342.
Kojouharova, M., Reid, K. and Gadjeva, M. (2010) 'New insights into the molecular mechanisms of classical complement activation', *Molecular immunology*. Elsevier, 47(13), pp. 2154–2160.
Kremer, L. *et al.* (2002) 'Mycolic acid biosynthesis and enzymic characterization of the β-ketoacyl-ACP synthase A-condensing enzyme from Mycobacterium tuberculosis', *Biochemical Journal*. Portland Press, 364(2), pp. 423–430.
Kristian, S. A. *et al.* (2008) 'Biofilm formation induces C3a release and protects Staphylococcus epidermidis from IgG and complement deposition and from neutrophil-dependent killing', *The Journal of infectious diseases*. The University of Chicago Press, 197(7), pp. 1028–1035.
Kulka, K., Hatfull, G. and Ojha, A. K. (2012) 'Growth of Mycobacterium tuberculosis biofilms', *JoVE (Journal of Visualized Experiments)*, (60), pp. e3820–e3820. doi: 10.3791/3820.
de L. Costello, A. M. *et al.* (1992) 'Does antibody to mycobacterial antigens, including lipoarabinomannan, limit dissemination in childhood tuberculosis?', *Transactions of the Royal Society of Tropical Medicine and Hygiene*. Royal Society of Tropical Medicine and Hygiene, 86(6), pp. 686–692.
Laddy, D. J. *et al.* (2018) 'Toward tuberculosis vaccine development: recommendations for nonhuman primate study design', *Infection and immunity*. Am Soc Microbiol, 86(2), pp. e00776-17.
Lambert, P. (2002) 'Cellular impermeability and uptake of biocides and antibiotics in gram-positive bacteria and mycobacteria.', *J Appl Microbiol*, 92, p. 46S–54S. doi: 10.1046/j.1365-2672.92.5s1.19.x.

Lea-Smith, D. J. *et al.* (2007) 'The reductase that catalyzes mycolic motif synthesis is required for efficient attachment of mycolic acids to arabinogalactan', *Journal of Biological Chemistry*. ASBMB, 282(15), pp. 11000–11008.

Lefebvre, C. *et al.* (2018) 'HadD, a novel fatty acid synthase type II protein, is essential for alpha-and epoxy-mycolic acid biosynthesis and mycobacterial fitness', *Scientific reports*. Nature Publishing Group, 8(1), pp. 1–15.

Lenaerts, A. J. *et al.* (2007) 'Location of persisting mycobacteria in a guinea pig model of tuberculosis revealed by R207910', *Antimicrobial Agents and Chemotherapy*, 51(9), pp. 3338–3345. doi: 10.1128/AAC.00276-07.

Li, H. and Javid, B. (2018) 'Antibodies and tuberculosis: finally coming of age?', *Nature Reviews Immunology*. Nature Publishing Group, 18(9), pp. 591–596.

Luo, F. *et al.* (2013) 'Ficolin-2 defends against virulent Mycobacteria tuberculosis infection in vivo, and its insufficiency is associated with infection in humans', *PloS one*. Public Library of Science, 8(9), p. e73859.

Luo, L. *et al.* (2019) 'Anaphylatoxins enhance recruitment of nonclassical monocytes via chemokines produced by pleural mesothelial cells in tuberculous pleural effusion', *American journal of respiratory cell and molecular biology*. American Thoracic Society, 60(4), pp. 454–464.

Madigan, C. A. *et al.* (2017) 'A macrophage response to Mycobacterium leprae phenolic glycolipid initiates nerve damage in leprosy', *Cell*. Elsevier, 170(5), pp. 973–985.

Mahamed, D. *et al.* (2017) 'Intracellular growth of Mycobacterium tuberculosis after macrophage cell death leads to serial killing of host cells', *Elife*. eLife Sciences Publications Limited, 6, p. e22028.

Malik, Z. A., Denning, G. M. and Kusner, D. J. (2000) 'Inhibition of Ca(2+) signaling by Mycobacterium tuberculosis is associated with reduced phagosome-lysosome fusion and increased survival within human macrophages.', *The Journal of experimental medicine*. The Rockefeller University Press, 191(2), pp. 287–302. Available at: http://www.ncbi.nlm.nih.gov/pubmed/10637273 (Accessed: 29 July 2018).

Marc, M. M. *et al.* (2004) 'Complement factors c3a, c4a, and c5a in chronic obstructive pulmonary disease and asthma', *American journal of respiratory cell and molecular biology*. American Thoracic Society, 31(2), pp. 216–219.

Marrakchi, H., Lanéelle, G. and Quémard, A. (2000) 'InhA, a target of the antituberculous drug isoniazid, is involved in a mycobacterial fatty acid elongation system, FAS-II', *Microbiology*. Microbiology Society, 146(2), pp. 289–296.

Marrakchi, H., Lanéelle, M.-A. A. and Daffé, M. (2014) 'Mycolic acids: structures, biosynthesis, and beyond', *Chemistry & biology*. Elsevier, 21(1), pp. 67–85. doi: 10.1016/j.chembiol.2013.11.011.

Marriner, G. A. *et al.* (2011) 'The medicinal chemistry of tuberculosis chemotherapy', in *Third World Diseases*. Springer, pp. 47–124.

Marsollier, L. *et al.* (2005) 'Colonization of the salivary glands of Naucoris cimicoides by Mycobacterium ulcerans requires host plasmatocytes and a macrolide toxin, mycolactone', *Cellular microbiology*. Wiley Online Library, 7(7), pp. 935–943.

Martínez, A., Torello, S. and Kolter, R. (1999) 'Sliding motility in mycobacteria', *Journal of bacteriology*. Am Soc Microbiol, 181(23), pp. 7331–7338.

Mathew, R. *et al.* (2006) 'Deletion of the rpoZ gene, encoding the ω subunit of RNA polymerase, results in pleiotropic surface-related phenotypes in Mycobacterium smegmatis', *Microbiology*. Microbiology Society, 152(6), pp. 1741–1750.

Matsushita, M. *et al.* (2005) 'Human M-Ficolin Is a Secretory Protein That', *J Immunol*. Citeseer, 175, pp. 3150–3156.

McShane, H. *et al.* (2004) 'Recombinant modified vaccinia virus Ankara expressing antigen 85A boosts BCG-primed and naturally acquired antimycobacterial immunity in humans', *Nature medicine*. Nature Publishing Group, 10(11), pp. 1240–1244.

Melo, M. D. *et al.* (2000) 'Utilization of CD11b knockout mice to characterize the role of complement receptor 3 (CR3, CD11b/CD18) in the growth of Mycobacterium tuberculosis in macrophages',

Cellular immunology. Elsevier, 205(1), pp. 13–23.
Meluleni, G. J. *et al.* (1995) 'Mucoid Pseudomonas aeruginosa growing in a biofilm in vitro are killed by opsonic antibodies to the mucoid exopolysaccharide capsule but not by antibodies produced during chronic lung infection in cystic fibrosis patients.', *The Journal of Immunology*. Am Assoc Immnol, 155(4), pp. 2029–2038.
Menozzi, F. D. *et al.* (1996) 'Identification of a heparin-binding hemagglutinin present in mycobacteria.', *Journal of Experimental Medicine*. Rockefeller University Press, 184(3), pp. 993–1001.
Merle, N. S. *et al.* (2015) 'Complement system part I - molecular mechanisms of activation and regulation', *Frontiers in Immunology*, 6(JUN), pp. 1–30. doi: 10.3389/fimmu.2015.00262.
Middlebrook, G., Dubos, R. J. and Pierce, C. (1947) 'Virulence and morphological characteristics of mammalian tubercle bacilli', *The Journal of experimental medicine*. Rockefeller University Press, 86(2), pp. 175–184.
Mikusova, K. *et al.* (1995) 'Biogenesis of the mycobacterial cell wall and the site of action of ethambutol.', *Antimicrobial agents and chemotherapy*. American Society for Microbiology (ASM), 39(11), p. 2484.
Minnikin, D. E. (1982) 'Complex lipids, their chemistry biosynthesis and roles', *The biology of mycobacteria*. Academic Press, 1, pp. 95–184.
Minnikin, D. E. *et al.* (2015) 'Pathophysiological implications of cell envelope structure in Mycobacterium tuberculosis and related taxa', *Tuberculosis-expanding knowledge*. BoD, pp. 145–175.
Mishra, A. K. *et al.* (2011) 'Lipoarabinomannan and related glycoconjugates: structure, biogenesis and role in Mycobacterium tuberculosis physiology and host–pathogen interaction', *FEMS microbiology reviews*. Blackwell Publishing Ltd Oxford, UK, 35(6), pp. 1126–1157.
Morgan, B. P. and Gasque, P. (1997) 'Extrahepatic complement biosynthesis: where, when and why?', *Clinical and experimental immunology*. Wiley-Blackwell, 107(1), p. 1.
Moulton, R. A. *et al.* (2007) 'Complement C5a anaphylatoxin is an innate determinant of dendritic cell-induced Th1 immunity to Mycobacterium bovis BCG infection in mice', *Journal of leukocyte biology*. Wiley Online Library, 82(4), pp. 956–967.
Mukamolova, G. V *et al.* (2010) 'Resuscitation-promoting factors reveal an occult population of tubercle bacilli in sputum', *American journal of respiratory and critical care medicine*. American Thoracic Society, 181(2), pp. 174–180.
Murphy, K. (2012) *Janeway's Immunobiology*. 8th editio. Garland Science.
Nakedi, K. C. *et al.* (2015) 'Comparative Ser/Thr/Tyr phosphoproteomics between two mycobacterial species: the fast growing Mycobacterium smegmatis and the slow growing Mycobacterium bovis BCG', *Frontiers in microbiology*. Frontiers Media SA, 6.
Naresh, K. *et al.* (2011) 'Synthesis, biological studies of linear and branched arabinofuranoside-containing glycolipids and their interaction with surfactant protein A', *Glycobiology*. Oxford University Press, 21(9), pp. 1237–1254.
Nataraj, V. *et al.* (2015) 'Mycolic acids: Deciphering and targeting the Achilles' heel of the tubercle bacillus', *Molecular Microbiology*, 98(1), pp. 7–16. doi: 10.1111/mmi.13101.
Neill, M. A. and Klebanoff, S. J. (1988) 'The effect of phenolic glycolipid-1 from Mycobacterium leprae on the antimicrobial activity of human macrophages.', *The Journal of experimental medicine*, 167(1), pp. 30–42.
Nguyen, K. T. *et al.* (2010) 'Mycobacterial biofilms facilitate horizontal DNA transfer between strains of Mycobacterium smegmatis.', *Journal of bacteriology*, 192(19), pp. 5134–42. doi: 10.1128/JB.00650-10.
Nguyen, L., Chinnapapagari, S. and Thompson, C. J. (2005) 'FbpA-dependent biosynthesis of trehalose dimycolate is required for the intrinsic multidrug resistance, cell wall structure, and colonial morphology of Mycobacterium smegmatis', *Journal of bacteriology*. Am Soc Microbiol, 187(19), pp. 6603–6611.
Nigou, J., Gilleron, M. and Puzo, G. (2003) 'Lipoarabinomannans: from structure to biosynthesis', *Biochimie*. Elsevier, 85(1–2), pp. 153–166.

Nilsson, U. R. and Nilsson, B. (1984) 'Simplified assays of hemolytic activity of the classical and alternative complement pathways', *Journal of immunological methods*. Elsevier, 72(1), pp. 49–59.

Noll, H. *et al.* (1956) 'The chemical structure of the cord factor of Mycobacterium tuberculosis', *Biochimica et biophysica acta*. Elsevier, 20, pp. 299–309.

Nyka, W. (1963) 'Studies on Mycobacterium tuberculosis in lesions of the human lung: a new method of staining tubercle bacilli in tissue sections', *American Review of Respiratory Disease*. American Lung Association, 88(5), pp. 670–679.

Nyka, W. (1967) 'Method for staining both acid-fast and chromophobic tubercle bacilli with carbolfuschsin.', *Journal of bacteriology*. American Society for Microbiology (ASM), 93(4), p. 1458.

Nyka, W. (1977) 'The chromophobic tubercle bacilli and the problem of endogenous reactivation of tuberculosis.', *Materia medica Polona. Polish journal of medicine and pharmacy*, 9(3), pp. 175–185.

Nyka, W. and O'Neill, E. F. (1970) 'A new approach to the study of non-acid-fast mycobacteria', *Annals of the New York Academy of Sciences*. Wiley Online Library, 174(2), pp. 862–871.

O'Garra, A. *et al.* (2013) 'The immune response in tuberculosis.', *Annual review of immunology*, 31(1), pp. 475–527. doi: 10.1146/annurev-immunol-032712-095939.

Ojha, A. *et al.* (2005) 'GroEL1: a dedicated chaperone involved in mycolic acid biosynthesis during biofilm formation in mycobacteria', *Cell*. Elsevier, 123(5), pp. 861–873.

Ojha, A. and Hatfull, G. F. (2007) 'The role of iron in Mycobacterium smegmatis biofilm formation: the exochelin siderophore is essential in limiting iron conditions for biofilm formation but not for planktonic growth', *Molecular microbiology*. Wiley Online Library, 66(2), pp. 468–483.

Ojha, A. K. *et al.* (2008) 'Growth of Mycobacterium tuberculosis biofilms containing free mycolic acids and harbouring drug-tolerant bacteria', *Molecular Microbiology*, 69(1), pp. 164–174. doi: 10.1111/j.1365-2958.2008.06274.x.

Ojha, A. K. *et al.* (2010) 'Enzymatic hydrolysis of trehalose dimycolate releases free mycolic acids during mycobacterial growth in biofilms', *Journal of Biological Chemistry*. ASBMB, 285(23), pp. 17380–17389. doi: 10.1074/jbc.M110.112813.

Orme, I. M. (2014) 'A new unifying theory of the pathogenesis of tuberculosis', *Tuberculosis*. Elsevier, 94(1), pp. 8–14.

Ortalo-Magne, A. *et al.* (1995) 'Molecular composition of the outermost capsular material of the tubercle bacillus', *Microbiology*. Microbiology Society, 141(7), pp. 1609–1620.

Pabst, M. J. *et al.* (1988) 'Inhibition of macrophage priming by sulfatide from Mycobacterium tuberculosis.', *The Journal of Immunology*. Am Assoc Immnol, 140(2), pp. 634–640.

Pacheco, S. A. *et al.* (2013) 'MmpL11 protein transports mycolic acid-containing lipids to the mycobacterial cell wall and contributes to biofilm formation in Mycobacterium smegmatis', *Journal of Biological Chemistry*. Elsevier, 288(33), pp. 24213–24222.

Pang, J. M. *et al.* (2012) 'The polyketide Pks1 contributes to biofilm formation in Mycobacterium tuberculosis', *Journal of bacteriology*. Am Soc Microbiol, 194(3), pp. 715–721.

Parish, T. and Stoker, N. G. N. G. (2015) 'Mycobacteria Protocols', *Methods in Molecular Biology*. New Jersey: Humana Press, 101, pp. 77–103. doi: 10.1385/0896034712.

Parsek, M. R. and Singh, P. K. (2003) 'Bacterial biofilms: an emerging link to disease pathogenesis', *Annu.Rev.Microbiol.*, 57(0066–4227 (Print)), pp. 677–701. doi: 10.1146/annurev.micro.57.030502.090720.

Patterson, B. *et al.* (2017) 'Detection of Mycobacterium tuberculosis bacilli in bio-aerosols from untreated TB patients', *Gates open research*. Gates Foundation-Open Access, 1.

Peñuelas-Urquides, K. *et al.* (2013) 'Measuring of Mycobacterium tuberculosis growth: a correlation of the optical measurements with colony forming units', *Brazilian journal of microbiology*. SciELO Brasil, 44(1), pp. 287–290.

Perley, C. C. *et al.* (2014) 'The human antibody response to the surface of Mycobacterium tuberculosis', *PloS one*. Public Library of Science, 9(6), p. e98938.

Pieters, J. (2008) 'Mycobacterium tuberculosis and the Macrophage: Maintaining a Balance', *Cell Host*

and Microbe, 3(6), pp. 399–407. doi: 10.1016/j.chom.2008.05.006.
Polotsky, V. Y. *et al.* (1997) 'Interaction of human mannose-binding protein with Mycobacterium avium', *Journal of Infectious Diseases*. The University of Chicago Press, 175(5), pp. 1159–1168.
Quidel (2018) 'The Complement System'.
Qvist, T. *et al.* (2015) 'Chronic pulmonary disease with Mycobacterium abscessus complex is a biofilm infection.', *The European respiratory journal*. European Respiratory Society, 46(6), pp. 1823–6. doi: 10.1183/13993003.01102-2015.
Ramanathan, V. D., Curtis, J. and Turk, J. L. (1980) 'Activation of the alternative pathway of complement by mycobacteria and cord factor', *Infection and Immunity*, 29(1), pp. 30–35.
Ramsugit, S. *et al.* (2013) 'Pili contribute to biofilm formation in vitro in Mycobacterium tuberculosis', *Antonie Van Leeuwenhoek*. Springer, 104(5), pp. 725–735.
Recht, J. *et al.* (2000) 'Genetic Analysis of Sliding Motility inMycobacterium smegmatis', *Journal of bacteriology*. Am Soc Microbiol, 182(15), pp. 4348–4351.
Recht, J. and Kolter, R. (2001) 'Glycopeptidolipid acetylation affects sliding motility and biofilm formation in Mycobacterium smegmatis', *Journal of bacteriology*. Am Soc Microbiol, 183(19), pp. 5718–5724.
Remel (2004) *No Title*, *TB Auramine O*. Available at: https://assets.thermofisher.com/TFS-Assets/MBD/Instructions/IFU40086.pdf.
Remel (2013) *No Title*, *TB ZIEHL-NEELSEN CARBOLFUCHSIN*.
Ren, H. *et al.* (2007) 'Identification of the lipooligosaccharide biosynthetic gene cluster from Mycobacterium marinum', *Molecular microbiology*. Wiley Online Library, 63(5), pp. 1345–1359.
Ricklin, D., Reis, E. S. and Lambris, J. D. (2016) 'Complement in disease: a defence system turning offensive', *Nature Reviews Nephrology*, 12(7), pp. 383–401. doi: 10.1038/nrneph.2016.70.
Riojas, M. A. *et al.* (2018) 'Phylogenomic analysis of the species of the Mycobacterium tuberculosis complex demonstrates that Mycobacterium africanum, Mycobacterium bovis, Mycobacterium caprae, Mycobacterium microti and Mycobacterium pinnipedii are later heterotypic synonyms of Mycobacterium tuberculosis', *International journal of systematic and evolutionary microbiology*. Microbiology Society, 68(1), pp. 324–332.
Rodriguez-Rivera, F. P. *et al.* (2017) 'Visualization of mycobacterial membrane dynamics in live cells', *Journal of the American Chemical Society*, p. jacs.6b12541. doi: 10.1021/jacs.6b12541.
Rooyakkers, A. W. J. and Stokes, R. W. (2005) 'Absence of complement receptor 3 results in reduced binding and ingestion of Mycobacterium tuberculosis but has no significant effect on the induction of reactive oxygen and nitrogen intermediates or on the survival of the bacteria in resident and interferon-gamma activated macrophages', *Microbial pathogenesis*. Elsevier, 39(3), pp. 57–67.
Röse, L., Kaufmann, S. H. E. and Daugelat, S. (2004) 'Involvement of Mycobacterium smegmatis undecaprenyl phosphokinase in biofilm and smegma formation', *Microbes and infection*. Elsevier, 6(11), pp. 965–971.
Roumenina, L. T. *et al.* (2008) 'Interaction of the globular domain of human C1q with Salmonella typhimurium lipopolysaccharide', *Biochimica et Biophysica Acta (BBA)-Proteins and Proteomics*. Elsevier, 1784(9), pp. 1271–1276.
Ryan, G. J. *et al.* (2010) 'Multiple M. tuberculosis phenotypes in mouse and guinea pig lung tissue revealed by a dual-staining approach.', *PloS one*. Edited by J. Nigou. Public Library of Science, 5(6), p. e11108. doi: 10.1371/journal.pone.0011108.
Sambandan, D. *et al.* (2013) 'Keto-Mycolic Acid-Dependent Pellicle Formation Confers Tolerance to Drug-Sensitive Mycobacterium tuberculosis', *mBio*, 4(3), pp. e00222-13. doi: 10.1128/mBio.00222-13.Editor.
Sani, M. *et al.* (2010) 'Direct visualization by Cryo-EM of the mycobacterial capsular layer: A labile structure containing ESX-1-secreted proteins', *PLoS Pathogens*, 6(3). doi: 10.1371/journal.ppat.1000794.
Sass, L. A. *et al.* (2015) 'Complement effectors of inflammation in cystic fibrosis lung fluid correlate with clinical measures of disease', *PLoS One*. Public Library of Science San Francisco, CA

USA, 10(12), p. e0144723.
Sax, H. *et al.* (2015) 'Prolonged outbreak of Mycobacterium chimaera infection after open-chest heart surgery', *Clinical Infectious Diseases*. Oxford University Press, 61(1), pp. 67–75. doi: 10.1093/cid/civ198.
Schlesinger, L. S. *et al.* (1990) 'Phagocytosis of Mycobacterium tuberculosis is mediated by human monocyte complement receptors and complement component C3.', *The Journal of Immunology*. Am Assoc Immnol, 144(7), pp. 2771–2780.
Schlesinger, L. S. (1993) 'Macrophage phagocytosis of virulent but not attenuated strains of Mycobacterium tuberculosis is mediated by mannose receptors in addition to complement receptors.', *The Journal of Immunology*. Am Assoc Immnol, 150(7), pp. 2920–2930.
Schlesinger, L. S. and Horwitz, M. (1990) 'Phagocytosis of leprosy bacilli is mediated by complement receptors CR1 and CR3 on human monocytes and complement component C3 in serum.', *Journal of Clinical Investigation*. American Society for Clinical Investigation, 85(4), p. 1304.
Schlesinger, L. S. and Horwitz, M. A. (1991) 'Phagocytosis of Mycobacterium leprae by human monocyte-derived macrophages is mediated by complement receptors CR1 (CD35), CR3 (CD11b/CD18), and CR4 (CD11c/CD18) and IFN-gamma activation inhibits complement receptor function and phagocytosis of this bacterium.', *The Journal of Immunology*. Am Assoc Immnol, 147(6), pp. 1983–1994.
Schlesinger, L. S. and Horwitz, M. A. (1991) 'Phenolic glycolipid-1 of Mycobacterium leprae binds complement component C3 in serum and mediates phagocytosis by human monocytes.', *Journal of Experimental Medicine*. Rockefeller University Press, 174(5), pp. 1031–1038.
Schlesinger, L. S. and Horwitz, M. A. (1994) 'A role for natural antibody in the pathogenesis of leprosy: antibody in nonimmune serum mediates C3 fixation to the Mycobacterium leprae surface and hence phagocytosis by human mononuclear phagocytes.', *Infection and immunity*. American Society for Microbiology (ASM), 62(1), pp. 280–9. Available at: http://www.ncbi.nlm.nih.gov/pubmed/8262640 (Accessed: 22 October 2018).
Schneider, C. A., Rasband, W. S. and Eliceiri, K. W. (2012) 'NIH Image to ImageJ: 25 years of image analysis', *Nature methods*. Nature Publishing Group, 9(7), pp. 671–675.
Schorey, J. S., Carroll, M. C. and Brown, E. J. (1997) 'A macrophage invasion mechanism of pathogenic mycobacteria', *Science*. American Association for the Advancement of Science, 277(5329), pp. 1091–1093.
Schroeder, H. W. and Cavacini, L. (2010) 'Structure and function of immunoglobulins', *Journal of Allergy and Clinical Immunology*. Elsevier, 125(2), pp. S41–S52.
Schulze-Röbbecke, R., Janning, B. and Fischeder, R. (1992) 'Occurrence of mycobacteria in biofilm samples', *Tubercle and Lung Disease*. Elsevier, 73(3), pp. 141–144.
Sefidi, F. J. *et al.* (2017) 'Improvement of thermal stability of BCG vaccine', *Iranian biomedical journal*. Pasteur Institute of Iran, 21(6), p. 406.
Seiler, B. T. *et al.* (2019) 'Broad-spectrum capture of clinical pathogens using engineered Fc-mannose-binding lectin enhanced by antibiotic treatment', *F1000Research*. Faculty of 1000 Ltd, 8.
Selander, B. *et al.* (2006) 'Mannan-binding lectin activates C3 and the alternative complement pathway without involvement of C2', *The Journal of clinical investigation*. Am Soc Clin Investig, 116(5), pp. 1425–1434.
Shaler, C. R. *et al.* (2013) 'Within the enemy's camp: Contribution of the granuloma to the dissemination, persistence and transmission of Mycobacterium tuberculosis', *Frontiers in Immunology*, 4(FRB), pp. 1–8. doi: 10.3389/fimmu.2013.00030.
Sharpe, S. *et al.* (2016) 'Ultra low dose aerosol challenge with Mycobacterium tuberculosis leads to divergent outcomes in rhesus and cynomolgus macaques', *Tuberculosis*. Elsevier, 96, pp. 1–12.
Shiloh, M. U. and Champion, P. A. D. (2010) 'To catch a killer. What can mycobacterial models teach us about Mycobacterium tuberculosis pathogenesis?', *Current opinion in microbiology*. Elsevier, 13(1), pp. 86–92.
Silva Miranda, M. *et al.* (2012) 'The tuberculous granuloma: an unsuccessful host defence mechanism

providing a safety shelter for the bacteria?', *Clinical and Developmental Immunology*. Hindawi, 2012. doi: 10.1155/2012/139127.

Simmons, W. L. and Dybvig, K. (2007) 'Biofilms protect Mycoplasma pulmonis cells from lytic effects of complement and gramicidin', *Infection and immunity*. American Society for Microbiology (ASM), 75(8), p. 3696.

Sinsimer, D. *et al.* (2008) 'The phenolic glycolipid of Mycobacterium tuberculosis differentially modulates the early host cytokine response but does not in itself confer hypervirulence', *Infection and immunity*. Am Soc Microbiol, 76(7), pp. 3027–3036.

Sochorová, Z. *et al.* (2014) 'Morphological and proteomic analysis of early stage air-liquid interface biofilm formation in Mycobacterium smegmatis.', *Microbiology (Reading, England)*, p. mic.0.076174-0-. doi: 10.1099/mic.0.076174-0.

Spargo, B. J. *et al.* (1991) 'Cord factor (alpha, alpha-trehalose 6, 6'-dimycolate) inhibits fusion between phospholipid vesicles', *Proceedings of the National Academy of Sciences*. National Acad Sciences, 88(3), pp. 737–740.

Stewart, G. R. *et al.* (2005) 'Mycobacterial mutants with defective control of phagosomal acidification', *PLoS Pathog*. Public Library of Science, 1(3), p. e33.

Stewart, G. R., Robertson, B. D. and Young, D. B. (2003) 'Tuberculosis: a problem with persistence', *Nat.Rev.Microbiol.*, 1(1740–1526 (Print)), pp. 97–105. doi: Doi 10.1038/Nrmicro749.

Strunk, R. C., Eidlen, D. M. and Mason, R. J. (1988) 'Pulmonary alveolar type II epithelial cells synthesize and secrete proteins of the classical and alternative complement pathways.', *The Journal of clinical investigation*. Am Soc Clin Investig, 81(5), pp. 1419–1426.

Swartz, R. P. *et al.* (1988) 'Differences in uptake of mycobacteria by human monocytes: a role for complement.', *Infection and immunity*. Am Soc Microbiol, 56(9), pp. 2223–2227. Available at: http://www.ncbi.nlm.nih.gov/pubmed/3137162 (Accessed: 7 May 2018).

Świerzko, A. S. *et al.* (2016) 'Mycobacterial antigen 85 complex (Ag85) as a target for ficolins and mannose-binding lectin', *International Journal of Medical Microbiology*. Elsevier, 306(4), pp. 212–221.

Syal, K. *et al.* (2016) 'Synthetic arabinomannan glycolipids impede mycobacterial growth, sliding motility and biofilm structure', *Glycoconjugate journal*. Springer, 33(5), pp. 763–777.

Syal, K. *et al.* (2017) 'Synthetic (p) ppGpp analogue is an inhibitor of stringent response in mycobacteria', *Antimicrobial agents and chemotherapy*. Am Soc Microbiol, 61(6).

Tabouret, G. *et al.* (2010) 'Mycobacterium leprae phenolglycolipid-1 expressed by engineered M. bovis BCG modulates early interaction with human phagocytes', *PLoS Pathog*. Public Library of Science, 6(10), p. e1001159.

Tahlan, K. *et al.* (2012) 'SQ109 targets MmpL3, a membrane transporter of trehalose monomycolate involved in mycolic acid donation to the cell wall core of Mycobacterium tuberculosis', *Antimicrobial agents and chemotherapy*. Am Soc Microbiol, 56(4), pp. 1797–1809.

Takayama, K., Wang, L. and Merkal, R. S. (1973) 'Scanning electron microscopy of the H37Ra strain of Mycobacterium tuberculosis exposed to isoniazid', *Antimicrobial agents and chemotherapy*. American Society for Microbiology (ASM), 4(1), p. 62.

Tameris, M. D. *et al.* (2013) 'Safety and efficacy of MVA85A, a new tuberculosis vaccine, in infants previously vaccinated with BCG: a randomised, placebo-controlled phase 2b trial', *The Lancet*. Elsevier, 381(9871), pp. 1021–1028.

Tanner, R. *et al.* (2019) 'The humoral immune response to BCG vaccination', *Frontiers in immunology*. Frontiers, 10, p. 1317.

Taylor, S. *et al.* (2008) 'Development of a high-throughput antibody-mediated complement deposition assay for the assessment of meningococcal vaccines', *Molecular Immunology*. Pergamon, 45(16), p. 4168.

Thanky, N. R., Young, D. B. and Robertson, B. D. (2007) 'Unusual features of the cell cycle in mycobacteria: polar-restricted growth and the snapping-model of cell division', *Tuberculosis*. Elsevier, 87(3), pp. 231–236.

Thavarajah, R. *et al.* (2012) 'Chemical and physical basics of routine formaldehyde fixation', *Journal of oral and maxillofacial pathology: JOMFP*. Wolters Kluwer--Medknow Publications, 16(3), p.

400.
Thornton, B. P. *et al.* (1996) 'Analysis of the sugar specificity and molecular location of the beta-glucan-binding lectin site of complement receptor type 3 (CD11b/CD18).', *The Journal of Immunology*. Am Assoc Immnol, 156(3), pp. 1235–1246.
Thorson, L. M. *et al.* (2001) 'Effect of mycobacterial phospholipids on interaction of Mycobacterium tuberculosis with macrophages', *Infection and immunity*. Am Soc Microbiol, 69(4), pp. 2172–2179.
Toba, H., Crawford, J. T. and Ellner, J. J. (1989) 'Pathogenicity of Mycobacterium avium for human monocytes: absence of macrophage-activating factor activity of gamma interferon.', *Infection and immunity*. Am Soc Microbiol, 57(1), pp. 239–244.
Todar, K. (2006) 'Todar's online textbook of bacteriology'. University of Wisconsin-Madison Department of Bacteriology Madison, Wis, USA.
Torrelles, J. B. *et al.* (2002) 'Characterization of virulence, colony morphotype and the glycopeptidolipid of Mycobacterium avium strain 104.', *Tuberculosis (Edinburgh, Scotland)*. Elsevier, 82(6), pp. 293–300. doi: 10.1054/TUBE.2002.0373.
Totani, T. *et al.* (2017) 'Effects of nutritional and ambient oxygen condition on biofilm formation in Mycobacterium avium subsp. hominissuis via altered glycolipid expression.', *Scientific reports*. Nature Publishing Group, 7, p. 41775. doi: 10.1038/srep41775.
Trivedi, A. *et al.* (2016) 'Thiol reductive stress induces cellulose-anchored biofilm formation in Mycobacterium tuberculosis', *Nature communications*. Nature Publishing Group, 7(1), pp. 1–15.
Ulrichs, T. *et al.* (2005) 'Modified immunohistological staining allows detection of Ziehl–Neelsen-negative Mycobacterium tuberculosis organisms and their precise localization in human tissue', *The Journal of Pathology: A Journal of the Pathological Society of Great Britain and Ireland*. Wiley Online Library, 205(5), pp. 633–640.
Urbanowski, M. E. *et al.* (2020) 'Cavitary tuberculosis: the gateway of disease transmission', *The Lancet Infectious Diseases*. Elsevier.
Vega-Dominguez, P. *et al.* (2020) 'Biofilms of the non-tuberculous Mycobacterium chelonae form an extracellular matrix and display distinct expression patterns', *The Cell Surface*. Elsevier, 6, p. 100043.
Venkataswamy, M. M. *et al.* (2012) 'In vitro culture medium influences the vaccine efficacy of Mycobacterium bovis BCG', *Vaccine*. Elsevier, 30(6), pp. 1038–1049.
Vilchèze, C. *et al.* (2000) 'Inactivation of the inhA-encoded fatty acid synthase II (FASII) enoyl-acyl carrier protein reductase induces accumulation of the FASI end products and cell lysis of Mycobacterium smegmatis', *Journal of bacteriology*. Am Soc Microbiol, 182(14), pp. 4059–4067. doi: 10.1128/JB.182.14.4059-4067.2000.
Villeneuve, C. *et al.* (2005) 'Mycobacteria use their surface-exposed glycolipids to infect human macrophages through a receptor-dependent process', *Journal of lipid research*. ASBMB, 46(3), pp. 475–483. doi: 10.1194/jlr.M400308-JLR200.
Vogt, S. *et al.* (2020) 'Local and Systemic Concentrations of Pattern Recognition Receptors of the Lectin Pathway of Complement in a Cohort of Patients With Interstitial Lung Diseases', *Frontiers in immunology*. Frontiers, 11, p. 2412.
Wallace, R. J. *et al.* (2013) 'Absence of Mycobacterium intracellulare and presence of Mycobacterium chimaera in household water and biofilm samples of patients in the United States with Mycobacterium avium complex respiratory disease', *Journal of clinical microbiology*. Am Soc Microbiol, 51(6), pp. 1747–1752.
Warrier, T. *et al.* (2012) 'Antigen 85C inhibition restricts Mycobacterium tuberculosis growth through disruption of cord factor biosynthesis', *Antimicrobial agents and chemotherapy*. Am Soc Microbiol, 56(4), pp. 1735–1743.
Watford, W. T. *et al.* (2000) 'Complement-mediated host defense in the lung', 27710, pp. 790–798.
Welch, N. G. *et al.* (2017) 'Orientation and characterization of immobilized antibodies for improved immunoassays', *Biointerphases*. American Vacuum Society, 12(2), p. 02D301.
Welsh, K. J. *et al.* (2008) 'A role for tumour necrosis factor-α, complement C5 and interleukin-6 in the

initiation and development of the mycobacterial cord factor trehalose 6, 6′-dimycolate induced granulomatous response', *Microbiology (Reading, England)*. NIH Public Access, 154(Pt 6), p. 1813.

Welsh, K. J. *et al.* (2012) 'Complement factor C7 contributes to lung immunopathology caused by Mycobacterium tuberculosis', *Clinical and Developmental Immunology*. Hindawi Publishing Corporation, 2012.

WHO (2017) 'Guidelines for treatment of drug-susceptible tuberculosis and patient care'. World Health Organization.

WHO (2020a) 'Global tuberculosis report 2020'. World Health Organization.

WHO (2020b) 'WHO consolidated guidelines on tuberculosis: module 4: treatment: drug-resistant tuberculosis treatment: online annexes'. World Health Organization.

Wiseman, M. E. and Frank, C. W. (2012) 'Antibody adsorption and orientation on hydrophobic surfaces', *Langmuir*. ACS Publications, 28(3), pp. 1765–1774.

Wolf, Y. I. *et al.* (2001) 'Genome trees constructed using five different approaches suggest new major bacterial clades.', *BMC evolutionary biology*, 1, p. 8. doi: 11734060.

Woodruff, P. J. *et al.* (2004) 'Trehalose is required for growth of Mycobacterium smegmatis', *Journal of Biological Chemistry*. ASBMB, 279(28), pp. 28835–28843.

Xie, L. *et al.* (2015) 'Proteome-wide lysine acetylation profiling of the human pathogen Mycobacterium tuberculosis', *The international journal of biochemistry & cell biology*. Elsevier, 59, pp. 193–202.

Yamazaki, Y. *et al.* (2006) 'The ability to form biofilm influences Mycobacterium avium invasion and translocation of bronchial epithelial cells', *Cellular microbiology*. Wiley Online Library, 8(5), pp. 806–814. doi: 10.1111/j.1462-5822.2005.00667.x.

Yang, Y. *et al.* (2013) 'Exposure to a cutinase-like serine esterase triggers rapid lysis of multiple mycobacterial species', *Journal of Biological Chemistry*. ASBMB, 288(1), pp. 382–392.

Yasuda, K. (1999) 'Complement activation by mycoloyl glycolipids from Mycobacterium tuberculosis and Rhodococcus ruber.', *Osaka city medical journal*, 45(2), pp. 159–174.

Zaffran, Y., Zhang, L. and Ellner, J. J. (1998) 'Role of CR4 in Mycobacterium tuberculosis-human macrophages binding and signal transduction in the absence of serum', *Infection and immunity*. Am Soc Microbiol, 66(9), pp. 4541–4544.

Zhai, W. *et al.* (2019) 'The immune escape mechanisms of Mycobacterium tuberculosis', *International journal of molecular sciences*. Multidisciplinary Digital Publishing Institute, 20(2), p. 340.

Zhang, J.-H., Chung, T. D. Y. and Oldenburg, K. R. (1999) 'A simple statistical parameter for use in evaluation and validation of high throughput screening assays', *Journal of biomolecular screening*. Sage Publications Sage CA: Thousand Oaks, CA, 4(2), pp. 67–73.

Zhang, L. *et al.* (1988) 'Effect of Mycobacterium tuberculosis-derived sulfolipid I on human phagocytic cells.', *Infection and immunity*. American Society for Microbiology (ASM), 56(11), p. 2876.

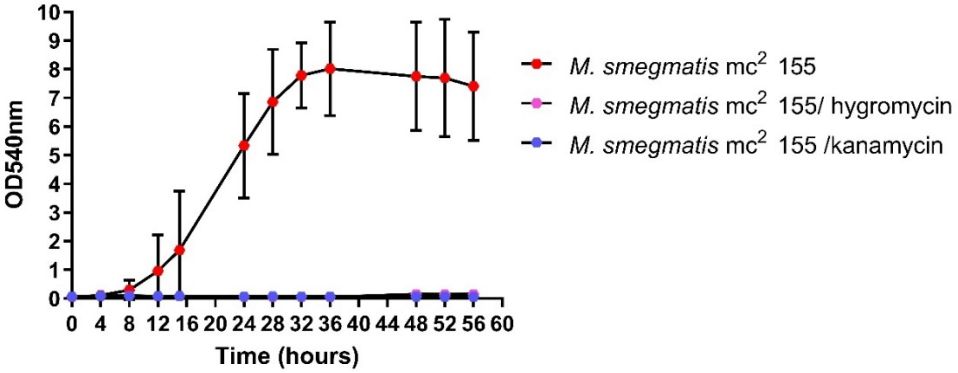
Zhang, Y. *et al.* (2014) 'Mechanisms of pyrazinamide action and resistance', *Molecular Genetics of Mycobacteria*. Wiley Online Library, pp. 479–491.

Zimmerli, S., Edwards, S. and Ernst, J. D. (1996) 'Selective receptor blockade during phagocytosis does not alter the survival and growth of Mycobacterium tuberculosis in human macrophages.', *American journal of respiratory cell and molecular biology*. American Public Health Association, 15(6), pp. 760–770.

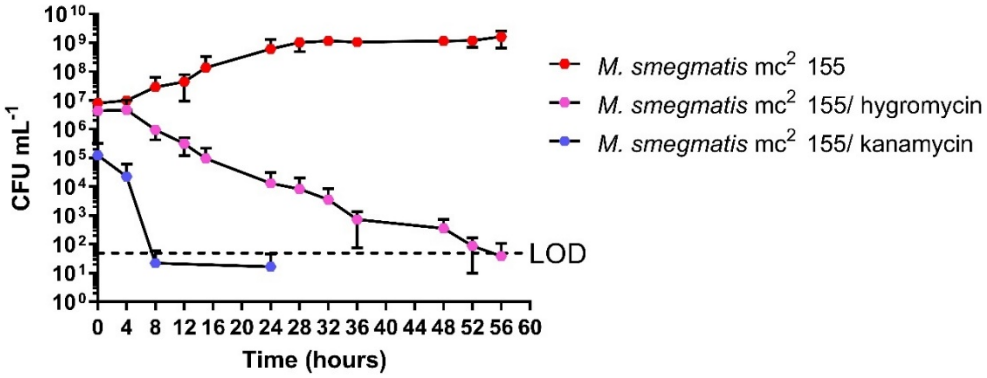
Zwerling, A. and Pai, M. (2011) 'The BCG world atlas: a new, open-access resource for clinicians and researchers', *Expert Review of Anti-infective Therapy*. Taylor & Francis, 9(8), pp. 559–561. doi: 10.1586/eri.11.71.

Appendix 1

A



B



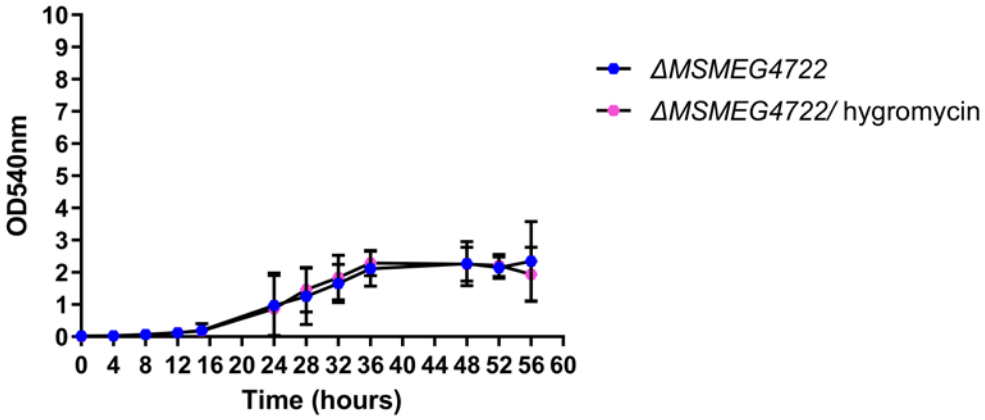
C

Strain	Doubling time based on $OD540_{nm}$	Doubling time based on CFU mL^{-1}
M. smegmatis mc^2 155	4:12 [±1:22]	4:07 [±0:47]

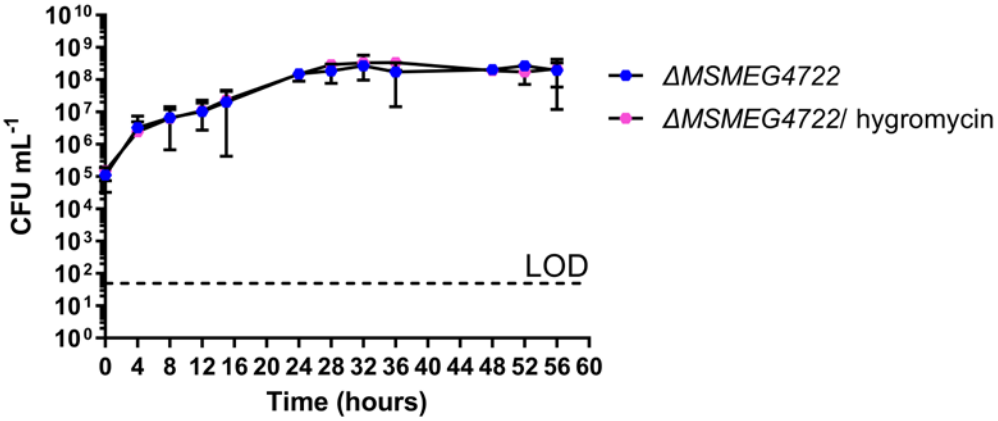
Figure A.1.1: Culture of *M. smegmatis* mc^2 155 with and without selective antibiotics.

$OD540_{nm}$ and CFU mL^{-1} of *M. smegmatis* mc^2 155 cultured in Middlebrook 7H9 supplemented with 10% OADC + 0.05% Tween-80 either with no addition of antibiotics (red), or the addition of either 50µg mL^{-1} hygromycin (pink) or 50µg mL^{-1} kanamycin (lilac) measured over a 56-hour time course. (A) $OD540_{nm}$ over 56-hours at intervals of approximately every 4-hours. (B) CFU mL^{-1} over 56-hours at intervals of approximately every 4-hours. (C) Calculated bacterial doubling time based of $OD540_{nm}$ or CFU mL^{-1}. Three independent biological replicates. Error bars = standard deviation. LOD = limit of detection (50 CFU mL^{-1}).

A



B



C

Strain	Doubling time based on $OD540_{nm}$	Doubling time based on CFU mL^{-1}
ΔMSMEG4722	4:26 [±0:16]	3:23 [±0:58]
ΔMSMEG4722/ hygromycin	4:37 [±0:34]	3:23 [±0:54]

Figure A.1.2: Culture of *ΔMSMEG4722* with and without the addition of hygromycin.

$OD540_{nm}$ and CFU mL^{-1} of *ΔMSMEG4722* cultured in Middlebrook 7H9 supplemented with 10% OADC + 0.05% Tween-80 and; no antibiotics (blue) or 50µg mL^{-1} hygromycin (pink) (A) $OD540_{nm}$ over 56-hours at intervals of approximately every 4-hours (B) CFU mL^{-1} over 56-hours at intervals of approximately every 4-hours. (C) Calculated bacterial doubling time based on $OD540_{nm}$ or CFU mL^{-1}. Three independent biological replicates. Error bars = standard deviation. LOD = limit of detection (50 CFU mL^{-1}). Statistical analysis was performed by matched two-way ANOVA ($OD540_{nm}$) or matched mixed effect analysis (CFU mL^{-1}) using the Geisser-Greenhouse correction.

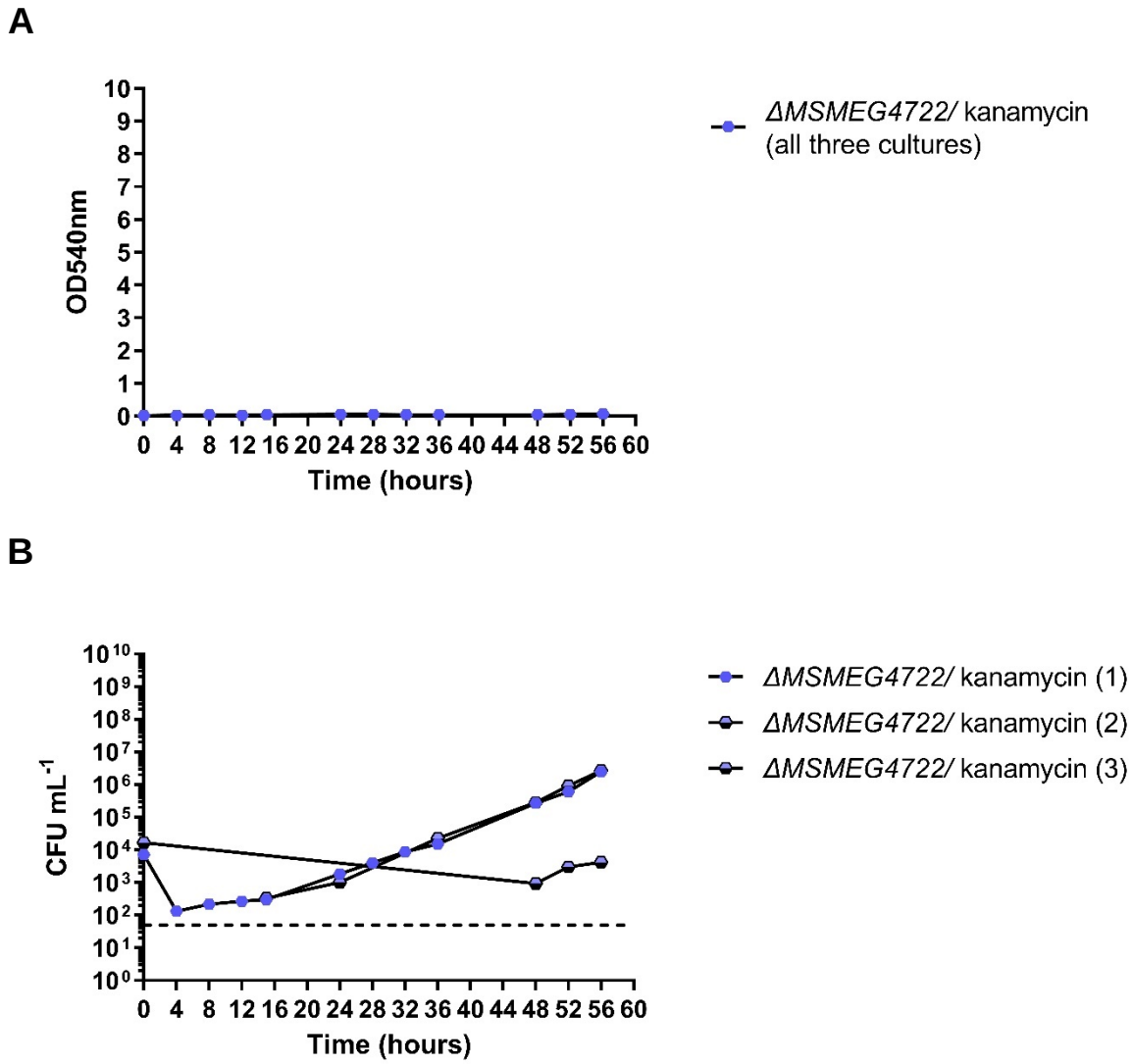
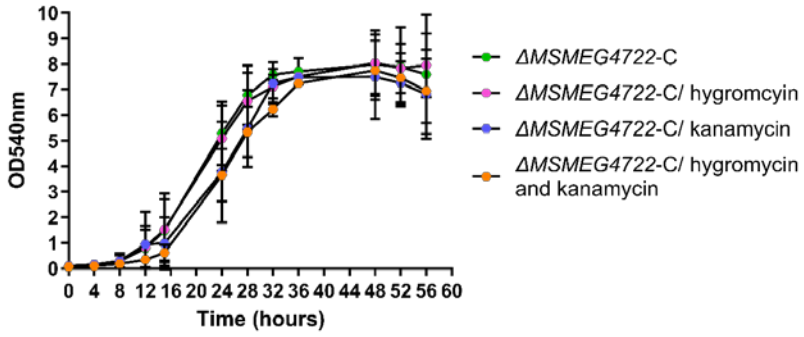


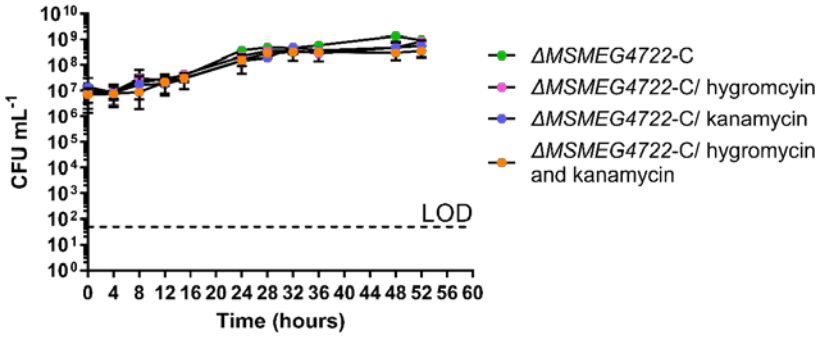
Figure A.1.3: Culture of *ΔMSMEG4722* with the addition of kanamycin.

$OD540_{nm}$ and CFU mL^{-1} of *ΔMSMEG4722* cultured Middlebrook 7H9 + 10% OADC + 0.05% Tween-80 and 50µg mL^{-1} kanamycin. (A) $OD540_{nm}$ over 56-hours at intervals of approximately every 4-hours for all three biological replicates. (B) CFU mL^{-1} over 56-hours at intervals of approximately every 4-hours for culture one (lilac) culture two (upper half lilac) and culture three (lower half lilac). LOD = limit of detection (50 CFU mL^{-1}).

A



B



C

Strain	Doubling time based on $OD540_{nm}$	Doubling time based on CFU mL^{-1}
ΔMSMEG4722-C	4:14 [±1:00]	3:45 [±0:43]
ΔMSMEG4722-C/ hygromycin	4:22 [±1:14]	4:46 [±1:34]
ΔMSMEG4722-C/ kanamycin	4:34 [±1:10]	4:49 [±0:49]
ΔMSMEG4722-C/ hygromycin and kanamycin	4:52 [±1:12]	4:04 [±0:17]

Figure A.1.4: Culture of *ΔMSMEG4722*-C with and without selective antibiotics.

$OD540_{nm}$ and CFU mL^{-1} of *ΔMSMEG4722*-C cultured in Middlebrook 7H9 supplemented with 10% OADC + 0.05% Tween-80; no antibiotic (green), 50µg mL^{-1} hygromycin (pink), 50µg mL^{-1} kanamycin (lilac) or 50µg mL^{-1} hygromycin and kanamycin (orange). (A) $OD540_{nm}$ over 56-hours at intervals of approximately every 4-hours (B) CFU mL^{-1} measurements over 56-hours at intervals of approximately every 4-hours. (C) Calculated doubling time based on $OD540_{nm}$ or CFU mL^{-1}. Three independent biological replicates. Error bars = standard deviation. LOD = limit of detection (50 CFU mL^{-1}). Statistical analysis by a matched two-way ANOVA ($OD540_{nm}$) or matched mixed effect analysis (CFU mL^{-1}) using the Geisser-Greenhouse correction.

Appendix 2

Outer apolar lipids

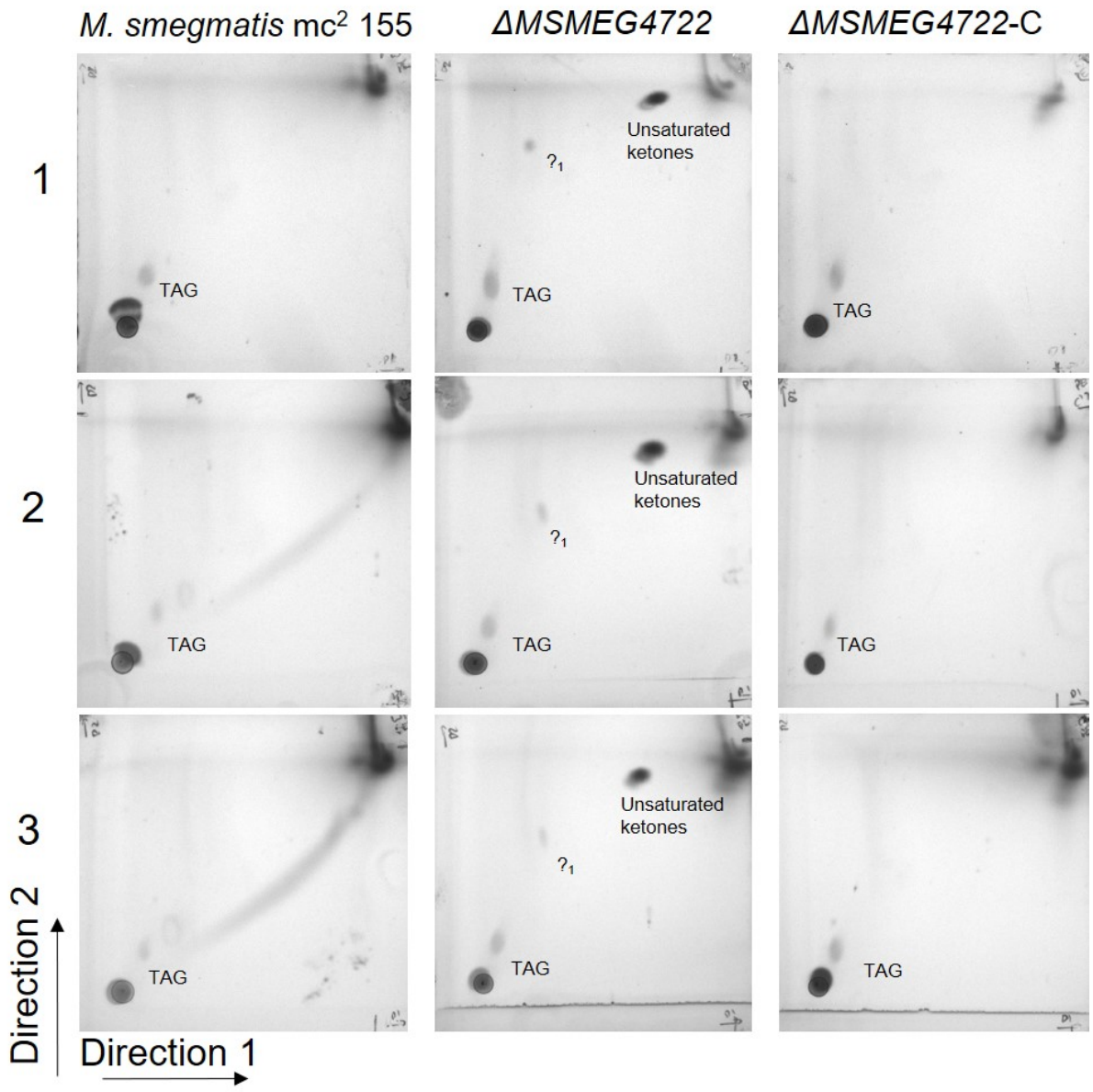


Figure A.2.1: Outer apolar lipid analysis of *M. smegmatis* mc^2 155, *ΔMSMEG4722* and *ΔMSMEG4722*-C (solvent system A).

2D-TLC plates of outer apolar lipid fractions. Three independent biological replicates. Developed in petroleum ether 60-80^{o}C: ethyl acetate (98:2 v/v) x3 and petroleum ether 60-80^{o}C: acetone (98:2 v/v) x1 and stained with MPA. Triacylglycerol (TAG), unsaturated ketones, unidentified lipid 1 (?$_1$).

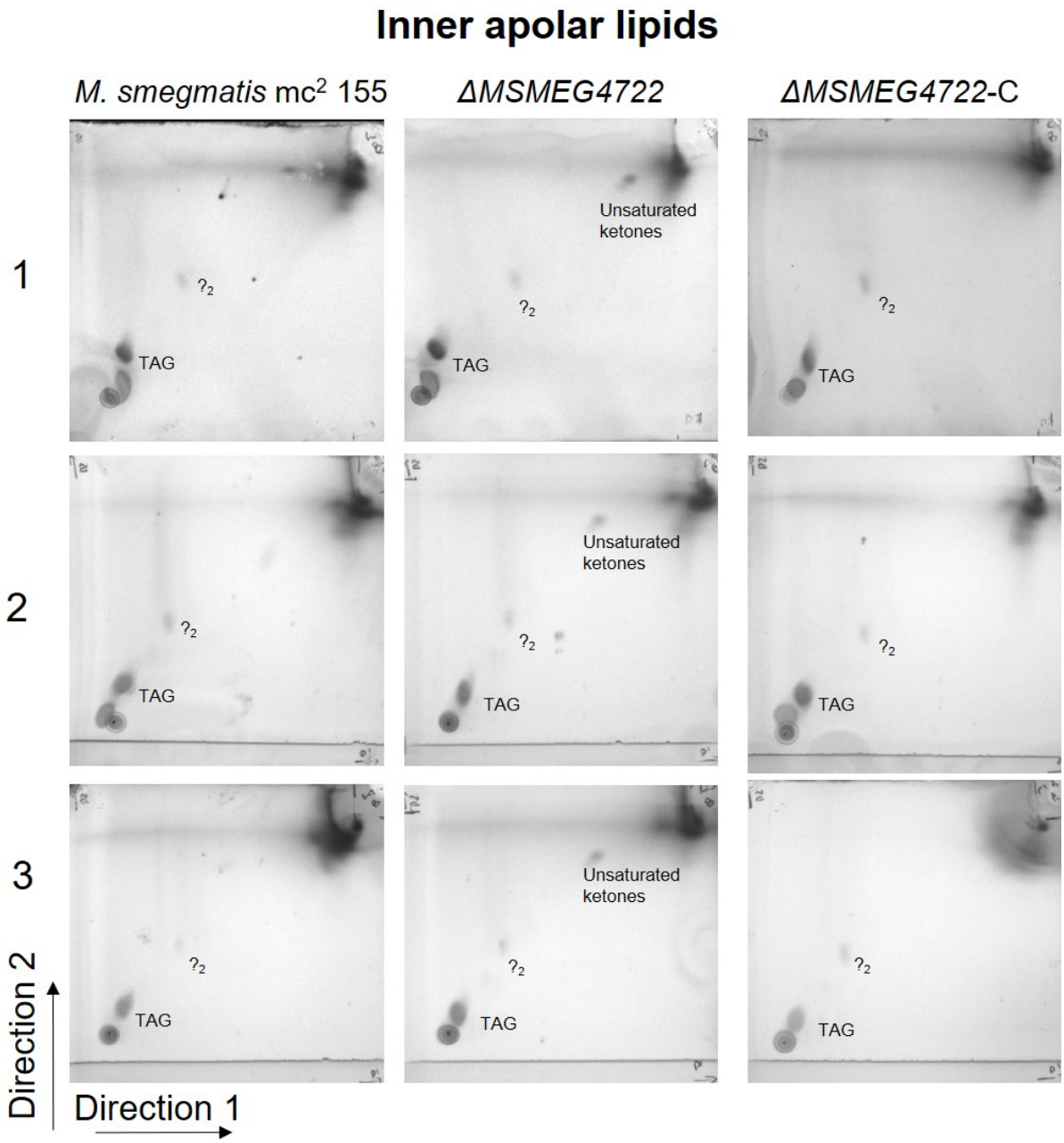


Figure A.2.2: Inner apolar lipid analysis of *M. smegmatis* mc² 155, *ΔMSMEG4722* and *ΔMSMEG4722*-C (solvent system A).

2D-TLC plates of inner apolar lipid fractions. Three independent biological replicates. Developed in petroleum ether 60-80ºC: ethyl acetate (98:2 v/v) x3 and petroleum ether 60-80ºC: acetone (98:2 v/v) x1 and stained with MPA. Triacylglycerol (TAG), unsaturated ketones, unidentified lipid 2 (?2).

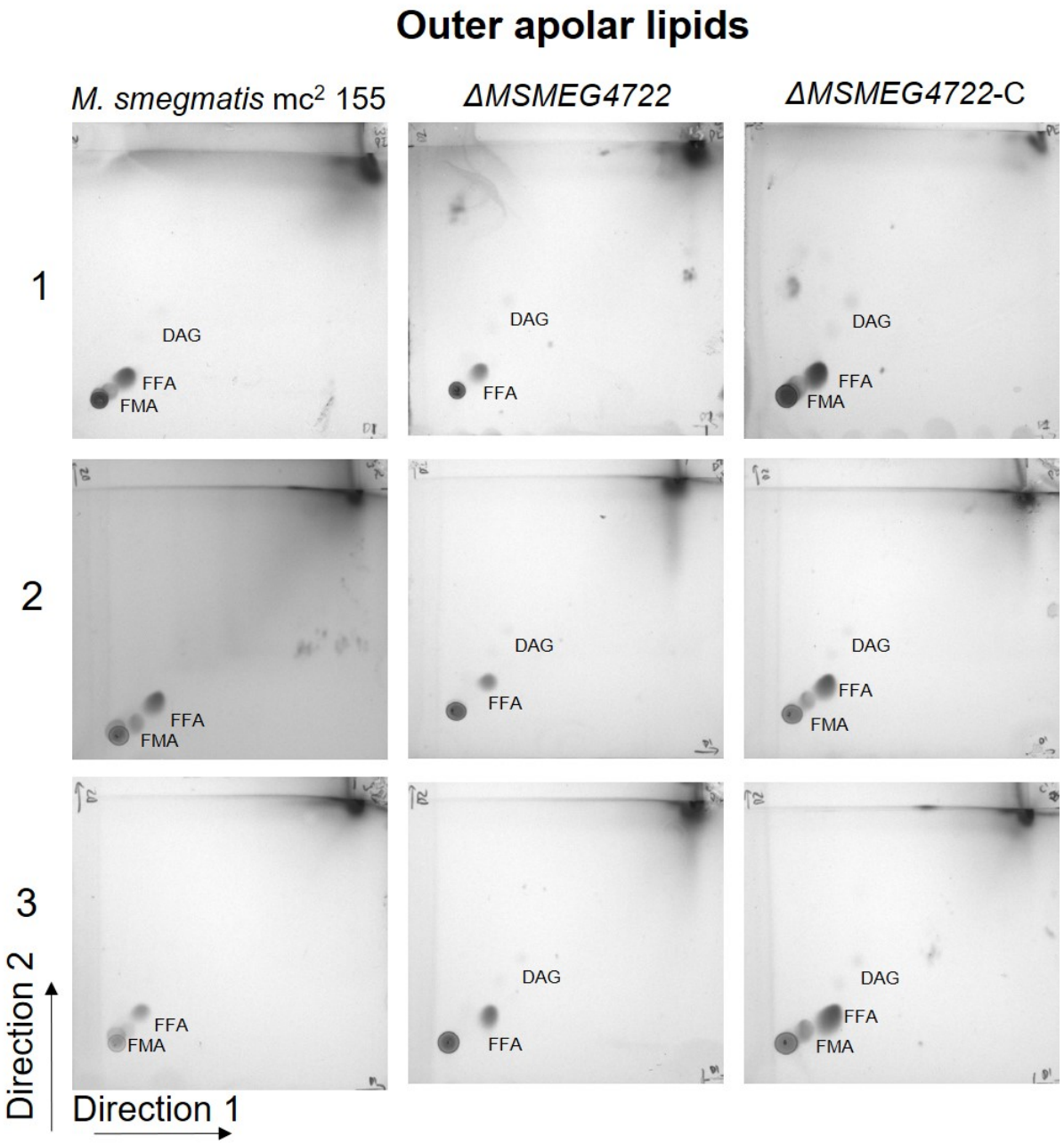


Figure A.2.3: Outer apolar lipid analysis of *M. smegmatis* mc² 155, *ΔMSMEG4722* and *ΔMSMEG4722*-C (solvent system B).

2D-TLC plates of outer apolar lipid fractions. Three independent biological replicates. Developed in petroleum ether 60-80ºC: acetone (92:8 v/v) x3 and toluene: acetone (95:5 v/v) x1 and stained with MPA. Free fatty acid (FFA), free mycolic acid (FMA), diglyceride (DAG).

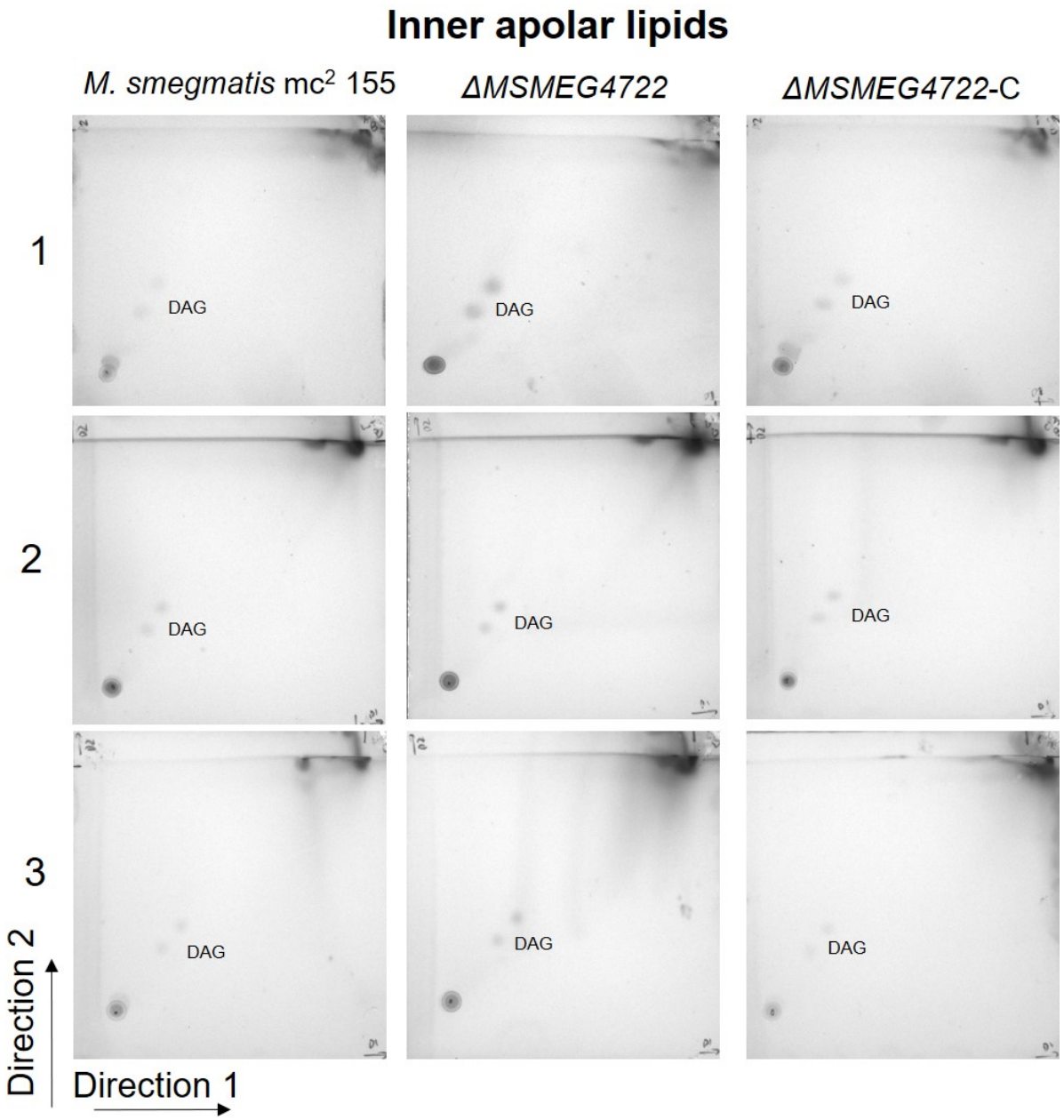


Figure A.2.4: Inner apolar lipid analysis of *M. smegmatis* mc² 155, *ΔMSMEG4722* and *ΔMSMEG4722*-C (solvent system B).

2D-TLC plates of inner apolar lipid fractions. Three independent biological replicates. Developed in petroleum ether 60-80ºC: acetone (92:8 v/v) x3 and toluene: acetone (95:5 v/v) x1 and stained with MPA. Diglyceride (DAG).

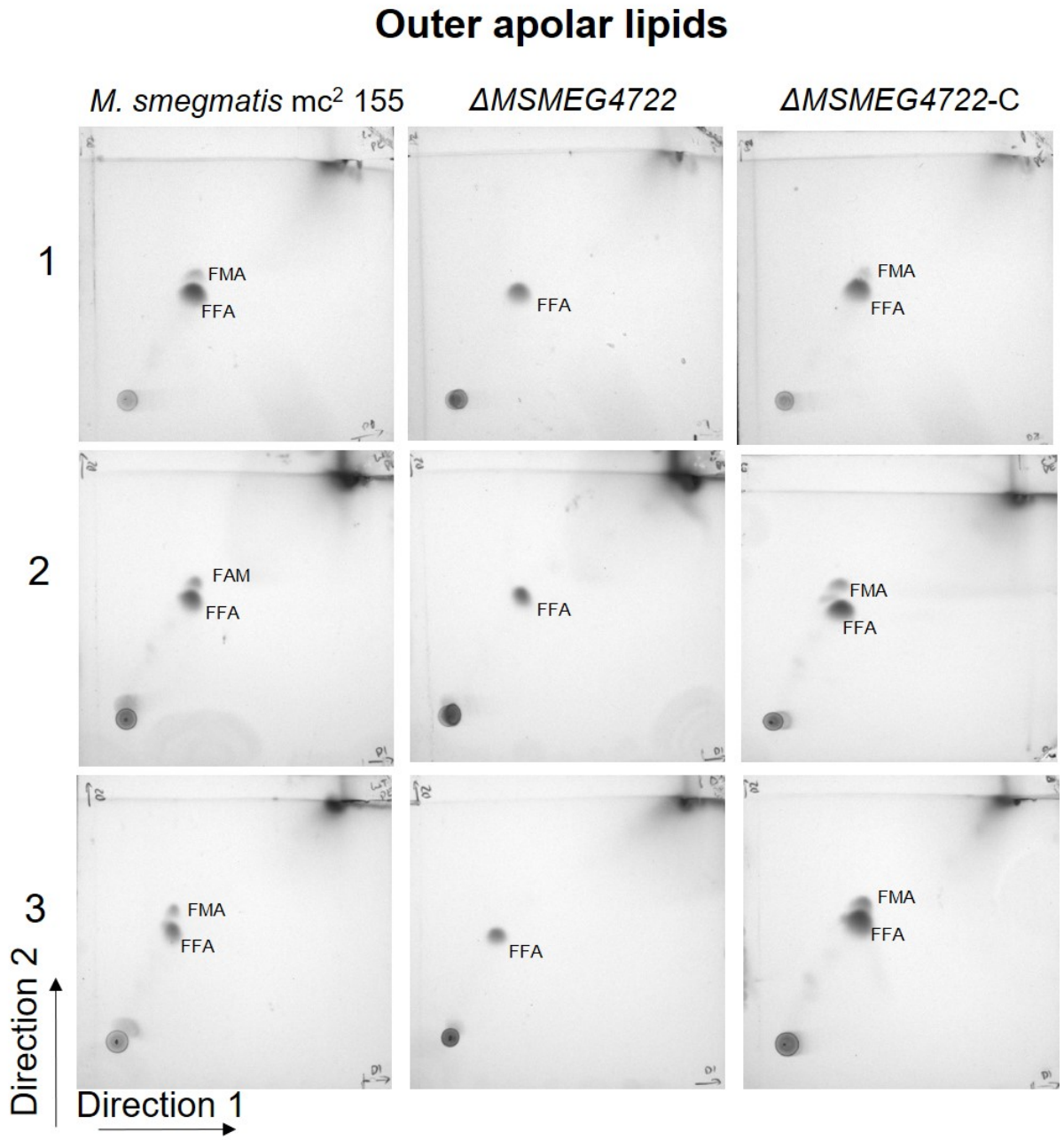


Figure A.2.5: Outer apolar lipid analysis of *M. smegmatis* mc² 155, *ΔMSMEG4722* and *ΔMSMEG4722*-C (solvent system C).

2D-TLC plates of outer apolar lipid fractions. Developed in chloroform: methanol (96:4 v/v) x1 and toluene: acetone (80:20 v/v) x1 and stained with MPA. Free mycolic acids (FMA), free fatty acids (FFA).

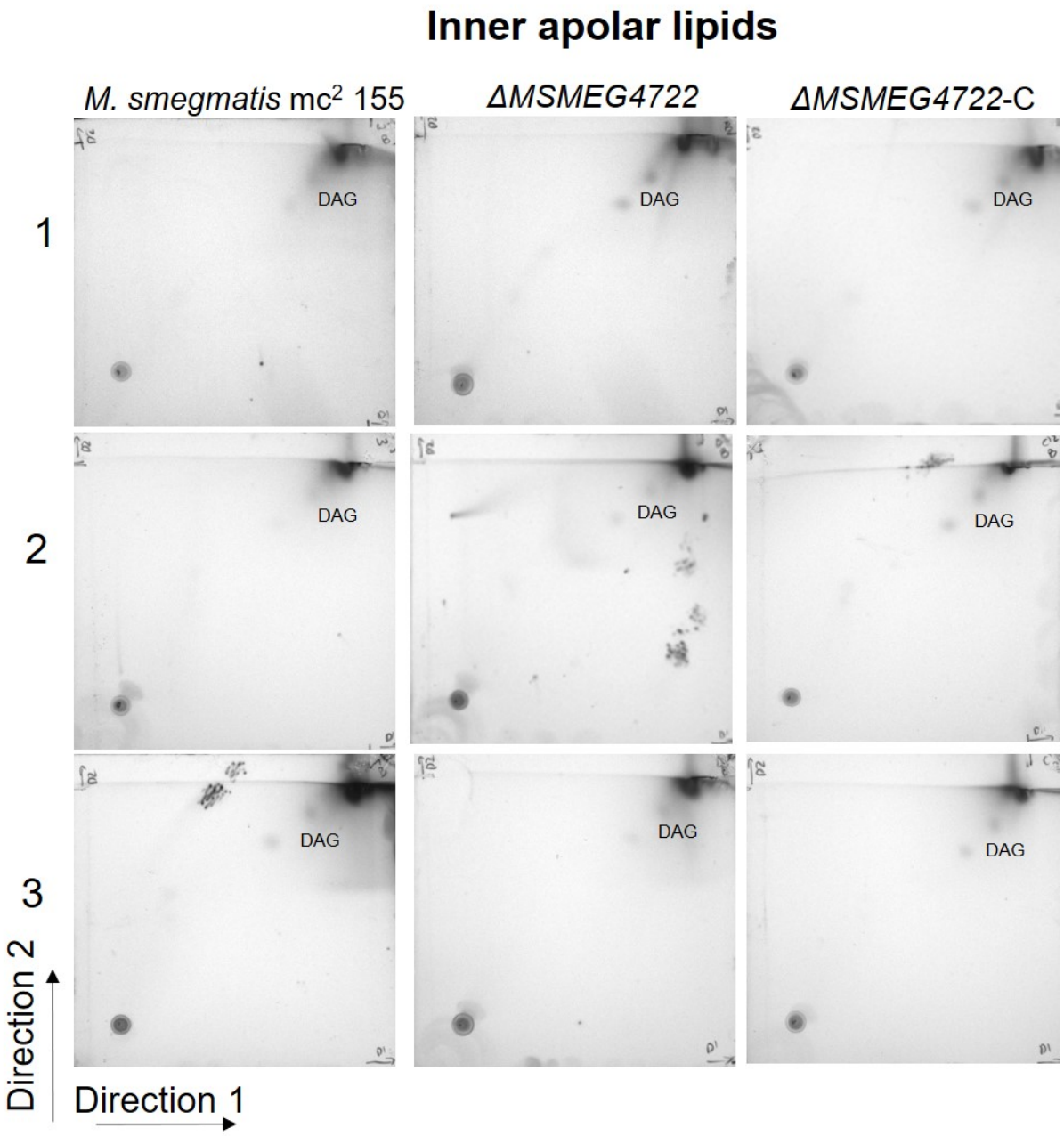


Figure A.2.6: Inner apolar lipid analysis of *M. smegmatis* mc^2 155, *ΔMSMEG4722* and *ΔMSMEG4722*-C (solvent system C).

2D-TLC plates of outer apolar lipid fractions. Developed in chloroform: methanol (96:4 v/v) x1 and toluene: acetone (80:20 v/v) x1 and stained with MPA. Diglyceride (DAG).

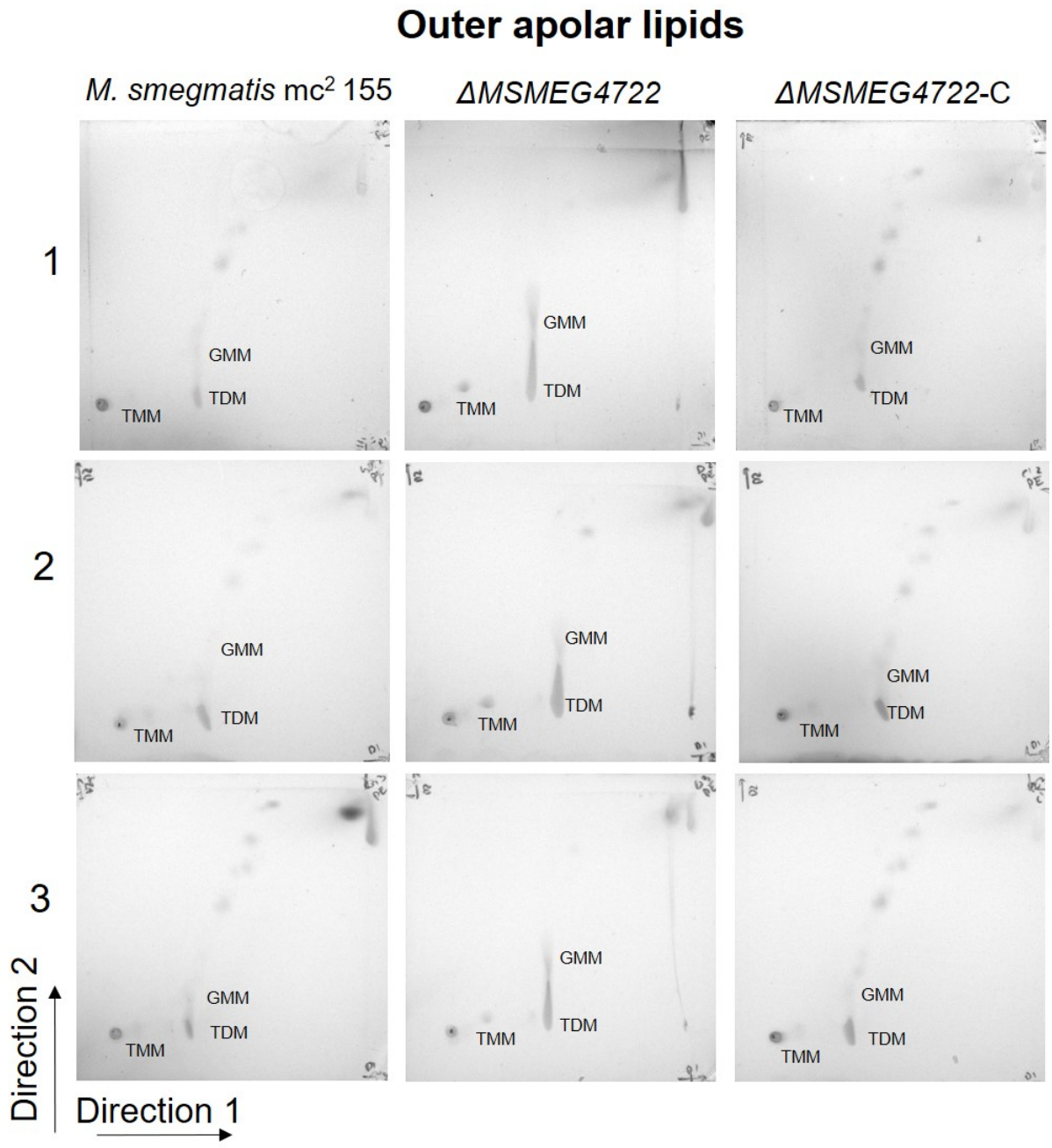


Figure A.2.7: Outer apolar lipid fraction analysis of *M. smegmatis* mc^2 155, *ΔMSMEG4722* and *ΔMSMEG4722*-C (solvent system D).

2D-TLC plates of the outer apolar lipid fractions. Developed in chloroform: methanol: deionised water (100:14:0.8 v/v/v) x1 and chloroform: acetone: methanol: deionized water (50:60:2.5:3 v/v/v/v) x1 and stained with α-naphthol. Trehalose monomycolate (TMM), trehalose dimycolate (TDM), glucose monomycolate (GMM).

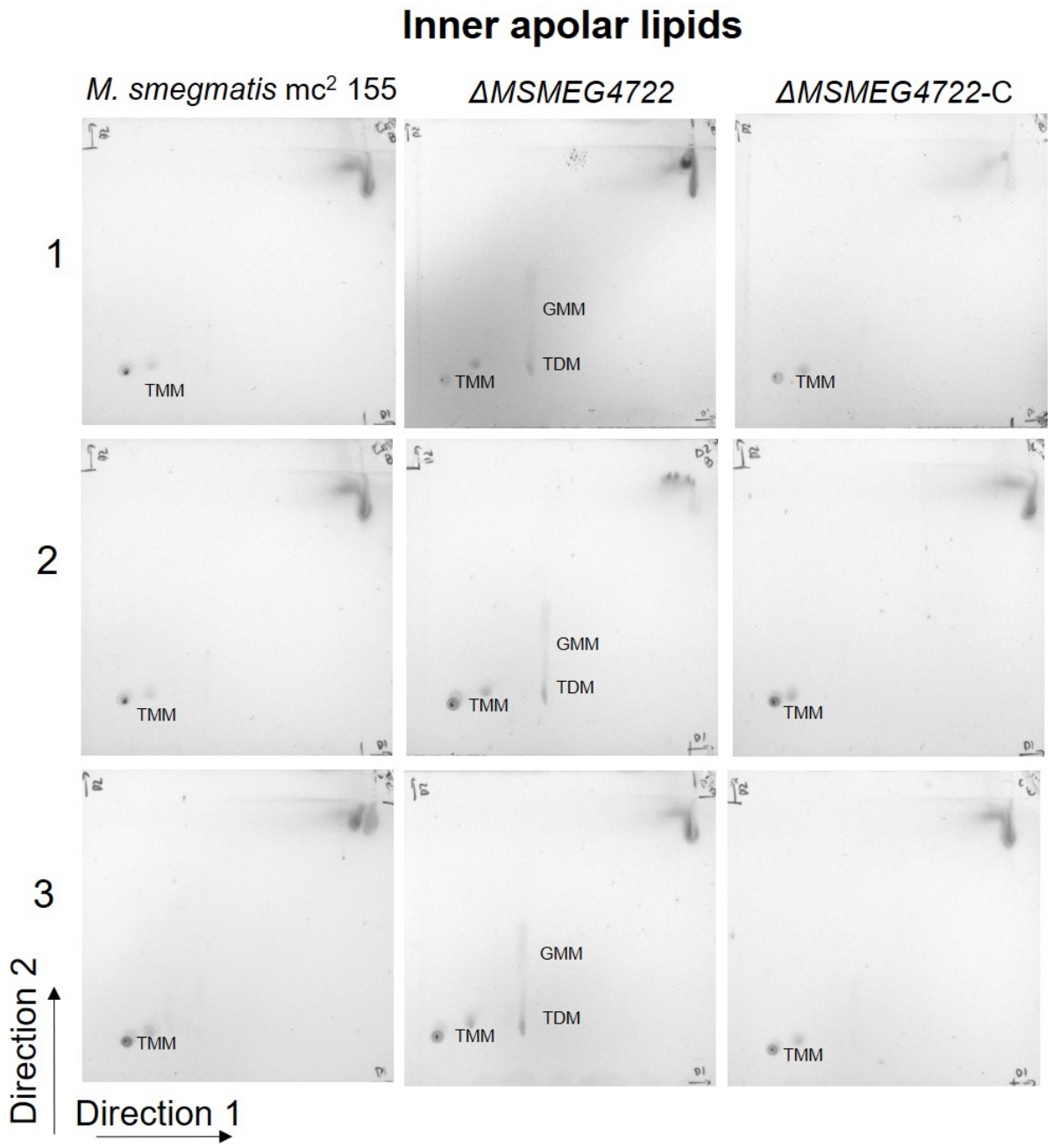


Figure A.2.8: Inner apolar lipid fraction analysis of *M. smegmatis* mc² 155, *ΔMSMEG4722* and *ΔMSMEG4722*-C (solvent system D).

2D-TLC plates of the inner apolar lipid fractions. Developed in chloroform: methanol: deionised water (100:14:0.8 v/v/v) x1 and chloroform: acetone: methanol: deionized water (50:60:2.5:3 v/v/v/v) x1 and stained with α-naphthol. Trehalose monomycolate (TMM), trehalose dimycolate (TDM), glucose monomycolate (GMM).

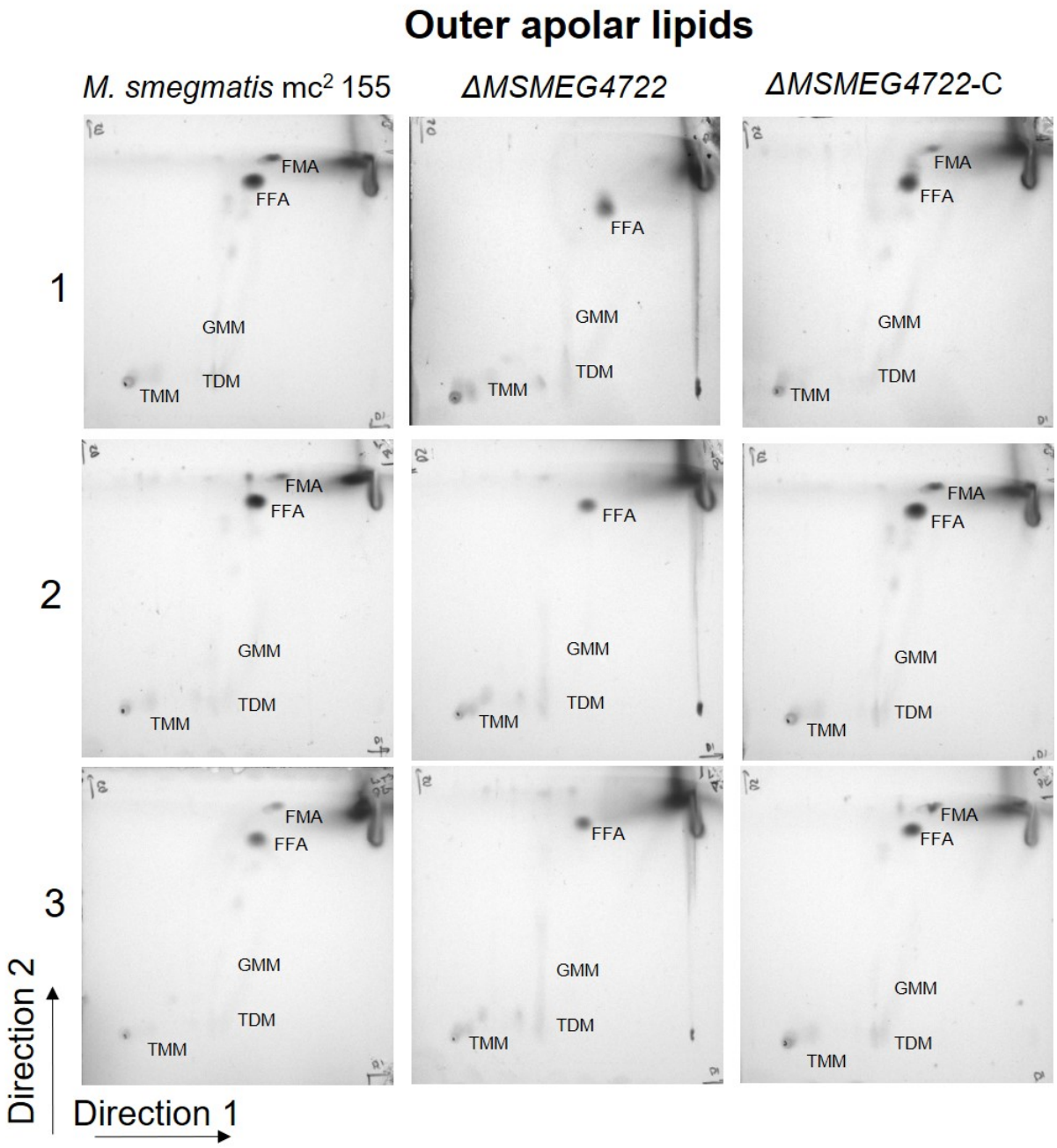


Figure A.2.9: Outer apolar lipid fraction analysis of *M. smegmatis* mc^2 155, *ΔMSMEG4722* and *ΔMSMEG4722*-C (solvent system D).

2D-TLC plates of the outer apolar lipid fractions. Developed in chloroform: methanol: deionised water (100:14:0.8 v/v/v) x1 and chloroform: acetone: methanol: deionized water (50:60:2.5:3 v/v/v/v) x1 and stained with MPA. Trehalose monomycolate (TMM), trehalose dimycolate (TDM), glucose monomycolate (GMM), free mycolic acid (FMA), free fatty acid (FFA).

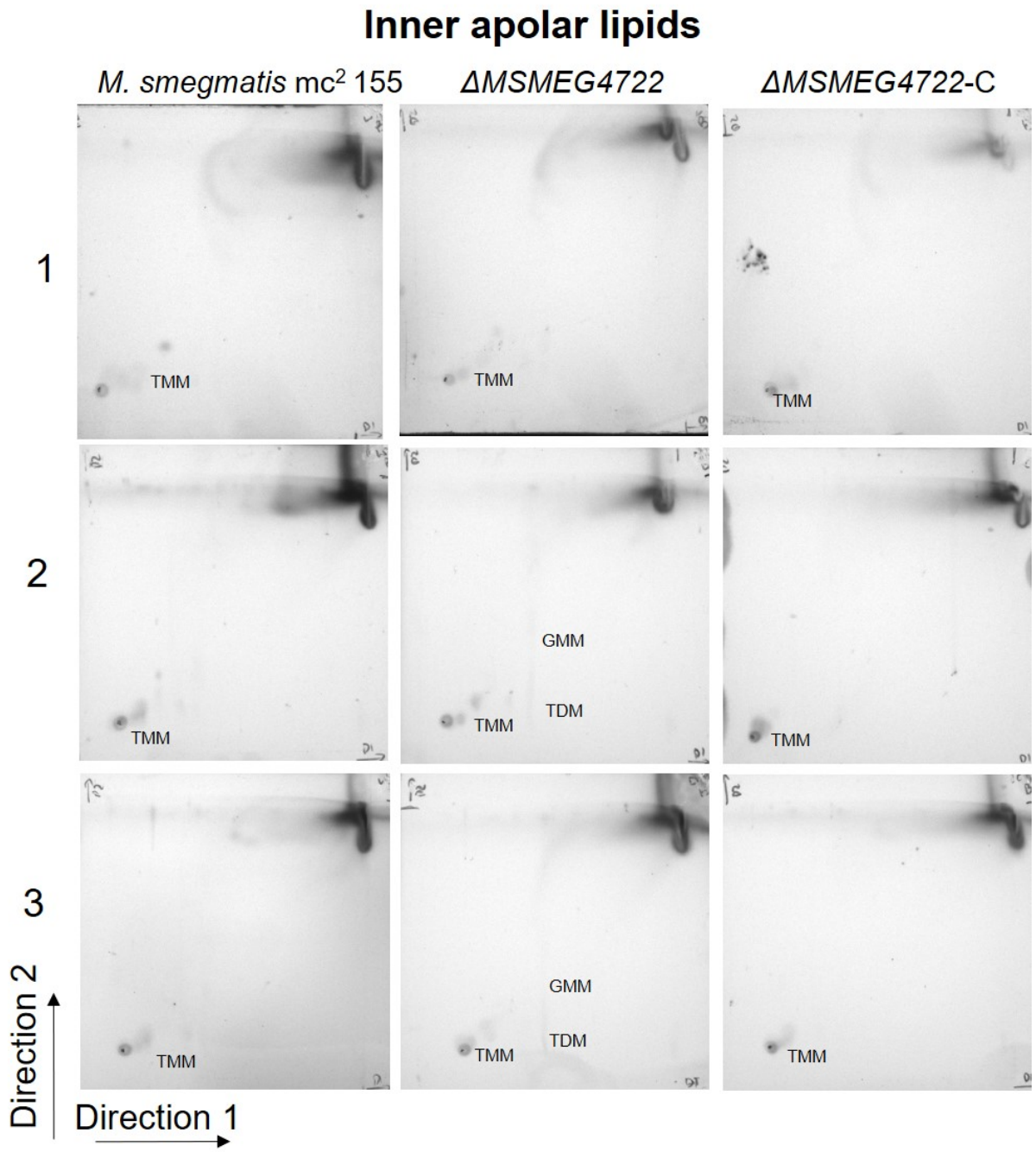


Figure A.2.10: Inner apolar lipid fraction analysis of *M. smegmatis* mc² 155, *ΔMSMEG4722* and *ΔMSMEG4722*-C (solvent system D).

2D-TLC plates of the inner apolar lipid fractions. Developed in chloroform: methanol: deionised water (100:14:0.8 v/v/v) x1 and chloroform: acetone: methanol: deionized water (50:60:2.5:3 v/v/v/v) x1 and stained with MPA. Trehalose monomycolate (TMM), trehalose dimycolate (TDM), glucose monomycolate (GMM).

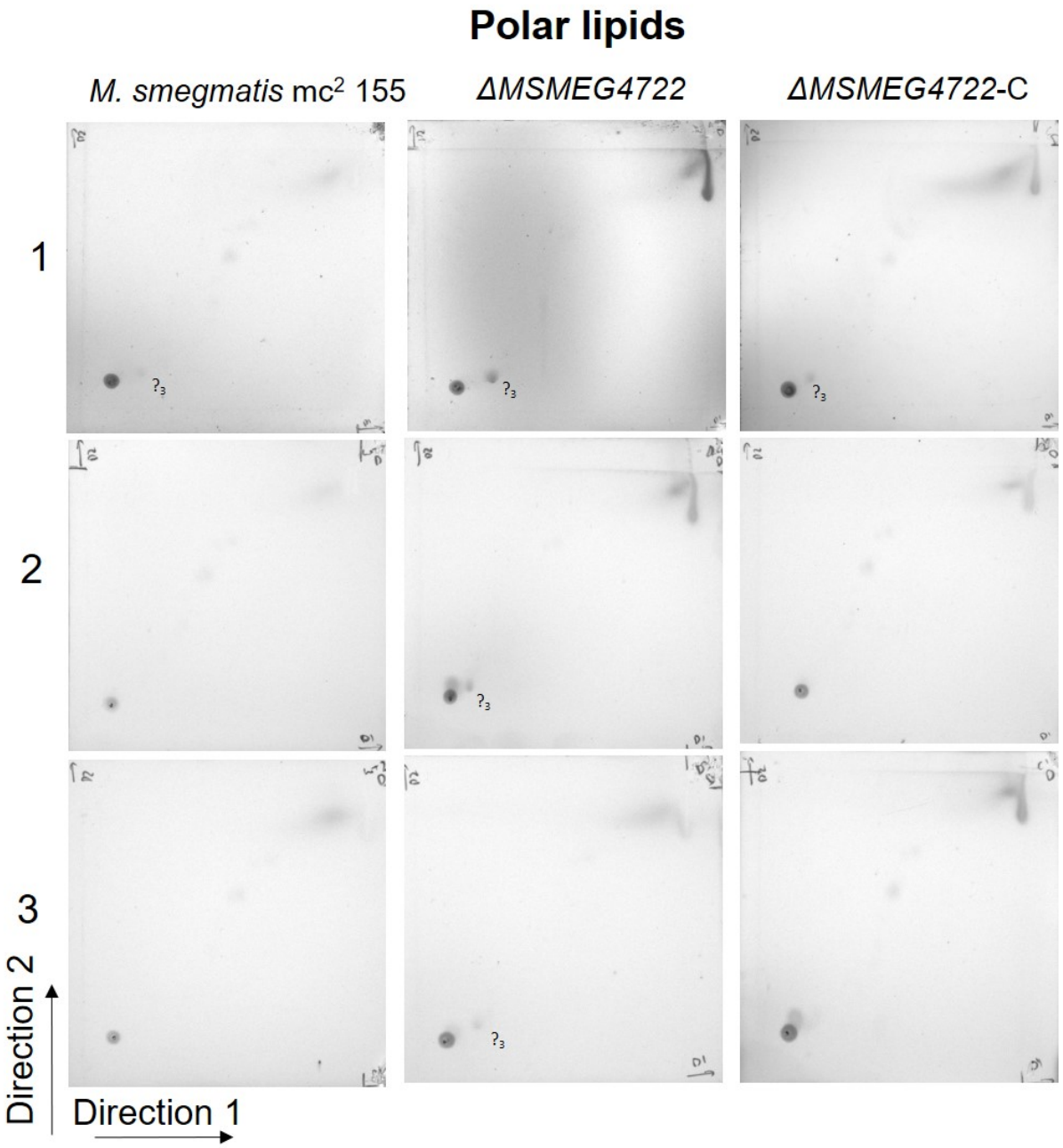


Figure A.2.11: Polar lipid analysis of *M. smegmatis* mc^2 155, *ΔMSMEG4722* and *ΔMSMEG4722*-C (solvent system D).

Representative 2D-TLC plates of polar lipid fractions. Developed in chloroform: methanol: deionized water (100:14:0.8 v/v/v) x1 and chloroform: acetone: methanol: deionised water (50:60:2.5:3 v/v/v/v) x1 stained with α-naphthol. Unidentified lipid 3 ($?_3$).

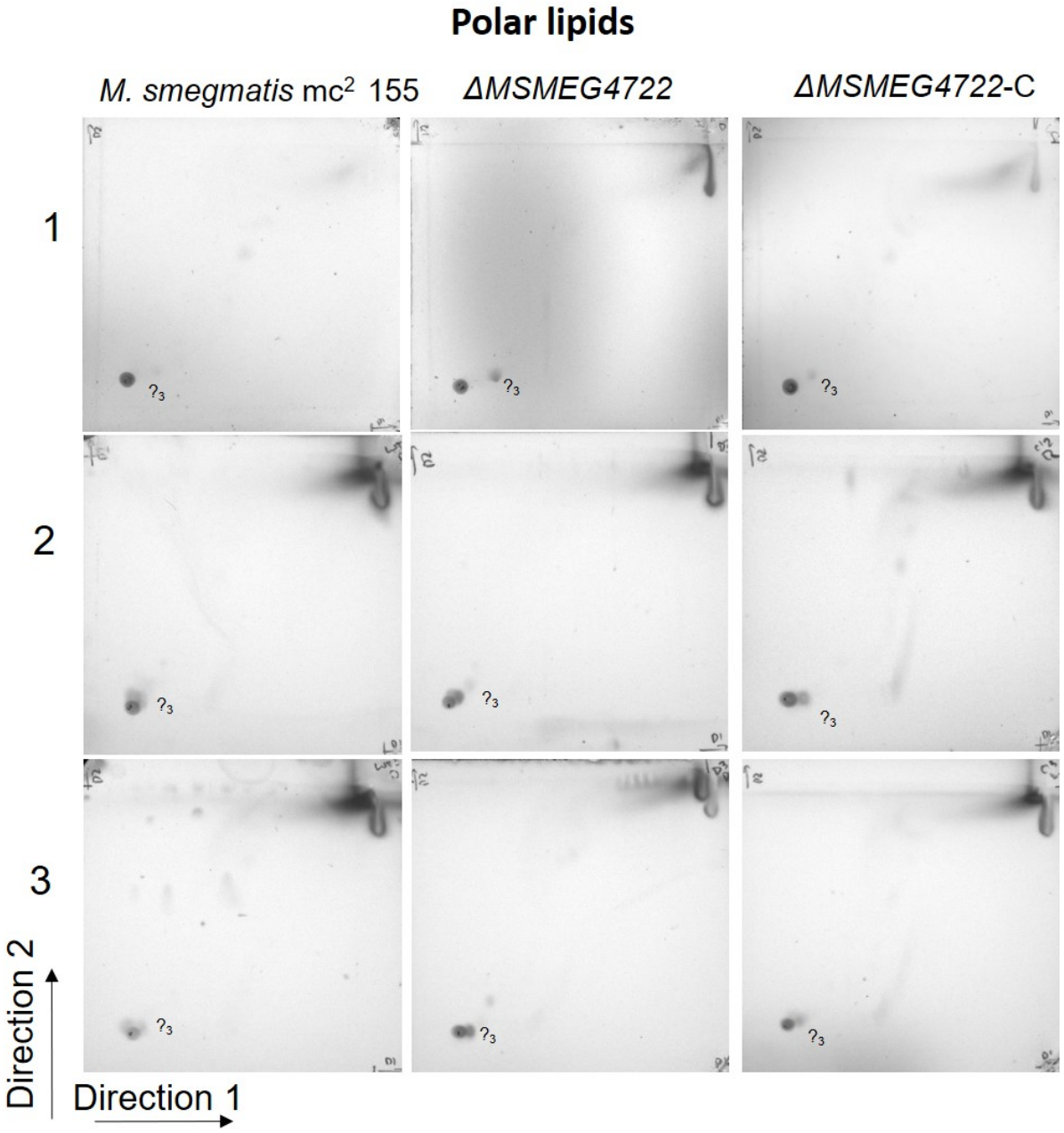


Figure A.2.12: Polar lipid analysis of *M. smegmatis* mc^2 155, *ΔMSMEG4722* and *ΔMSMEG4722*-C (solvent system D).

Representative 2D-TLC plates of polar lipid fractions. Developed in chloroform: methanol: deionized water (100:14:0.8 v/v/v) x1 and chloroform: acetone: methanol: deionised water (50:60:2.5:3 v/v/v/v) x1 stained with MPA. Unidentified lipid 3 (?$_3$).

Appendix 2

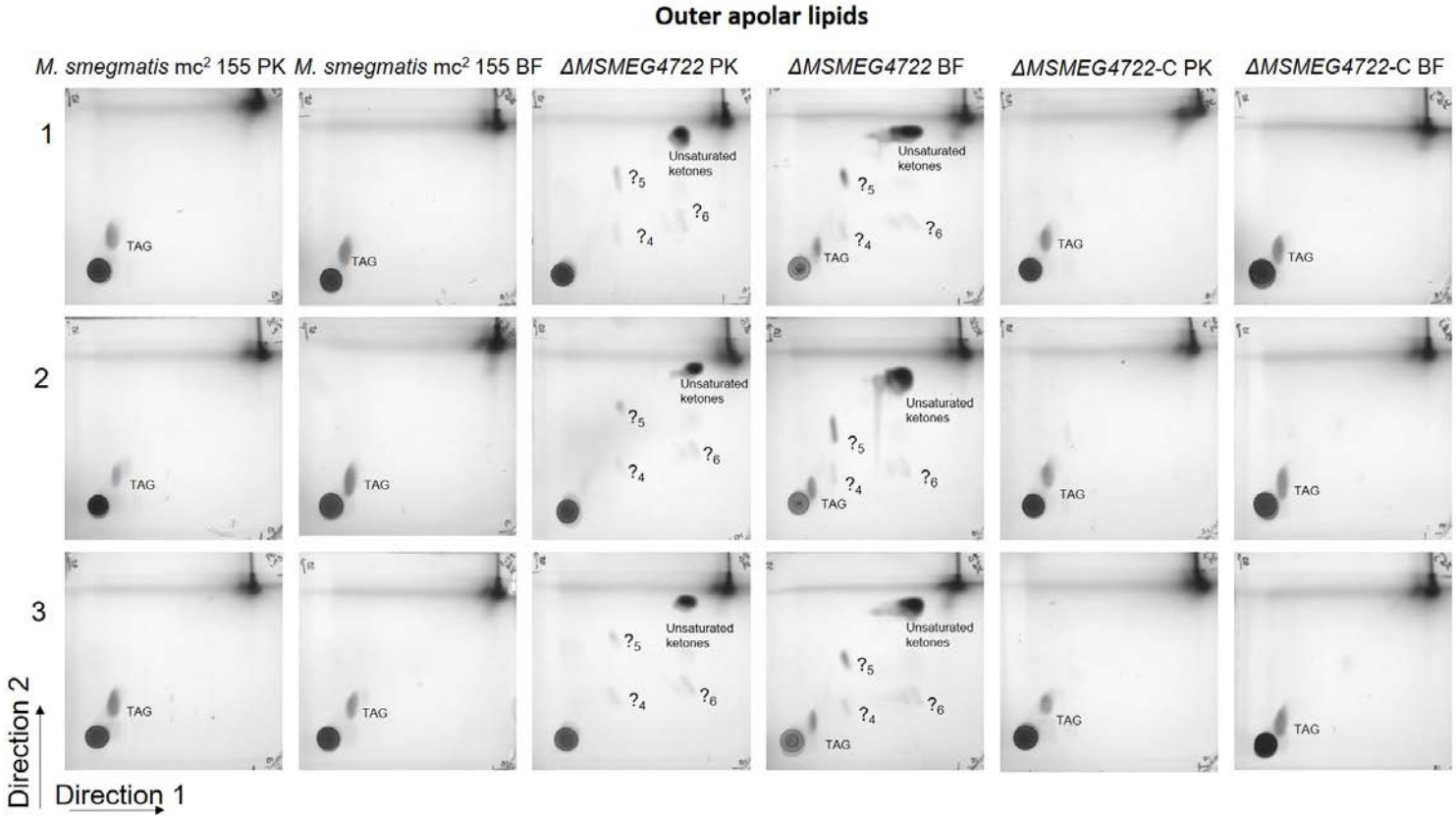


Figure A.2.13: Outer apolar lipid analysis of planktonic and biofilm *M. smegmatis* mc² 155, *ΔMSMEG4722* and *ΔMSMEG4722*-C (solvent system A).

2D-TLC plates of all three strains cultured either as planktonic or pellicle biofilms. Developed in petroleum ether 60-80ºC: ethyl acetate (98:2 v/v) x3 and petroleum ether 60-80ºC: acetone (98:2 v/v) x1 and stained with MPA. Triacylglycerol (TAG), unsaturated ketones, unidentified lipid 4 (?$_4$), unidentified lipid 5 (?$_5$), unidentified lipid 6 (?$_6$).

Appendix 2

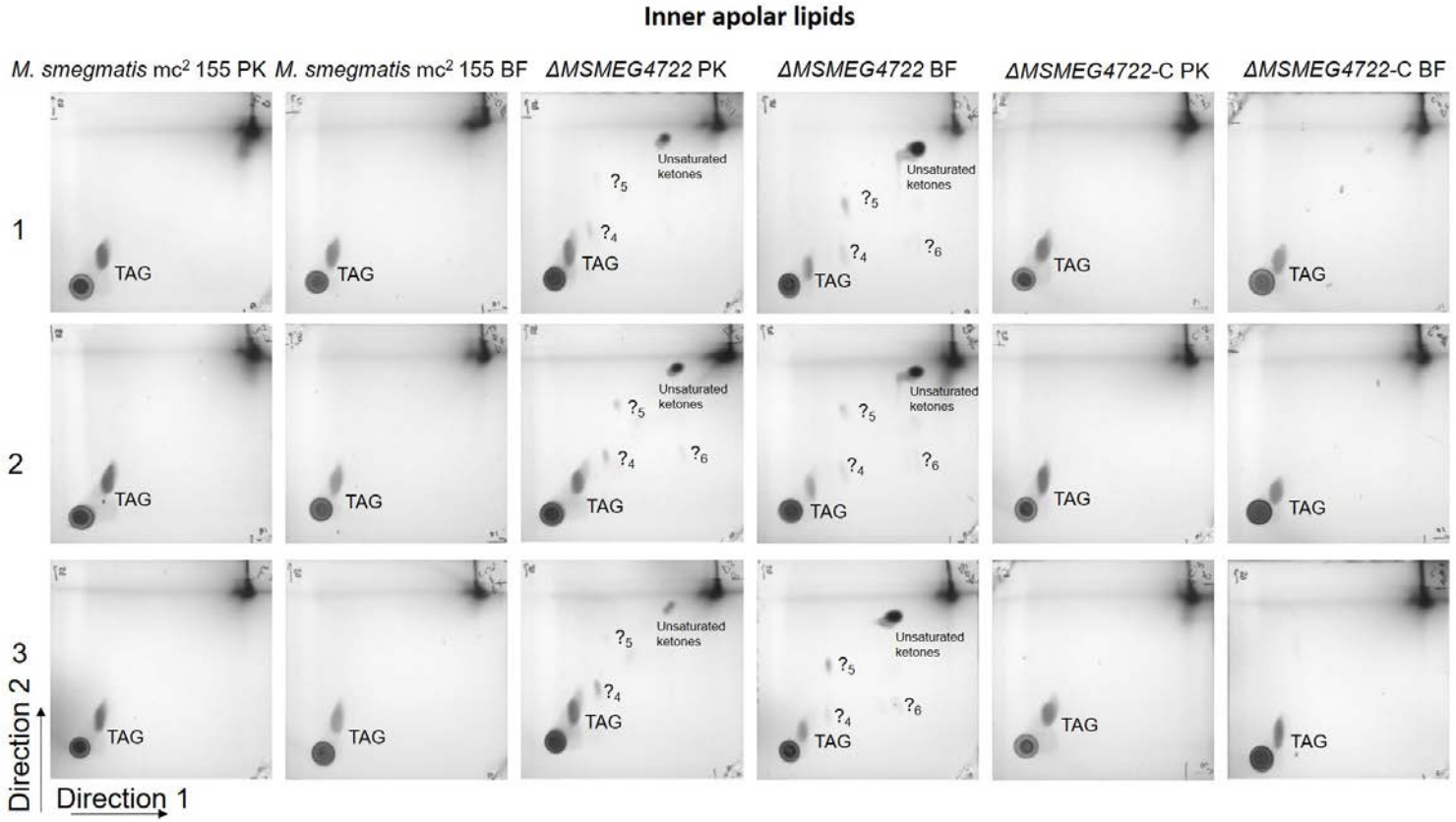


Figure A.2.14: Inner apolar lipid analysis of planktonic and biofilm *M. smegmatis* mc² 155, *ΔMSMEG4722* and *ΔMSMEG4722*-C (solvent system A).

2D-TLC plates of all three strains cultured either as planktonic or pellicle biofilms. Developed in petroleum ether 60-80ºC: ethyl acetate (98:2 v/v) x3 and petroleum ether 60-80ºC: acetone (98:2 v/v) x1 and stained with MPA. Triacylglycerol (TAG), unsaturated ketones, unidentified lipid 4 (?$_4$), unidentified lipid 5 (?$_5$), unidentified lipid 6 (?$_6$).

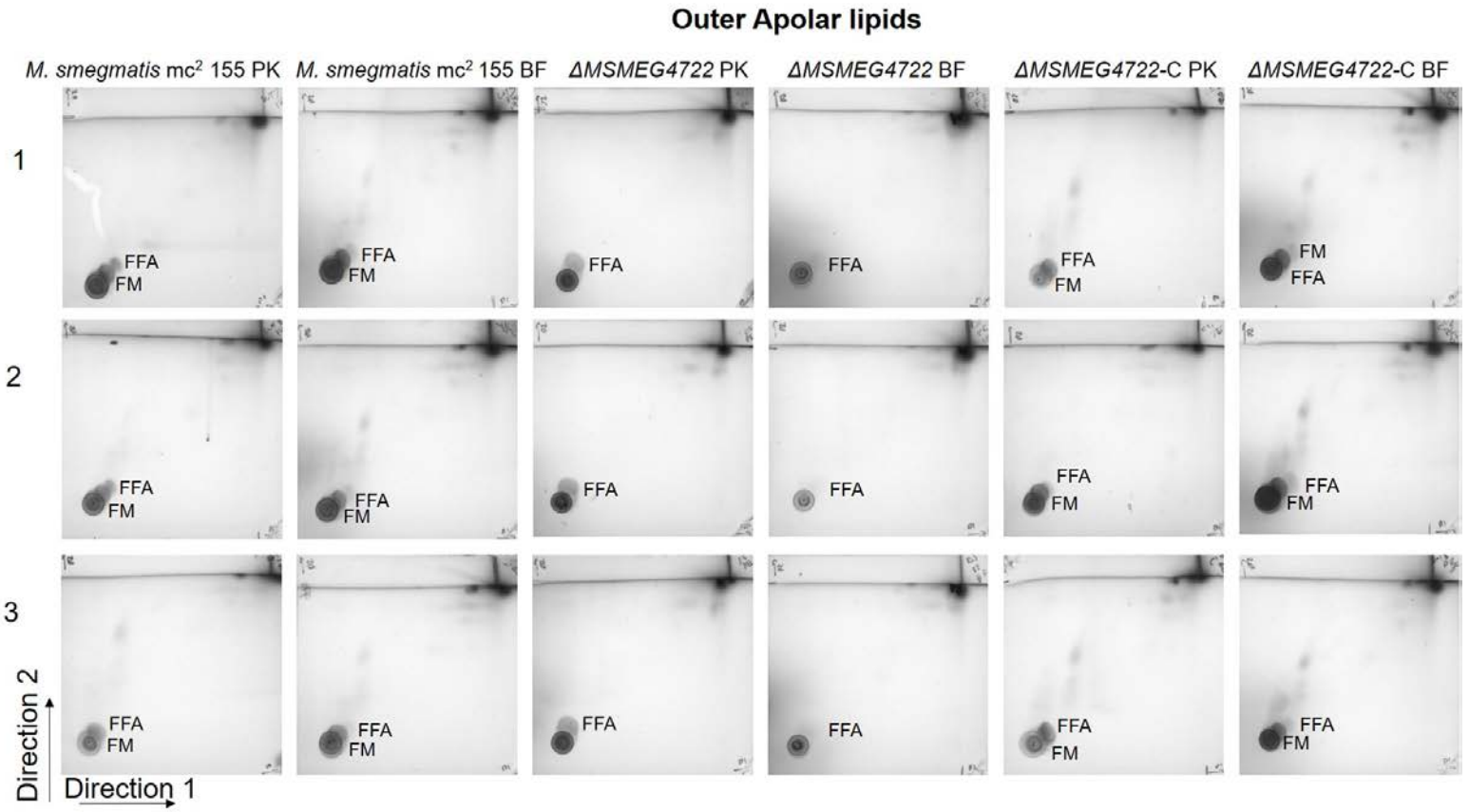


Figure A.2.15: Outer apolar lipid analysis of planktonic and biofilm *M. smegmatis* mc² 155, *ΔMSMEG4722* and *ΔMSMEG4722*-C (solvent system B).

2D-TLC plates of all three strains cultured either as planktonic or pellicle biofilms. Three independent biological replicates. Developed in petroleum ether 60-80ºC: acetone (92:8 v/v) x3 and toluene: acetone (95:5 v/v) x1 and stained with MPA. Free fatty acid (FFA).

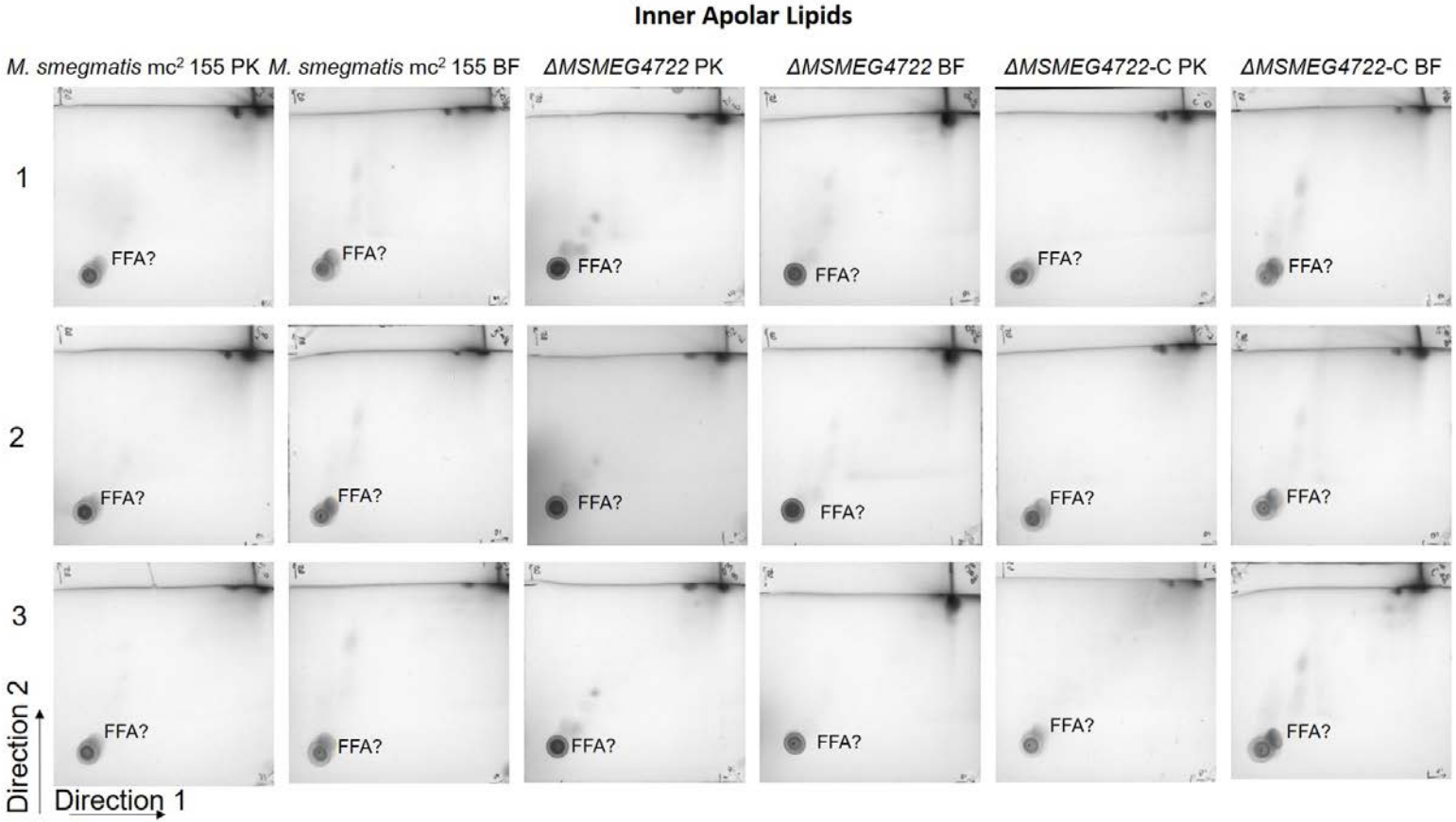


Figure A.2.16: Inner apolar lipid analysis of planktonic and biofilm *M. smegmatis* mc² 155, *ΔMSMEG4722* and *ΔMSMEG4722*-C (solvent system B).

2D-TLC plates of all three strains cultured either as planktonic or pellicle biofilms. Three independent biological replicates. Developed in petroleum ether 60-80ºC: acetone (92:8 v/v) x3 and toluene: acetone (95:5 v/v) x1 and stained with MPA. Free fatty acid (FFA).

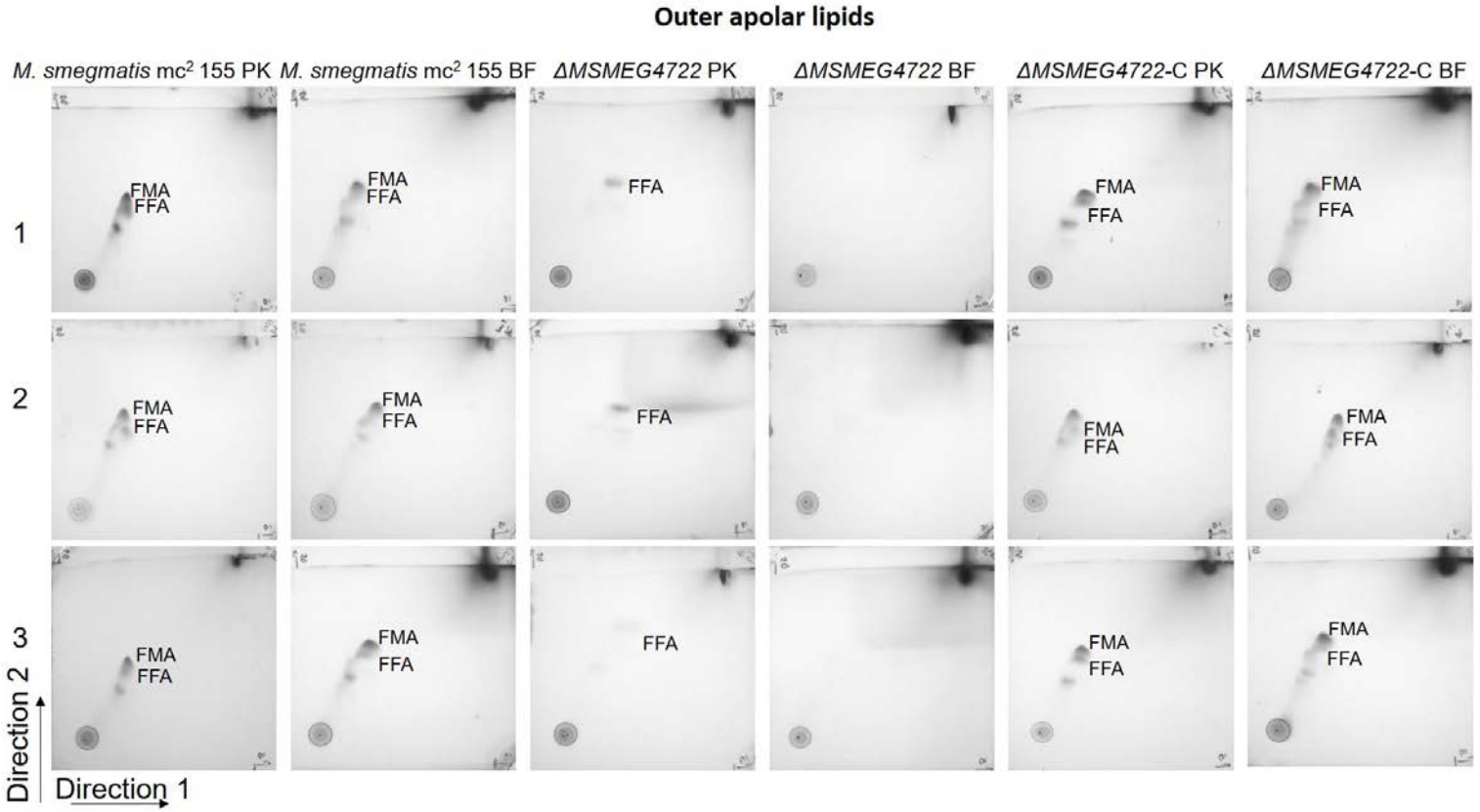


Figure A.2.17: Outer apolar lipid analysis of planktonic and biofilm *M. smegmatis* mc² 155, *ΔMSMEG4722* and *ΔMSMEG4722*-C (solvent system C).

2D-TLC plates of outer apolar lipid fractions of all three strains cultured as planktonic or pellicle biofilms. Developed in chloroform: methanol (96:4 v/v) x1 and toluene: acetone (80:20 v/v) x1 and stained with MPA. Free fatty acid (FFA), free mycolic acid (FMA), unidentified lipid 7 ($?_7$), unidentified lipid 8 ($?_8$), unidentified lipid 9 ($?_9$).

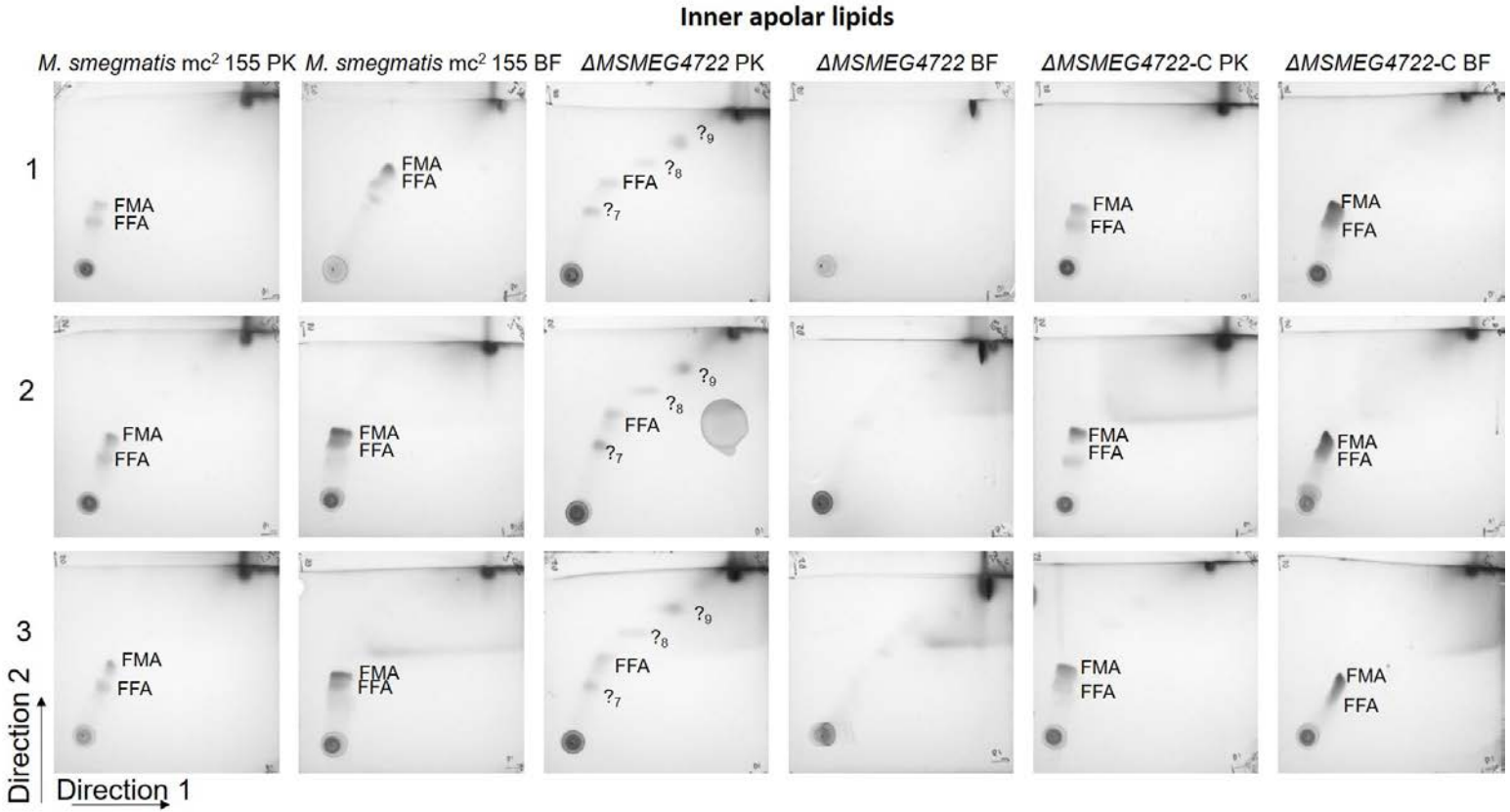


Figure A.2.18: Inner apolar lipid analysis of planktonic and biofilm *M. smegmatis* mc² 155, *ΔMSMEG4722* and *ΔMSMEG4722*-C (solvent system C).

2D-TLC plates of inner apolar lipid fractions of all three strains cultured as planktonic or pellicle biofilms. Developed in chloroform: methanol (96:4 v/v) x1 and toluene: acetone (80:20 v/v) x1 and stained with MPA. Free fatty acid (FFA), free mycolic acid (FMA), unidentified lipid 7 ($?_7$), unidentified lipid 8 ($?_8$), unidentified lipid 9 ($?_9$).

Appendix 2

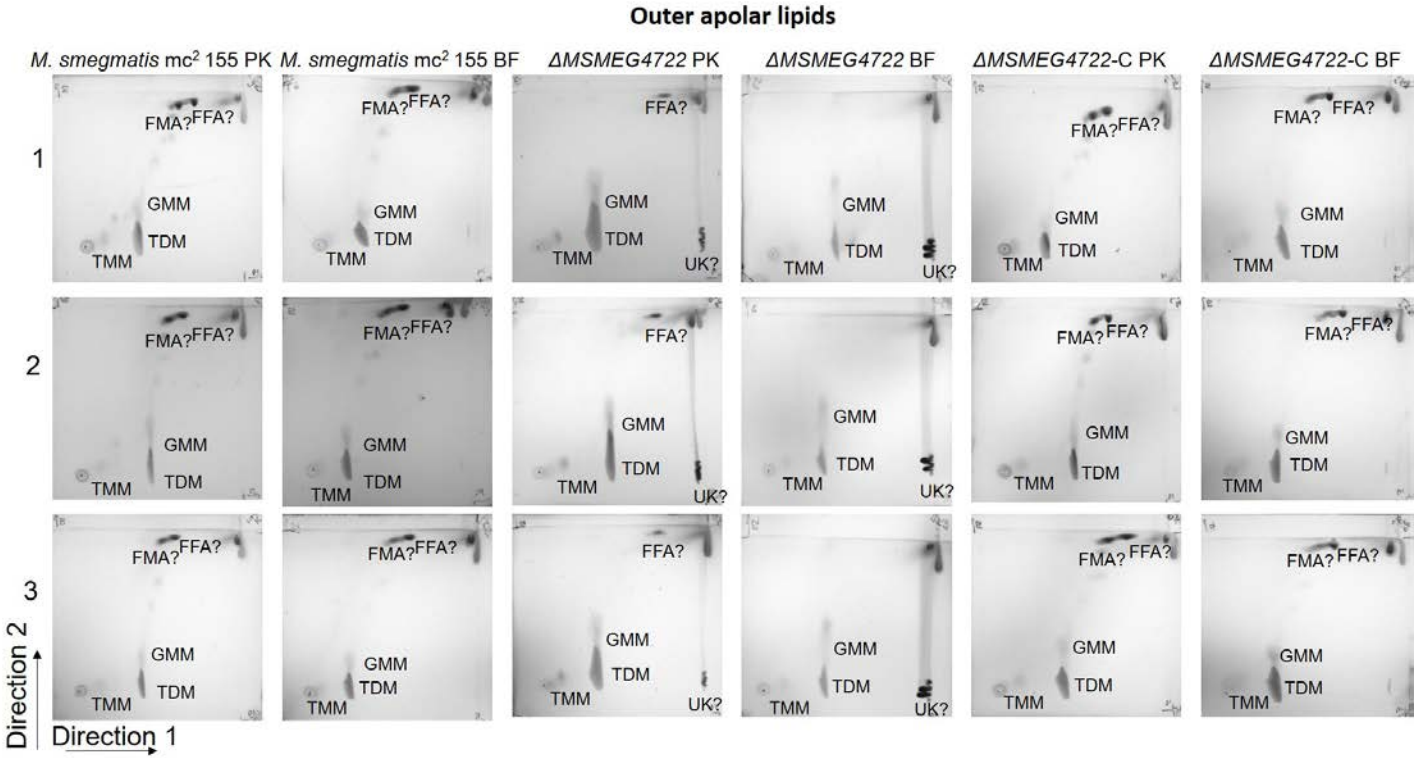


Figure A.2.19: Outer apolar lipid analysis of planktonic and biofilm *M. smegmatis* mc² 155, *ΔMSMEG4722* and *ΔMSMEG4722*-C (solvent system D).

2D-TLC plates of outer apolar lipid fractions of all three strains cultured as planktonic or pellicle biofilms. Developed in chloroform: methanol: deionised water (100:14:0.8 v/v/v) x1 and chloroform: acetone: methanol: deionised water (50:60:2.5:3 v/v/v/v) x1 and stained with α-naphthol. Trehalose monomycolate (TMM), trehalose dimycolate (TDM), glucose monomycolate (GMM), free fatty acid (FFA), free mycolic acid (FMA) and unsaturated ketones (UK).

Appendix 2

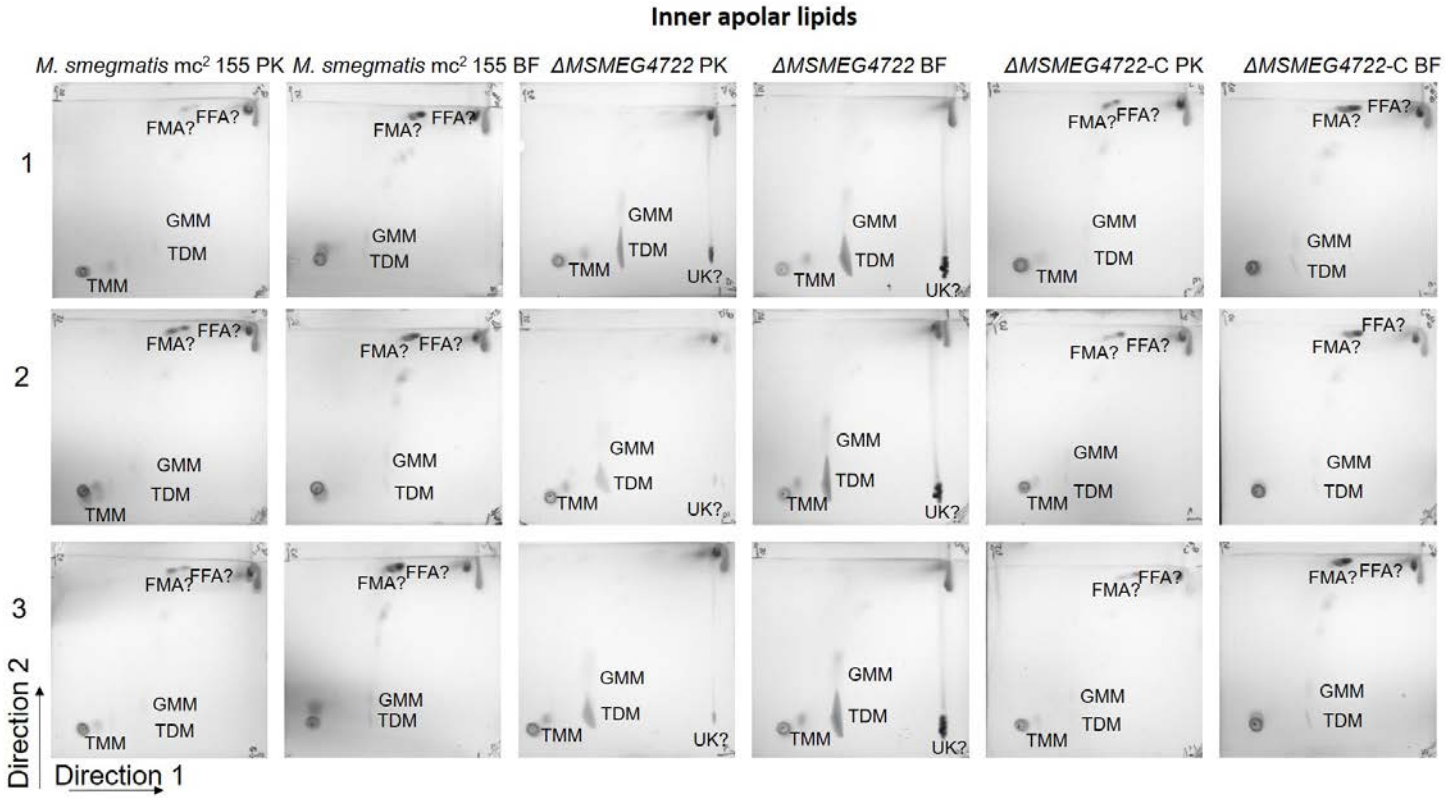


Figure A.2.20: Inner apolar lipid analysis of planktonic and biofilm *M. smegmatis* mc² 155, *ΔMSMEG4722* and *ΔMSMEG4722*-C (solvent system D).

2D-TLC plates of inner apolar lipid fractions of all three strains cultured as planktonic or pellicle biofilms. Developed in chloroform: methanol: deionised water (100:14:0.8 v/v/v) x1 and chloroform: acetone: methanol: deionised water (50:60:2.5:3 v/v/v/v) x1 and stained with α-naphthol. Trehalose monomycolate (TMM), trehalose dimycolate (TDM), glucose monomycolate (GMM), free fatty acid (FFA), free mycolic acid (FMA) and unsaturated ketones (UK).

Appendix 2

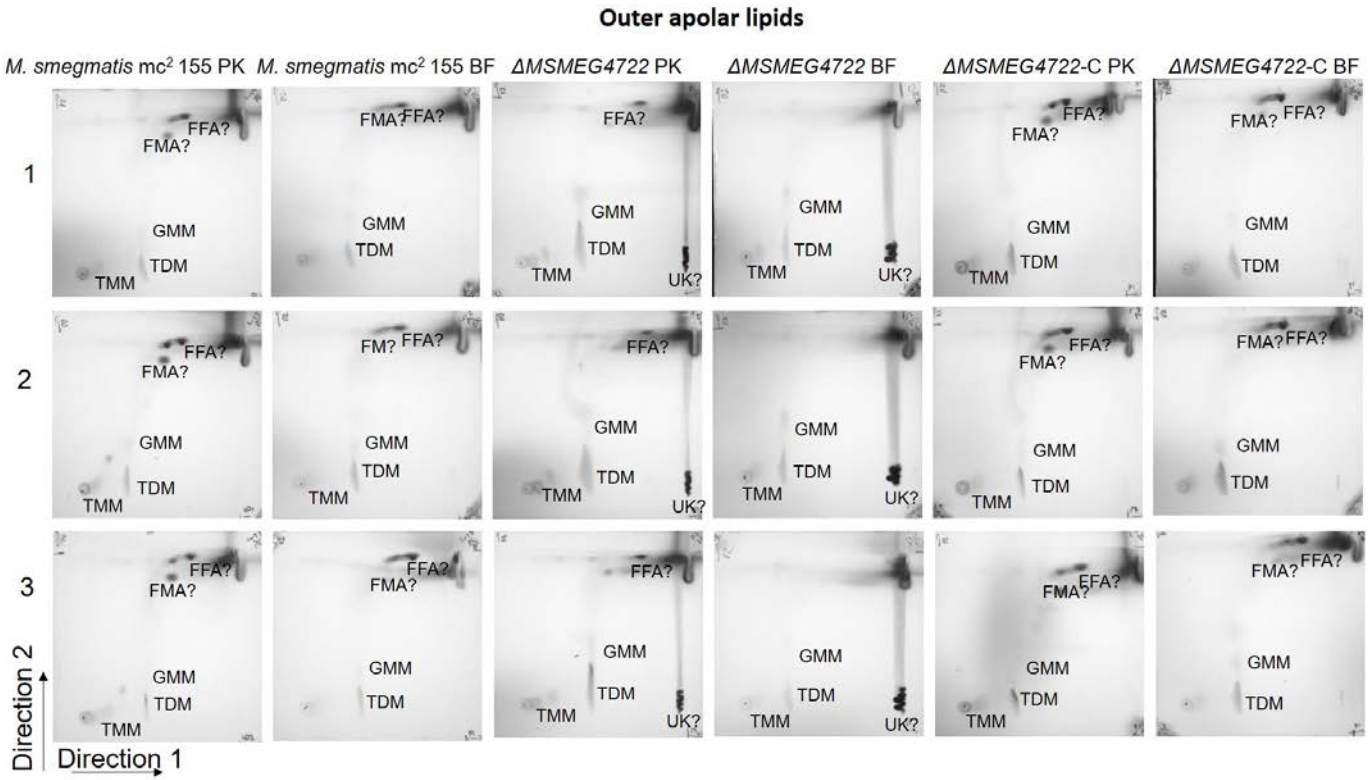


Figure A.2.21: Outer apolar lipid analysis of planktonic and biofilm *M. smegmatis* mc² 155, *ΔMSMEG4722* and *ΔMSMEG4722*-C (solvent system D).

2D-TLC plates of outer apolar lipid fractions of all three strains cultured as planktonic or pellicle biofilms. Developed in chloroform: methanol: deionised water (100:14:0.8 v/v/v) x1 and chloroform: acetone: methanol: deionised water (50:60:2.5:3 v/v/v/v) x1 and stained with MPA. Trehalose monomycolate (TMM), trehalose dimycolate (TDM), glucose monomycolate (GMM), free fatty acid (FFA), free mycolic acid (FMA) and unsaturated ketones (UK).

Appendix 2

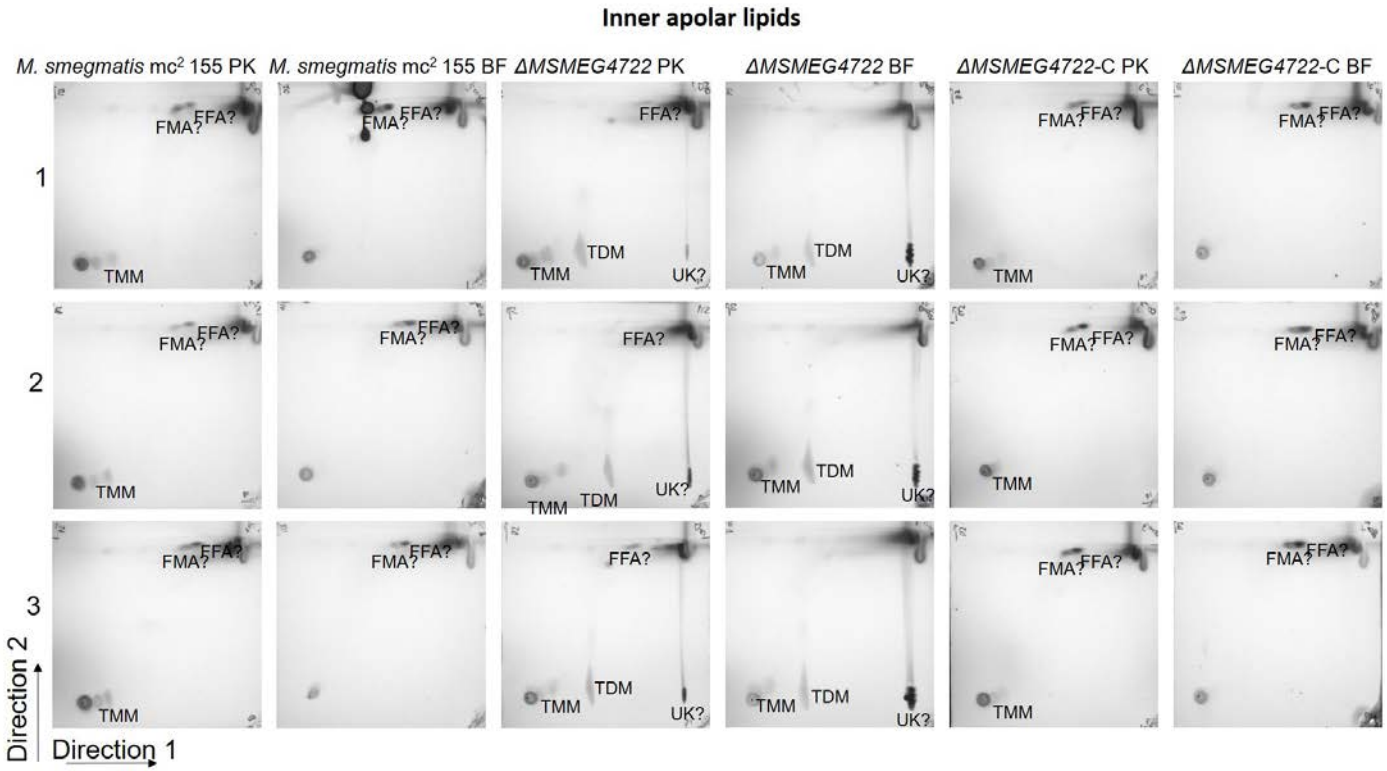


Figure A.2.22: Inner apolar lipid analysis of planktonic and biofilm *M. smegmatis* mc² 155, *ΔMSMEG4722* and *ΔMSMEG4722*-C (solvent system D).

2D-TLC plates of inner apolar lipid fractions of all three strains cultured as planktonic or biofilm phenotype. Developed in chloroform: methanol: deionised water (100:14:0.8 v/v/v) x1 and chloroform: acetone: methanol: deionised water (50:60:2.5:3 v/v/v/v) x1 and stained with MPA. Trehalose monomycolate (TMM), trehalose dimycolate (TDM), glucose monomycolate (GMM), free fatty acid (FFA), free mycolic acid (FMA) and unsaturated ketones (UK).

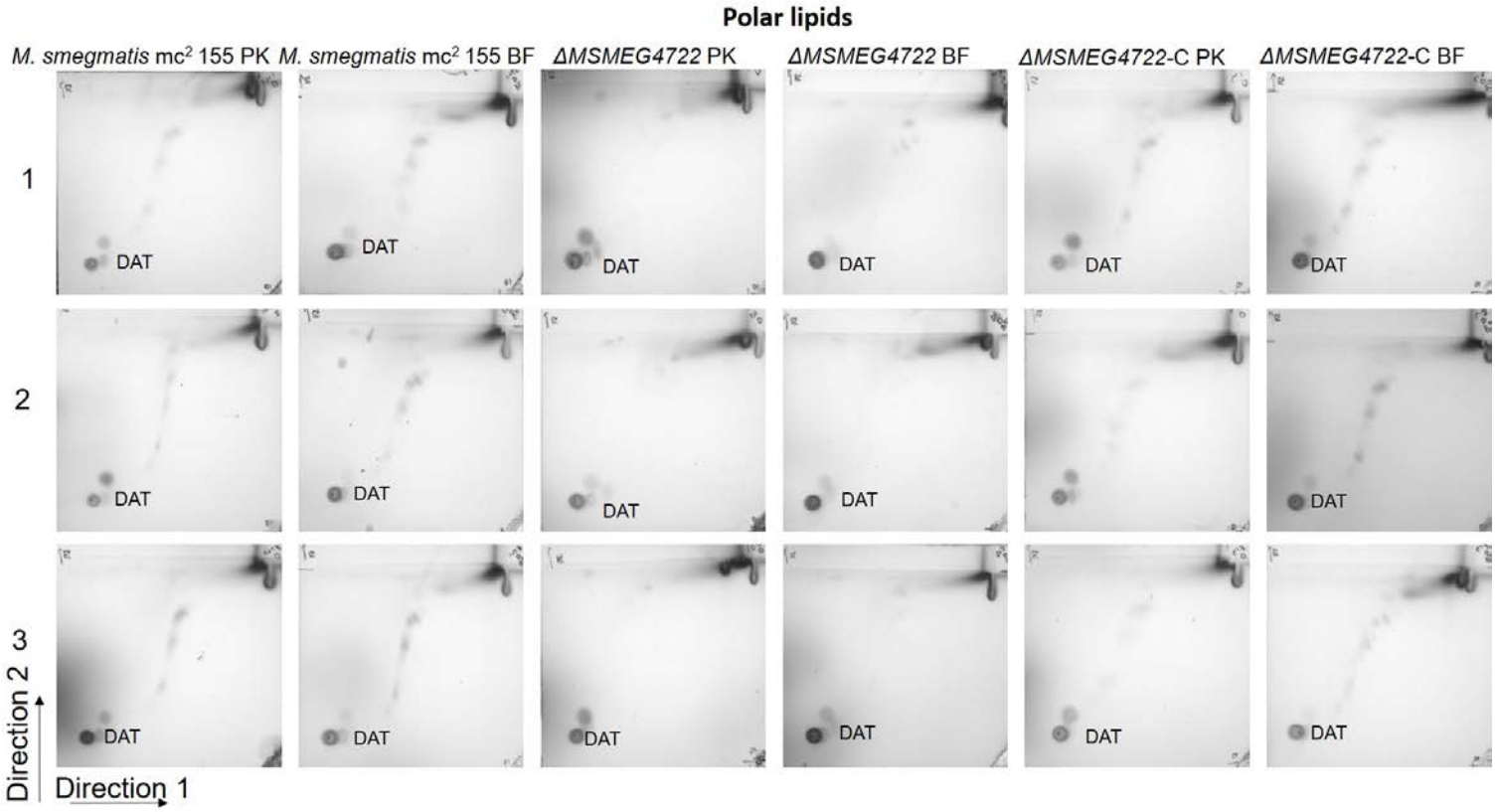


Figure A.2.23: Polar lipid analysis of planktonic and biofilm culture *M. smegmatis* mc² 155, *ΔMSMEG4722* and *ΔMSMEG4722*-C (solvent system D).

2D-TLC plates of polar lipid fractions of all three strains cultured as planktonic or biofilm phenotype. Developed in chloroform: methanol: deionised water (100:14:0.8 v/v/v) x1 and chloroform: acetone: methanol: deionised water (50:60:2.5:3 v/v/v/v) x1 and stained with α-naphthol.

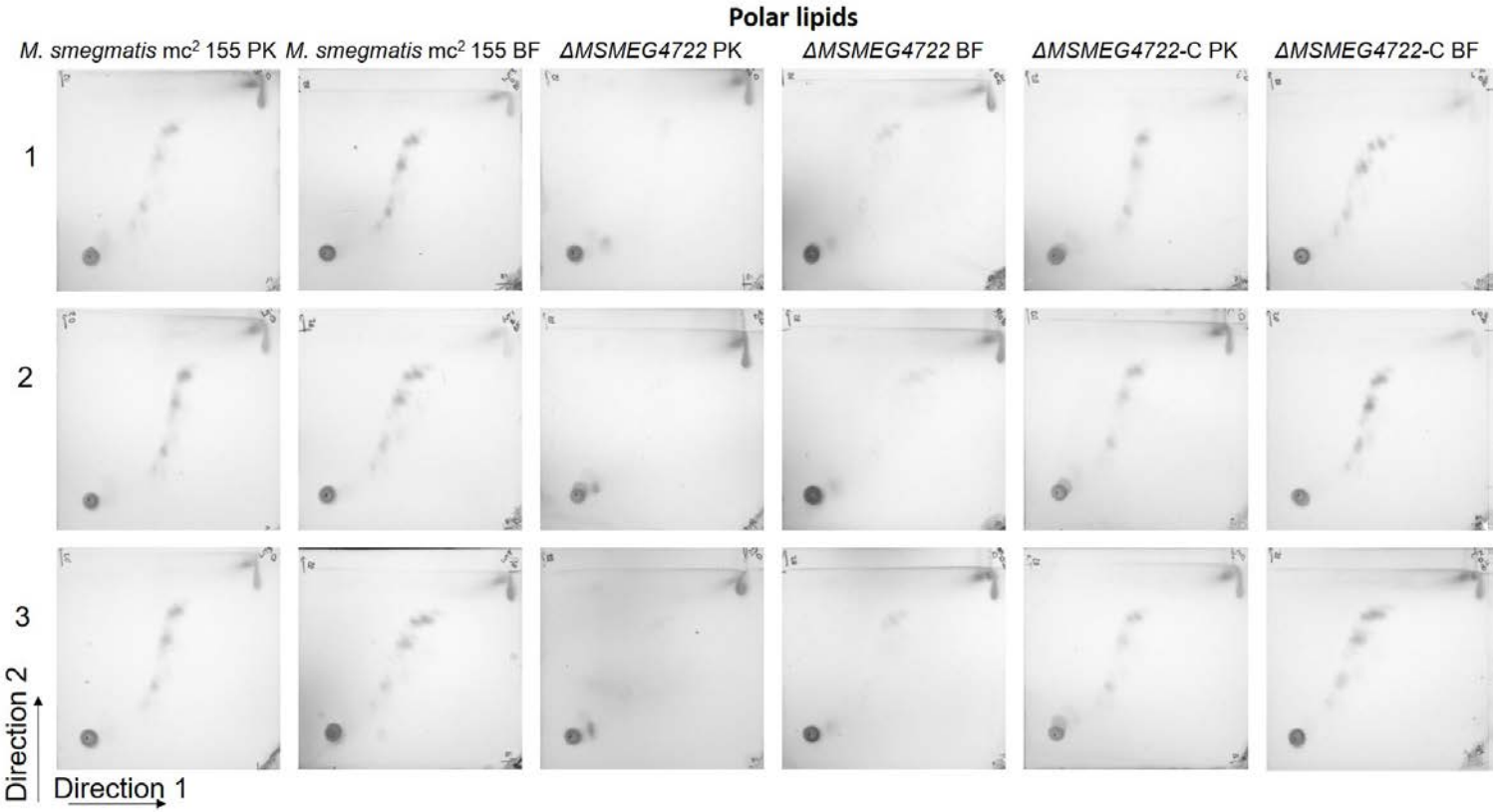


Figure A.2.24: Polar lipid analysis of planktonic and biofilm culture *M. smegmatis* mc² 155, *ΔMSMEG4722* and *ΔMSMEG4722*-C (solvent system D).

2D-TLC plates of polar lipid fractions of all three strains cultured as planktonic or pellicle biofilms. Developed in chloroform: methanol: deionised water (100:14:0.8 v/v/v) x1 and chloroform: acetone: methanol: deionised water (50:60:2.5:3 v/v/v/v) x1 and stained with MPA.

Appendix 2

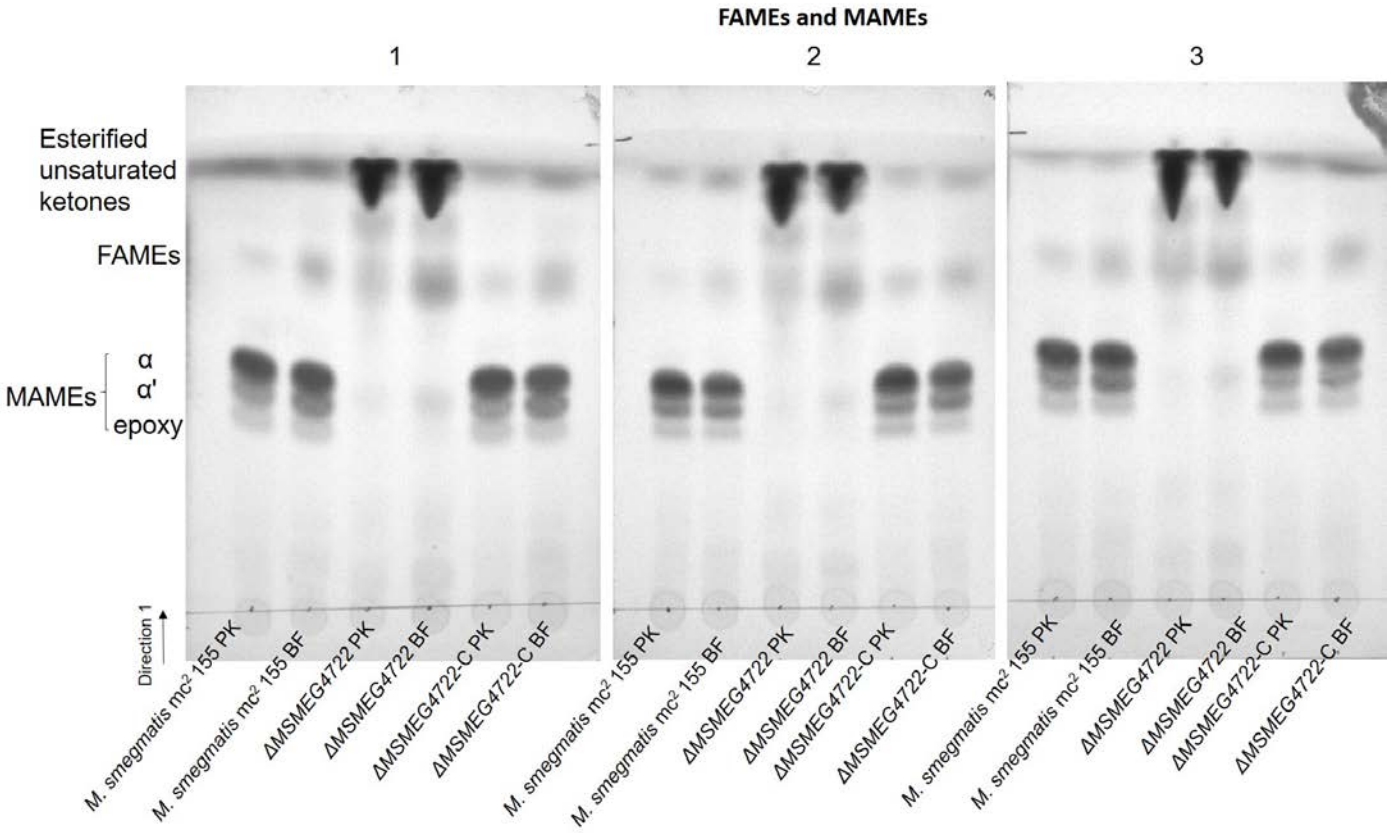


Figure A.2.25: FAMEs and MAMEs analysis of planktonic and biofilm *M. smegmatis* mc² 155, *ΔMSMEG4722* and *ΔMSMEG4722*-C.

1D-TLC using a FAMEs and MAMEs solvent system of all three strains cultured either as the planktonic or pellicle biofilms. Developed in petroleum ether 60-80ºC: acetone (95:5) x3 and stained with MPA. Esterified unsaturated ketones, α, α' and epoxy-mycolic acid methyl esters (MAMEs) and fatty acid methyl esters (FAMEs).

Appendix 3

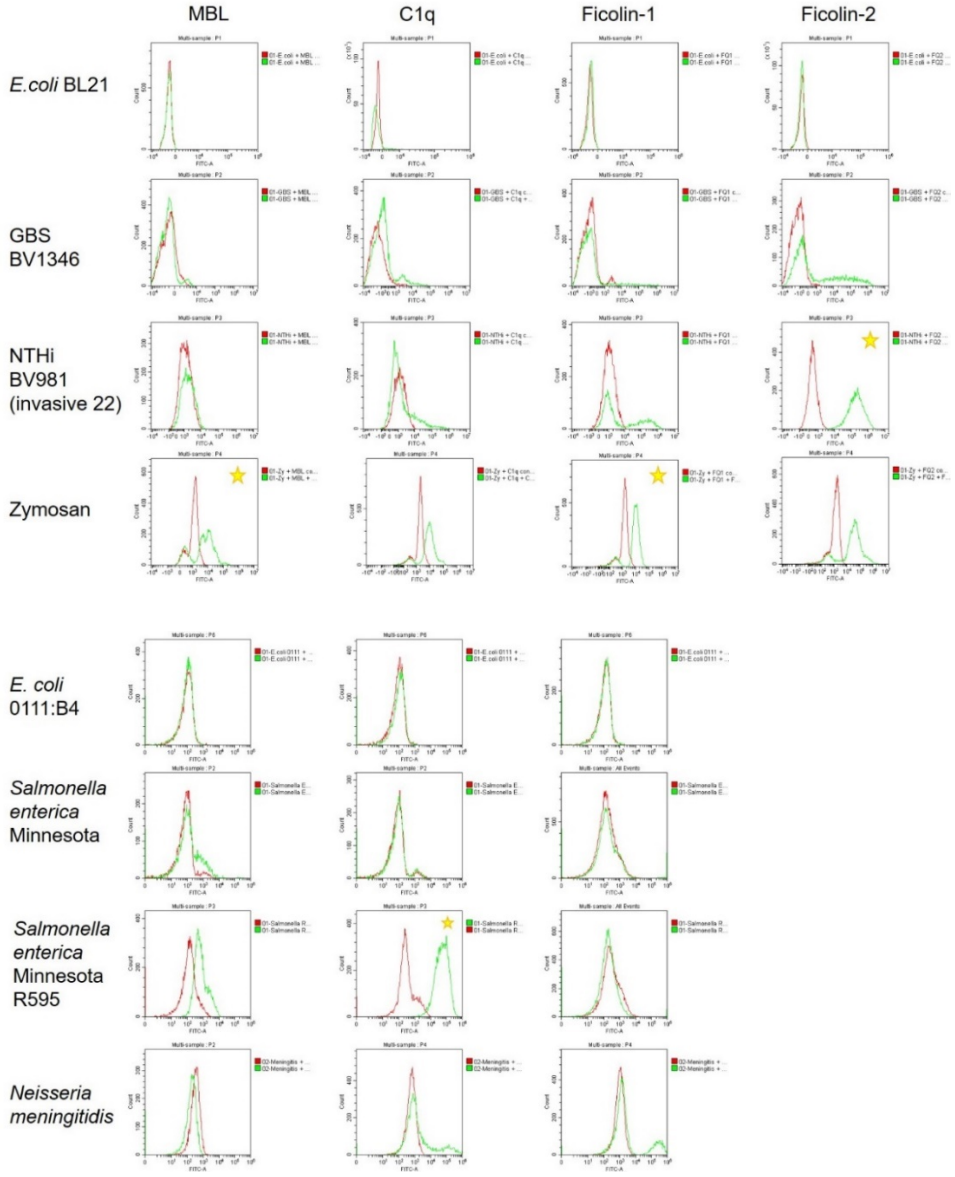


Figure A.3.1: Complement activator binding screen for positive controls.

5µg mL^{-1} purified C1q, rMBL, rficolin-1 and rficolin-2 were screened for binding to a range of bacteria (all $1x10^7$ bacteria mL^{-1}) and zymosan ($5.14x10^7$ particles mL^{-1}) to determine positive controls for activator-based flow cytometry assays. Overlay histograms of bacteria or zymosan incubated with (green) and without (red) purified or recombinant activator. Yellow stars indicate highest binder for that activator; *S. enterica* Minnesota R595 (Clq), NTHi BV981 (invasive 22) (ficolin-2) and zymosan (MBL and ficolin-1).

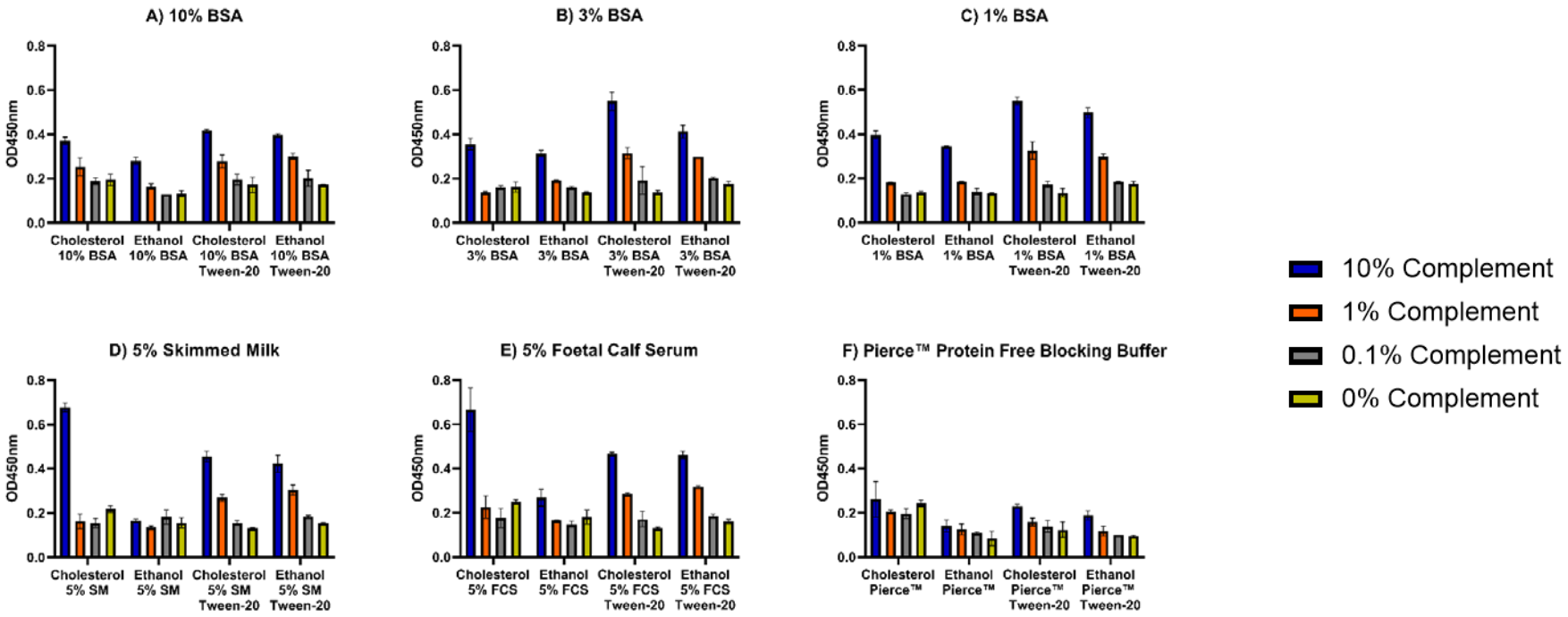


Figure A.3.2: Initial blocking buffer screen for the lipid-based C3b/iC3b ELISA.

Cholesterol was re-suspended in 2:1 chloroform: methanol to 500µg mL^{-1}, then diluted to 25µg mL^{-1} in ethanol. For background fluorescence, 2:1 chloroform: methanol diluted in ethanol (same dilution as cholesterol) was used to coat the plates. Wells were coated with 100µl. 150µl of six blocking buffers ± 0.05% Tween-20 were incubated for 1 hour. (A) 10% BSA, (B) 3% BSA, (C) 1% BSA (D) 5% Skimmed Milk (SM), (E) 5% Foetal Calf Serum (FCS) or (F) Pierce™ Protein Free Blocking Buffer (Pierce™). This was followed by a 1 hour incubation at 37ºC with 100µl 10% (blue), 1% (orange), 0.1% (grey) or 0% (yellow) complement before labelling with pAb anti-C3c HRP for 1 hour. Plates were developed by the addition of TMB substrate and quenched after 10 minutes before absorbance was read at $OD450_{nm}$.

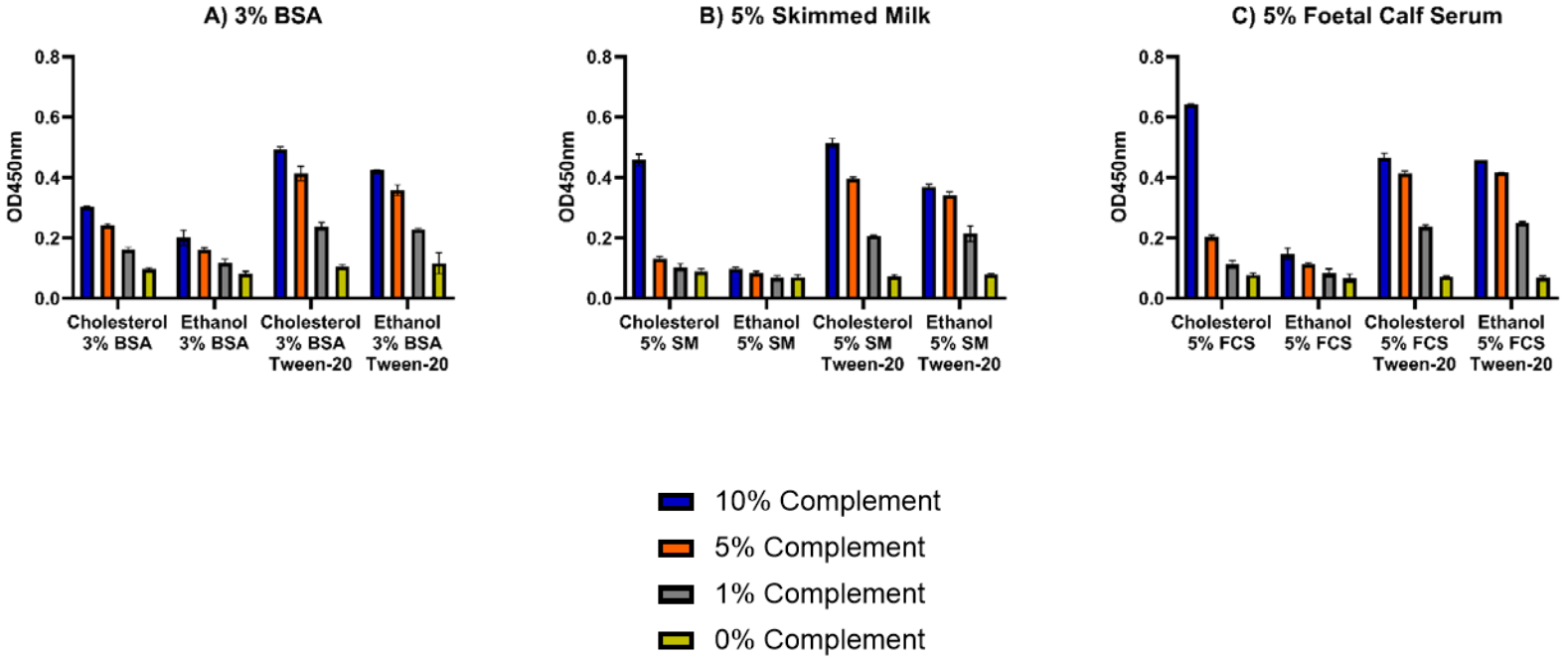
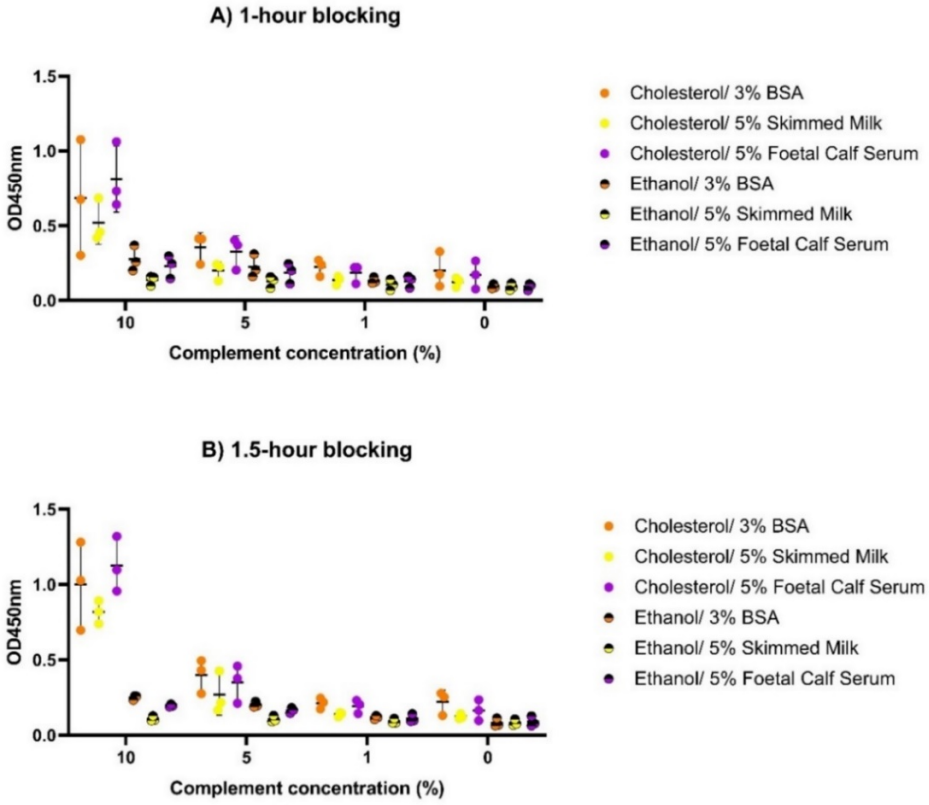


Figure A.3.3: Second blocking buffer screen for the lipid-based C3b/iC3b ELISA.

Cholesterol was re-suspended in 2:1 chloroform: methanol to 500µg mL^{-1}, then diluted to 25µg mL^{-1} in ethanol. For background fluorescence, 2:1 chloroform: methanol diluted in ethanol (same dilution as cholesterol) was used to coat the plates. Wells were coated with 100µl. 150µl of three blocking buffers ± 0.05% Tween-20 were incubated for 1 hour. (A) 3% BSA, (B) 5% Skimmed Milk (SM) or (C) 5% Foetal Calf Serum (FCS). This was followed by a 1 hour incubation at 37ºC with 100µl 10% (blue), 5% (orange), 1% (grey) or 0% (yellow) complement before labelling with pAb anti-C3c HRP for 1 hour. Plates were developed by the addition of TMB substrate and quenched after 10 minutes before absorbance was read at $OD450_{nm}$.



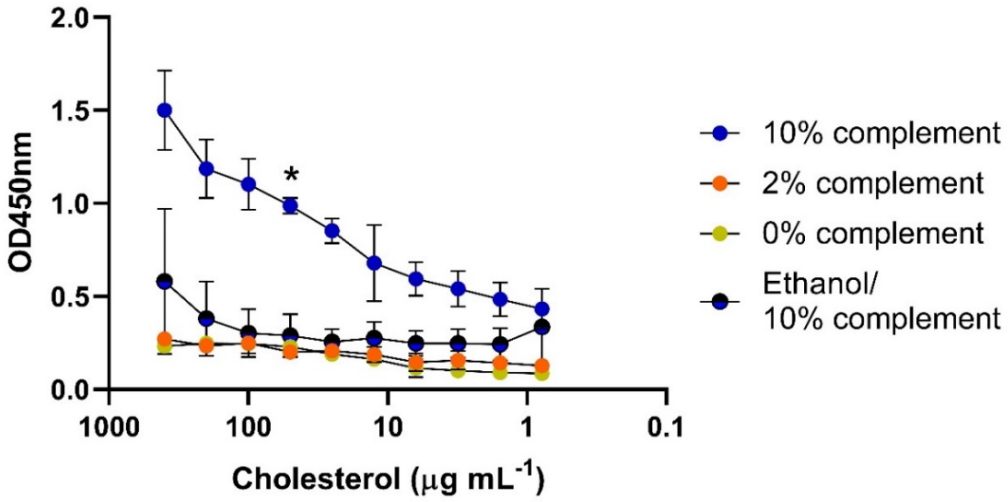
C

10% complement / blocking buffer	1 hour block	1.5-hour block
3% BSA	-1.823	-0.01
5% Skimmed Milk	-0.139	0.678
5% Foetal Calf Serum	-0.256	**0.495**

Figure A.3.4: Third blocking buffer screen for the lipid-based C3b/iC3b ELISA.

Cholesterol was re-suspended in 2:1 chloroform: methanol to 500µg mL^{-1}, then diluted to 25µg mL^{-1} in ethanol. For background controls (block colour/ black), 2:1 chloroform: methanol diluted in ethanol (same dilution as cholesterol) was used to coat the plates. Wells were coated with 100µl. 200µl of the blocking buffers tested were 3% BSA (orange), 5% Skimmed Milk (yellow), and 5% Foetal Calf Serum (purple) incubated for (A) 1 hour or (B) 1.5 hours. Background fluorescence controls; 3% BSA (orange/black), 5% Skimmed Milk (yellow/black), and 5% Foetal Calf Serum (purple/black). This was followed by a 1 hour incubation at 37ºC with 100µl 10%, 5%, 1% or 0% complement before labelling with pAb anti-C3c HRP for 1 hour. Plates were developed by the addition of TMB substrate and quenched after 10 minutes before absorbance was read at $OD450_{nm.}$ (C) Statistical analysis performed was Z-factor. Error bars = standard deviation of three biological replicates. Green = excellent, yellow = marginal and red = negative. Chosen blocking conditions were 5% Foetal Calf Serum for 1.5 hours.

A



B

10% complement / cholesterol (µg mL^{-1})	Z-Factor
400	-0.39522
200	-0.08683
100	0.185594
50	**0.453591**
25	0.441529
12.5	-0.78371
6.25	-0.10312
3.125	-0.4361
1.56	-0.78117
0.78	-7.00079

Figure A.3.5: Optimal lipid coating concentration for the C3b/iC3b lipid-based ELISA.

(A) Checkerboard ELISA of complement concentration against cholesterol concentration. Cholesterol was re-suspended to 40mg mL^{-1} in 2:1 chloroform: methanol, then diluted to 400µg mL^{-1} in ethanol. 1:2 serial dilution of cholesterol (400µg mL^{-1} to 0.78µg mL^{-1}) in ethanol was performed. Wells were coated with 100µl and blocked with 5% Foetal Calf Serum for 1.5 hours. Complement concentrations tested were 10% (blue), 2% (orange) and 0% (mustard) incubated at 37^{o}C for 1 hour. The equivalent 2:1 chloroform: methanol diluted in ethanol was used to determine complement-mediated background fluorescence incubated with 10% complement (blue/black circles). Complement deposition labelling was pAb anti-C3c HRP for 1 hour. Plates were developed by the addition of TMB substrate and quenched after 10 minutes before absorbance was read at OD450$_{nm.}$ (B) Statistical analysis performed was Z-Factor. Error bars = standard deviation of three biological replicates. Yellow = marginal and red = negative. The chosen coating concentration was 50µg mL^{-1}.

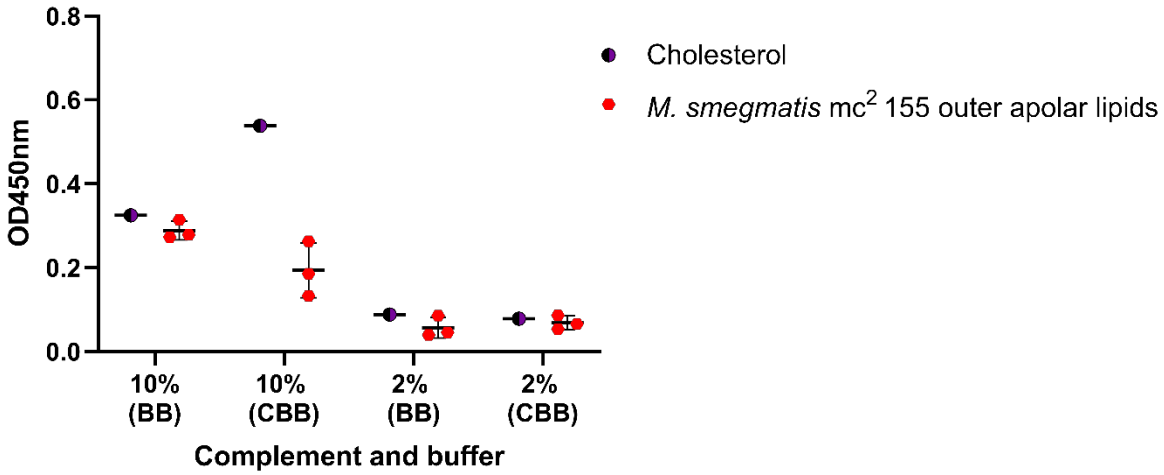


Figure A.3.6: Evaluating the effect of barbitone on complement activation in the lipid-based C3b/iC3b ELISA.

Samples tested were the positive control cholesterol (purple and black circle) and three independent biological replicates of the outer apolar lipid fractions extracted from *M. smegmatis* mc^2 155 (red hexagon) re-suspended in 2:1 chloroform: methanol to 5mg mL^{-1} diluted in ethanol to 50µg mL^{-1}. Wells were coated with 100µl, then blocked with 5% Foetal Calf Serum for 1.5 hours. Samples were incubated with 10% or 2% complement at 37°C for 1 hour before labelling with pAb anti-C3c FITC. Plates were developed by the addition of TMB substrate and quenched after 10 minutes before absorbance was read at $OD450_{nm.}$ Complement and anti-C3c (FITC) were diluted in Binding Buffer (BB: 2% BSA in PBS) or Complement Binding Buffer (CBB: 2% BSA in PBS + barbitone). Background fluorescence was derived from the incubation of 10% or 2% complement with chloroform: methanol diluted in ethanol only coated-wells and subtracted from samples.

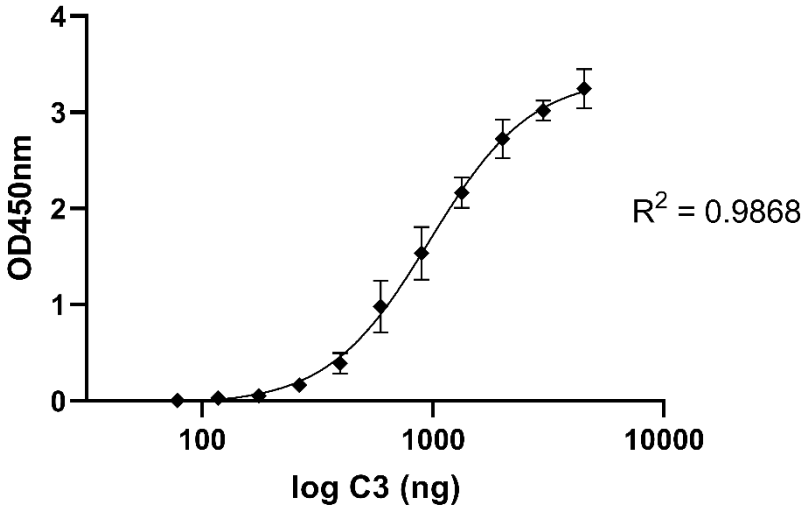


Figure A.3.7: C3 standard curve.

A 12-point standard curve of well-bound purified C3. A 2:3 serial dilution was performed ranging from 4514ng to 52ng. Wells were blocked with 1% BSA for 1.5 hours then labelled with the pAb anti-C3c HRP. The C3 standard curve was plotted using the Sigmoidal, 4PL, x is log(concentration) curve fitting analysis. Error bars = standard deviation from five replicate curves.

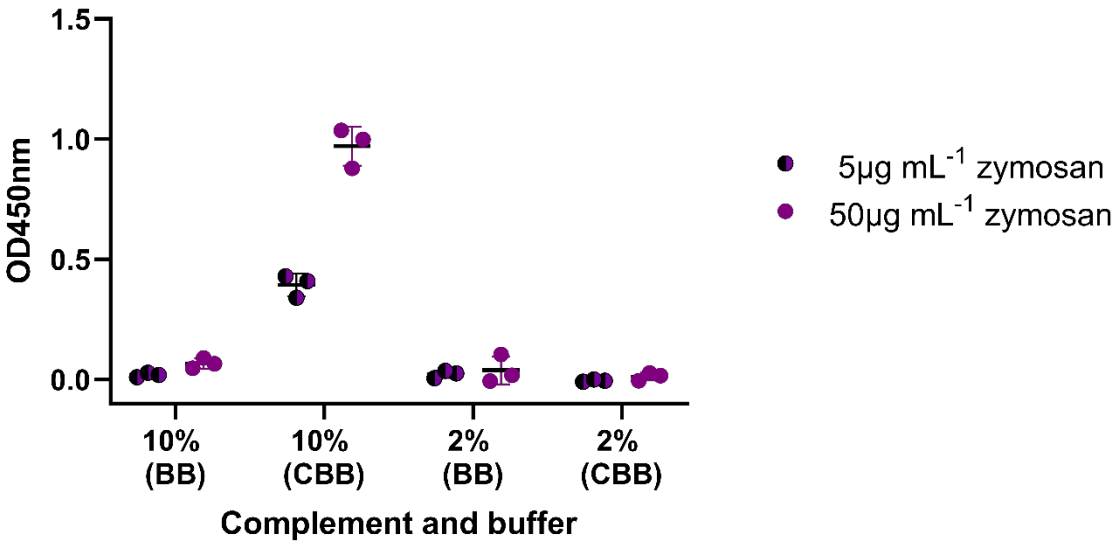
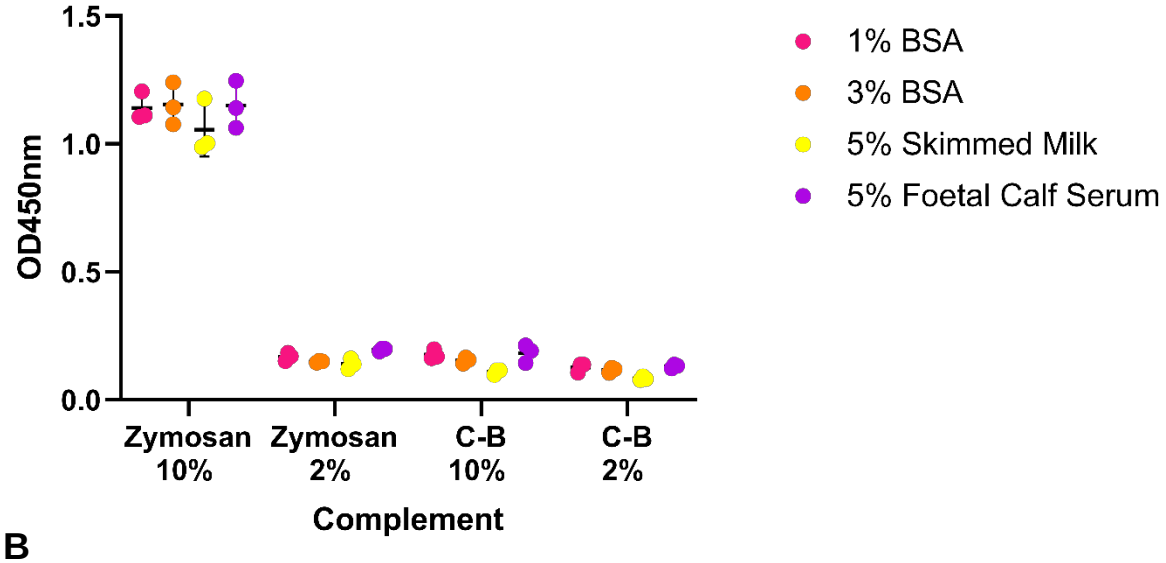


Figure A.3.8: Evaluating the effect of barbitone on complement activation in the carbohydrate-based C3b/iC3b ELISA.

The positive control zymosan was tested at 50µg mL^{-1} (back/purple circles) and 5µg mL^{-1} (purple circles). Wells were blocked with 1% BSA for 1.5 hours. Zymosan was incubated with 10% complement or 2% complement at 37°C for 1 hour. Complement and anti-C3c (FITC) were diluted in Binding Buffer (BB: 2% BSA in PBS) or Complement Binding Buffer (CBB: 2% BSA in PBS + barbitone). Background fluorescence was derived from the incubation of 10% or 2% complement with carbonate-bicarbonate (C-B) only coated-wells and subtracted from samples.

A



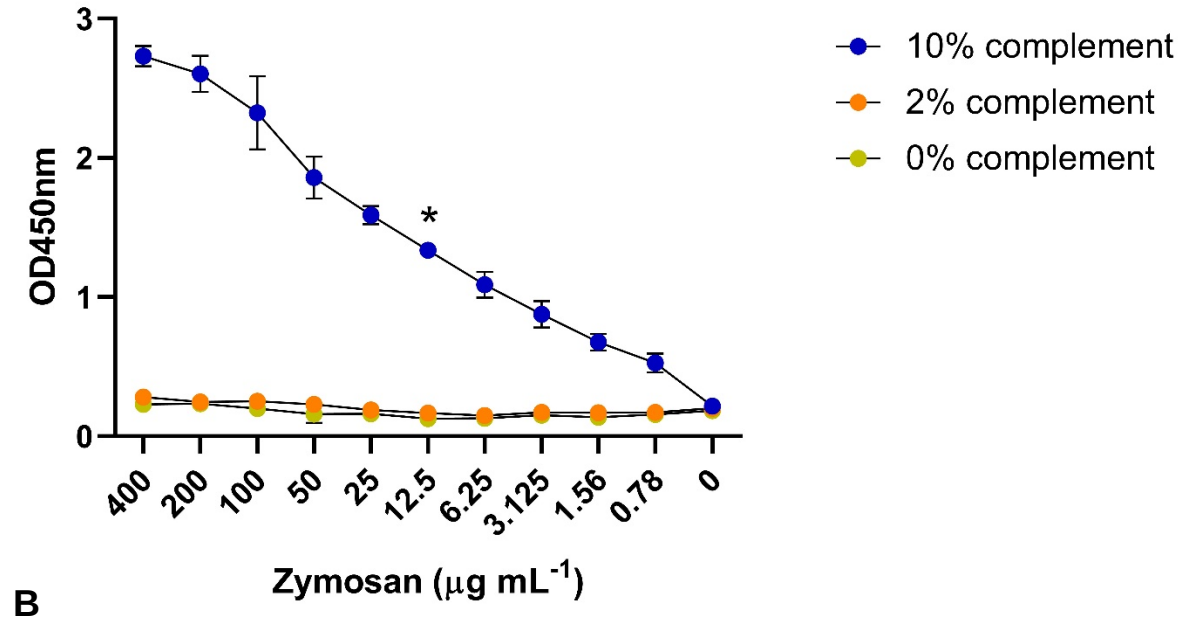
B

10% complement / blocking buffer	Z-Factor
1% BSA	**0.81023**
3% BSA	0.76979
5% Skimmed Milk	0.70139
5% Foetal Calf Serum	0.67749

Figure A.3.9: Blocking buffer screen for the C3b/iC3b carbohydrate-based ELISA.

(A) Zymosan was diluted to 50µg mL^{-1} and 100µl coated to the plates before blocking with 1% BSA (pink), 3% BSA (orange), 5% Skimmed Milk (yellow) or 5% Foetal Calf Serum (purple) for 1.5 hours. Carbonate-bicarbonate buffer (C-B) only coated wells were blocked then incubated with 10% or 2% complement in CBB to determine background fluorescence. (B) Statistical analysis performed was Z-factor. Error bars are the standard deviation of three biological replicates. Green = excellent. 1% BSA was chosen as the optimal blocking buffer.

A



B

10% complement / zymosan (µg mL^{-1})	Z-Factor
400	0.838955
200	0.764336
100	0.596505
50	0.635076
25	0.751752
12.5	**0.803194**
6.25	0.635184
3.125	0.514449
1.56	0.519345
0.78	0.328133

Figure A.3.10: Determining the optimal coating concentration for the C3b/iC3b carbohydrate-based ELISA.

(A) A 1:2 serial dilution of zymosan (400µg mL^{-1} to 0.78 µg mL^{-1} in carbonate-bicarbonate) was performed and each well coated with 100µl. The wells were blocked for 1.5 hours with 1% BSA. Complement concentrations tested were 10% (blue), 2% (orange) and 0% (mustard). Background control was 10% complement incubated with wells coated with carbonate-bicarbonate only (zymosan 0µg mL^{-1}) for Z-factor analysis. (B) Statistical analysis performed was Z-Factor. Error bars are the standard deviation of three biological replicates. Green = excellent and yellow = marginal. 12.5µg mL^{-1} was the optimal coating concentration.

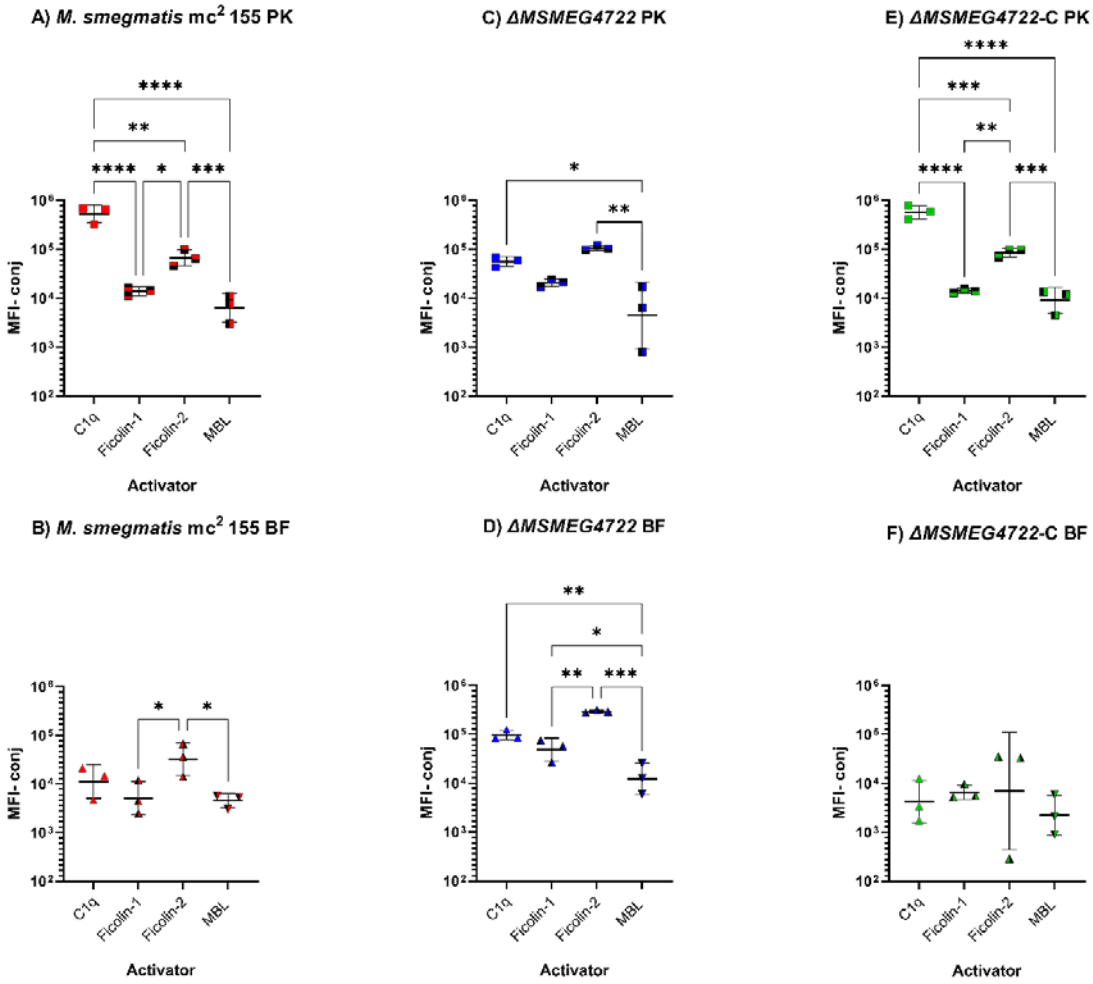


Figure A.3.11: Activator binding to planktonic and biofilm-derived bacteria for each strain.

Median fluorescence intensity – conjugate only fluorescence (MFI – conj) corresponding to binding of complement activator C1q, ficolin-1, ficolin-2 and MBL binding onto planktonic and pellicle biofilm-derived *M. smegmatis* mc^2 155, *ΔMSMEG4722* and *ΔMSMEG4722*-C. (A) *M. smegmatis* mc^2 155 planktonic (B) *M. smegmatis* mc^2 155 pellicle biofilm (C) *ΔMSMEG4722* planktonic (D) *ΔMSMEG4722* pellicle biofilm (E) *ΔMSMEG4722*-C planktonic (F) *ΔMSMEG4722*-C pellicle biofilm. Planktonic (PK) and pellicle biofilm (BF). Error bars = standard deviation of three biological replicates. For statistical analysis, data was log10 transformed before performing a one-way ANOVA with Tukey's multiple comparison correction. (A) * P = 0.0118, ** P = 0.0023, *** P = 0.0010, **** P < 0.0001 (B) * P = 0.0487 (Ficolin-2 vs Ficolin-1) * P = 0.0364 (Ficolin-2 vs MBL) (C) * P = 0.0194, ** P = 0.0054 (D) * P = 0.0285, ** P = 0.0029 (C1q vs MBL), ** P = 0.0066 (Ficolin-2 vs Ficolin-1), *** P = 0.0002 (E) ** P = 0.0013, *** P = 0.0009 (C1q vs Ficolin-2), *** P = 0.0003 (Ficolin-2 vs MBL), **** P < 0.0001.